Regulation of immunometabolic processes in atherosclerosis and nonalcoholic fatty liver disease by liver receptor homolog 1

Stein, Matthias Alexander Sokrates

Habilitationsschrift

Regulation of Immunometabolic Processes in Atherosclerosis and Nonalcoholic Fatty Liver Disease by Liver Receptor Homolog 1

Zur Erlangung der Venia Legendi der Universität Zürich

Verfasst von

Matthias Alexander Sokrates Stein

Zürich, 8. Mai 2018

Preface

In this habilitation treatise I focus on the work that was performed to analyze the function of the nuclear receptor liver receptor homolog 1 (LRH-1) in the development of atherosclerosis and nonalcoholic fatty liver disease.

I started exploring transcriptional networks in the fruit fly *Drosophila melanogaster* during my Master (diploma) thesis. This study in developmental biology was carried out at the Max Planck Institute for Developmental Biology in Tübingen and performed under the supervision of Ingrid Lohmann. I also got substantial support from Petra Stöbe and Zhongzhao Zhai to analyze the interaction of the transcription factor *Deformed* during *Drosophila* embryogenesis.

Christian Matter introduced me to the atherosclerosis research during an interview for a PhD thesis early in 2008. The impact of this disease as the leading cause of mortality in the world on one side, and the fascinating biomedical complexity on the other side caught my attention. Atherogenesis is triggered and influenced by genetic, epigenetic and environmental factors and encompasses various organs and many different cell types. Therefore, there is a lot be learned and discover at various levels, from small molecular protein interactions to metabolic processes affecting whole-body physiology. I joined Christian Matter's group to perform my PhD thesis, and since then my primary research interest has been to study how molecular network affect the development of this chronic immunometabolic disease.

During my PhD thesis at the Institute of Physiology at the University of Zurich I studied the role of a specific protein deacetylase in atherosclerosis in mice and primary human cells. During this time, I got valuable support from my thesis committee members and lab colleagues, including Christian Matter, Burkhard Becher, Michael Hottiger, Walter Wahli, Alexander Breitenstein, Christian Besler, Stephan Winnik, Gabriela Kania, and Przemyslaw Blyszczuk. Our studies revealed important anti-inflammatory functions of this deacetylase in athero-thrombotic diseases, which are summarized and discussed in my PhD thesis.

After completion of my PhD in March 2011, I moved to Lausanne to perform my postdoctoral work in the lab of Kristina Schoonjans at the École Polytechnique Fédérale de Lausanne. In her lab I analyzed the function of the transcription factor LRH-1 in atherosclerosis and nonalcoholic fatty liver disease, another important chronic metabolic disease. During this time, I greatly benefited from the input and help of Kristina Schoonjans, Johan Auwerx, Pan Xu, Vera Lemos, Dongryeol Ryu, Alessia Perino, Maaike Oosterveer, Xu Wang, Li Hao, Karim Gariani, Jef Verbeek, and Norman Moullan. We discovered exciting mechanisms involved in the metabolic regulation of atherosclerosis and nonalcoholic fatty liver disease using mouse models and exploring human data. Moreover, during these years I expanded my research field from a rather focused view on the arteries and the cells within the atherosclerotic plaques towards a systemic view, taking into account the systemic effects driven by other organs, especially the liver.

Supported by an Ambizione Grant of the Swiss National Science Foundation, I lead my own independent research team at the Center for Molecular Cardiology at the University of Zurich since February 2016. My incorporation into the center was possible due to the kind support of the chairman and the director of the Center for Molecular Cardiology, i.e. Thomas Lüscher and Giovanni Camici. I would like to also acknowledge my current team members, Sara Oppi and Stefanie Nusser-Stein, who are paving up a common scientific path by contributing most valuable ideas and experiments. Currently, we are studying the function of two transcriptional corepressors in atherogenesis in mice, cell models, human data, and also building up bed-to-benchside collaborations with clinical teams. Here again we are benefiting from the fruitful collaborations with national and international colleagues, including Maaike Oosterveer, Dongryeol Ryu, Kristina Schoonjans, Johan Auwerx, Fatima Bosch, Fumio Matsuzaki, Christian Matter, Elena Osto, Theofanis Karayannis, Evan Williams, Alexander Leitner, Martin Geiger, and Zoran Rancic.

Table of Contents

1. Abstract

The metabolic syndrome is a cluster of interconnected diseases, including insulin resistance, obesity, hypertension, and dyslipidemias, and it is tightly associated with the development of atherosclerosis, nonalcoholic fatty liver disease (NAFLD), and type 2 diabetes mellitus. NALFD is one of the primary causes of liver disease in the world and it is strongly associated with cardiovascular risk factors. The disease encompasses different stages of liver disorders, starting with the excessive massive accumulation of hepatic triglycerides. Atherosclerosis is the primary cause of myocardial infarction and stroke, two of the leading causes of mortality in the world. One hallmark of the disease is the excessive accumulation of cholesterol in monocyte-derived macrophages within atherosclerotic lesions. Both atherosclerosis and NAFLD are immunometabolic diseases, i.e. chronic diseases that are affected by both metabolic and immunological triggers and signaling networks.

The signaling cascades that are activated by inflammatory and metabolic mediators converge at key transcriptional regulators, which in turn coordinate the expression of specific target genes. Together with colleagues I demonstrated that the nuclear receptor homolog-1 (LRH-1) affects the development of both atherosclerosis and NAFLD by regulating immunometabolic processes. We showed that atherosclerosis-prone mice carrying a mutation that abolishes the SUMOylation of the nuclear receptor (i.e. LRH-1 K289R) are significantly protected from atherosclerosis development in mice challenged with a high-cholesterol diet. This atheroprotection was regulated by the corepressor prospero-related homeobox 1 (PROX1), which normally transrepresses the transcription of genes involved in hepatic reverse cholesterol transport. On the other side, we showed that this same LRH-1 mutation promotes the development of NAFLD and early signs of steatohepatitis if mice are challenged with a lipogenic high-fat high-sucrose diet. These studies highlighted that a single posttranslational modification of a specific residue of a transcriptional regulator is sufficient to modulate the function of the protein and the corresponding cellular and metabolic processes, which consequently can affect the development of these complex chronic diseases.

In this habilitation I will summarize these two major studies as well as other work that underline the crucial function that this nuclear receptor exerts in the liver and macrophages under different genetic backgrounds and dietary challenges. These studies are of high translational potential given the availability of specific LRH-1 agonists and antagonists that could potentially be used to modulate the development and/or progression of these chronic diseases.

2. Atherosclerosis and nonalcoholic fatty liver disease

Atherosclerosis is the primary cause of myocardial infarction and stroke, two of the leading causes of mortality in the world (1, 2). In a simplified view one could describe atherosclerosis as a disease characterized by the thickening of blood vessels due to atherosclerotic plaques that are caused by the accumulation of immune cells and lipids, especially cholesterol. The disease most likely co-evolved with humans: Special 3 dimensional computer tomography-based imaging reconstructions of old mummified corpses revealed that the people living up to 4000 years ago had atherosclerotic lesions (3). These lesions could be detected in mummies from archaic to middle age periods, from different cultures, and found in different places of the world (3).

Atherosclerosis is a chronic immunometabolic disease, and its development starts early in a human life. One hallmark of the disease is the excessive accumulation of cholesterol in monocyte-derived macrophages within atherosclerotic lesions. The first fatty streak lesions may arise during embryonic development, and clinical correlation studies suggest that maternal hypercholesterolemia might promote the formation of lesion in the fetus (4, 5). The complex pathophysiology is triggered by genetic and environmental risk factors (6, 7). Moreover, disease progression is affected by medical complications, such as diabetes and obesity, and environmental factors, such as dietary metabolites (e.g. cholesterol, specific fatty acids, carnitine) (6-8). Importantly, these risk factors converge on various molecular processes, including inflammatory and/or metabolic responses**,** in diverse organs and the cells within atherosclerotic plaques. The developmental process of atheromatous plaque formation is locally driven by the interaction between modified lipoproteins, activated endothelial cells, an cell from the innate and adaptive immune system (1). The main steps in the development of atherosclerotic plaques are illustrated in Figure 1.

The signaling cascades that are activated by inflammatory and metabolic mediators converge at key transcriptional regulators, which in turn coordinate the expression of specific target genes (9). Whether individual target genes are activated or repressed depends on several other factors, such as folding and compaction of the chromatin, posttranslational modifications of histones by chromatin-modifying enzymes, functional alterations by noncoding RNAs, and recruitment of the transcriptional machinery, including transcription factors and importantly also transcription cofactors, i.e. transcriptional corepressors and coactivators (10-12).

Mouse models of atherosclerosis

Most wildtype mouse strains display a different lipoprotein profile than humans and are resistant to develop atherosclerosis (13). Therefore, genetic mouse models with a ‘humanized’ lipoprotein profile are commonly used to study atherosclerosis in mice, including *apolipoprotein E* (*Apoe*$^{-/-}$) and *LDL receptor* (*Ldlr*$^{-/-}$) knockout mice, as well as the *E3L.CETP* mice (14-17). *Apoe* knockout mice develop marked hypercholesterolemia, having most cholesterol in the VLDL subfractions, develop atherosclerosis spontaneously, and display a strong immunologically-driven phenotype (16). *Ldlr*

knockout mice have most cholesterol in the LDL fractions, comparable to humans, develop atherosclerotic plaques upon high cholesterol feeding, and are the preferred model to study cholesterol metabolism (15). *E3L.CETP* are *Apoe* knockout mice that additionally contain a human cholesteryl ester transfer protein (CETP) gene, which is normally not present in mice, and therefore can be used to study processes linked to CETP function (17). The atherosclerotic phenotype of these mice is aggravated after feeding them a high-cholesterol plus high-fat diet.

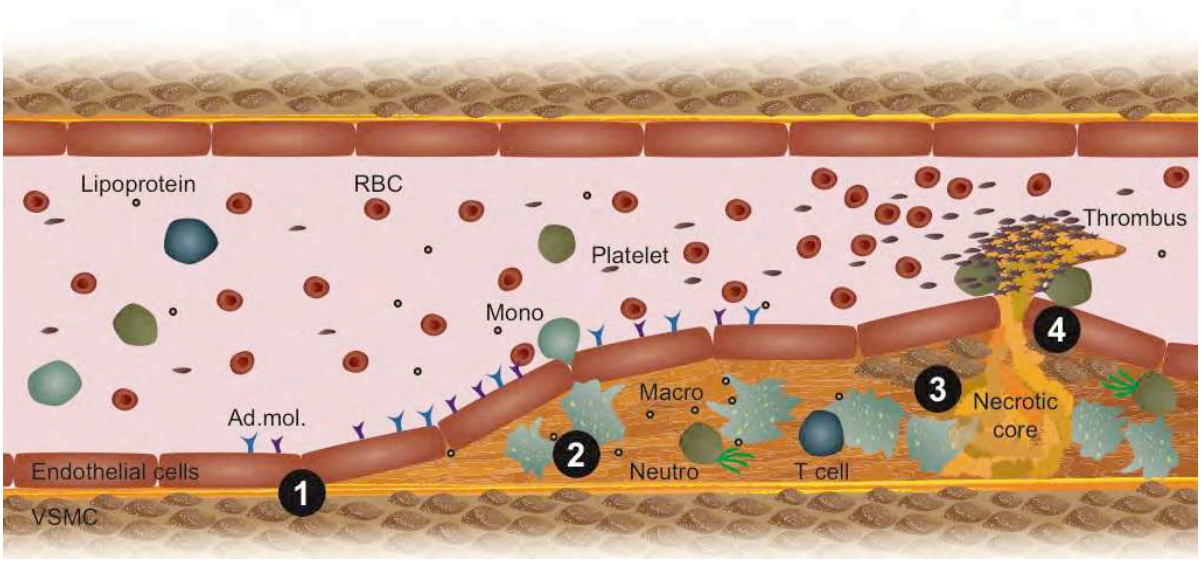

Figure 1. Model of atherogenesis. This scheme illustrates the development of an atherosclerotic plaque from left to right in a longitudinal section of an arterial vessel. (1) Upon activation by metabolic or inflammatory triggers, endothelial cells express adhesion molecules (Ad. mol.) that promote the recruitment of immune cells, such as blood monocytes (Mono). These cells then infiltrate the arterial intima, where monocyte differentiate into macrophages (Macro) and interact with other immune cells, such as neutrophils (Neutro) and T cells. (2) Increased uptake of modified lipoproteins via scavenger receptors or decreased cholesterol efflux accelerates the accumulation of intracellular free cholesterol and cholesteryl ester-loaded lipid droplets that promote foam cell formation. (3) Macrophage foam cells eventually die and fall apart, thereby forming a necrotic core. (4) Advanced, vulnerable plaques can rupture and thereby form an arterial thrombus, which can lead to a myocardial infarction or stroke. RBC, red blood cell; VSMC, vascular smooth muscle cell.

Nonalcoholic fatty liver disease

Nonalcoholic fatty liver disease (NAFLD) is one of the primary causes of liver disease in the world. Its prevalence correlates with the incidence of obesity, but also lean persons are affected (18). NAFLD encompasses different stages of liver disorders. The earliest stage of the disease is characterized by the massive accumulation of triglycerides in the liver, which is termed hepatic steatosis and is considered a benign condition. Chronic exposure to these lipids can lead to more severe stages of the diseases, such as nonalcoholic steatohepatitis (NASH), which is further characterized by ballooning of the hepatocytes, infiltration of immune cells, and formation of fibrotic lesions into the liver. NASH may further progress to cirrhosis, in which scar tissue replaces hepatocytes, and promote the development of hepatocellular carcinoma (Figure 2A) (19-21).

The development of hepatic steatosis is highly heterogeneous, and the excessive accumulation of triglycerides can be caused by an imbalance between the acquisition and disposal of fatty acids. Different processes coordinate this balance, such as the uptake of dietary fatty acids from chylomicrons, the uptake of free fatty acids from lipolysis in the adipose tissue, the storage of fatty acids as triglycerides in hepatic lipid droplets, the secretion of triglycerides into VLDL particles, the breakdown of fatty acids in mitochondrial beta oxidation, and the synthesis of fatty acids (de novo lipogenesis) (Figure 2B) (19, 22, 23).

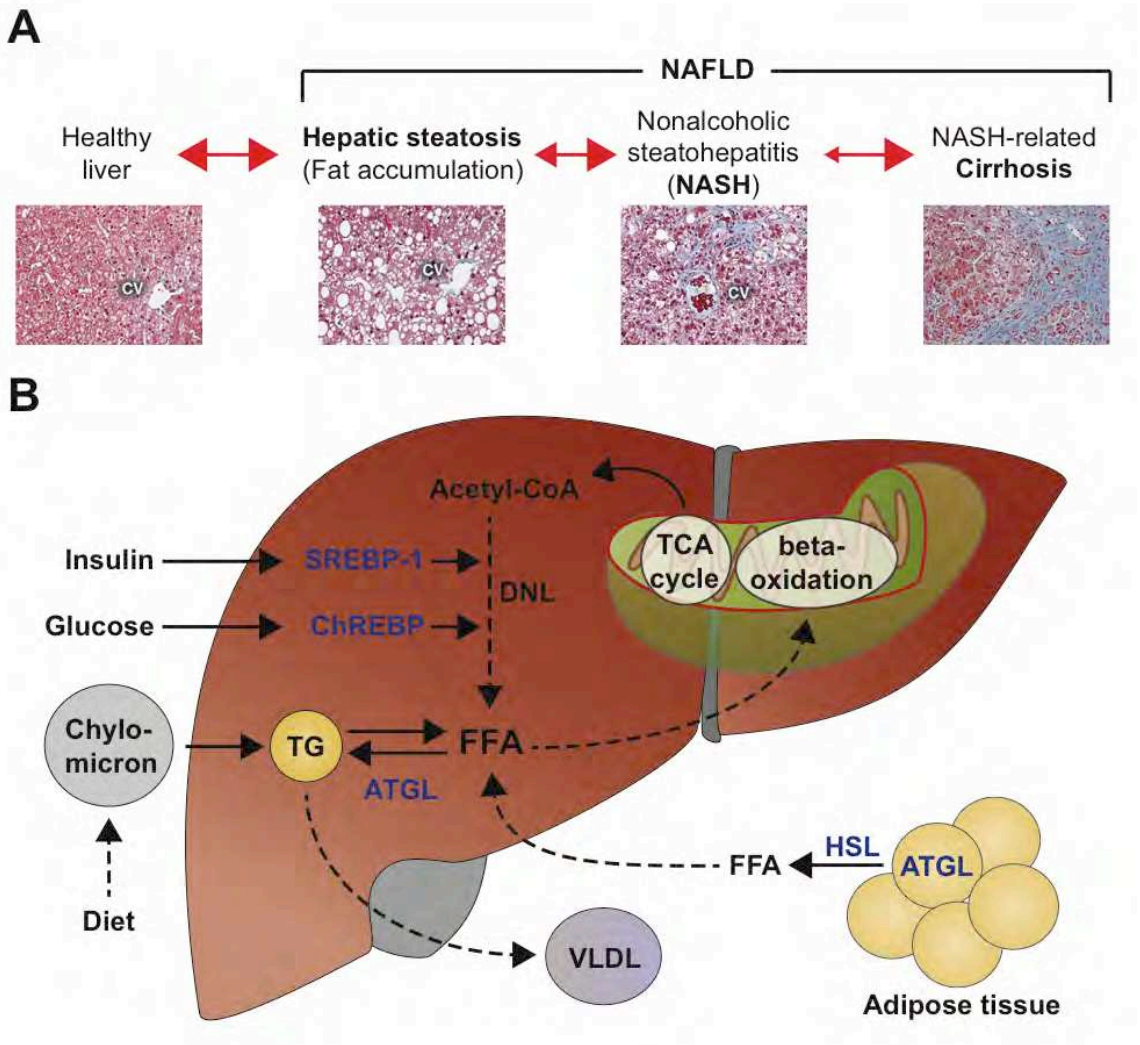

Figure 2. Stages of nonalcoholic fatty liver disease (NAFLD) and hepatic fatty acid metabolism. (A) Masson's trichrome staining of representative liver sections from different stages of NAFLD. CV, central vein. (B) Scheme illustrating the major processes regulating fatty acid metabolism in the liver and highlighting important enzymes. SREBP-1, sterol regulatory element binding transcription factor 1; ChREBP, carbohydrate-responsive element-binding protein; ATGL, adipose triglyceride lipase; HSL, hormone-sensitive lipase. Adapted from (19).

Dietary models of NAFLD

Different dietary approaches can be undertaken to study NAFLD in mice, rat and other experimental animal models. The first experimental model that was used was a methionine- and choline-deficient

diet, which induces hepatic fibrosis upon chronic treatment. However, mice under a methionine- and choline-deficient diet loose body weight and do not develop hepatic insulin resistance, and are therefore only partially comparable to NALFD in humans. Newer dietary approaches include a high-fat diet alone, or a moderate to high-fat diet in combination with other lipogenic supplements or fibrosis-inducing agents, such as cholesterol, fructose, sucrose or bleomycin. These diets do also better resemble the pathophysiological changes observed in NAFLD patients (24-29).

Association of NAFLD with cardiovascular disease

NALFD is the hepatic component of the metabolic syndrome, and it is strongly associated with insulin resistance, obesity, hypertension, and dyslipidemia, which are well established cardiovascular risk factors. Clinical studies demonstrated that patients with NAFLD have increased circulating and hepatic proinflammatory and procoagulant markers according to the stage of their disease (30, 31). Moreover, the expression of classical atherogenic genes is impaired in patients with NASH. This leads to adverse cardiovascular function in NAFLD patients, such as increased oxidative stress and endothelial dysfunction, hypercoagulability, and accelerated development of atherosclerosis (30-32). This impaired cardiovascular function is the primary cause of premature mortality and morbidity in NAFLD patients (30-33).

3. The beneficial hepatic role of LRH-1 in atherogenesis

Liver receptor homolog 1 (LRH-1 or NR5A2) is a nuclear receptor with diverse biological functions ranging from follicle maturation in the ovary to cell cycle regulation in different tissues. In the liver, LRH-1 is an important regulator of cholesterol and bile salt metabolism (34-37). Previous studies suggested that LRH-1 might play an important function in the pathogenesis of atherosclerosis (38-41). For example, LRH-1 regulates the hepatic expression of *Scavenger receptor B type I* (*Scarb1*) (40), a gene that is highly expressed in the liver, where it facilitates the uptake of cholesteryl esters from high-density lipoproteins (HDL), and thus plays a crucial role in the reverse cholesterol transport. The reverse cholesterol transport is an anti-atherogenic process in which excessive cholesterol from peripheral tissues is transported to the liver via high-density lipoproteins, where it can be further converted into bile acids or be excreted with the bile (Figure 3) (42). Dysfunctional reverse cholesterol transport may lead to excessive accumulation of cholesterol in peripheral tissues or the liver, and therefore stimulate macrophage foam cell formation and disease progression (43).

Unlike many other nuclear receptors, murine LRH-1 does not require ligand binding to be activated (44), although recent studies suggest that specific phospholipid species might act as endogenous LRH-1 ligands (45). Instead, LRH-1 transcriptional activity is significantly modified upon interaction with transcriptional repressors (46-48), and/or by posttranslational modifications like SUMOylation and phosphorylation (49-51). Whereas LRH-1 phosphorylation results in an increase in its transcriptional activity, SUMOylation represses its function. Although it has not yet been established which physiological stimuli trigger LRH-1 SUMOylation, two models show how the SUMOylated form might

be kept transcriptionally inactive: (1) The SUMOylated protein translocates into nuclear bodies and is thereby physically separated from the chromatin; (2) the recruitment of corepressor complexes leads to a transrepression of target genes (49, 52, 53).

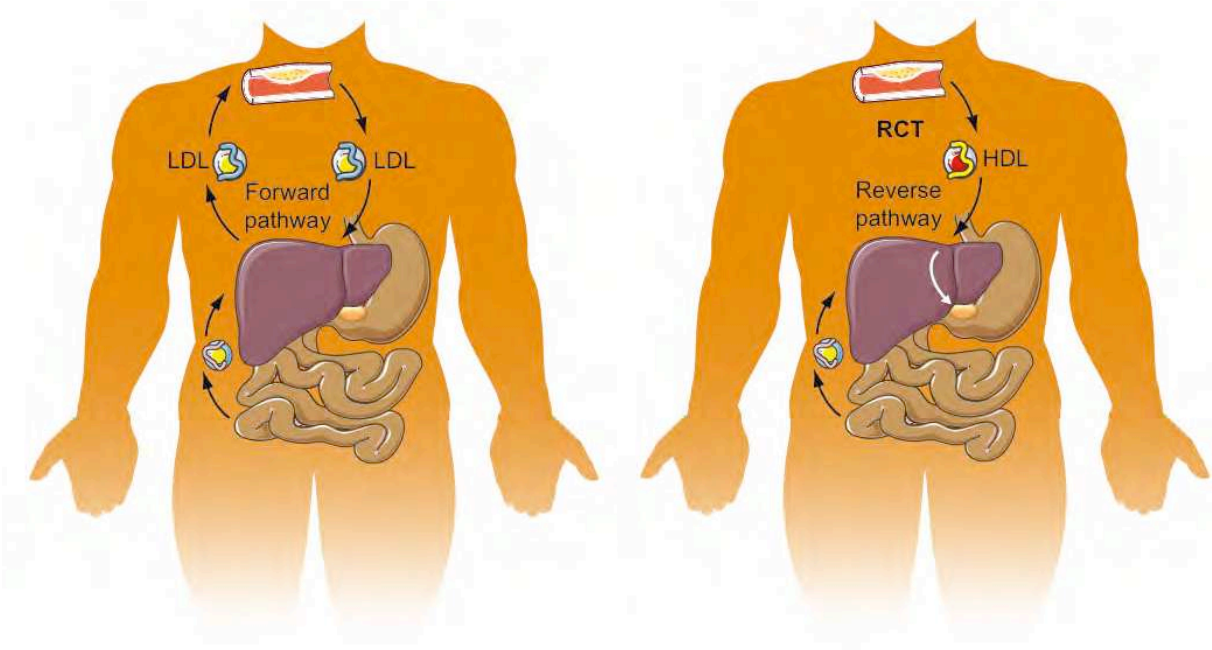

Figure 3. Forward and reverse cholesterol transport (RCT). Left side, scheme illustrating the forward, cyclic cholesterol transport that is mainly mediated via low-density lipoproteins (LDLs). Right side, the main carriers in the reverse cholesterol transport pathway are high-density lipoproteins (HDLs), which transport peripheral cholesterol back to the liver.

SUMOylation of LRH-1 reduces its transcriptional activity

We mutated 4 different lysine residues to study potential SUMOylation-defective forms of LRH-1 in vitro (Figure 4A). Importantly, we discovered that mutating the endogenous lysine K289 to arginine (K289R) increased the transcriptional activity of LRH-1 (gain-of-function) and prevented the SUMOylation of the protein (Figure 4B, C) (54). We then generated a mouse model which contains a single nucleotide substitution at DNA level that leads to the LRH-1 K289R mutation at protein level (54).

SUMOylation-defective LRH-1 mice develop less atherosclerotic lesions

To analyzed how atherosclerosis development is affected in this LRH-1 gain-of-function mouse model, we crossbred it to atherosclerosis-prone *Ldlr* knockout mice and challenged the mice with a high cholesterol diet. Importantly, our initial hypothesis that LRH-1 may be an atheroprotective factor hold true as the *Ldlr*$^{-/-}$ *Lrh-1 K289R* (LL-K289R) mice developed significantly less atheromatous lesions than the *Ldlr*$^{-/-}$ *Lrh-1 WT* (LL-WT) control mice after being exposed to a high-cholesterol diet (HCD) for 14 weeks (Figure 5) (54).

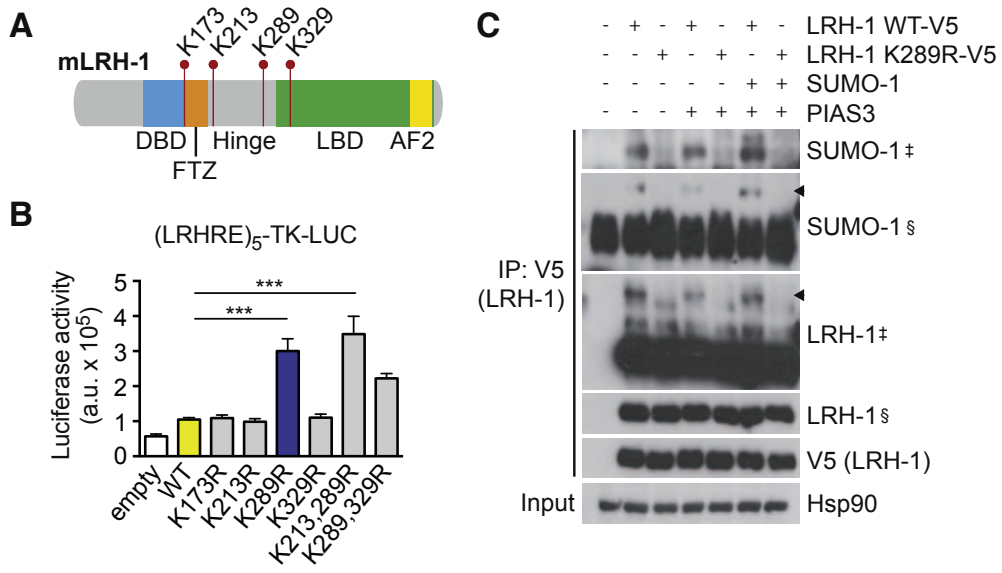

Figure 4. LRH-1 K289R blocks SUMOylation and displays increased transcriptional activity in vitro. (A) Model of LRH-1 highlighting the lysine residues that were mutated. DBD, DNA-binding domain; FTZ, Fushi-tarazu homology domain; LBD, ligand-binding domain; AF2, activation function 2 domain. (B) Luciferase assay performed in HEK 293T cells that were co-transfected with a pGL3::(LRHRE)5-TK-LUC and a pCMV plasmid coding for the wildtype or indicated mutant LRH-1 constructs. (C) Immunoprecipitation of V5-tagged LRH-1 to detect the SUMOylated band of LRH-1 (arrowheads). HEK 293T cells were transfected with pCMV-V5::LRH-1 WT or pCMV-V5::LRH-1 K289R, pCMV::PIAS3, and/or pcDNA-HA::SUMO-1-HA. Mean ± s.e.m., **p<0.01, ***p<0.001. Adapted from (54).

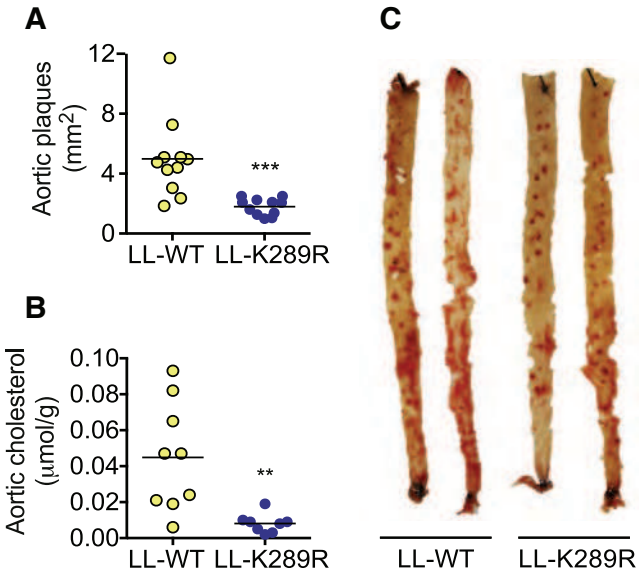

Figure 5. LRH-1 gain-of-function prevents atherogenesis. (A, B) Quantification of atherosclerotic lesions (A) and cholesterol content (B) in thoraco-abdominal aortas of *Ldlr*$^{-/-}$ *Lrh-1 K289R* (LL-K289R) and *Ldlr*$^{-/-}$ *Lrh-1 WT* (LL-WT) mice fed a high-cholesterol diet for 14 weeks. (C) Representative images of thoraco-abdominal aortae stained with Oil-Red O to visualize neutral lipids. Scatter plot displaying the mean. **p<0.01, ***p<0.001. Adapted from (54).

We further demonstrated that LRH-1 K289R promotes reverse cholesterol transport, accelerates biliary flow, and thus enhances fecal excretion of cholesterol. This enhanced hepatic reverse cholesterol transport in LL-K289R mice was a consequence of an increased expression of genes involved in cholesterol transport, such as *Scarb1*, *Abcg5* and *Abcg8*. Moreover, we showed that the increased expression of these cholesterol transporters is secondary to a compromised interaction of LRH-1 K289R with an important transcriptional corepressor, i.e. PROX1. In wildtype mice, LRH-1 interacts with PROX1 to transrepress reverse cholesterol transport genes. In LL-K289R mice, the LRH-1-PROX1 interaction is impaired, leading to an enhanced expression of the cholesterol transporters, and thereby promotes the hepatic reverse cholesterol transport (Figure 6) (37, 54).

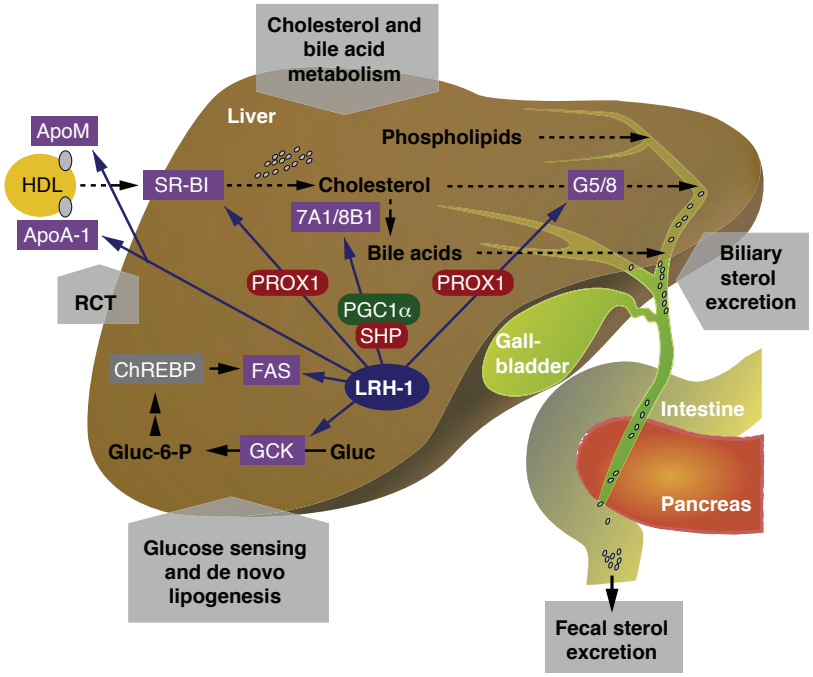

Figure 6. Athero-protection by LRH-1. Scheme illustrating how LRH-1 regulates central hepatic functions, including bile acid synthesis, lipid metabolism and reverse cholesterol transport, and glucose sensing. Adapted from (37).

4. The protective function of LRH-1 in macrophages

LRH-1 is primarily expressed in organs of the enterohepatic axis (34-37), and its expression is much lower in macrophages compared to the liver (54). However, together with colleagues from the University of Toulouse we discovered that its expression can be modulated in macrophages according to their polarization (55). In fact, stimulation of macrophages with the strong pro-inflammatory lipopolysaccharide (LPS) further reduced the expression of *Lrh-1* (*Nr5a2*) to almost undetectable levels (Figure 7a). Conversely, stimulation with anti-inflammatory cytokines increased its expression in murine and human macrophages (Figure 7a, b), suggesting that LRH-1 could play an important function in alternative macrophage polarization.

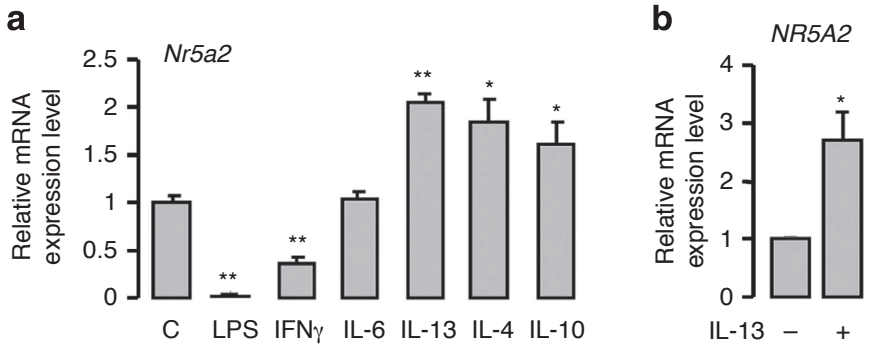

Figure 7. *Lrh-1* expression is induced in interleukin 13 (IL-13)-stimulated macrophages. Mouse (a) and human (b) macrophages were stimulated with the indicated endotoxin or cytokines. Mean ± s.e.m., *p<0.05, **p<0.01. Adapted from (55).

Further experiments demonstrated that STAT6 regulates the expression of *Lrh-1* upon interleukin 13 (IL-13) treatment (55). Myeloid cell-specific deletion of the nuclear receptor confirmed that LRH-1 plays an important role in the regulation of alternative macrophage polarization. The expression of several anti-inflammatory (M2 polarization) genes was increased, whereas the expression of various pro-inflammatory (M1 polarization) genes was reduced in control mice (*Lrh-1*$^{M+/+}$) treated with IL-13 (Figure 8). Importantly, these transcriptional effects were lost myeloid cell-specific *Lrh-1* knockout (*Lrh-1*$^{M-/-}$) mice (Figure 8) (55).

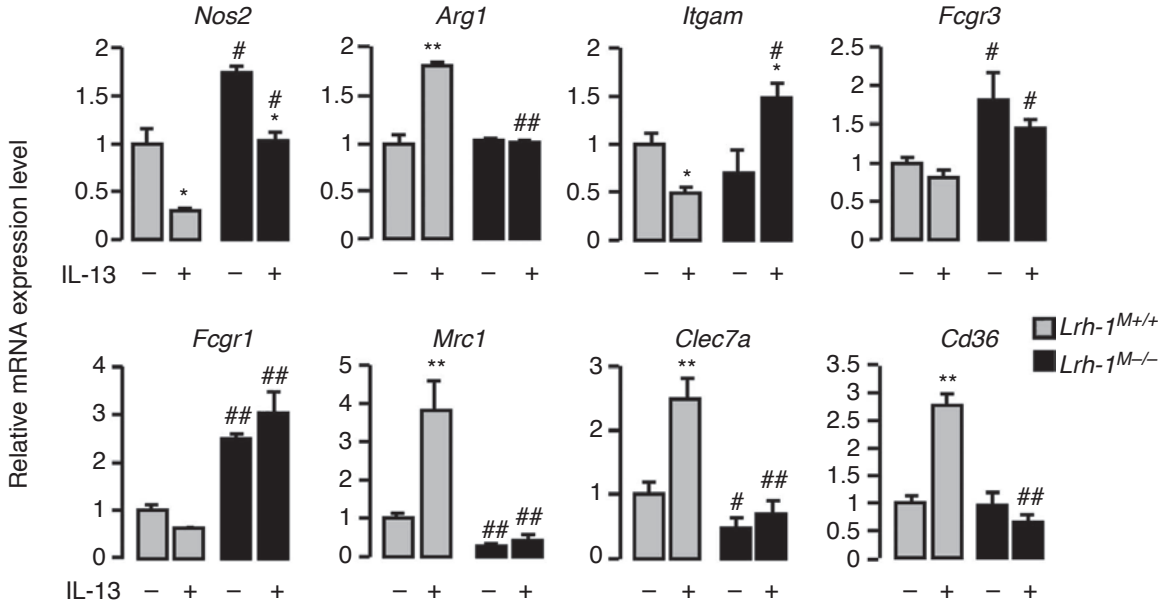

Figure 8. LRH-1 promotes alternative macrophage polarisation. Expression of pro- or anti-inflammatory genes in IL-13 stimulated peritoneal macrophages from myeloid cell-specific *Lrh-1* knockout (*Lrh-1*$^{M-/-}$) or control mice (*Lrh-1*$^{M+/+}$). Mean ± s.e.m., *p<0.05, **p<0.01 compared to the untreated control, $^{\#}$p<0.05, $^{\#\#}$p<0.01 compared to *Lrh-1*$^{M+/+}$ stimulated with IL-13. Adapted from (55).

Further experiments revealed that LRH-1 regulates the expression of two cytochrome… genes, i.e. *Cyp1a1* and *Cyp1b1*. The transcriptional regulation of these genes by LRH-1 was confirmed in luciferase reporter assays combined with site-directed mutagenesis (Figure 9). These two cytochrome P450-family enzymes convert arachidonic acid (AA) into 15-hydroxyeicosatetraenoic acid (15-HETE), an endogenous PPARγ activator, which in turn mediates the downstream polarization effects of LRH-1 (55). Our collaborators could further demonstrate that this pathway plays a protective antifungal function upon *Candida albicans* infection in mice (55).

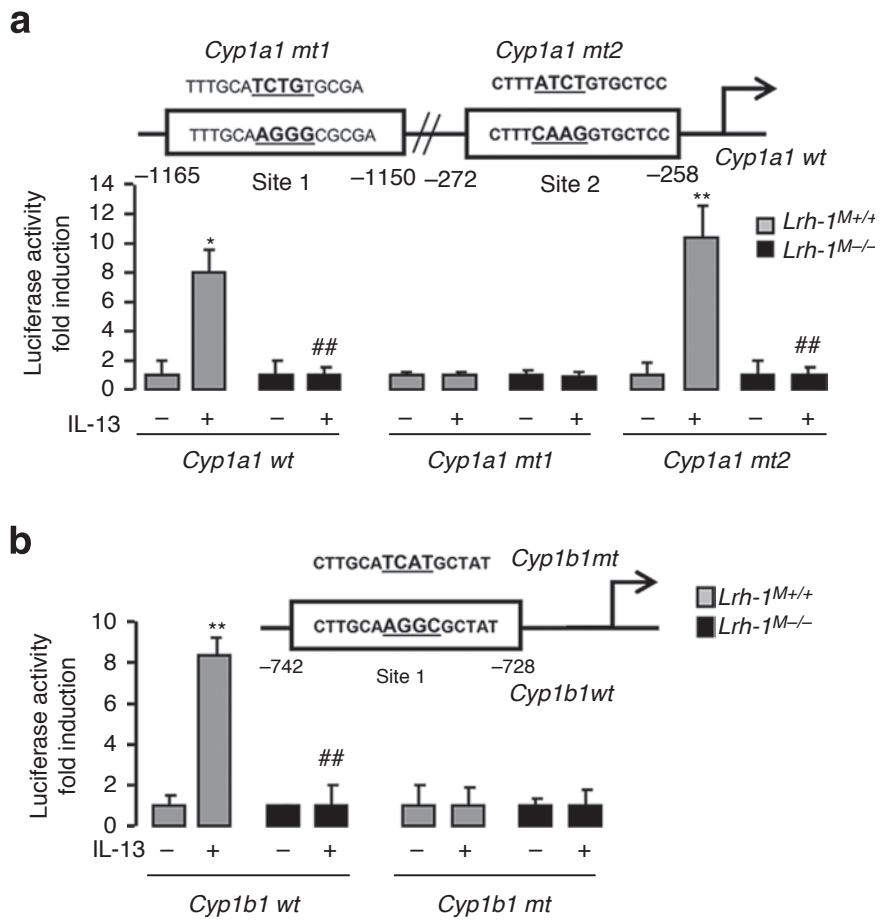

Figure 9. LRH-1 induces the expression of *Cyp1a1* and *Cyp1b1*. A luciferase plasmid with the *Cyp1a1* (a) or *Cyp1b1* (b) wildtype or mutant promoter was transfected into peritoneal macrophages from *Lrh-1*$^{M-/-}$ or control *Lrh-1*$^{M+/+}$ mice. Cells were stimulated with IL-13 to assess the reporter activity. Mean ± s.e.m., *p<0.05, **p<0.01 compared to the untreated control, and $^{\#\#}$p<0.01 compared to *Lrh-1*$^{M+/+}$. Adapted from (55).

5. The deleterious role of LRH-1 in liver steatosis

The two previous studies presented in this cumulative thesis showed that LRH-1 exerts protective effects in the liver in the context of atherosclerosis development, and in macrophages to activate anti-inflammatory pathways. Other previous studies demonstrated that hepatic LRH-1 also regulates glucose and lipid metabolism, and activation of LRH-1 with the ligand phospholipid dilauroylphosphatidylcholine (DLPC) protected insulin resistant mice against hepatic steatosis and improved glucose homeostasis (45, 56-58). Since DLPC exerted these beneficial effects in the liver, we were wondering if the same would be observed in our gain-of-function mouse model. Therefore,

we performed a series of studies to assess the role of nonSUMOylatable LRH-1 K289R in de novo lipogenesis and fatty liver development.

The best way to study de novo lipogenesis in mice is to fast them for a prolonged period and then refed them for few hours prior to analysis. During the fasting period the hepatic de novo lipogenesis process, including the transcription of various lipogenesis gene and their enzymatic function, is shut down. Upon refeeding this process is then quickly reactivated at both transcriptional and posttranslational level (59). We used two experimental groups to analyze de novo lipogenesis: the 'fasted' group was fasted for 24 hours, and the 'refed' group was fasted for 18 hours and then refed for 6 hours (Figure 10A) (60).

We performed these fast-refeeding experiments with both the *Lrh-1 WT* and *Lrh-1 K289R* mice. Notably, we observed that the posttranslational cleavage and activity of sterol regulatory element binding transcription factor 1 (SREBP-1) was strongly increased in *Lrh-1 K289R* compared to *Lrh-1 WT* mice (Figure 10B, C). SREBP-1 is a master regulator of de novo lipogenesis genes and it is activated upon posttranslational cleavage by specific endopeptidases at the Golgi apparatus, thereby rendering a transcriptionally active protein that migrates to the nucleus and activates target gene expression (61).

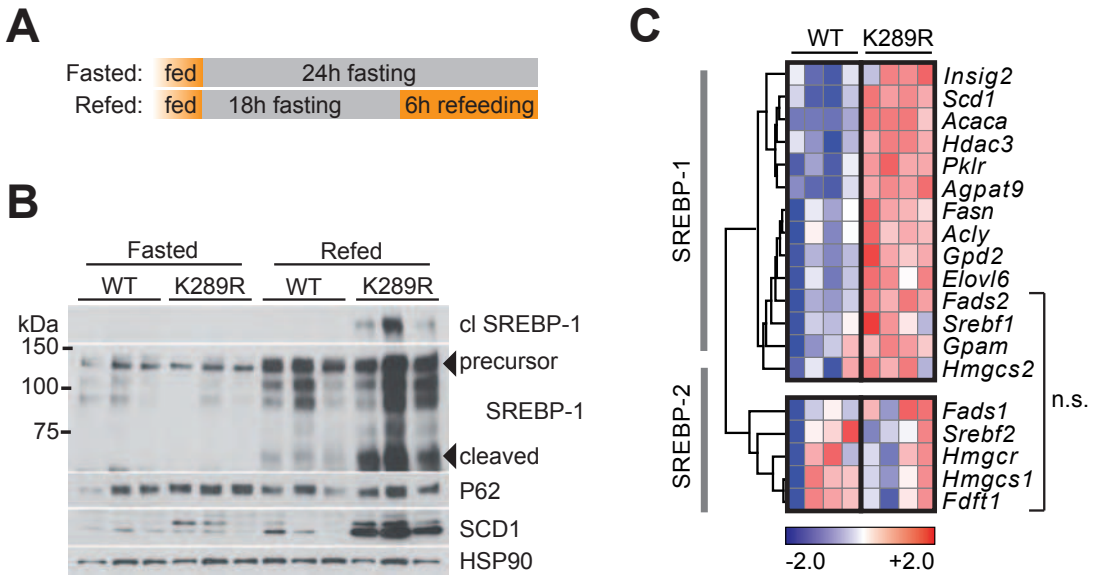

Figure 10. LRH-1 K289R affects the posttranslational processing of SREBP-1. (A) Experimental setup displaying the fasted and refed mouse groups. (B) Western blot of SREBP-1, P62, SCD1, and HSP90 on hepatic lysates from fasted or refed *Lrh-1 WT* or *K289R* mice. (C) Heatmap of the microarray expression analysis of SREBP-1 and SREBP-2 target genes. Log_2 scale. n.s., not significant, for all other transcripts $p<0.05$. Adapted from (60).

We also assessed if the increased processing and activity of SREBP-1 drives de novo lipogenesis in vivo. Staining of liver section with Oil-red O and analysis of hepatic triglyceride content displayed increased lipid content in the liver of *Lrh-1 K289R* compared to *Lrh-1 WT* mice (Figure 11A, B).

Furthermore, the fractional de novo synthesis of different fatty acids was also enhanced in *Lrh-1 K289R* mice (Figure 11C-E), while the chain elongation of preexisting fatty acids was not altered (60).

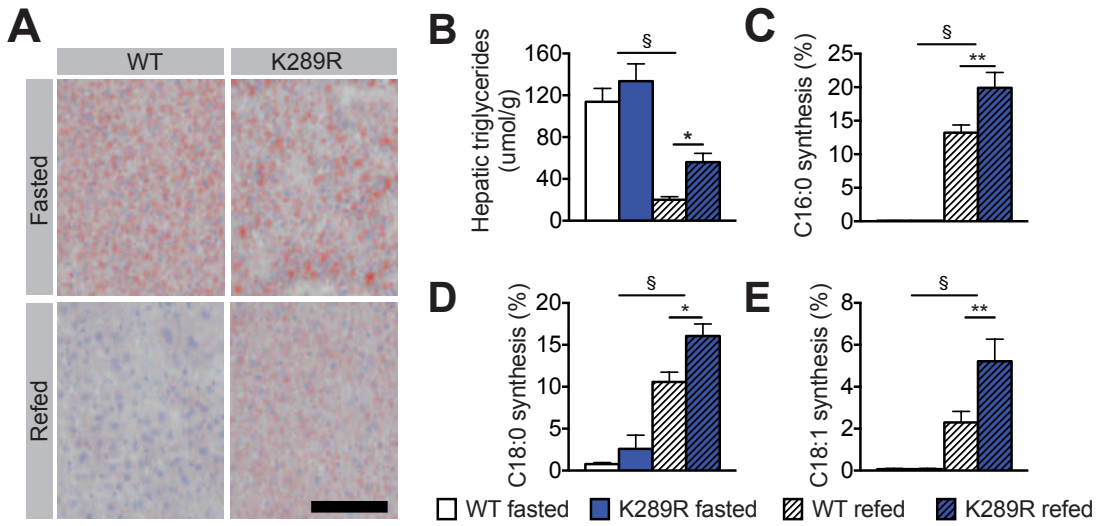

Figure 11. *Lrh-1 K289R* mice display increased de novo lipogenesis. (A) Representative Oil-red O stained liver sections from *Lrh-1 WT* or *K289R* mice. (B) Quantification of hepatic triglcerides in *Lrh-1 WT* or *K289R* livers. (C-E) Fractional de novo synthesis of palmitate (C), stearate (D), and oleate (E) in *Lrh-1 WT* or *K289R* mice. Mean ± s.e.m., *p<0.05, **p<0.01 relative to *Lrh-1 WT*. §p<0.001 relative to fasted mice. Adapted from (60).

In order to identify the link between LRH-1 (a transcriptional factor that is only localized in nuclei) and SREBP-1 (whose processing happens at the ER and Golgi apparatus), we analyzed transcriptomic data to identify hits that could affect SREBP-1 processing. In this manner we identified oxysterol binding protein-like 3 (OSBPL3), a member of a lipid transfer protein family that transfers lipids between the plasma and endoplasmic reticulum membrane (62-64). The expression of OSBPL3 was strongly increased at mRNA and protein level in *Lrh-1 K289R* compared to *Lrh-1 WT* livers (Figure 12A-D), and we further revealed that *Osbpl3* is a direct LRH-1 target gene (60). Consistently, others reporter that the expression of *Osbpl3* is strongly reduced in mice with hepatic *Lrh-1* deficiency (65). Moreover, by using in vivo *Osbpl3* silencing or overexpression approaches we demonstrated that the processing of SREBP-1 was altered, suggesting that the LRH-1-OSBPL3 axis induces SREBP-1 maturation and de novo lipogenesis (60).

To assess the role of LRH-1 K289R in a chronic NAFLD model, we treated mice with a high-fat high sucrose (HFHS) diet for 17 weeks. Interestingly, *Lrh-1 K289R* mice developed a stronger fatty liver phenotype compared to *Lrh-1 WT* livers (Figure 13A), which was associated with increased hepatic expression levels of OSBPL3 and enhanced plasma levels of alanine transaminase (ALAT) and aspartate aminotransferase (ASAT) (Figure 13B-D).

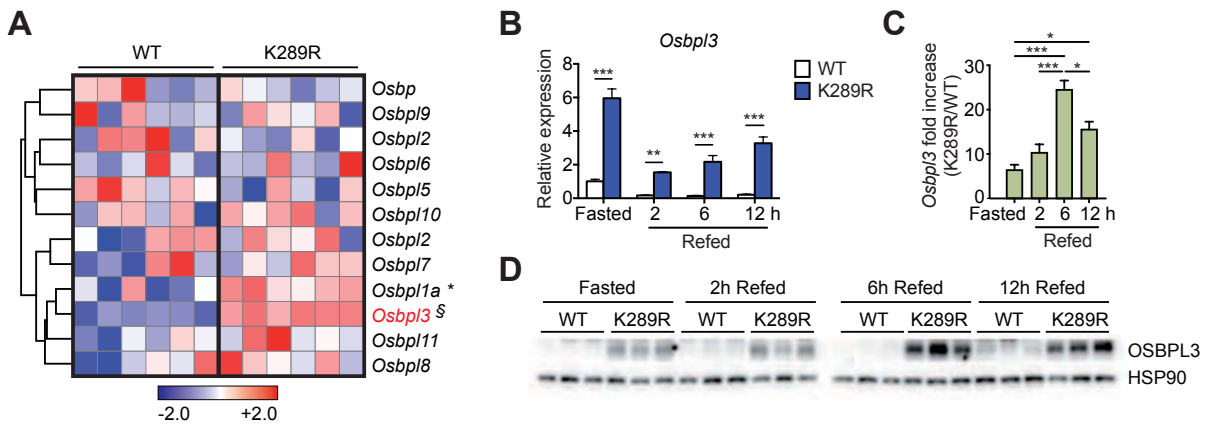

Figure 12. LRH-1 K289R affects the posttranslational processing of SREBP-1. (A) Heatmap of the microarray expression analysis of oxysterol-binding protein family members. Log_2 scale. (B-D) Expression of *Osbpl3* mRNA (B, C), and Western blot of OSBPL3 and HSP90 on hepatic lysates from fasted or refed *Lrh-1 WT* or *K289R* mice. Mean ± s.e.m., *p<0.05, §p<0.01. Adapted from (60).

To evaluate if OSBPL3 could also play a role in NAFLD in humans, we analyzed *OSBPL3* expression levels in different human NALFD and NASH studies, including a human study that was undertaken to compare patients with mild versus advanced NAFLD (66). Interestingly, the expression *OSBPL3* clearly increased in patients with advanced NAFLD and tightly clustered with markers of fibrosis (Figure 14).

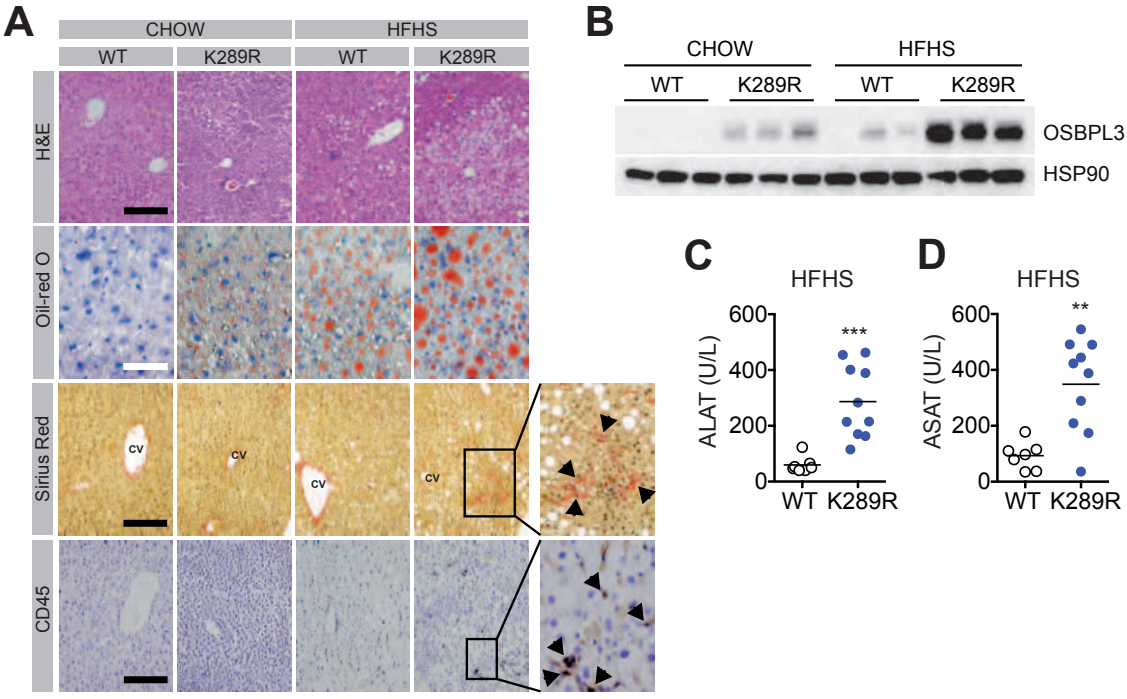

Figure 13. LRH-1 K289R affects the posttranslational processing of SREBP-1. (A) Representative liver sections of *Lrh-1 WT* or *K289R* mice with the indicated staining. (B) Western blot of OSBPL3 on hepatic lysates *Lrh-1 WT* or *K289R* mice. (C, D) Plasma levels of ALAT and ASAT in *Lrh-1 WT* or *K289R* mice. Mean ± s.e.m., **p<0.01, ***p<0.001. Adapted from (60).

This study highlighted that the LRH-1-OSBPL3-SREBP-1 axis play a significant function in de novo lipogenesis and the development of NALFD in mice, and suggests that the same pathway might also be relevant in humans with NAFLD.

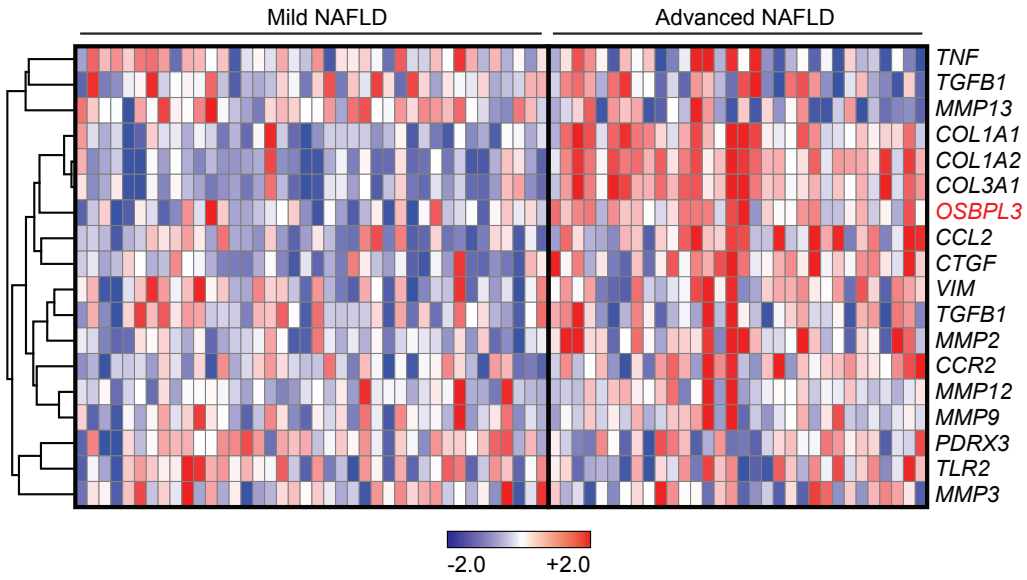

Figure 14. LRH-1 K289R affects the posttranslational processing of SREBP-1. Heatmap of the microarray expression analysis of OSBPL3 and markers of inflammation and fibrosis in mild and advanced NAFLD patients. Log_2 scale. Adapted from (60), raw data from (66).

6. The detrimental contribution of LRH-1 to hepatocellular carcinoma

Besides regulating glucose and lipid metabolism, LRH-1 also coordinates cell proliferation and cancer development in the intestine and pancreas (67-70). These findings raised the question about its contribution in liver cancer development. Since earlier studies suggested that LRH-1 would act as an oncogene, we primarily analyzed the development of hepatic cancer in mice lacking *Lrh-1* specifically in the liver (*Lrh-1*$^{hep-/-}$ mice) (57). We treated the mice with diethylnitrosamine (DEN), a chemical that is known to induce hepatocellular carcinoma in experimental animal models (71).

Upon DEN treatment control wildtype *Lrh-1*$^{hep+/+}$ mice developed many and large hepatic tumors (Figure 15A-C). Conversely, *Lrh-1*$^{hep-/-}$ mice developed markedly less liver tumors upon DEN treatment (Figure 15A-C). Moreover, analysis of the transcriptome of the livers from both genotypes, revealed that the expression of several genes involved in the metabolism of amino acids and derivatives was strongly downregulated in *Lrh-1*$^{hep-/-}$ mice (Figure 15D) (72).

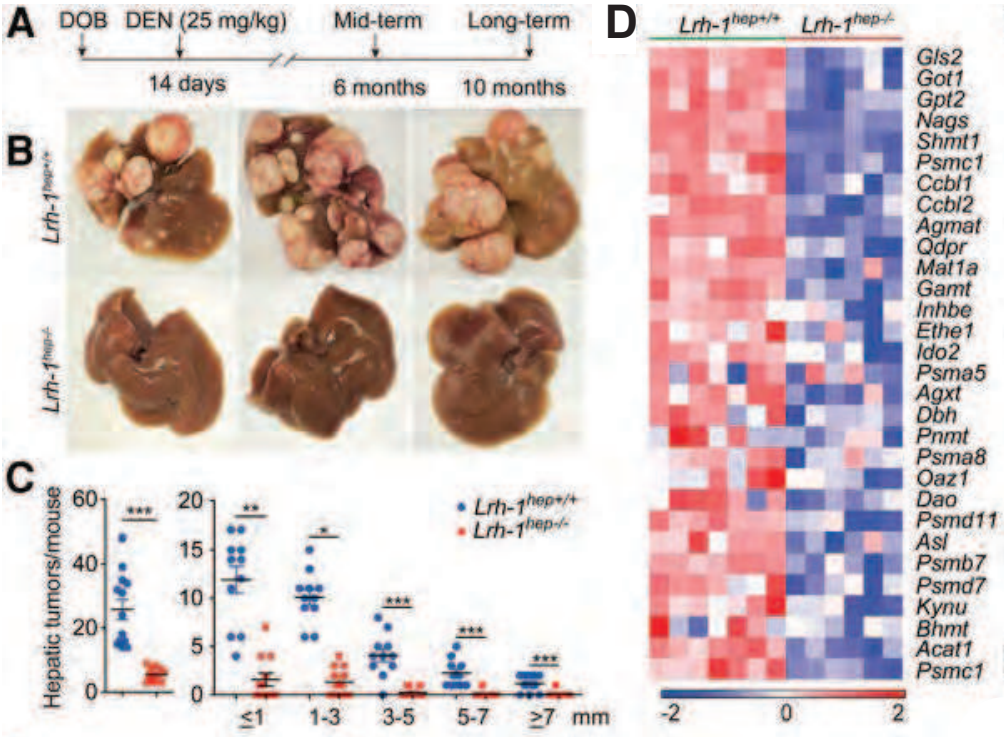

Figure 15. Hepatic deletion of *Lrh-1* protects against DEN-induced liver cancer. (A) Experimental setup displaying the injection time of DEN and assessment of the phenotype at 6 and 10 moths of age. (B) Representative images of livers from 10-month-old *Lrh-1*$^{hep-/-}$ and *Lrh-1*$^{hep+/+}$ mice. (C) Total tumor count (left side) and tumor size distribution (right side) from 10-month-old *Lrh-1*$^{hep-/-}$ and *Lrh-1*$^{hep+/+}$ mice. (D) Heatmap of the microarray expression analysis from genes involved in metabolism of amino acids and derivatives. Log_2 scale. Mean ± s.e.m., *p<0.05, **p<0.01, ***p<0.001. Adapted from (72).

Cancer cells alter several metabolic processes to promote tumor development and progression. One common phenomenon if the switch from an oxidative to a glycolytic metabolic state (73). During this transition glucose is converted into lactate instead of entering the tricarboxylic acid (TCA) cycle. As a consequence, cancer cells rely more on glutamine to refill TCA cycle intermediates (74, 75). Such a 'refilling' of intermediates of a metabolic pathway is termed anaplerosis (73).

Subsequent characterization of *Lrh-1*$^{hep-/-}$ and *Lrh-1*$^{hep+/+}$ mice, combined with a series of in vitro experiments and in vivo glutamine flux analysis, revealed that LRH-1 is a direct transcriptional activator of *glutaminase 2* (*Gls2*), and consequently controls glutamine-induced anaplerosis, regulates mTOR pathway activity, and induces cell proliferation (72).

In line with these finding, shRNA mediated silencing of *Lrh-1* or *Gls2* in Hepa 1.6 cells induced significantly less tumor growth after injection into athymic nude mice (Figure 16A). Taken together, these experiments demonstrated that LRH-1 plays a critical role in glutamine processing and has a striking impact on hepatocellular cancer development in mice (Figure 16B).

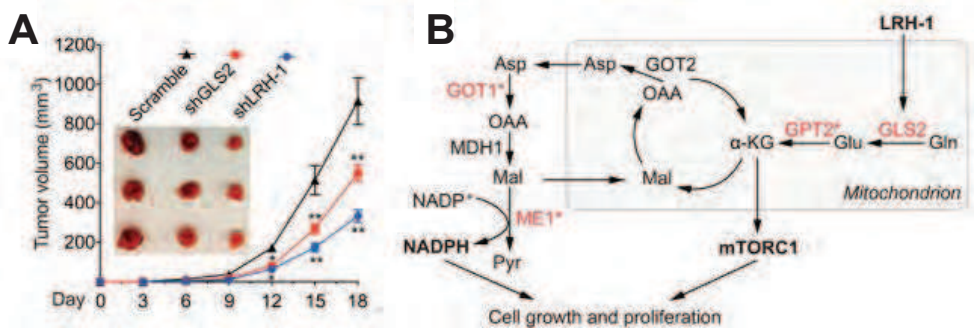

Figure 16. The LRH-1-GLS2 axis promotes tumor development. (A) Tumor development in athymic nude mice injected with *Lrh-1* or *Gls2*-silenced Hepa 1.6 cells. (B) Model displaying how the LRH-1-GLS2 axis promotes glutamine-induced anaplerosis, cell growth and proliferation. Mean ± s.e.m., **p<0.01. Adapted from (72).

7. The protective function of SIRT7 in hepatic steatosis

SIRT7 is a member of the family of sirtuins deacetylases that is primarily localized in the nucleus. In collaboration with Dongryeol Ryu, Young Suk Jo, Giuseppe Lo Sasso, Johan Auwerx, and other colleagues, we studied the metabolic function of SIRT7. Interestingly, we could demonstrate that whole-body *Sirt7* knockout mice displayed a dysmorphic phenotype, including cardiac dysfunction, reduced exercise performance, hepatic microvesicular steatosis, and age-related hearing loss (76). To verify if these functions also occur upon targeted deletion of *Sirt7* in specific tissues, we generated and phenotyped a liver-specific knockout mouse line. Consistently with the whole-body *Sirt7* knockout, the liver-specific knockout mice developed liver microvesicular steatosis, which is characterized by excessive triglyceride accumulation (Figure 17A-C) (76).

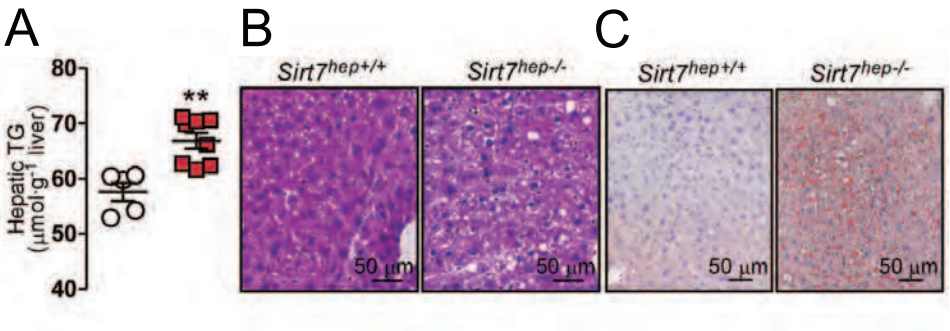

Figure 17. Liver-specific deletion of *Sirt7* promotes hepatic steatosis. (A) Quantification of hepatic triglycerides in 55-week-old male $Sirt7^{hep+/+}$ (white dots) or $Sirt7^{hep-/-}$ (red squares) mice. (B, C) Representative hematoxylin & eosin (B), and Oil Red O staining (C). Mean ± s.e.m., **p<0.01. Adapted from (76).

Liver-specific *Sirt7* knockout mice had an impaired expression of several important nuclear-encoded mitochondrial proteins, which led to a reduction in mitochondrial oxidative phosphorylation (OXPHOS) complex formation and oxygen consumption rate (OCR) (Figure 18A-C) (76).

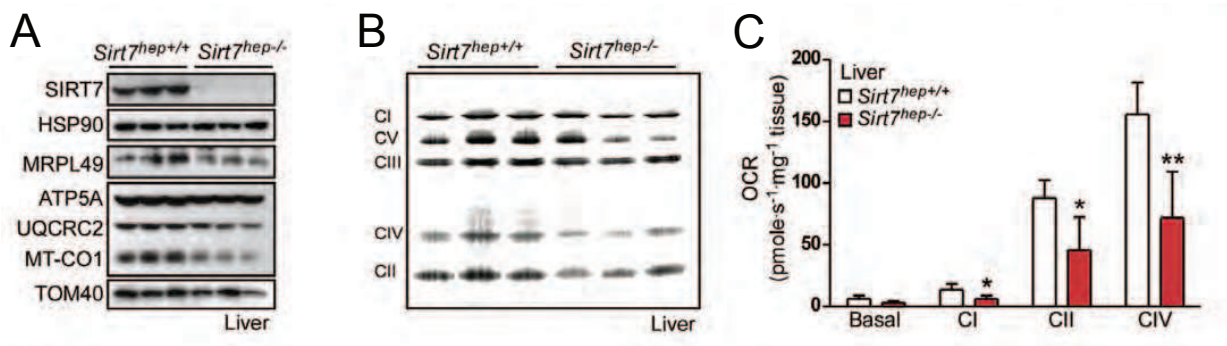

Figure 18. Liver-specific deletion of *Sirt7* leads to mitochondrial dysfunction. (A) Western blot analysis showing SIRT7, MRPL49, various OXPHOS subunits, and TOM40 in liver of *Sirt7*$^{hep+/+}$ and *Sirt7*$^{hep-/-}$. (B) Blue native-PAGE of hepatic OXPHOS complexes. (C) OCR of liver lysates from 42-week-old male *Sirt7*$^{hep+/+}$ and *Sirt7*$^{hep-/-}$ mice. (n = 5 per group). Mean ± s.e.m., *p<0.05, **p<0.01. Adapted from (76).

All these phenotypes are related to mitochondrial dysfunction. Indeed, our data showed that SIRT7 deacetylates distinct lysine residues of GA repeat binding protein beta 1 (GABPβ1), a master regulator of nuclear-encoded mitochondrial genes. Therefore, genetic deletion of *Sirt7* enhances multisystemic mitochondrial dysfunction (76). Of note, the precise function of this important sirtuin in atherosclerosis has not yet been studied and/or published.

8. Conclusions and perspectives

The central function of transcriptional complexes in chronic immunometabolic diseases

The field of immunometabolic regulation in chronic inflammatory diseases got substantial attention in the last years (77-85). The research studies presented here – as well as my previous and ongoing studies – clearly demonstrate that transcription factors and cofactors play a central role in

(i) integrating the information from upstream intracellular signaling pathways,

(ii) coordinating the expression of target genes,

(iii) regulating the downstream response of the cell,

(iv) and thereby affecting the development of chronic inflammatory diseases, such as atherosclerosis and NAFLD (54, 55, 60, 76, 86-90).

Several of the transcriptional regulators that I studied in the past were known to affect metabolic processes, such as the LRH-1, SIRT1, and PGC-1α. Interestingly, our studies demonstrated that these factors also affect inflammatory pathways in different organs and tissues. For examples, we showed that the SIRT1 mediates immunometabolic functions in endothelial cells, macrophages, and the liver by deacetylating and thereby suppressing the NF-kB signaling pathway and by regulating hepatic proprotein convertase subtilisin/kexin type 9 (PCSK9) expression (86-89). The work shown here indicates how LRH-1 regulates central metabolic and inflammatory processes in the liver and macrophages, thereby affecting the development of atherosclerosis, NAFLD, liver cancer, and fungal infection (37, 54, 55, 60, 72).

In conclusion, these studies demonstrated that specific transcriptional complexes, consisting of transcription factors and cofactors, exert a central function to integrate upstream information and regulate the expression of downstream target genes, and thereby act as central immunometabolic regulators. While the role of many transcription factors is well described, we know much less about transcription cofactors. About 300 transcription cofactors are known to exist in mice and human cells (91). However, only a fraction of those is expressed in a specific cell type or tissue, and their function is restricted to certain pathways and transcription factors (11, 12). Some of these factors are involved in inflammatory mechanisms, others known to exert metabolic functions. The identification of transcriptional regulators that exert important immunometabolic functions in chronic diseases, such as atherosclerosis and nonalcoholic fatty liver disease, will be a major focus of my future research.

LRH-1 as a therapeutic target

Our study revealed that gain-of-function of LRH-1 prevented the development of atherosclerosis in an atherosclerosis-prone mouse model, but promoted hepatic steatosis in a dietary NAFLD model (54, 60). Moreover, hepatic deletion of *Lrh-1* led to a clear protection against the development of

hepatocellular carcinoma (72). The identification of small molecule agonists and antagonists as well as the discovery that specific phospholipid species act as endogenous agonists of LRH-1 (45, 92-94), suggest that the receptor could be a *bona fide* druggable target. Activation of LRH-1 with small molecule agonists could be beneficial to promote reverse cholesterol transport and biliary cholesterol excretion to prevent atherosclerosis development (Figure 19) (38, 54, 95) as well as to treat diabetes (45, 56). An alternative would be the development of drugs that activate specific isopeptidases that remove the SUMO peptide from LRH-1, thereby increasing its transcriptional activity (49, 52, 54, 60, 96, 97). On the other side, inhibition of hepatic LRH-1 might be a therapeutic approach to prevent the development of NAFLD and hepatic cancer (Figure 19). Future studies will be necessary to:

- Describe the mechanistic difference leading to these unexpected and controversial phenotypes, i.e. atherosclerotic protection on one side and the potential development of NAFLD on the other side. For instance, it was demonstrated that specific phospholipid species may act as endogenous LRH-1 activators (45). A different content and composition of these phospholipids in the different diets could lead to protective effects in one disease model, while promote the progression of another model.

- To reveal the impact of pharmacological LRH-1 modulation using specific LRH-1 agonist and/or antagonist on these diseases and analyze potential adverse effects (92-94, 98, 99).

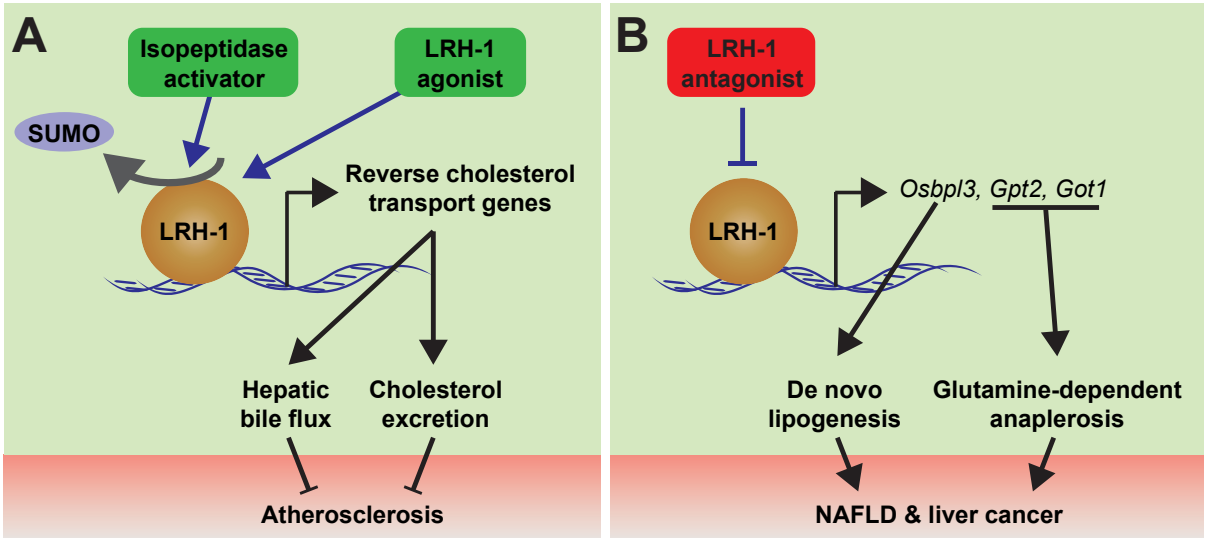

Figure 19. Potential therapeutic applications by modulating LRH-1 function. Scheme illustrating the (A) beneficial anti-atherogenic effect that could be driven by pharmacological LRH-1 activation, and (B) the protective effects on NAFLD and liver cancer that could be mediated via LRH-1 inhibition.

9. References

1. Hansson GK. Inflammation, atherosclerosis, and coronary artery disease. *N Engl J Med.* 2005;352(16):1685-95.

2. Mortality GBD, and Causes of Death C. Global, regional, and national age-sex specific all-cause and cause-specific mortality for 240 causes of death, 1990-2013: a systematic analysis for the Global Burden of Disease Study 2013. *Lancet.* 2015;385(9963):117-71.

3. Thompson RC, Allam AH, Lombardi GP, Wann LS, Sutherland ML, Sutherland JD, Soliman MA, Frohlich B, Mininberg DT, Monge JM, Vallodolid CM, Cox SL, Abd el-Maksoud G, Badr I, Miyamoto MI, el-Halim Nur el-Din A, Narula J, Finch CE, and Thomas GS. Atherosclerosis across 4000 years of human history: the Horus study of four ancient populations. *Lancet.* 2013;381(9873):1211-22.

4. Napoli C, D'Armiento FP, Mancini FP, Postiglione A, Witztum JL, Palumbo G, and Palinski W. Fatty streak formation occurs in human fetal aortas and is greatly enhanced by maternal hypercholesterolemia. Intimal accumulation of low density lipoprotein and its oxidation precede monocyte recruitment into early atherosclerotic lesions. *J Clin Invest.* 1997;100(11):2680-90.

5. Palinski W, and Napoli C. The fetal origins of atherosclerosis: maternal hypercholesterolemia, and cholesterol-lowering or antioxidant treatment during pregnancy influence in utero programming and postnatal susceptibility to atherogenesis. *FASEB J.* 2002;16(11):1348-60.

6. Weber C, and Noels H. Atherosclerosis: current pathogenesis and therapeutic options. *Nat Med.* 2011;17(11):1410-22.

7. Libby P, Ridker PM, and Hansson GK. Progress and challenges in translating the biology of atherosclerosis. *Nature.* 2011;473(7347):317-25.

8. Jonsson AL, and Backhed F. Role of gut microbiota in atherosclerosis. *Nat Rev Cardiol.* 2017;14(2):79-87.

9. Hopkins PN. Molecular biology of atherosclerosis. *Physiol Rev.* 2013;93(3):1317-542.

10. Margueron R, and Reinberg D. Chromatin structure and the inheritance of epigenetic information. *Nat Rev Genet.* 2010;11(4):285-96.

11. Smith E, and Shilatifard A. The chromatin signaling pathway: diverse mechanisms of recruitment of histone-modifying enzymes and varied biological outcomes. *Mol Cell.* 2010;40(5):689-701.

12. Mouchiroud L, Eichner LJ, Shaw RJ, and Auwerx J. Transcriptional coregulators: fine-tuning metabolism. *Cell Metab.* 2014;20(1):26-40.

13. Paigen B, Holmes PA, Mitchell D, and Albee D. Comparison of atherosclerotic lesions and HDL-lipid levels in male, female, and testosterone-treated female mice from strains C57BL/6, BALB/c, and C3H. *Atherosclerosis.* 1987;64(2-3):215-21.

14. Plump AS, Smith JD, Hayek T, Aalto-Setala K, Walsh A, Verstuyft JG, Rubin EM, and Breslow JL. Severe hypercholesterolemia and atherosclerosis in apolipoprotein E-deficient mice created by homologous recombination in ES cells. *Cell.* 1992;71(2):343-53.

15. Ishibashi S, Brown MS, Goldstein JL, Gerard RD, Hammer RE, and Herz J. Hypercholesterolemia in low density lipoprotein receptor knockout mice and its reversal by adenovirus-mediated gene delivery. *J Clin Invest.* 1993;92(2):883-93.

16. Zhang SH, Reddick RL, Piedrahita JA, and Maeda N. Spontaneous hypercholesterolemia and arterial lesions in mice lacking apolipoprotein E. *Science.* 1992;258(5081):468-71.

17. Westerterp M, van der Hoogt CC, de Haan W, Offerman EH, Dallinga-Thie GM, Jukema JW, Havekes LM, and Rensen PC. Cholesteryl ester transfer protein decreases high-density lipoprotein and severely aggravates atherosclerosis in APOE*3-Leiden mice. *Arterioscler Thromb Vasc Biol.* 2006;26(11):2552-9.

18. Younossi Z, Anstee QM, Marietti M, Hardy T, Henry L, Eslam M, George J, and Bugianesi E. Global burden of NAFLD and NASH: trends, predictions, risk factors and prevention. *Nat Rev Gastroenterol Hepatol.* 2018;15(1):11-20.

19. Cohen JC, Horton JD, and Hobbs HH. Human fatty liver disease: old questions and new insights. *Science.* 2011;332(6037):1519-23.

20. Baffy G, Brunt EM, and Caldwell SH. Hepatocellular carcinoma in non-alcoholic fatty liver disease: an emerging menace. *J Hepatol.* 2012;56(6):1384-91.

21. Tilg H, and Moschen AR. Evolution of inflammation in nonalcoholic fatty liver disease: the multiple parallel hits hypothesis. *Hepatology.* 2010;52(5):1836-46.

22. Postic C, and Girard J. Contribution of de novo fatty acid synthesis to hepatic steatosis and insulin resistance: lessons from genetically engineered mice. *J Clin Invest.* 2008;118(3):829-38.

23. Kawano Y, and Cohen DE. Mechanisms of hepatic triglyceride accumulation in non-alcoholic fatty liver disease. *J Gastroenterol.* 2013;48(4):434-41.

24. Lau JK, Zhang X, and Yu J. Animal models of non-alcoholic fatty liver disease: current perspectives and recent advances. *J Pathol.* 2017;241(1):36-44.

25. Machado MV, Michelotti GA, Xie G, Almeida Pereira T, Boursier J, Bohnic B, Guy CD, and Diehl AM. Mouse models of diet-induced nonalcoholic steatohepatitis reproduce the heterogeneity of the human disease. *PLoS One.* 2015;10(5):e0127991.

26. Charlton M, Krishnan A, Viker K, Sanderson S, Cazanave S, McConico A, Masuoko H, and Gores G. Fast food diet mouse: novel small animal model of NASH with ballooning, progressive fibrosis, and high physiological fidelity to the human condition. *American journal of physiology Gastrointestinal and liver physiology.* 2011;301(5):G825-34.

27. Ishimoto T, Lanaspa MA, Rivard CJ, Roncal-Jimenez CA, Orlicky DJ, Cicerchi C, McMahan RH, Abdelmalek MF, Rosen HR, Jackman MR, Maclean PS, Diggle CP, Asipu A, Inaba S, Kosugi T, Sato W, Maruyama S, Sanchez-Lozada LG, Sautin YY, Hill JO, Bonthron DT, and

Johnson RJ. High-fat and high-sucrose (western) diet induces steatohepatitis that is dependent on fructokinase. *Hepatology.* 2013;58(5):1632-43.

28. Cutting out the liver fat. *Nat Med.* 2017;23(12):1385.

29. Verbeek J, Jacobs A, Spincemaille P, and Cassiman D. Development of a Representative Mouse Model with Nonalcoholic Steatohepatitis. *Curr Protoc Mouse Biol.* 2016;6(2):201-10.

30. Anstee QM, Targher G, and Day CP. Progression of NAFLD to diabetes mellitus, cardiovascular disease or cirrhosis. *Nat Rev Gastroenterol Hepatol.* 2013;10(6):330-44.

31. Byrne CD, and Targher G. NAFLD: a multisystem disease. *J Hepatol.* 2015;62(1 Suppl):S47-64.

32. Bhatia LS, Curzen NP, Calder PC, and Byrne CD. Non-alcoholic fatty liver disease: a new and important cardiovascular risk factor? *Eur Heart J.* 2012;33(10):1190-200.

33. Targher G, Day CP, and Bonora E. Risk of cardiovascular disease in patients with nonalcoholic fatty liver disease. *N Engl J Med.* 2010;363(14):1341-50.

34. Fayard E, Auwerx J, and Schoonjans K. LRH-1: an orphan nuclear receptor involved in development, metabolism and steroidogenesis. *Trends Cell Biol.* 2004;14(5):250-60.

35. Lazarus KA, Wijayakumara D, Chand AL, Simpson ER, and Clyne CD. Therapeutic potential of Liver Receptor Homolog-1 modulators. *J Steroid Biochem Mol Biol.* 2012;130(3-5):138-46.

36. Lee YK, and Moore DD. Liver receptor homolog-1, an emerging metabolic modulator. *Front Biosci.* 2008;13:5950-8.

37. Stein S, and Schoonjans K. Molecular basis for the regulation of the nuclear receptor LRH-1. *Curr Opin Cell Biol.* 2015;33:26-34.

38. Venteclef N, Haroniti A, Tousaint JJ, Talianidis I, and Delerive P. Regulation of anti-atherogenic apolipoprotein M gene expression by the orphan nuclear receptor LRH-1. *J Biol Chem.* 2008;283(7):3694-701.

39. Venteclef N, Smith JC, Goodwin B, and Delerive P. Liver receptor homolog 1 is a negative regulator of the hepatic acute-phase response. *Mol Cell Biol.* 2006;26(18):6799-807.

40. Schoonjans K, Annicotte JS, Huby T, Botrugno OA, Fayard E, Ueda Y, Chapman J, and Auwerx J. Liver receptor homolog 1 controls the expression of the scavenger receptor class B type I. *EMBO Rep.* 2002;3(12):1181-7.

41. Freeman LA, Kennedy A, Wu J, Bark S, Remaley AT, Santamarina-Fojo S, and Brewer HB, Jr. The orphan nuclear receptor LRH-1 activates the ABCG5/ABCG8 intergenic promoter. *J Lipid Res.* 2004;45(7):1197-206.

42. Rosenson RS, Brewer HB, Jr., Davidson WS, Fayad ZA, Fuster V, Goldstein J, Hellerstein M, Jiang XC, Phillips MC, Rader DJ, Remaley AT, Rothblat GH, Tall AR, and Yvan-Charvet L.

Cholesterol efflux and atheroprotection: advancing the concept of reverse cholesterol transport. *Circulation.* 2012;125(15):1905-19.

43. Li AC, and Glass CK. The macrophage foam cell as a target for therapeutic intervention. *Nat Med.* 2002;8(11):1235-42.

44. Sablin EP, Krylova IN, Fletterick RJ, and Ingraham HA. Structural basis for ligand-independent activation of the orphan nuclear receptor LRH-1. *Mol Cell.* 2003;11(6):1575-85.

45. Lee JM, Lee YK, Mamrosh JL, Busby SA, Griffin PR, Pathak MC, Ortlund EA, and Moore DD. A nuclear-receptor-dependent phosphatidylcholine pathway with antidiabetic effects. *Nature.* 2011;474(7352):506-10.

46. Goodwin B, Jones SA, Price RR, Watson MA, McKee DD, Moore LB, Galardi C, Wilson JG, Lewis MC, Roth ME, Maloney PR, Willson TM, and Kliewer SA. A regulatory cascade of the nuclear receptors FXR, SHP-1, and LRH-1 represses bile acid biosynthesis. *Mol Cell.* 2000;6(3):517-26.

47. Lu TT, Makishima M, Repa JJ, Schoonjans K, Kerr TA, Auwerx J, and Mangelsdorf DJ. Molecular basis for feedback regulation of bile acid synthesis by nuclear receptors. *Mol Cell.* 2000;6(3):507-15.

48. Steffensen KR, Holter E, Bavner A, Nilsson M, Pelto-Huikko M, Tomarev S, and Treuter E. Functional conservation of interactions between a homeodomain cofactor and a mammalian FTZ-F1 homologue. *EMBO Rep.* 2004;5(6):613-9.

49. Chalkiadaki A, and Talianidis I. SUMO-dependent compartmentalization in promyelocytic leukemia protein nuclear bodies prevents the access of LRH-1 to chromatin. *Mol Cell Biol.* 2005;25(12):5095-105.

50. Lee MB, Lebedeva LA, Suzawa M, Wadekar SA, Desclozeaux M, and Ingraham HA. The DEAD-box protein DP103 (Ddx20 or Gemin-3) represses orphan nuclear receptor activity via SUMO modification. *Mol Cell Biol.* 2005;25(5):1879-90.

51. Lee YK, Choi YH, Chua S, Park YJ, and Moore DD. Phosphorylation of the hinge domain of the nuclear hormone receptor LRH-1 stimulates transactivation. *J Biol Chem.* 2006;281(12):7850-5.

52. Venteclef N, Jakobsson T, Ehrlund A, Damdimopoulos A, Mikkonen L, Ellis E, Nilsson LM, Parini P, Janne OA, Gustafsson JA, Steffensen KR, and Treuter E. GPS2-dependent corepressor/SUMO pathways govern anti-inflammatory actions of LRH-1 and LXRbeta in the hepatic acute phase response. *Genes Dev.* 2010;24(4):381-95.

53. Venteclef N, Jakobsson T, Steffensen KR, and Treuter E. Metabolic nuclear receptor signaling and the inflammatory acute phase response. *Trends in endocrinology and metabolism: TEM.* 2011;22(8):333-43.

54. Stein S, Oosterveer MH, Mataki C, Xu P, Lemos V, Havinga R, Dittner C, Ryu D, Menzies KJ, Wang X, Perino A, Houten SM, Melchior F, and Schoonjans K. SUMOylation-dependent LRH-1/PROX1 interaction promotes atherosclerosis by decreasing hepatic reverse cholesterol transport. *Cell Metab.* 2014;20(4):603-13.

55. Lefevre L, Authier H, Stein S, Majorel C, Couderc B, Dardenne C, Eddine MA, Meunier E, Bernad J, Valentin A, Pipy B, Schoonjans K, and Coste A. LRH-1 mediates anti-inflammatory and antifungal phenotype of IL-13-activated macrophages through the PPARgamma ligand synthesis. *Nat Commun.* 2015;6:6801.

56. Musille PM, Pathak MC, Lauer JL, Hudson WH, Griffin PR, and Ortlund EA. Antidiabetic phospholipid-nuclear receptor complex reveals the mechanism for phospholipid-driven gene regulation. *Nat Struct Mol Biol.* 2012;19(5):532-7, S1-2.

57. Oosterveer MH, Mataki C, Yamamoto H, Harach T, Moullan N, van Dijk TH, Ayuso E, Bosch F, Postic C, Groen AK, Auwerx J, and Schoonjans K. LRH-1-dependent glucose sensing determines intermediary metabolism in liver. *J Clin Invest.* 2012;122(8):2817-26.

58. Mataki C, Magnier BC, Houten SM, Annicotte JS, Argmann C, Thomas C, Overmars H, Kulik W, Metzger D, Auwerx J, and Schoonjans K. Compromised intestinal lipid absorption in mice with a liver-specific deficiency of liver receptor homolog 1. *Mol Cell Biol.* 2007;27(23):8330-9.

59. Strable MS, and Ntambi JM. Genetic control of de novo lipogenesis: role in diet-induced obesity. *Crit Rev Biochem Mol Biol.* 2010;45(3):199-214.

60. Stein S, Lemos V, Xu P, Demagny H, Wang X, Ryu D, Jimenez V, Bosch F, Luscher TF, Oosterveer MH, and Schoonjans K. Impaired SUMOylation of nuclear receptor LRH-1 promotes nonalcoholic fatty liver disease. *J Clin Invest.* 2017;127(2):583-92.

61. Horton JD, Goldstein JL, and Brown MS. SREBPs: activators of the complete program of cholesterol and fatty acid synthesis in the liver. *J Clin Invest.* 2002;109(9):1125-31.

62. Chung J, Torta F, Masai K, Lucast L, Czapla H, Tanner LB, Narayanaswamy P, Wenk MR, Nakatsu F, and De Camilli P. INTRACELLULAR TRANSPORT. PI4P/phosphatidylserine countertransport at ORP5- and ORP8-mediated ER-plasma membrane contacts. *Science.* 2015;349(6246):428-32.

63. Moser von Filseck J, Copic A, Delfosse V, Vanni S, Jackson CL, Bourguet W, and Drin G. INTRACELLULAR TRANSPORT. Phosphatidylserine transport by ORP/Osh proteins is driven by phosphatidylinositol 4-phosphate. *Science.* 2015;349(6246):432-6.

64. Maeda K, Anand K, Chiapparino A, Kumar A, Poletto M, Kaksonen M, and Gavin AC. Interactome map uncovers phosphatidylserine transport by oxysterol-binding proteins. *Nature.* 2013;501(7466):257-61.

65. Miranda DA, Krause WC, Cazenave-Gassiot A, Suzawa M, Escusa H, Foo JC, Shihadih DS, Stahl A, Fitch M, Nyangau E, Hellerstein M, Wenk MR, Silver DL, and Ingraham HA. LRH-1 regulates hepatic lipid homeostasis and maintains arachidonoyl phospholipid pools critical for phospholipid diversity. *JCI Insight.* 2018;3(5).

66. Moylan CA, Pang H, Dellinger A, Suzuki A, Garrett ME, Guy CD, Murphy SK, Ashley-Koch AE, Choi SS, Michelotti GA, Hampton DD, Chen Y, Tillmann HL, Hauser MA, Abdelmalek MF, and Diehl AM. Hepatic gene expression profiles differentiate presymptomatic patients with mild versus severe nonalcoholic fatty liver disease. *Hepatology.* 2014;59(2):471-82.

67. Schoonjans K, Dubuquoy L, Mebis J, Fayard E, Wendling O, Haby C, Geboes K, and Auwerx J. Liver receptor homolog 1 contributes to intestinal tumor formation through effects on cell cycle and inflammation. *Proc Natl Acad Sci U S A.* 2005;102(6):2058-62.

68. Botrugno OA, Fayard E, Annicotte JS, Haby C, Brennan T, Wendling O, Tanaka T, Kodama T, Thomas W, Auwerx J, and Schoonjans K. Synergy between LRH-1 and beta-catenin induces G1 cyclin-mediated cell proliferation. *Mol Cell.* 2004;15(4):499-509.

69. Benod C, Vinogradova MV, Jouravel N, Kim GE, Fletterick RJ, and Sablin EP. Nuclear receptor liver receptor homologue 1 (LRH-1) regulates pancreatic cancer cell growth and proliferation. *Proceedings of the National Academy of Sciences of the United States of America.* 2011;108(41):16927-31.

70. Petersen GM, Amundadottir L, Fuchs CS, Kraft P, Stolzenberg-Solomon RZ, Jacobs KB, Arslan AA, Bueno-de-Mesquita HB, Gallinger S, Gross M, Helzlsouer K, Holly EA, Jacobs EJ, Klein AP, LaCroix A, Li D, Mandelson MT, Olson SH, Risch HA, Zheng W, Albanes D, Bamlet WR, Berg CD, Boutron-Ruault MC, Buring JE, Bracci PM, Canzian F, Clipp S, Cotterchio M, de Andrade M, Duell EJ, Gaziano JM, Giovannucci EL, Goggins M, Hallmans G, Hankinson SE, Hassan M, Howard B, Hunter DJ, Hutchinson A, Jenab M, Kaaks R, Kooperberg C, Krogh V, Kurtz RC, Lynch SM, McWilliams RR, Mendelsohn JB, Michaud DS, Parikh H, et al. A genome-wide association study identifies pancreatic cancer susceptibility loci on chromosomes 13q22.1, 1q32.1 and 5p15.33. *Nat Genet.* 2010;42(3):224-8.

71. Tolba R, Kraus T, Liedtke C, Schwarz M, and Weiskirchen R. Diethylnitrosamine (DEN)-induced carcinogenic liver injury in mice. *Lab Anim.* 2015;49(1 Suppl):59-69.

72. Xu P, Oosterveer MH, Stein S, Demagny H, Ryu D, Moullan N, Wang X, Can E, Zamboni N, Comment A, Auwerx J, and Schoonjans K. LRH-1-dependent programming of mitochondrial glutamine processing drives liver cancer. *Genes Dev.* 2016;30(11):1255-60.

73. Vander Heiden MG, and DeBerardinis RJ. Understanding the Intersections between Metabolism and Cancer Biology. *Cell.* 2017;168(4):657-69.

74. DeBerardinis RJ, Mancuso A, Daikhin E, Nissim I, Yudkoff M, Wehrli S, and Thompson CB. Beyond aerobic glycolysis: transformed cells can engage in glutamine metabolism that exceeds the requirement for protein and nucleotide synthesis. *Proc Natl Acad Sci U S A.* 2007;104(49):19345-50.

75. Yuneva M, Zamboni N, Oefner P, Sachidanandam R, and Lazebnik Y. Deficiency in glutamine but not glucose induces MYC-dependent apoptosis in human cells. *J Cell Biol.* 2007;178(1):93-105.

76. Ryu D, Jo YS, Lo Sasso G, Stein S, Zhang H, Perino A, Lee JU, Zeviani M, Romand R, Hottiger MO, Schoonjans K, and Auwerx J. A SIRT7-dependent acetylation switch of GABPbeta1 controls mitochondrial function. *Cell Metab.* 2014;20(5):856-69.

77. Lackey DE, and Olefsky JM. Regulation of metabolism by the innate immune system. *Nat Rev Endocrinol.* 2016;12(1):15-28.

78. McNelis JC, and Olefsky JM. Macrophages, immunity, and metabolic disease. *Immunity.* 2014;41(1):36-48.

79. Saltiel AR, and Olefsky JM. Inflammatory mechanisms linking obesity and metabolic disease. *J Clin Invest.* 2017;127(1):1-4.

80. Ertunc ME, and Hotamisligil GS. Lipid signaling and lipotoxicity in metaflammation: indications for metabolic disease pathogenesis and treatment. *J Lipid Res.* 2016;57(12):2099-114.

81. Hotamisligil GS. Foundations of Immunometabolism and Implications for Metabolic Health and Disease. *Immunity.* 2017;47(3):406-20.

82. Hotamisligil GS. Inflammation, metaflammation and immunometabolic disorders. *Nature.* 2017;542(7640):177-85.

83. Lee YS, Wollam J, and Olefsky JM. An Integrated View of Immunometabolism. *Cell.* 2018;172(1-2):22-40.

84. Buck MD, Sowell RT, Kaech SM, and Pearce EL. Metabolic Instruction of Immunity. *Cell.* 2017;169(4):570-86.

85. Pearce EJ, and Pearce EL. Immunometabolism in 2017: Driving immunity: all roads lead to metabolism. *Nat Rev Immunol.* 2017.

86. Breitenstein A, Stein S, Holy EW, Camici GG, Lohmann C, Akhmedov A, Spescha R, Elliott PJ, Westphal CH, Matter CM, Luscher TF, and Tanner FC. Sirt1 inhibition promotes in vivo arterial thrombosis and tissue factor expression in stimulated cells. *Cardiovasc Res.* 2011;89(2):464-72.

87. Miranda MX, van Tits LJ, Lohmann C, Arsiwala T, Winnik S, Tailleux A, Stein S, Gomes AP, Suri V, Ellis JL, Lutz TA, Hottiger MO, Sinclair DA, Auwerx J, Schoonjans K, Staels B, Luscher TF, and Matter CM. The Sirt1 activator SRT3025 provides atheroprotection in Apoe-/- mice by reducing hepatic Pcsk9 secretion and enhancing Ldlr expression. *Eur Heart J.* 2015;36(1):51-9.

88. Stein S, Lohmann C, Schafer N, Hofmann J, Rohrer L, Besler C, Rothgiesser KM, Becher B, Hottiger MO, Boren J, McBurney MW, Landmesser U, Luscher TF, and Matter CM. SIRT1 decreases Lox-1-mediated foam cell formation in atherogenesis. *Eur Heart J.* 2010;31(18):2301-9.

89. Stein S, Schafer N, Breitenstein A, Besler C, Winnik S, Lohmann C, Heinrich K, Brokopp CE, Handschin C, Landmesser U, Tanner FC, Luscher TF, and Matter CM. SIRT1 reduces endothelial activation without affecting vascular function in ApoE-/- mice. *Aging (Albany NY).* 2010;2(6):353-60.

90. Stein S, Lohmann C, Handschin C, Stenfeldt E, Boren J, Luscher TF, and Matter CM. ApoE-/- PGC-1alpha-/- mice display reduced IL-18 levels and do not develop enhanced atherosclerosis. *PLoS One.* 2010;5(10):e13539.

91. Zhang HM, Chen H, Liu W, Liu H, Gong J, Wang H, and Guo AY. AnimalTFDB: a comprehensive animal transcription factor database. *Nucleic Acids Res.* 2012;40(Database issue):D144-9.

92. Benod C, Carlsson J, Uthayaruban R, Hwang P, Irwin JJ, Doak AK, Shoichet BK, Sablin EP, and Fletterick RJ. Structure-based Discovery of Antagonists of Nuclear Receptor LRH-1. *The Journal of biological chemistry.* 2013;288(27):19830-44.

93. Whitby RJ, Dixon S, Maloney PR, Delerive P, Goodwin BJ, Parks DJ, and Willson TM. Identification of small molecule agonists of the orphan nuclear receptors liver receptor homolog-1 and steroidogenic factor-1. *J Med Chem.* 2006;49(23):6652-5.

94. Whitby RJ, Stec J, Blind RD, Dixon S, Leesnitzer LM, Orband-Miller LA, Williams SP, Willson TM, Xu R, Zuercher WJ, Cai F, and Ingraham HA. Small molecule agonists of the orphan nuclear receptors steroidogenic factor-1 (SF-1, NR5A1) and liver receptor homologue-1 (LRH-1, NR5A2). *J Med Chem.* 2011;54(7):2266-81.

95. Delerive P, Galardi CM, Bisi JE, Nicodeme E, and Goodwin B. Identification of liver receptor homolog-1 as a novel regulator of apolipoprotein AI gene transcription. *Mol Endocrinol.* 2004;18(10):2378-87.

96. Yang FM, Pan CT, Tsai HM, Chiu TW, Wu ML, and Hu MC. Liver receptor homolog-1 localization in the nuclear body is regulated by sumoylation and cAMP signaling in rat granulosa cells. *FEBS J.* 2009;276(2):425-36.

97. Priest C, and Tontonoz P. SUMOylation places LRH-1 in PROXimity to lipid metabolism. *Cell Metab.* 2014;20(4):558-9.

98. Cobo-Vuilleumier N, Lorenzo PI, Rodriguez NG, Herrera Gomez IG, Fuente-Martin E, Lopez-Noriega L, Mellado-Gil JM, Romero-Zerbo SY, Baquie M, Lachaud CC, Stifter K, Perdomo G, Bugliani M, De Tata V, Bosco D, Parnaud G, Pozo D, Hmadcha A, Florido JP, Toscano MG, de Haan P, Schoonjans K, Sanchez Palazon L, Marchetti P, Schirmbeck R, Martin-Montalvo A, Meda P, Soria B, Bermudez-Silva FJ, St-Onge L, and Gauthier BR. LRH-1 agonism favours an immune-islet dialogue which protects against diabetes mellitus. *Nat Commun.* 2018;9(1):1488.

99. Mays SG, Okafor CD, Whitby RJ, Goswami D, Stec J, Flynn AR, Dugan MC, Jui NT, Griffin PR, and Ortlund EA. Crystal Structures of the Nuclear Receptor, Liver Receptor Homolog 1, Bound to Synthetic Agonists. *J Biol Chem.* 2016;291(49):25281-91.

10. Original articles

1. **SUMOylation-Dependent LRH-1/PROX1 Interaction Promotes Atherosclerosis by Decreasing Hepatic Reverse Cholesterol Transport.**

   Stein S, Oosterveer MH, Mataki C, Xu P, Lemos V, Havinga R, Dittner C, Ryu D, Menzies KJ, Wang X, Perino A, Houten SM, Melchior F, Schoonjans K. (2014). *Cell Metab* 20, 603-613.

2. **Molecular Basis for the Regulation of the Nuclear Receptor LRH-1.**

   Stein S and Schoonjans S (2015). *Curr Opin Cell Biol* 33, 26-34.

3. **LRH-1 mediates anti-inflammatory and antifungal phenotype of IL-13-activated macrophages through the PPARgamma ligand synthesis.**

   Lefevre L, Authier H, Stein S, Majorel C, Couderc B, Dardenne C, Eddine MA, Meunier E, Bernad J, Valentin A, Pipy B, Schoonjans K, Coste A. (2015). *Nat Commun* 6, 6801.

4. **Impaired SUMOylation of nuclear receptor LRH-1 promotes nonalcoholic fatty liver disease.**

   Stein S, Lemos V, Xu P, Demagny H, Wang X, Ryu D, Jimenez V, Bosch F, Lüscher TF, Oosterveer MH, Schoonjans K. (2017). *J Clin Invest* 127, 583-592.

5. **LRH-1-dependent programming of mitochondrial glutamine processing drives liver cancer.**

   Xu P, Oosterveer MH*, Stein S*, Demagny H, Ryu D, Moullan N, Wang X, Can E, Zamboni N, Comment A, Auwerx J, Schoonjans K. (2016). *Genes Dev* 30, 1255-1260. *Equal contribution.

6. **A SIRT7-Dependent Acetylation Switch of GABPbeta1 Controls Mitochondrial Function.**

   Ryu D, Jo YS*, Lo Sasso G*, Stein S*, Zhang H, Perino A, Lee JU, Zeviani M, Romand R, Hottiger MO, Schoonjans K, Auwerx J. (2014). *Cell Metab* 20, 856-869. *Equal contribution.

Cell Metabolism
Article

SUMOylation-Dependent LRH-1/PROX1 Interaction Promotes Atherosclerosis by Decreasing Hepatic Reverse Cholesterol Transport

Sokrates Stein,[1] Maaike H. Oosterveer,[2] Chikage Mataki,[1] Pan Xu,[1] Vera Lemos,[1] Rick Havinga,[2] Claudia Dittner,[3,4] Dongryeol Ryu,[1] Keir J. Menzies,[1] Xu Wang,[1] Alessia Perino,[1] Sander M. Houten,[5] Frauke Melchior,[3] and Kristina Schoonjans[1,*]

[1]Metabolic Signaling, Institute of Bioengineering, School of Life Sciences, Ecole Polytechnique Fédérale de Lausanne, 1015 Lausanne, Switzerland

[2]Department of Pediatrics, Center for Liver Digestive and Metabolic Diseases, University of Groningen, University Medical Center Groningen, 9700 RB Groningen, the Netherlands

[3]Zentrum für Molekulare Biologie Heidelberg (ZMBH), DKFZ-ZMBH Alliance, 69120 Heidelberg, Germany

[4]Joint Division Molecular Metabolic Control, Zentrum für Molekulare Biologie Heidelberg, Deutsches Krebsforschungszentrum (DKFZ) and University Hospital Heidelberg, DKFZ-ZMBH Alliance, 69120 Heidelberg, Germany

[5]Department of Genetics and Genomic Sciences, Icahn School of Medicine at Mount Sinai, New York, NY 10029, USA

*Correspondence: kristina.schoonjans@epfl.ch

http://dx.doi.org/10.1016/j.cmet.2014.07.023

SUMMARY

Reverse cholesterol transport (RCT) is an antiatherogenic process in which excessive cholesterol from peripheral tissues is transported to the liver and finally excreted from the body via the bile. The nuclear receptor liver receptor homolog 1 (LRH-1) drives expression of genes regulating RCT, and its activity can be modified by different posttranslational modifications. Here, we show that atherosclerosis-prone mice carrying a mutation that abolishes SUMOylation of LRH-1 on K289R develop less aortic plaques than control littermates when exposed to a high-cholesterol diet. The mechanism underlying this atheroprotection involves an increase in RCT and its associated hepatic genes and is secondary to a compromised interaction of LRH-1 K289R with the corepressor prospero homeobox protein 1 (PROX1). Our study reveals that the SUMOylation status of a single nuclear receptor lysine residue can impact the development of a complex metabolic disease such as atherosclerosis.

INTRODUCTION

Atherosclerosis is a disease characterized by excessive cholesterol accumulation in vessel walls. It evolves from a complex interplay between hypercholesterolemia, dyslipidemia, and chronic inflammation and encompasses several tissues and organs (Weber and Noels, 2011). Rupture of an atherosclerotic plaque may lead to a myocardial infarction or stroke, two of the primary causes of morbidity and mortality in the world (Weber and Noels, 2011).

Liver receptor homolog 1 (LRH-1 or NR5A2) is a member of the NR5A subfamily of nuclear receptors (NRs) that binds as a monomer to its response elements (Fayard et al., 2004). The transcriptional activity of LRH-1 is governed by multiple factors, including the binding of ligands and posttranslational modifications, which together define its interaction with transcriptional coregulators (Fernandez-Marcos et al., 2011; Lee and Moore, 2008). LRH-1 is highly expressed in tissues of the enterohepatic axis, where it has diverse molecular and physiological functions (Fayard et al., 2004) ranging from local glucocorticoid production in the intestine (Coste et al., 2007) to glucose sensing in the liver (Oosterveer et al., 2012). Interestingly, one of the first described LRH-1 target genes is *scavenger receptor B type 1* (*Scarb1*) (Schoonjans et al., 2002), a gene that is expressed in many tissues and plays important functions in reverse cholesterol transport (RCT), an antiatherogenic process in which excessive cholesterol from peripheral tissues is transported to the liver and finally excreted via the bile (Rosenson et al., 2012). Although several other LRH-1 target genes involved in cholesterol metabolism have been identified, including *carboxl ester lipase* (*Cel*) (Fayard et al., 2003), *ATP binding cassette member subfamily G5* (*Abcg5*), *Abcg8* (Freeman et al., 2004), and *apolipoprotein M* (*Apom*) (Venteclef et al., 2008), so far no study has demonstrated that LRH-1 activity is critical for proper RCT or atherogenesis.

LRH-1 is targeted for SUMOylation by E3-SUMO ligases at several lysine residues, and this conserved reversible posttranslational modification affects its transcriptional activity (Chalkiadaki and Talianidis, 2005; Lee et al., 2005; Talamillo et al., 2013; Venteclef et al., 2010; Ward et al., 2013). SUMOylation of human LRH-1 is considered to attenuate its transcriptional activity, yet the mechanistic basis underlying this repression is poorly understood. Although one study reported that the SUMOylated form of LRH-1 is sequestered into promyelocytic leukemia (PML) protein bodies (Chalkiadaki and Talianidis, 2005), another study proposed that SUMO modification of LRH-1 stabilizes the recruitment of the transcriptional nuclear receptor corepressor 1 and histone deacetylase 3 (NCoR1/Hdac3) corepressor complex through its association with G protein pathway suppressor 2 (GPS2) (Venteclef et al., 2010).

In this study, we demonstrate that mice carrying a mutation on lysine 289 of LRH-1 (*Lrh1 K289R* mice) display reduced LRH-1

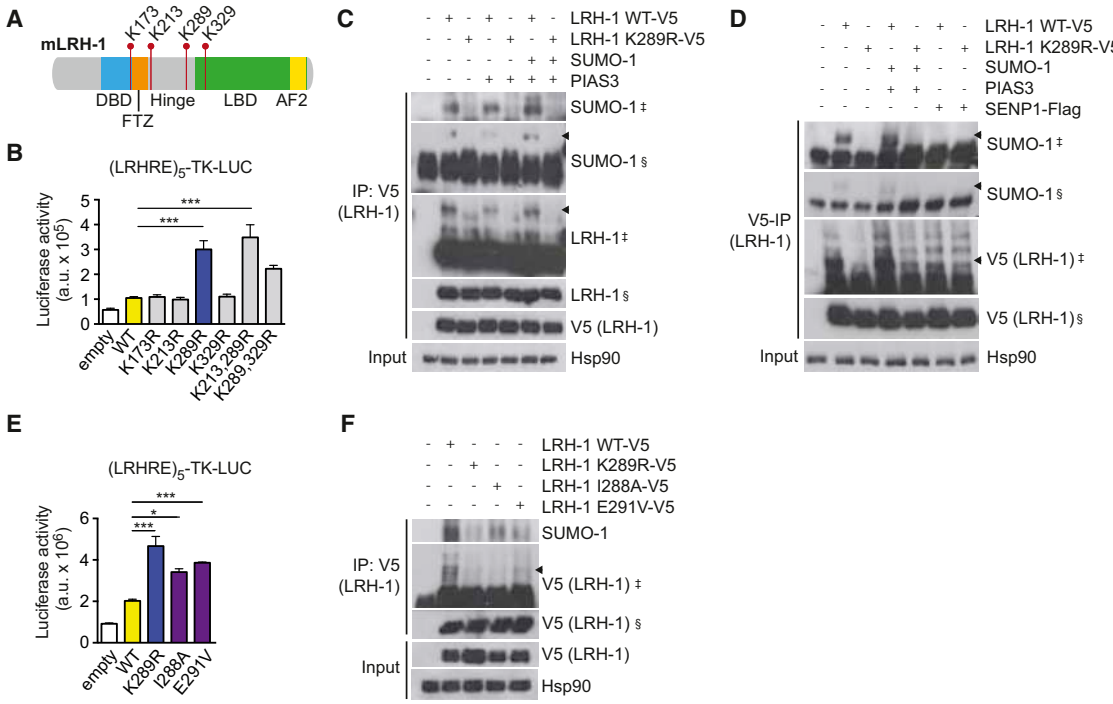

Figure 1. Non-SUMOylatable LRH-1 K289R Displays Increased Reporter Activity and Impaired SUMOylation In Vitro

(A) Schematic overview of LRH-1 highlighting the lysine residues that were mutated. DBD, DNA binding domain; FTZ, fushi tarazu homology domain; LBD, ligand binding domain; AF2, activation function 2 domain.

(B) Luciferase assay performed in HEK293T cells that were cotransfected with a pGL3::$(LRHRE)_5$-TK-LUC and a pCMV plasmid coding for LRH-1 WT or the outlined mutant constructs. n = 3. The experiment was replicated three times.

(C) Immunoprecipitation of V5-tagged LRH-1 to detect the SUMOylated band of LRH-1 (arrowheads). HEK293T cells were transfected with pCMV-V5::LRH-1 WT or pCMV-V5::LRH-1 K289R, pCMV::PIAS3, and/or pcDNA-HA::SUMO-1-HA. The experiment was replicated at least three times.

(D) Immunoprecipitation of V5-tagged LRH-1 to detect the SUMOylated band of LRH-1 in HEK293T cells that were transfected with pCMV-V5::LRH-1 (WT or K289R) and pCMV-FLAG::SENP1. The experiment was replicated at least three times.

(E) Residues adjacent to K289 are required for SUMOylation and function of LRH-1 activity. Luciferase assay was performed in HEK293T cells that were cotransfected with a pGL3::$(LRHRE)_5$-TK-LUC and pCMV plasmid coding for LRH-1 WT or the outlined mutant constructs. n = 3 from three separate experiments.

(F) Immunoprecipitation of V5-tagged LRH-1 to detect SUMOylation of the different mutant constructs used in (E).

Data are represented as means ± SEM. *p < 0.05, **p < 0.01, ***p < 0.001 relative to *Lrh-1 WT*, as determined by ANOVA and Bonferonni post hoc or Student's t test. Arrowheads, LRH-1*SUMO-1 band; §, short exposure; ‡,long exposure.

SUMOylation and increased expression of genes regulating cholesterol transport. When crossbred to atherosclerosis-prone *low-density lipoprotein receptor* (*Ldlr*) knockout mice, *Ldlr−/− Lrh-1 K289R* mice show improved RCT and diminished atherosclerosis development in comparison to control mice. Mechanistically, this effect is attributed to the specific loss of interaction of the mutated form of LRH-1 with the corepressor PROX1, thereby increasing the expression of LRH-1 target genes involved in RCT.

RESULTS

Non-SUMOylatable LRH-1 K289R Displays Increased Transcriptional Activity In Vitro

The murine LRH-1 protein has several lysine (K) residues that could be SUMOylated. They are located in the DNA binding domain, hinge region, or ligand binding domain (Figure 1A). On the basis of previous studies (Lee et al., 2005), we mutated the most relevant K residues to non-SUMOylatable arginines (R) and analyzed their potential to *trans*-activate a heterologous LRH-1 reporter by transient transfection assays (Figure 1B). Interestingly, the K289R mutation displayed the highest transcriptional activity, whereas the remaining K mutations (K173R, K213R, or K329R) had neither an effect as single mutations nor an additive effect when mutated together with K289R (Figure 1B). Next, we analyzed whether the enhanced activity of LRH-1 K289R was also associated with a reduction in the SUMOylation status. Human embryonic kidney 293T (HEK293T) cells transfected with either LRH-1 wild-type (WT) or LRH-1 K289R were cotransfected with either PIAS3 SUMO ligase alone or in combination with SUMO-1 substrate. Basal LRH-1 WT SUMOylation was clearly detectable, whereas it was nearly undetectable in LRH-1 K289R (Figure 1C). Cotransfection with PIAS3 and SUMO-1 slightly increased SUMOylation of LRH-1 WT (Figure 1C). Notably, LRH-1 K289R SUMOylation remained low after PIAS3 and SUMO-1 cotransfection, showing that mutating a single K residue can affect the total SUMOylation status of the transcription factor (Figure 1C). Moreover, cotransfection of LRH-1 WT or LRH-1 K289R with the isopeptidase sentrin/SUMO-specific protease 1 (SENP1) efficiently removed the SUMO modification from only LRH-1 WT (Figure 1D). The SUMO acceptor

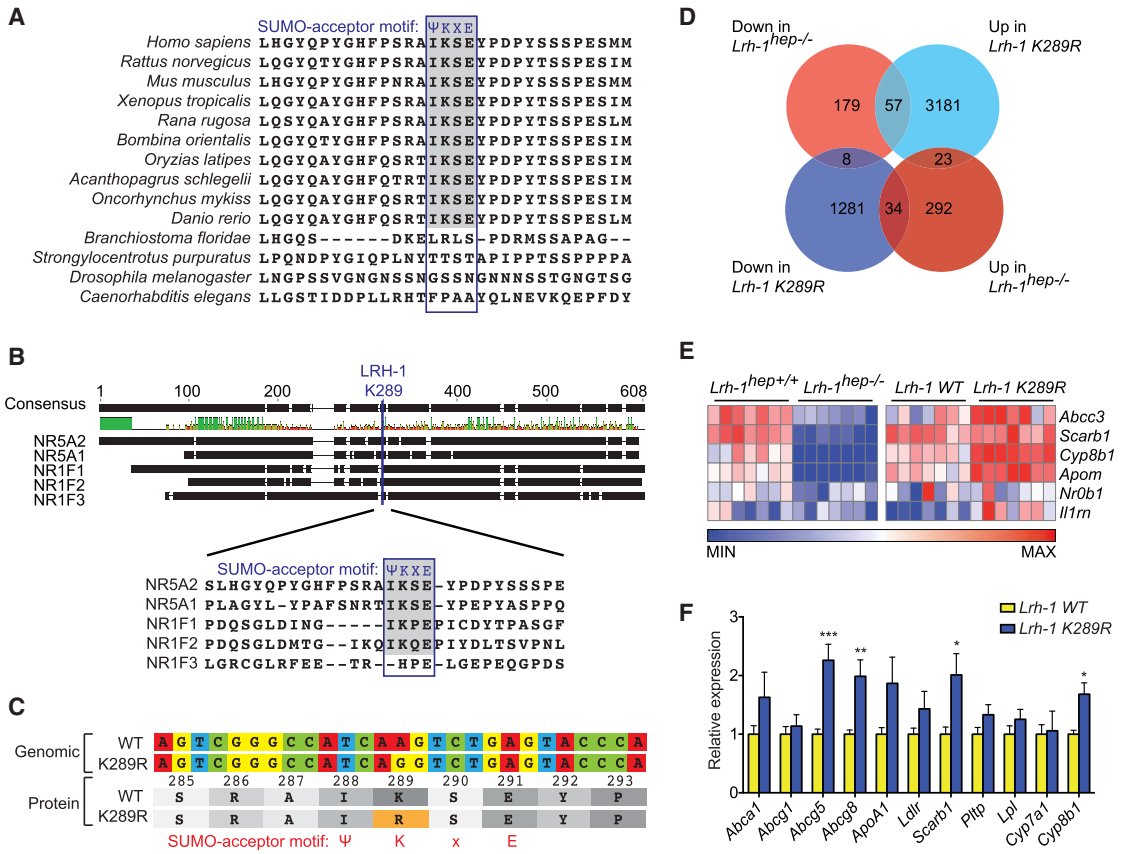

Figure 2. The LRH-1 SUMO Acceptor Motif Is Conserved in Vertebrates, and Mutation of Its Lysine Triggers Activation of Cholesterol Homeostasis Genes In Vivo

(A) Alignment of the amino acid sequence surrounding the murine LRH-1 K289 residue with other species. The blue-lined box highlights the aligned amino acids homologous to the SUMO acceptor motif, and the gray shading marks the sequences with an intact SUMO acceptor sequence.

(B) Protein alignment of LRH-1 (NR5A2) with other monomeric NR showing conserved sequences surrounding the LRH-1 K289 residue. Green, high homology; red, low homology.

(C) Overview of the genomic and protein sequence surrounding the K289R mutation. Mutation of a single nucleotide (AAG → AGG) at genomic level leads to K289R mutation of the translated protein.

(D) Venn diagram depicting the number of genes that are significantly up- or downregulated in *Lrh-1*$^{hep-/-}$ (n = 8) in comparison to *Lrh-1*$^{hep+/+}$ (Oosterveer et al., 2012) (n = 8) as well as *Lrh-1 K289R* (n = 7) in comparison to *Lrh-1 WT* (n = 7) mice.

(E) Heatmap displaying the expression of selected LRH-1 target genes in the corresponding genotypes (n = 4 per genotype).

(F) Hepatic expression of genes that regulate cholesterol homeostasis in *Lrh-1 WT* (n = 8) and *Lrh-1 K289R* (n = 9) mice.

Data are represented as means ± SEM. *p < 0.05, **p < 0.01, ***p < 0.001 relative to *Lrh-1 WT*, as determined by Student's t test. See also Figures S1 and S2.

motif Ψ-K-x-E is found in many SUMOylated proteins. Although the lysine residue can be targeted for SUMOylation, the adjacent hydrophobic (Ψ) and acidic glutamate (E) residues are also necessary to mediate the conjugation with the SUMO E2 enzyme Ubc9 (Bernier-Villamor et al., 2002). Mutation of these two sites (I288A and E291V) also increased LRHRE-driven reporter activity (Figure 1E) and reduced LRH-1 SUMOylation (Figure 1F), showing that not only the lysine but also an intact SUMO acceptor motif is crucial for the SUMO-dependent function of LRH-1.

LRH-1 K289R Activates Selected Target Genes In Vivo

To understand the relevance of this particular SUMO acceptor lysine residue, we carried out comparative alignment studies. Alignment of the amino acids surrounding the murine LRH-1 K289 with other species demonstrated that this particular SUMO acceptor motif is highly conserved in vertebrates but not in the chordate lancelet (*Branchiostoma floridae*), sea urchin (*Strongylocentrotus purpuratus*), fruit fly (*Drosophila melanogaster*), or roundworm (*Caenorhabditis elegans*; Figures 2A; Figure S1A available online). However, homologous proteins in *C. elegans* and *D. melanogaster* have other sites that can be targeted for SUMOylation (Talamillo et al., 2013; Ward et al., 2013). Next, we compared the murine LRH-1 protein sequence with other monomeric NRs with special focus on the highly variable and intrinsically disordered hinge region (Krasowski et al., 2008). Besides the close homolog NR5A1 (SF-1), only the retinoic-acid-receptor-related orphan receptors (RORs:NR1F1, NR1F2, and NR1F3) displayed somewhat homologous hinge regions (Figure S1B). Closer alignment of LRH-1 with NR5A1 and the three RORs showed that only NR1F1 and NR1F2 contain

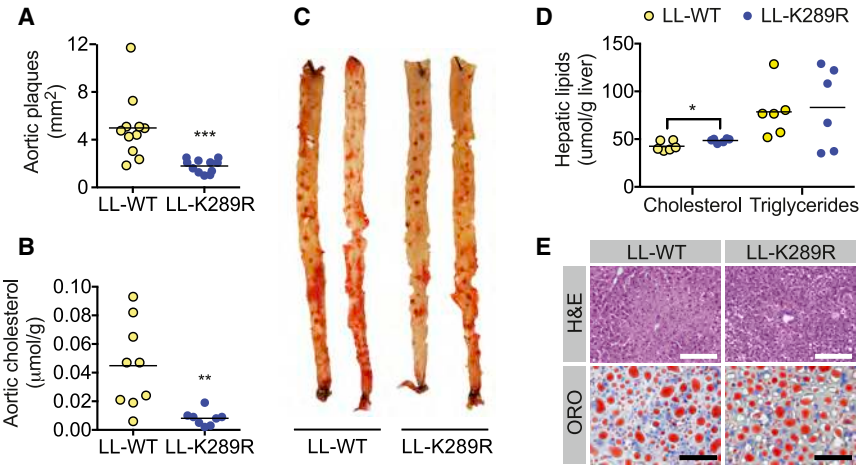

Figure 3. LRH-1 K289R Protects against Atherosclerosis Progression

(A) Quantification of aortic plaque area in *Ldlr*$^{-/-}$ *Lrh-1 WT* (LL-WT) or *Ldlr*$^{-/-}$ *Lrh-1 K289R* (LL-K289R) mice. n = 11 per genotype.

(B) Quantification of the cholesterol content in aortic lipid extracts of LL-WT (n = 9) and LL-K289R (n = 8) mice.

(C) Representative aortas of LL-WT and LL-K289R mice stained with Oil-Red O.

(D) Quantification of cholesterol and triglyceride contents in hepatic lipid extracts of LL-WT and LL-K289R mice. n = 6 per genotype.

(E) Representative images of hematoxylin and eosin and Oil-Red O (ORO) staining of hepatic sections of LL-WT and LL-K289R mice. The white scale bar represents 200 μm, and the black scale bar represents 50 μm.

Data are represented as means ± SEM. *p < 0.05, **p < 0.01, ***p < 0.001 relative to LL-WT, as determined by Mann-Whitney U or Student's t tests. See also Figure S3.

the conserved SUMO acceptor motif (Figure 2B). These bioinformatic data suggest that SUMOylation of this site is specific for a very small subset of NRs and highlights the functional importance of the hinge region in these selected NRs.

To analyze the physiological impact of the K289R mutation on LRH-1 function in vivo, we generated a knockin mouse line containing the K289R mutation *Lrh-1 K289R* (Figures 2C and S2A). The offspring of *Lrh-1 K289R* breeders were born under normal Mendelian and sex ratios, and no apparent dysmorphic phenotype could be observed in these mice (data not shown). The mutation did not affect the expression of LRH-1 in the liver in comparison to *Lrh-1 WT* and hepatocyte-specific *Lrh-1*$^{hep+/+}$ mice (Figure S2B). Then, we performed microarray analyses on livers in order to compare the transcriptome of hepatocyte-specific *Lrh-1*$^{hep-/-}$ (Oosterveer et al., 2012) and *Lrh-1 K289R* mice to their corresponding controls. Only 57 of the 244 genes (23.4%) whose expression was decreased in *Lrh-1*$^{hep-/-}$ mice were induced in *Lrh-1 K289R* mice (Figure 2D and Table S1). Several of the established LRH-1 target genes that are reduced in *Lrh-1*$^{hep-/-}$ mice were oppositely regulated in *Lrh-1 K289R* mice (Figure 2E). Intriguingly, most of the selected hepatic LRH-1 target genes involved in cholesterol metabolism were increased in *Lrh-1 K289R* in comparison to *Lrh-1 WT* mice, as determined by qPCR analyses (Figure 2F). Although hepatic expression of *Cyp8b1* was nearly absent in hepatocyte-specific *Lrh-1*$^{hep-/-}$ mice (Mataki et al., 2007), it was only mildly enhanced in *Lrh-1 K289R* mice (Figure 2F). This was reflected in the composition of bile acids in the gallbladder. Although the total bile acid content did not differ, *Lrh-1 K289R* mice had slightly increased tauro-conjugated cholic acid (tCA) and less tauro-conjugated muricholic acid (tMCA) (Figure S2C). Altogether, these data show that LRH-1 K289R exhibits increased transcriptional activity on a selected subset of LRH-1 target genes and cannot be described as a global constitutive active LRH-1 form.

LRH-1 K289R Protects against Atherosclerosis Development

Given that many of the genes affected in *Lrh-1 K289R* mice are involved in cholesterol homeostasis, we hypothesized that LRH-1 K289R may affect cholesterol metabolism, and hence hypercholesterolemia-driven diseases, such as atherosclerosis. To study the role of LRH-1 K289R in atherosclerosis, we crossbred *Lrh-1 WT* and *Lrh-1 K289R* mice to atherosclerotic-prone *Ldlr* knockout mice in order to generate *Ldlr*$^{-/-}$ *Lrh-1 WT* (LL-WT) or *Ldlr*$^{-/-}$ *Lrh-1 K289R* (LL-K289R) mice. Then, 8-week-old LL-WT or LL-K289R mice were subjected to a high-cholesterol diet (HCD) for 14 weeks. Body and liver weight (Figures S3A and S3B), and also gross morphology of other organs, were similar between the different genotypes (data not shown). Notably, en face plaque analyses of the thoraco-abdominal aorta demonstrated that LL-K289R mice developed significantly less atherosclerotic plaques than LL-WT mice and also accumulated less cholesterol in their aortas (Figures 3A–3C). Advanced plaque analyses of the aortic sinus stained for collagen imaging revealed no changes in necrotic core size, cap thickness, or collagen content in LL-K289R in comparison to LL-WT mice (Figures S3C–S3E). Total plasma cholesterol did not differ between the mice, and plasma triglyceride levels were only slightly reduced before administering the HCD and were not significantly changed upon HCD feeding (Figures S3F and S3G). Although no changes in triglyceride content were observed in the lipoprotein fractions, a small reduction in the cholesterol content of the low-density lipoprotein subfraction of LL-K289R mice could be noticed (Figures S3H and S3I). Furthermore, hepatic triglyceride content was not changed in overnight fasted LL-K289R mice, whereas cholesterol content was only slightly increased (Figure 3D). Stainings of liver cryosections showed no apparent difference in neutral lipid content and cellular morphology between the two genotypes (Figure 3E). These data demonstrate that LL-K289R mice develop less atherosclerosis, possibly as a consequence of improved RCT.

To assess a potential contribution of macrophages in the observed phenotype, we measured *Lrh-1* in isolated thioglycolate-elicited peritoneal macrophages. In comparison to its expression in the liver, *Lrh-1* was barely detectable in macrophages under the conditions analyzed (Figure S4A; bioGPS *Lrh-1* expression pattern, http://biogps.org/#goto=genereport&id=26424). Furthermore, treatment with acetylated LDL (acLDL) to trigger

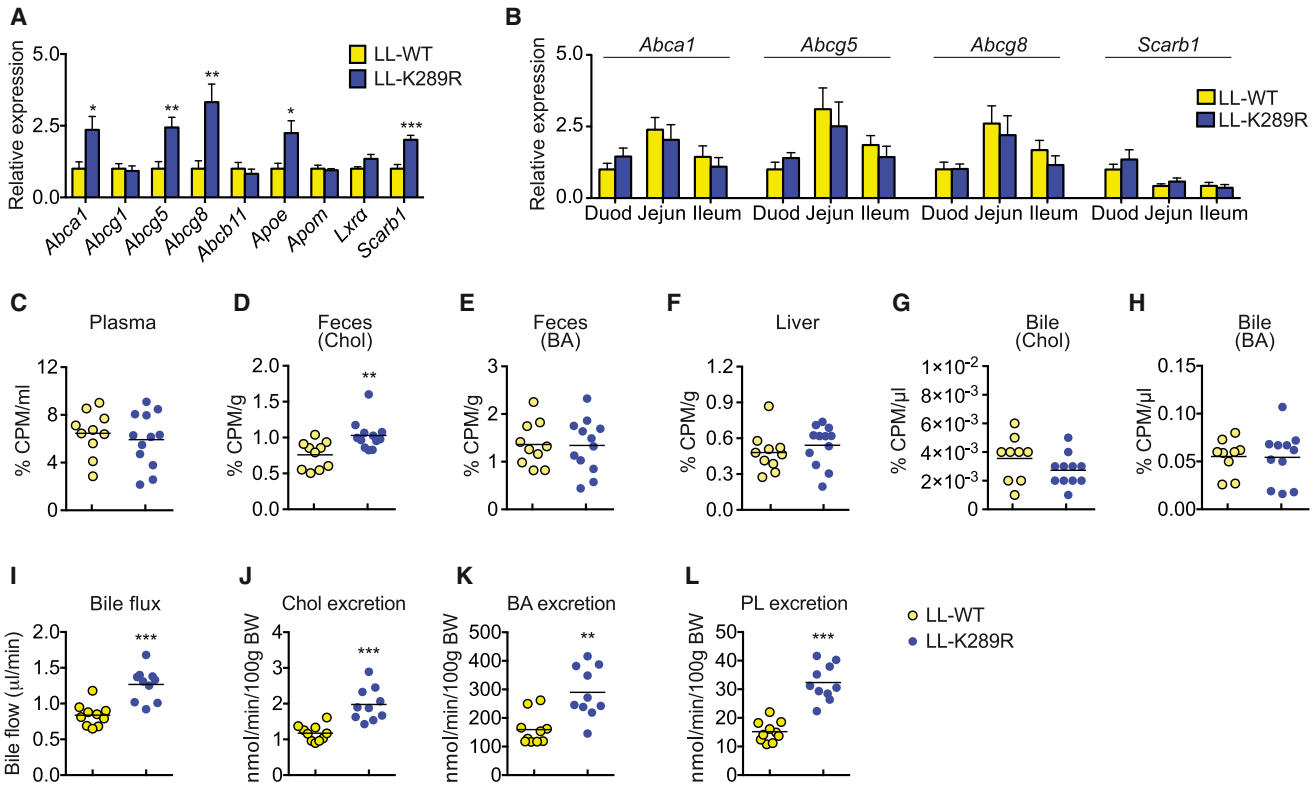

Figure 4. Improved Reverse Cholesterol Transport and Biliary Sterol Excretion in LL-K289R Mice

(A) Hepatic expression of genes affecting cholesterol metabolism in LL-WT and LL-K289R mice. n = 9 per genotype.

(B) Intestinal expression of genes affecting cholesterol metabolism in LL-WT and LL-K289R mice. Duod, duodenum; Jejun, jejunum. n = 9 per genotype.

(C–H) LL-WT and LL-K289R mice were injected with ^{3}H-cholesterol loaded LL-WT macrophages. Detection of ^{3}H-tracer in plasma (C), fecal cholesterol (Chol; D), fecal bile acids (BA; E), liver (F), bile cholesterol fraction (G), and bile BA fraction (H). n = 10 LL-WT; n = 12 LL-K289R.

(I–L) Bile excretion (I) and biliary secretion rates of Chol (J), BA (K), and phospholipids (PL; L). n = 10 per genotype.

Data are represented as means ± SEM. *p < 0.05, **p < 0.01, ***p < 0.001 relative to LL-WT, as determined by Mann-Whitney U or Student's t tests. See also Figure S4.

foam cell formation or lipopolysaccharide (LPS) in order to evaluate the inflammatory response did not trigger any significant difference in acetylated LDL accumulation, *Scarb1* expression, or inflammatory markers between *Lrh-1 WT* and *K289R* macrophages (Figures S4B–S4H), suggesting that the effects on aortic lipid accumulation are not likely related to differential macrophage function.

LRH-1 K289R Protects against Atherosclerosis by Promoting RCT

Intrigued by the marked decrease of atherosclerotic lesions in LL-K289R mice and the increased expression of genes involved in hepatic cholesterol homeostasis in *Lrh-1 K289R* mice (Figure 2F), we analyzed the expression of genes involved in RCT in the liver. Notably, hepatic expression of *Abca1*, *Abcg5*, *Abcg8*, *Apoe*, and *Scarb1* was significantly increased in LL-K289R in comparison to LL-WT mice (Figure 4A). Given that many of these genes are also expressed in the intestine and contribute to whole-body cholesterol homeostasis, we analyzed their expression pattern in the duodenum, jejunum, and ileum. Surprisingly, none of these transcripts was increased in any of the three intestinal sections (Figure 4B). Moreover, microarray analyses of jejunal sections from *Lrh-1 K289R* and *Lrh-1 WT* mice did not display differential expression of cholesterol and lipoprotein regulators that are expressed in livers and intestine (Figure S4I), indicating that LRH-1 K289R specifically induces the expression of cholesterol transport regulators in the liver.

To analyze whether the increased expression of RCT genes has physiological consequences, we performed in vivo macrophage-to-feces RCT and biliary flux studies. In vivo RCT analysis was performed by injecting peritoneal macrophages that were loaded with [^{3}H]-cholesterol (^{3}H tracer) ex vivo into recipient LL-K289R and LL-WT mice. ^{3}H-tracer counts were significantly increased in the fecal cholesterol fraction of LL-K289R in comparison to LL-WT mice, whereas no major differences were observed in the fecal bile acid pool or the plasma, hepatic, or biliary pools (Figures 4C–4H). Furthermore, gallbladder cannulation revealed that bile flow was increased in LL-K289R in comparison to LL-WT mice (Figure 4I). In line with the increased bile flow, biliary cholesterol, bile acids, and phospholipids excretion were also enhanced in LL-K289R in comparison to LL-WT mice (Figures 4J–4L). These data establish LRH-1 K289R as a potent mediator of bile secretion and RCT in vivo.

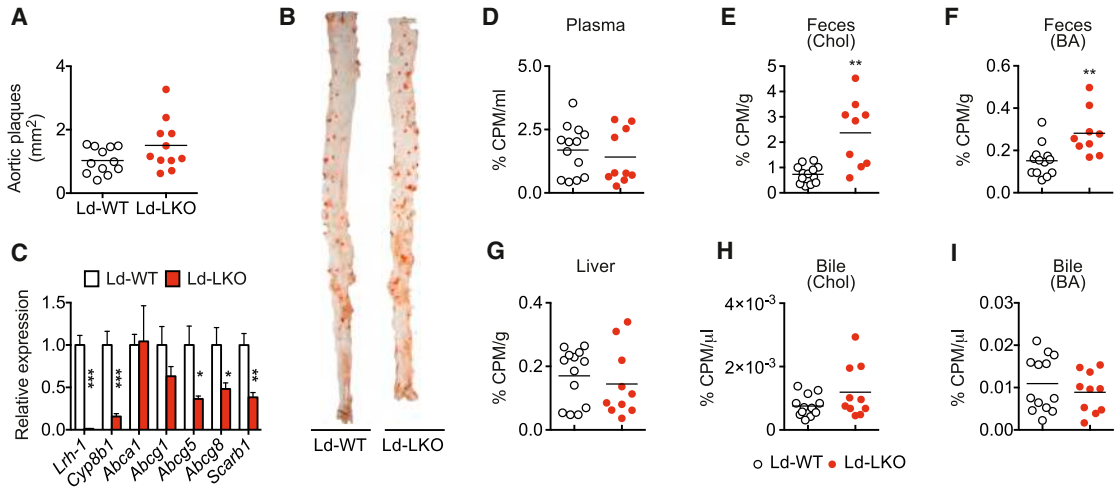

Figure 5. Liver-Specific *Lrh-1* Knockout Mice Do Not Develop More Atherosclerosis

(A) Quantification of aortic plaque area in *Ldlr*$^{-/-}$ *Lrh-1*$^{hep+/+}$ (Ld-WT, n = 12) or *Ldlr*$^{-/-}$ *Lrh-1*$^{hep-/-}$ (Ld-LKO, n = 11) mice.

(B) Representative aortas of Ld-WT and Ld-LKO mice stained with Oil-Red O.

(C) Hepatic expression of genes affecting cholesterol metabolism in Ld-WT and Ld-LKO mice. n = 9 per genotype.

(D–I) Ld-WT and Ld-LKO mice were injected with ^{3}H-cholesterol loaded Ld-WT macrophages. Detection of ^{3}H tracer in plasma (D), fecal cholesterol (E), fecal BA (F), liver (G), bile Chol fraction (H), and bile BA fraction (I). n = 13 Ld-WT; n = 10 Ld-LKO.

Data are represented as means ± SEM. *p < 0.05, **p < 0.01, ***p < 0.001 relative to LL-WT, as determined by Student's t test. See also Figure S5.

Liver-Specific *Lrh-1* Knockout Mice Do Not Develop Increased Atherosclerosis

Even though the transcriptome and targeted gene expression analyses argue against Lrh-1 K289R as a simple constitutively active form of LRH-1 (Figures 2D–2F), we nevertheless explored whether the hepatocyte-specific *Lrh-1*$^{hep-/-}$ mice would yield an opposite phenotype on RCT and atherosclerosis development. Therefore, we crossbred hepatocyte-specific *Lrh-1*$^{hep-/-}$ with *Ldlr*$^{-/-}$ mice in order to generate *Ldlr*$^{-/-}$ *Lrh-1*$^{hep+/+}$ (Ld-WT) or *Ldlr*$^{-/-}$ *Lrh-1*$^{hep-/-}$ (Ld-LKO) mice and fed them an HCD for 12 weeks. Body and liver weight did not differ between the genotypes (Figures S5A and S5B). Interestingly, Ld-LKO did not develop more atherosclerotic lesions than Ld-WT mice (Figures 5A and 5B), although the expression of the RCT regulators (Figure 5C) and binding of LRH-1 to the *Abcg5/Abcg8* intergenic promoter (Freeman et al., 2004) (Figure S5C) was significantly lower in the Ld-LKO liver. Moreover, in vivo RCT analysis demonstrated an increased fecal sterol content in Ld-LKO mice, which could explain why these mice do not develop more atherosclerotic lesions (Figures 5D–5I). The increase of fecal sterols in *Lrh-1*$^{hep-/-}$ mice most likely stems from the compromised intestinal sterol absorption, which was previously reported to be the consequence of reduced *Cyp8b1* in the liver shifting the bile acid pool toward more hydrophilic bile acids (Figure 5C) (Mataki et al., 2007; Out et al., 2011).

Compromised Binding of LRH-1 K289R with the Corepressor PROX1 Derepresses Hepatic RCT Genes

Several corepressors have been reported to fine-tune the activity of LRH-1 in a context specific manner. In the liver, corepressors such as small heterodimer partner (SHP or NR0B2) and prospero homeobox protein 1 (PROX1) as well as the NCOR1/HDAC3 corepressor complex can repress LRH-1 activity (Goodwin et al., 2000; Lee and Moore, 2002; Lu et al., 2000; Qin et al., 2004; Venteclef et al., 2010). To test the assumption that LRH-1 SUMOylation affects the interaction of LRH-1 with potential corepressors, we carried out coimmunoprecipitation experiments in HEK293T cells transfected with LRH-1 WT or LRH-1 K289R in the presence of the corepressor SHP, PROX1, or NCOR1. Surprisingly, we observed that the interaction between LRH-1 and PROX1 was lost or much weaker when LRH-1 K289R was ectopically expressed (Figure 6A), whereas no difference in interaction was observed with SHP or detected with NCOR1 (data not shown). This would suggest that optimal PROX1-LRH-1 interaction may at least require transient SUMOylation of K289 of LRH-1 WT. To assess this possibility, we coexpressed the isopeptidase SENP1 in order to enzymatically remove SUMO from its substrates. SENP1 robustly reduced the interaction between LRH-1 WT and PROX1, supporting the hypothesis that the SUMOylation status affects the interaction (Figure 6B), which might be direct or be mediated by a third partner. Interestingly, the weaker interaction observed between PROX1 and LRH-1 K289R was further reduced by addition of SENP1, suggesting that other SUMOylatable sites in the protein complex may enhance the interaction between the two proteins (Figure 6B). Given that loss of binding to the corepressor PROX1 would provide a mechanistic basis for explaining the enhanced activity of LRH-1 K289R, we next explored whether differential *Prox1* expression between liver and intestine could explain the absence of effects on intestinal RCT genes in *Lrh-1 K289R* mice (Figure 4B). Interestingly, *Prox1* mRNA was almost undetectable in the small intestine and only marginally expressed in the colon in comparison to liver (Figure 6C; bioGPS *Prox1* expression pattern, http://biogps.org/#goto=genereport&id=26424), thus most likely contributing to the differential expression of RCT genes between liver and intestine.

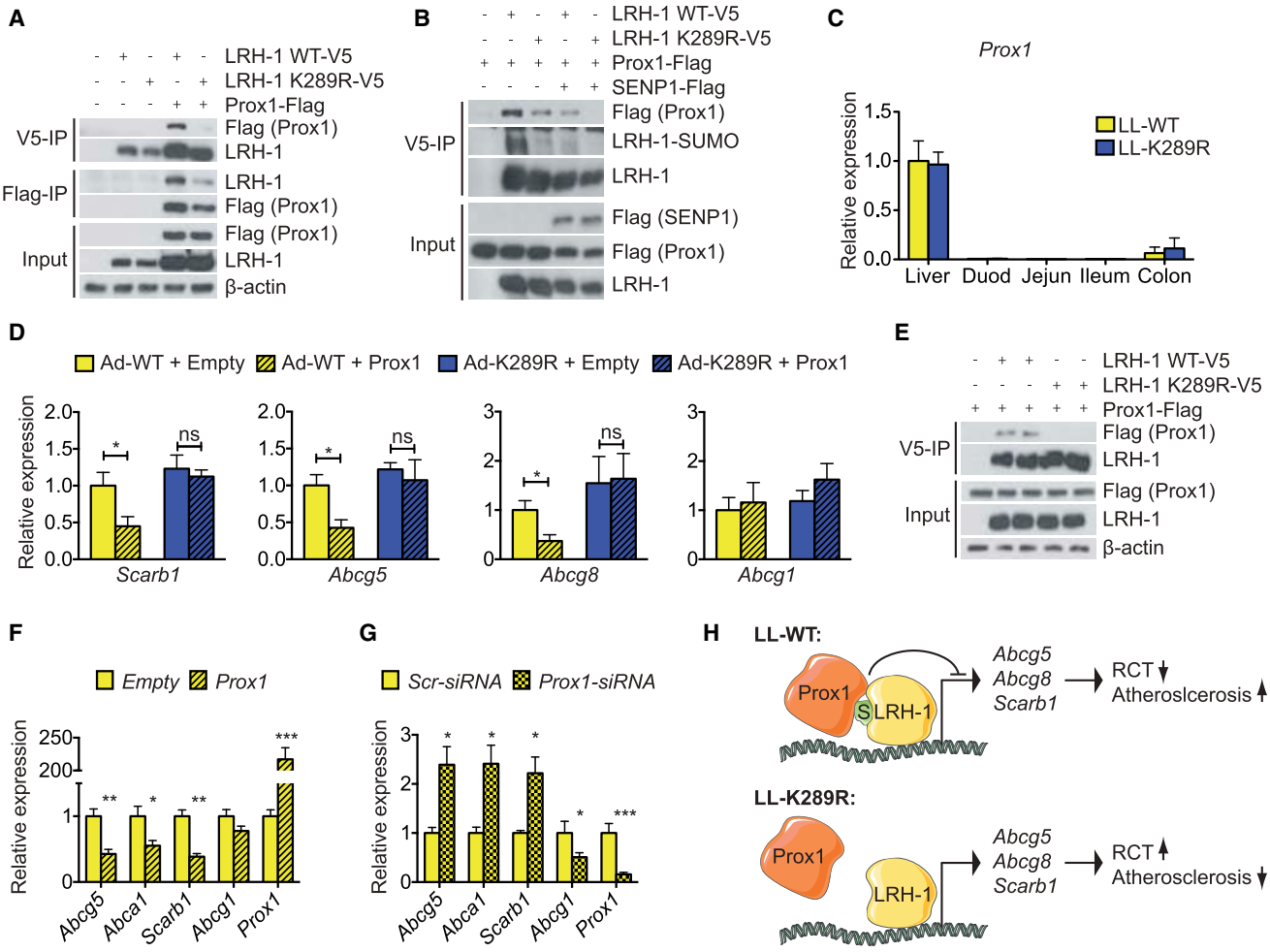

Figure 6. Compromised Binding of LRH-1 K289R with Prox1 Derepresses Hepatic RCT Genes

(A) LRH-1/Prox1 CoIP in HEK293T cells overexpressing V5-tagged LRH-1 (WT or K289R) and FLAG-tagged Prox1. The experiment was replicated at least three times.

(B) LRH-1/Prox1 CoIP in HEK293T cells overexpressing V5-tagged LRH-1 (WT or K289R), FLAG-tagged Prox1, and FLAG-tagged SENP1. The experiment was replicated three times.

(C) Comparative *Prox1* expression in liver, duodenum (Duod), jejunum (Jejun), ileum, and colon of LL-WT and LL-K289R mice. n = 9 per genotype.

(D) Expression of *Scarb1*, *Abcg5*, *Abcg8*, *Abca1*, and *Abcg1* in *Lrh-1*$^{hep-/-}$ primary hepatocytes that were infected or transfected with LRH-1 (WT or K289R) and Prox1. n = 3. The experiment was replicated with three batches of primary cells.

(E) LRH-1/Prox1 CoIP in primary hepatocytes that were infected or transfected with V5-tagged LRH-1 (WT or K289R) and FLAG-tagged Prox1. n = 2 from independent batches of primary hepatocytes.

(F and G) Effect of overexpression (F) and small-interfering-RNA-mediated silencing (G) of *Prox1* in WT primary hepatocytes n = 3. The experiment was replicated with two batches of primary cells.

(H) Model showing how LRH-1 WT and LRH-1 K289R regulate the expression of key genes controlling hepatic cholesterol transport and its consequence on RCT and atherosclerosis. S, SUMO-1.

Data are represented as means ± SEM. *p < 0.05 and **p < 0.01 relative to non-*Prox-1*-transfected controls, as determined by Student's t test. See also Figure S6.

To study the molecular effect of the PROX1-LRH-1 interaction in more detail, we decided to use primary hepatocytes. Notably, both *Lrh-1* and *Prox1* transcripts were reduced to ~25% of their expression in whole livers but were clearly detectable (Figure S6A). We isolated primary hepatocytes from *Lrh-1*$^{hep-/-}$ mice and infected them with an adenovirus containing the LRH-1 WT or K289R followed by ectopic expression of PROX1. Interestingly, while expression of *Abcg1* was not affected or rather increased in cells overexpressing PROX1, the expression of *Scarb1*, *Abcg5*, and *Abcg8* was diminished in cells in which LRH-1 WT, but not LRH-1 K289R, was reconstituted (Figures 6D and S6B), demonstrating that the repressive function of PROX1 on LRH-1 activity depends on an intact LRH-1 K289 SUMOylation site. Furthermore, LRH-1 K289R failed to bind PROX1 in transfected primary hepatocytes, whereas LRH-1 WT/PROX1 interaction was intact (Figure 6E), demonstrating that the LRH-1/PROX1 complex can assemble in vitro and ex vivo. To assess whether we could mimic the effect

of LRH-1/PROX1 interaction in a physiologically relevant cell model, we next overexpressed or silenced *Prox1* in WT primary hepatocytes. While overexpression of *Prox1* reduced the expression of the RCT regulators (Figure 6F), silencing of *Prox1* had the opposite effect (Figure 6G). Altogether, our data suggest that SUMOylated LRH-1 WT recruits the corepressor PROX1 and hence is unable to selectively activate the transcription of important cholesterol receptors and transporters (Figure 6H). If SUMOylation of LRH-1 is defective as in our LRH-1 K289R mutant, then the PROX1-mediated repression is weakened or lost, thereby facilitating the induction of RCT genes and diminishing the progression of atherosclerosis (Figure 6H).

DISCUSSION

Posttranslational modification by SUMO affects the function of a large number of nuclear proteins, including NRs (Geiss-Friedlander and Melchior, 2007; Treuter and Venteclef, 2011). Although various NRs have emerged as reversible SUMO targets modulating almost every aspect of NR function in cell models, very few studies have established in vivo functional roles of NR SUMOylation in health or disease. This is rather surprising given the prominent role of NRs in the pathogenesis of diseases and the repressive imprint of SUMOylation on NR activity. In this study, we have generated a mouse model harboring a K289R mutation that strongly affects LRH-1 SUMOylation and function. We demonstrate that loss of SUMOylation by mutating the critical lysine acceptor site in the LRH-1 protein is sufficient to protect mice against the development of a chronic metabolic disease such as atherosclerosis. More importantly, we provide evidence that the beneficial effect on atherosclerosis is caused by enhancing the transcription of hepatic RCT genes, such as *Abca1*, *Abcg5*, *Abcg8*, and *Scarb1*, without any involvement of gut- or macrophage-specific RCT genes. These findings are consistent with a recent study in *Drosophila* showing that SUMOylation of the LRH-1 homolog *Ftz-f1* affects the expression of the scavenger receptor *Snmp1*, which is required for cellular cholesterol uptake and subsequent steroid synthesis (Talamillo et al., 2013), suggesting that LRH-1 SUMOylation may impact on a similar physiologically conserved pathway.

Alignment of the protein sequence of LRH-1 with other NRs revealed that, aside from SF-1, only members of the ROR family have a hinge region that is comparable to that of LRH-1 (Figure 2B). Although in SF-1, mutation of two conserved SUMO acceptor lysine residues in the hinge region leads to a striking developmental phenotype in mice, characterized by inappropriate sonic hedgehog signaling and impaired endocrine tissue development (Lee et al., 2011a), our study shows that disruption of only one of these conserved SUMO sites in LRH-1 has a significant impact on adult homeostasis and protects against the development of a chronic disease. Surprisingly, SUMOylation of the homologous motif in RORα seems to activate instead of repressing its transcriptional activity (Hwang et al., 2009); however, its physiological properties have not been reported. These studies collectively indicate that SUMOylation of the hinge region has profound functional consequences among a very small subset of NRs.

The mechanistic features by which SUMO modulates the activity of NRs vary considerably and can range from interference with- to promotion of protein-protein interactions or alternatively competition with other PTMs (Geiss-Friedlander and Melchior, 2007; Jentsch and Psakhye, 2013). Our data suggest a role for LRH-1 SUMOylation in promoting protein-protein interactions. This finding is in line with previous studies showing that SUMOylation of LRH-1 K224, the human lysine residue corresponding to mouse LRH-1 K289, binds to a transcriptional corepressor complex consisting of NCOR1, HDAC3, and GPS2 and regulates the expression of acute phase response genes in human hepatoma cells (Venteclef et al., 2010). Interestingly, this study further demonstrated that mouse LRH-1 binding to the *haptoglobin* promoter was reduced in *Sumo1* knockout in comparison to WT livers. In our study, we reveal an unanticipated mechanism by demonstrating that LRH-1 K289R fails to bind another corepressor (i.e., PROX1), and we furthermore show that this impacts on the RCT genes, ultimately leading to enhanced bile flow and atheroprotection. The study by Venteclef et al. (2010), along with our work, propose that SUMOylation of a single K residue of LRH-1 promotes the recruitment of specific corepressor complexes. Importantly, our data demonstrate that the effect of LRH-1 SUMOylation depends on tissue-specific corepressor interaction.

The physiological stimuli and timing that affect LRH-1 SUMOylation in the liver are unknown. In primary granulosa cells, SUMO-driven sequestration of LRH-1 into nuclear bodies is abruptly reversed by cAMP and results in the induction of LRH-1 target genes (Yang et al., 2009). Intriguingly, this is accompanied by a robust reduction of the *Ubc9* and *Pias3* genes, which are part of the SUMO conjugation machinery. Conversely, expression of the SUMO-specific isopeptidase *Senp2* was increased. Although the crosstalk with the cAMP signaling has not been evaluated in the context of LRH-1 SUMOylation in liver cells, it is tempting to speculate that different physiological and/or pharmacological cues could trigger specific posttranslational modifications in LRH-1, which in turn could recruit specific corepressor complexes.

Several studies have identified natural or synthetic LRH-1 activators and inhibitors (Ingraham and Redinbo, 2005). A recent study has identified the unusual phospholipid dilauroyl phosphatidylcholine as an LRH-1 ligand (Lee et al., 2011b). Future studies should test whether ligand activation, posttranslational modifications such as SUMOylation, and coregulator recruitment are interconnected. The tissue and context-specific nature of such effects may offer an ideal therapeutic window for activating a receptor and exploit beneficial effects, without causing adverse effects that are common with NR therapeutics (Marciano et al., 2014). In this context, it is important to point out that the biological effects of LRH-1 K289R cannot be compared to those induced by a gain-of-function of LRH-1 or by a potential drug that would enhance the activity of LRH-1 in a broader manner. In fact, the *Lrh-1 K289R* mice show increased activation of selected LRH-1 target genes, whereas other targets are not affected. The *Lrh-1 K289R* mice also seem to display no effects on RCT in the gut, most likely because LRH-1 and PROX-1 are not coexpressed in the same cells of the crypt-villus epithelium (Botrugno et al., 2004) or because of the low abundance of PROX-1 in the intestinal mucosa (Figure 6C). Likewise, no changes on *Scarb1* gene expression could be detected in macrophages (Figure S4E). Such a restriction of the effects of LRH-1

to selected tissues—in this case, the liver—and a subset of target genes, may be the key to drive only antiatherogenic effects of LRH-1. A better understanding into how SUMOylation of LRH-1 and ensuing coregulator recruitment can be modulated will be instrumental and may provide opportunities for pharmacological intervention to combat common diseases, such as atherosclerosis.

EXPERIMENTAL PROCEDURES

Animal Studies

The generation of the *Lrh-1 K289R* mouse model is described in detail in the Supplemental Experimental Procedures. Congenic C57Bl/6J *Lrh-1 WT* or *Lrh-1 K289R* mice were crossbred with congenic C57Bl/6J *Ldlr* knockout mice in order to generate $Ldlr^{-/-}$ *Lrh-1 WT* (LL-WT) or $Ldlr^{-/-}$ *Lrh-1 K289R* (LL-K289R) mice. LL-WT and LL-K289R mice were kept on an HCD (1.25% total cholesterol, Harlan TD.94059) for 14 weeks starting at the age of 8 weeks. Similarly, congenic C57Bl/6J $Lrh\text{-}1^{hep-/-}$ and $Lrh\text{-}1^{hep+/+}$ mice (Oosterveer et al., 2012) were crossbred with $Ldlr^{-/-}$ mice in order to generate $Ldlr^{-/-}$ $Lrh\text{-}1^{hep+/+}$ (Ld-WT) or $Ldlr^{-/-}$ $Lrh\text{-}1^{hep-/-}$ (Ld-LKO) mice and fed a HCD for 12 weeks. All animal procedures were approved by the Swiss authorities (Canton of Vaud, animal protocols ID #2561 and #2768) and performed in accordance with our institutional guidelines.

Site-directed mutagenesis, subcellular fractionation of liver tissue, immunoprecipitation (IP), Coimmunoprecipitation (CoIP), and western blotting are explained in the Supplemental Experimental Procedures.

Protein Alignment

All protein alignments were performed with the standard Geneious (Blosum62 matrix) or ClustalW (BLOSUM matrix) algorithm from the Geneious software (http://www.geneious.com).

Gene Expression and Analysis

RNA was extracted from the livers and jejunums of ad libitum fed Lrh-1 WT (n = 7) and Lrh-1 K289R (n = 7) mice and from liver of ad libitum fed Lrh-$1hep^{+/+}$ (n = 8) and Lrh-$1hep^{-/-}$ (n = 8) mice with TRIZOL (Invitrogen) and purified with the RNeasy Cleanup Kit for Microarray Analysis (QIAGEN). For quantitative RT-PCR (qRT-PCR), cDNA was generated with the QuantiTect Reverse Transcription Kit (QIAGEN) and analyzed by qPCR with a LightCycler 480 Real-Time PCR System (Roche), and the primers are listed in the Table S2. Expression data were normalized to *36B4* or *B2M* mRNA levels. Microarray analysis was performed with the Affymetrix MouseGene 1.0 ST or Affymetrix MouseGene 2.0 ST array and normalized with the robust multiarray average method. A table of reciprocally regulated transcripts is provided in Table S1. Venn diagram analysis and heatmaps were performed with GENE-E (http://www.broadinstitute.org/cancer/software/GENE-E/index.html). For the Venn diagram, the overlap of nominally significantly changed genes ($p < 0.05$ and fold change ≥ 1.5) among the groups was analyzed.

Chromatin Immunoprecipitation

ChIP analysis was performed as described previously with minor modifications (Duggavathi et al., 2008). DNA was purified with the PCR Clean-up extraction kit (Macherey-Nagel), after which qPCR was performed as described previously (Mataki et al., 2007). Data were normalized to the input (fold differences = $2^{-(Ct\ sample\ -\ Ct\ input)}$). ChIP primer sequences are listed in Table S3.

Lipoprotein Separation

Pooled plasma samples were subjected to fast protein liquid chromatography gel filtration with a Superose 6 Column (GE Healthcare). Individual fractions were assayed for cholesterol and triglyceride concentrations with commercially available enzymatic assays (Roche).

Hepatic Lipid Analyses

Hepatic lipids were extracted according to the Bligh and Dyer (1959) protocol. Triglyceride and cholesterol contents in plasma and hepatic lipid fractions were quantified with enzymatic assays (Roche).

Cholesterol Uptake and LPS Stimulation of Peritoneal Macrophages

Thioglycolate-elicited peritoneal macrophages were harvested, cultured, and starved in vitro and then loaded with 50 μg/ml Dil-labeled acetylated LDL for 4 hr in order to assess the cholesterol uptake or 10 ng/ml LPS for 4 hr in order to analyze the expression of inflammatory markers.

Reverse Cholesterol Transport

RCT protocol was adapted from Meissner et al. (2010). In brief, thioglycolate-elicited mouse peritoneal macrophages were harvested, cultured in vitro, loaded with 50 μg/ml acetylated LDL and 3 μCi/ml 3H-cholesterol for 24 hr, and equilibrated in RPMI 1640 medium containing 1% penicillin/streptomycin and 0.2% BSA for 6 hr. For in vivo RCT, two million labeled LL-WT macrophages were injected intraperitoneally into recipient LL-WT or LL-K289R mice. Mice were sacrificed 48 hr postinjection, and plasma, liver, gallbladder, and feces were stored at −80°C until further analysis. Counts within liver were determined after the solubilization of the tissue. Fecal samples were dried, weighed, and thoroughly ground. Then, aliquots were separated into bile acid and neutral sterol fractions prior to liquid scintillation counting.

Bile Flow and Bile Composition

Bile duct cannulation was performed as described previously (Kruit et al., 2005) with LL-WT and LL-K289R mice. In brief, hepatic bile was collected for 30 min from the common bile duct via cannulation of the gallbladder, and bile flow was determined gravimetrically assuming a density of 1 g/ml for bile. Bile composition was analyzed by high performance liquid chromatography (HPLC) tandem mass spectrometry as described previously (Mataki et al., 2007).

Primary Cell Culture

Primary hepatocytes from hepatocyte-specific $Lrh\text{-}1^{hep-/-}$ mice were isolated with Liberase Blendzyme (Roche) perfusion as described previously with minor modifications (Ryu et al., 2011). $Lrh\text{-}1^{hep-/-}$ hepatocytes were plated in Dulbecco's modified Eagle's medium 4.5 g/l glucose with 10% fetal bovine serum. Cells were infected with an adenovirus expressing LRH-1 WT or LRH-1 K289R 4 hr after plating followed by transfection of a Prox1 plasmid with Lipofectamine 2000 (Invitrogen). Cells were lysed 48 hr postinfection and used for subsequent analysis.

Reporter Assays

Transient transfections in HEK293T cells were performed with Lipofectamine 2000 (Invitrogen) or JetPEI (Polyplus) as previously described (Oosterveer et al., 2012). In brief, cells were transfected with pTK-GL3 reporter constructs driven by a heterologous promoter consisting of multiple consensus LRH-1 response elements (pGL3::$(LRHRE)_5$-TK-LUC) in the presence of either pCMX::LRH-1 WT or the KR mutant constructs. Luciferase activities were measured 24 hr posttransfection and normalized to β-galactosidase activities.

Immunohistochemistry

En face plaque analysis was performed on thoraco-abdominal aortae that were fixed with 10% paraformaldehyde overnight and then stained with Oil-Red O (Stein et al., 2010). Aortic sinuses were cut into 5-μm-thick serial cryosections and stained with Sirius Red in order to measure necrotic core size, cap thickness, and collagen content (Stein et al., 2010). Means were taken from n = 6 mice per genotype, and three serial cryosections were evaluated from each mouse.

Statistical Analyses

Data are expressed as means ± SEM. Analysis of en face atherosclerotic plaque content and bile excretion rates was carried out with Mann-Whitney U tests. Comparison of differences between two groups of other experiments was assessed with unpaired two-tailed Student's t tests. Multiple group comparisons were assessed by one-way ANOVA and Bonferonni post hoc tests. $p < 0.05$ was considered statistically significant (*$p < 0.05$, **$p < 0.01$, ***$p < 0.001$).

ACCESSION NUMBERS

All microarray data are accessible at the NCBI Gene Expression Omnibus under number GSE59333.

SUPPLEMENTAL INFORMATION

Supplemental Information contains Supplemental Experimental Procedures, six figures, and three tables and can be found with this article online at http://dx.doi.org/10.1016/j.cmet.2014.07.023.

AUTHOR CONTRIBUTIONS

S.S. carried out most of the experiments, data analysis, and prepared the figures and the manuscript. M.H.O. and R.H. performed lipoprotein analysis and the bile cannulation experiment. C.M. made the initial mutant LRH-1 constructs and carried out reporter assays. P.X. helped with qPCR, stainings, and CoIP experiments. V.L. and A.P. helped with lipid extractions and macrophage isolation. D.R. assisted with the generation of adenoviral constructs. K.J.M. helped with the isolation of primary hepatocytes. X.W. helped with microarray and bioinformatic analyses. C.D. and F.M. helped with SUMOylation assays. S.M.H. performed HPLC analysis of the bile. K.S. designed the experiments and supervised all aspects of the work.

ACKNOWLEDGMENTS

We thank S. Bichet, N. Moullan, and T. Clerc for technical help and Xavier Warot and the Institut Clinique de la Souris for the generation of the LRH-1 K289R mouse. The pcDNA3.1-FLAG::Prox1 plasmid was kindly provided by Panagiotis Politis. This study was supported by EPFL funding and grants from the Swiss Heart Foundation and the Swiss Cancer League (KLS-2809-08-2011). S.S. is supported by a postdoctoral fellowship from the German Academy of Sciences Leopoldina (LPDS 2011-6).

Received: March 4, 2014
Revised: June 12, 2014
Accepted: July 24, 2014
Published: August 28, 2014

REFERENCES

Bernier-Villamor, V., Sampson, D.A., Matunis, M.J., and Lima, C.D. (2002). Structural basis for E2-mediated SUMO conjugation revealed by a complex between ubiquitin-conjugating enzyme Ubc9 and RanGAP1. Cell *108*, 345–356.

Bligh, E.G., and Dyer, W.J. (1959). A rapid method of total lipid extraction and purification. Can. J. Biochem. Physiol. *37*, 911–917.

Botrugno, O.A., Fayard, E., Annicotte, J.S., Haby, C., Brennan, T., Wendling, O., Tanaka, T., Kodama, T., Thomas, W., Auwerx, J., and Schoonjans, K. (2004). Synergy between LRH-1 and beta-catenin induces G1 cyclin-mediated cell proliferation. Mol. Cell *15*, 499–509.

Chalkiadaki, A., and Talianidis, I. (2005). SUMO-dependent compartmentalization in promyelocytic leukemia protein nuclear bodies prevents the access of LRH-1 to chromatin. Mol. Cell. Biol. *25*, 5095–5105.

Coste, A., Dubuquoy, L., Barnouin, R., Annicotte, J.S., Magnier, B., Notti, M., Corazza, N., Antal, M.C., Metzger, D., Desreumaux, P., et al. (2007). LRH-1-mediated glucocorticoid synthesis in enterocytes protects against inflammatory bowel disease. Proc. Natl. Acad. Sci. USA *104*, 13098–13103.

Duggavathi, R., Volle, D.H., Mataki, C., Antal, M.C., Messaddeq, N., Auwerx, J., Murphy, B.D., and Schoonjans, K. (2008). Liver receptor homolog 1 is essential for ovulation. Genes Dev. *22*, 1871–1876.

Fayard, E., Schoonjans, K., Annicotte, J.S., and Auwerx, J. (2003). Liver receptor homolog 1 controls the expression of carboxyl ester lipase. J. Biol. Chem. *278*, 35725–35731.

Fayard, E., Auwerx, J., and Schoonjans, K. (2004). LRH-1: an orphan nuclear receptor involved in development, metabolism and steroidogenesis. Trends Cell Biol. *14*, 250–260.

Fernandez-Marcos, P.J., Auwerx, J., and Schoonjans, K. (2011). Emerging actions of the nuclear receptor LRH-1 in the gut. Biochim. Biophys. Acta *1812*, 947–955.

Freeman, L.A., Kennedy, A., Wu, J., Bark, S., Remaley, A.T., Santamarina-Fojo, S., and Brewer, H.B., Jr. (2004). The orphan nuclear receptor LRH-1 activates the ABCG5/ABCG8 intergenic promoter. J. Lipid Res. *45*, 1197–1206.

Geiss-Friedlander, R., and Melchior, F. (2007). Concepts in sumoylation: a decade on. Nat. Rev. Mol. Cell Biol. *8*, 947–956.

Goodwin, B., Jones, S.A., Price, R.R., Watson, M.A., McKee, D.D., Moore, L.B., Galardi, C., Wilson, J.G., Lewis, M.C., Roth, M.E., et al. (2000). A regulatory cascade of the nuclear receptors FXR, SHP-1, and LRH-1 represses bile acid biosynthesis. Mol. Cell *6*, 517–526.

Hwang, E.J., Lee, J.M., Jeong, J., Park, J.H., Yang, Y., Lim, J.S., Kim, J.H., Baek, S.H., and Kim, K.I. (2009). SUMOylation of RORalpha potentiates transcriptional activation function. Biochem. Biophys. Res. Commun. *378*, 513–517.

Ingraham, H.A., and Redinbo, M.R. (2005). Orphan nuclear receptors adopted by crystallography. Curr. Opin. Struct. Biol. *15*, 708–715.

Jentsch, S., and Psakhye, I. (2013). Control of nuclear activities by substrate-selective and protein-group SUMOylation. Annu. Rev. Genet. *47*, 167–186.

Krasowski, M.D., Reschly, E.J., and Ekins, S. (2008). Intrinsic disorder in nuclear hormone receptors. J. Proteome Res. *7*, 4359–4372.

Kruit, J.K., Plösch, T., Havinga, R., Boverhof, R., Groot, P.H., Groen, A.K., and Kuipers, F. (2005). Increased fecal neutral sterol loss upon liver X receptor activation is independent of biliary sterol secretion in mice. Gastroenterology *128*, 147–156.

Lee, Y.K., and Moore, D.D. (2002). Dual mechanisms for repression of the monomeric orphan receptor liver receptor homologous protein-1 by the orphan small heterodimer partner. J. Biol. Chem. *277*, 2463–2467.

Lee, Y.K., and Moore, D.D. (2008). Liver receptor homolog-1, an emerging metabolic modulator. Front. Biosci. *13*, 5950–5958.

Lee, M.B., Lebedeva, L.A., Suzawa, M., Wadekar, S.A., Desclozeaux, M., and Ingraham, H.A. (2005). The DEAD-box protein DP103 (Ddx20 or Gemin-3) represses orphan nuclear receptor activity via SUMO modification. Mol. Cell. Biol. *25*, 1879–1890.

Lee, F.Y., Faivre, E.J., Suzawa, M., Lontok, E., Ebert, D., Cai, F., Belsham, D.D., and Ingraham, H.A. (2011a). Eliminating SF-1 (NR5A1) sumoylation in vivo results in ectopic hedgehog signaling and disruption of endocrine development. Dev. Cell *21*, 315–327.

Lee, J.M., Lee, Y.K., Mamrosh, J.L., Busby, S.A., Griffin, P.R., Pathak, M.C., Ortlund, E.A., and Moore, D.D. (2011b). A nuclear-receptor-dependent phosphatidylcholine pathway with antidiabetic effects. Nature *474*, 506–510.

Lu, T.T., Makishima, M., Repa, J.J., Schoonjans, K., Kerr, T.A., Auwerx, J., and Mangelsdorf, D.J. (2000). Molecular basis for feedback regulation of bile acid synthesis by nuclear receptors. Mol. Cell *6*, 507–515.

Marciano, D.P., Chang, M.R., Corzo, C.A., Goswami, D., Lam, V.Q., Pascal, B.D., and Griffin, P.R. (2014). The therapeutic potential of nuclear receptor modulators for treatment of metabolic disorders: PPARγ, RORs, and Rev-erbs. Cell Metab. *19*, 193–208.

Mataki, C., Magnier, B.C., Houten, S.M., Annicotte, J.S., Argmann, C., Thomas, C., Overmars, H., Kulik, W., Metzger, D., Auwerx, J., and Schoonjans, K. (2007). Compromised intestinal lipid absorption in mice with a liver-specific deficiency of liver receptor homolog 1. Mol. Cell. Biol. *27*, 8330–8339.

Meissner, M., Nijstad, N., Kuipers, F., and Tietge, U.J. (2010). Voluntary exercise increases cholesterol efflux but not macrophage reverse cholesterol transport in vivo in mice. Nutr. Metab. (Lond) *7*, 54.

Oosterveer, M.H., Mataki, C., Yamamoto, H., Harach, T., Moullan, N., van Dijk, T.H., Ayuso, E., Bosch, F., Postic, C., Groen, A.K., et al. (2012). LRH-1-dependent glucose sensing determines intermediary metabolism in liver. J. Clin. Invest. *122*, 2817–2826.

Out, C., Hageman, J., Bloks, V.W., Gerrits, H., Sollewijn Gelpke, M.D., Bos, T., Havinga, R., Smit, M.J., Kuipers, F., and Groen, A.K. (2011). Liver receptor homolog-1 is critical for adequate up-regulation of Cyp7a1 gene transcription and bile salt synthesis during bile salt sequestration. Hepatology *53*, 2075–2085.

Qin, J., Gao, D.M., Jiang, Q.F., Zhou, Q., Kong, Y.Y., Wang, Y., and Xie, Y.H. (2004). Prospero-related homeobox (Prox1) is a corepressor of human liver

receptor homolog-1 and suppresses the transcription of the cholesterol 7-alpha-hydroxylase gene. Mol. Endocrinol. *18*, 2424–2439.

Rosenson, R.S., Brewer, H.B., Jr., Davidson, W.S., Fayad, Z.A., Fuster, V., Goldstein, J., Hellerstein, M., Jiang, X.C., Phillips, M.C., Rader, D.J., et al. (2012). Cholesterol efflux and atheroprotection: advancing the concept of reverse cholesterol transport. Circulation *125*, 1905–1919.

Ryu, D., Seo, W.Y., Yoon, Y.S., Kim, Y.N., Kim, S.S., Kim, H.J., Park, T.S., Choi, C.S., and Koo, S.H. (2011). Endoplasmic reticulum stress promotes LIPIN2-dependent hepatic insulin resistance. Diabetes *60*, 1072–1081.

Schoonjans, K., Annicotte, J.S., Huby, T., Botrugno, O.A., Fayard, E., Ueda, Y., Chapman, J., and Auwerx, J. (2002). Liver receptor homolog 1 controls the expression of the scavenger receptor class B type I. EMBO Rep. *3*, 1181–1187.

Stein, S., Lohmann, C., Schäfer, N., Hofmann, J., Rohrer, L., Besler, C., Rothgiesser, K.M., Becher, B., Hottiger, M.O., Borén, J., et al. (2010). SIRT1 decreases Lox-1-mediated foam cell formation in atherogenesis. Eur. Heart J. *31*, 2301–2309.

Talamillo, A., Herboso, L., Pirone, L., Pérez, C., González, M., Sánchez, J., Mayor, U., Lopitz-Otsoa, F., Rodriguez, M.S., Sutherland, J.D., and Barrio, R. (2013). Scavenger receptors mediate the role of SUMO and Ftz-f1 in Drosophila steroidogenesis. PLoS Genet. *9*, e1003473.

Treuter, E., and Venteclef, N. (2011). Transcriptional control of metabolic and inflammatory pathways by nuclear receptor SUMOylation. Biochim. Biophys. Acta *1812*, 909–918.

Venteclef, N., Haroniti, A., Tousaint, J.J., Talianidis, I., and Delerive, P. (2008). Regulation of anti-atherogenic apolipoprotein M gene expression by the orphan nuclear receptor LRH-1. J. Biol. Chem. *283*, 3694–3701.

Venteclef, N., Jakobsson, T., Ehrlund, A., Damdimopoulos, A., Mikkonen, L., Ellis, E., Nilsson, L.M., Parini, P., Jänne, O.A., Gustafsson, J.A., et al. (2010). GPS2-dependent corepressor/SUMO pathways govern anti-inflammatory actions of LRH-1 and LXRbeta in the hepatic acute phase response. Genes Dev. *24*, 381–395.

Ward, J.D., Bojanala, N., Bernal, T., Ashrafi, K., Asahina, M., and Yamamoto, K.R. (2013). Sumoylated NHR-25/NR5A regulates cell fate during C. elegans vulval development. PLoS Genet. *9*, e1003992.

Weber, C., and Noels, H. (2011). Atherosclerosis: current pathogenesis and therapeutic options. Nat. Med. *17*, 1410–1422.

Yang, F.M., Pan, C.T., Tsai, H.M., Chiu, T.W., Wu, M.L., and Hu, M.C. (2009). Liver receptor homolog-1 localization in the nuclear body is regulated by sumoylation and cAMP signaling in rat granulosa cells. FEBS J. *276*, 425–436.

Available online at www.sciencedirect.com

ScienceDirect

Current Opinion in Cell Biology

Molecular basis for the regulation of the nuclear receptor LRH-1

Sokrates Stein and Kristina Schoonjans

Liver receptor homolog-1 (LRH-1) is a nuclear receptor (NR) with diverse functions in development, differentiation and metabolism and has been extensively studied in the enterohepatic system. While initially described as an orphan NR, recent studies suggest that specific phospholipids act as endogenous LRH-1 ligands. Although binding of ligands may enhance its transcriptional activation, posttranslational modifications (PTMs) and binding of coregulators and other NRs have emerged as mechanisms to fine-tune the selective regulation of LRH-1 target genes. In this review article, we will discuss how LRH-1 is regulated by PTMs and binding of ligands and coregulators, and explain some metabolic consequences with a special focus on liver physiology.

Addresses
Metabolic Signaling, Institute of Bioengineering, Ecole Polytechnique Fédérale de Lausanne, SV IBI GR-SCH, Station 15, CH-1015 Lausanne, Switzerland

Corresponding author: Schoonjans, Kristina (kristina.schoonjans@epfl.ch)

Current Opinion in Cell Biology 2015, **33**:26–34

This review comes from a themed issue on **Cell regulation**

Edited by **Johan Auwerx** and **Jodi Nunnari**

http://dx.doi.org/10.1016/j.ceb.2014.10.007

Introduction

Liver receptor homolog-1 (LRH-1, also known as nuclear receptor subfamily 5 group A member 2 (Nr5a2), fushi tarazu factor I (FTZ-F1), α-fetoprotein transcription factor (FTF), pancreas homolog receptor 1 (PHR-1), human B1-binding factor (hB1F), and Cyp7A promoter-binding factor (CPF)) is a member of the NR5A subfamily of nuclear receptors (NRs) that was first identified in an evolutionary tree analysis of the *Drosophila* Ftz-F1 NR group [1]. LRH-1 is mainly expressed in exocrine pancreas, ovaries, and tissues of the enterohepatic axis and has diverse functions in development, differentiation and metabolism (Figure 1) [2–4]. In the ovaries LRH-1 regulates steroid synthesis and ovulation [5–12], and is crucial during mouse gestation [13•]. LRH-1 also affects ovarian follicle maturation and fertility through its actions in the hypothalamus [14•]. In the pancreas, LRH-1 is critically required for adequate production and secretion of the pancreatic digestive juice [15,16].

LRH-1 has been tightly linked with cell proliferation [17–19], local immune homeostasis [20,21] and cancer [17,22,23]. The recent identification of LRH-1 in the control of stemness [24,25••,26,27] may furthermore provide new insights that could be directly relevant to understand the protumorigenic actions of LRH-1.

The role of LRH-1 has been extensively characterized in the liver. In this review we will focus on the multiple factors that regulate the transcriptional activity of LRH-1, such as potential ligands, posttranslational modifications and binding of coregulators. These multiple modes of regulation will be discussed in the context of the emerging actions of LRH-1 in liver physiology.

Orphan or adopted?

LRH-1 was originally classified as an orphan NR based on its constitutive activity and the lack of known endogenous ligand. This simple view has been in part revisited with the structures of mouse and human LRH-1 LBD proteins. These studies revealed that different phospholipid species, including phosphatidyl glycerol, phosphatidyl ethanolamine and phosphatidyl choline, as well as the second messengers phosphatidyl inositols, can bind to the large ligand binding pocket of human LRH-1, but much less to mouse LRH-1 [28,29]. A cluster of non-conserved residues in the human LBD seems to be essential for proper binding of phospholipids [28]. Moreover, while structural modifications of the ligand-binding pocket do not affect the transcriptional activity of mouse LRH-1 [30], F342W I416W mutations at the LBD of human LRH-1 markedly reduce binding of specific phospholipid species, which in turn hinders the recruitment of coactivators and diminishes the transcriptional potential of LRH-1 [31]. Together these structural studies reveal important species differences, which may reflect differences in constitutive activity. Of interest, recent studies identified the phospholipid dilauroyl phosphatidylcholine (DLPC) as a potent ligand of human and mouse LRH-1 *in vitro*, and showed that LRH-1 is required to mediate the antidiabetic effects of DLPC in two independent mouse models of diabesity [32••,33•]. In line with previously established functions of LRH-1 [34,35], DLPC treatment of hepatocytes induced the expression of genes involved in bile acid synthesis, further supporting the notion that DLPC can induce LRH-1 activity. Taken together, these structural and functional studies

Figure 1

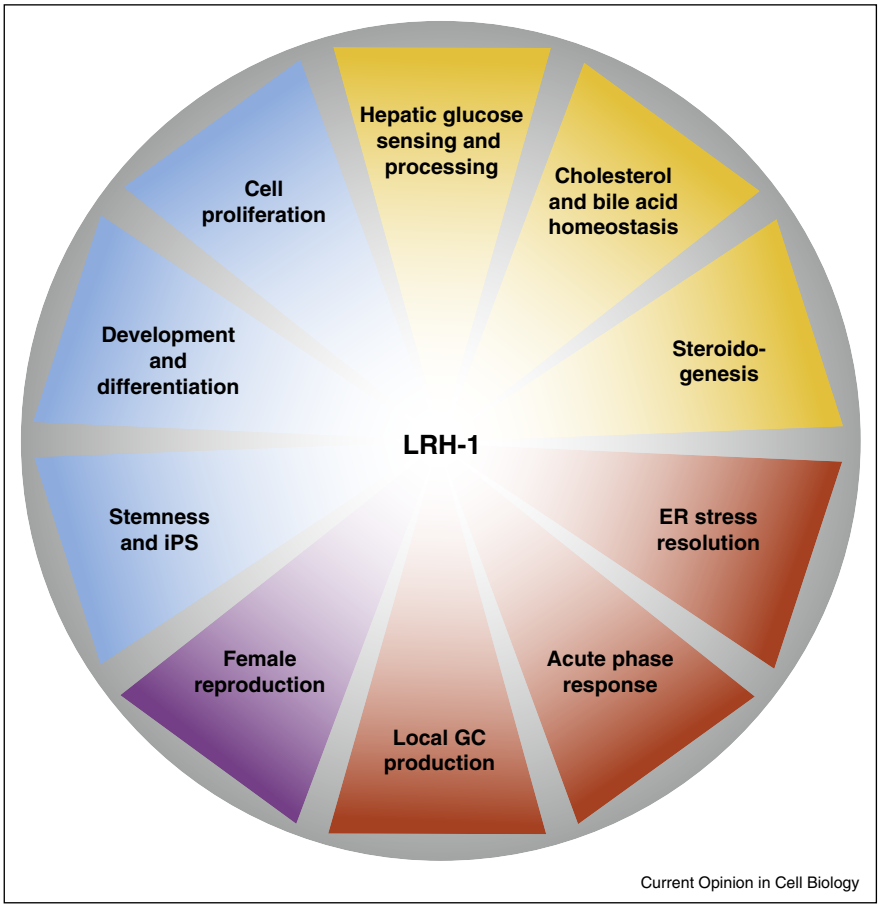

Overview of the diverse functions of LRH-1. Yellow shading, metabolic processes; red shading, adaptive stress responses; violet shading, female reproduction; blue shading, stemness, development and proliferation.

suggest that albeit LRH-1 can be active in the absence of ligand, specific phospholipid binding can further enhance its transcriptional activity.

Posttranslational regulation

Most NR are also targeted by different PTMs, including phosphorylation, acetylation, ubiquitination, and SUMOylation. Phosphorylation of the serine residues S238 and S243 in the hinge region of the human LRH-1 protein by the mitogen-activated protein kinase ERK1/2 has been shown to enhance its activity [36]. Another study suggests that LRH-1 is acetylated in the basal state and is bound by the small heterodimer partner (SHP)-sirtuin 1 (SIRT1) transrepressive complex. What is driving the acetylation and deacetylation of LRH-1 is not established, yet its acetylation status is surprisingly not modulated by SIRT1 [37]. It will be interesting to further establish the functional relevance and metabolic consequences of both PTMs in cellular and animal models.

Reversible covalent modification by small ubiquitin-like modifier-1 (SUMO-1) protein, or SUMOylation, has been extensively studied [38]. LRH-1 is targeted for SUMOylation by E3-SUMO ligases at both conserved and distinct lysine residues in different species, and reduces its transcriptional activity [39,40,41•,42,43•]. Different mechanisms have been proposed to explain how this transcriptional attenuation is achieved. Using different bioimaging techniques, it was shown that SUMOylation of LRH-1 translocates the transcription factor from the chromatin to promyelocytic leukemia protein (PML) nuclear bodies and prevents it from being transcriptionally active. Conversely, de-SUMOylation of the protein releases it from PML bodies and allows it to induce the expression of target genes [40]. Localization of SUMOylated LRH-1 to nuclear bodies can furthermore be suppressed by forskolin and cholera toxin treatment in rat primary granulosa cells, suggesting that cAMP signaling can modulate the SUMOylation status of LRH-1 and its localization to nuclear bodies [44].

Other studies suggest that the SUMOylation of LRH-1 affects the recruitment of co-regulators, which in turn modulates the expression of its target genes. This model has been described for two different corepressors of LRH-1. SUMOylation of LRH-1 was reported to stabilize a transcriptional corepressor complex comprised of the nuclear receptor corepressor 1 (NCOR1) and histone deacetylase 3 (HDAC3). The interaction of SUMOylated LRH-1 with this corepressor complex is mediated by the G protein pathway suppressor 2 (GPS2), and regulates the induction of several acute phase response proteins [41•]. Recent data from our own group suggest that another corepressor, prospero-related homeobox 1 (PROX1), is recruited to SUMOylated LRH-1 and transrepresses specific gene programs. Using non-SUMOylatable LRH-1 K289R knock-in mice on an atherosclerotic background, we could further demonstrate that loss of LRH-1 SUMOylation leads to increased expression of genes regulating reverse cholesterol transport (RCT) and enhanced RCT *in vivo* (Figure 2), hence culminating in the protection against the development of atherosclerosis [45••]. Another study performed in *Drosophila* demonstrated that SUMOylation of its LRH-1 homologue, Ftz-f1, impacts the metamorphosis process from larval to pupal transition by modulating the expression of the scavenger receptor *Snmp1*, which is required for proper lipid homeostasis in steroidogenic tissues [43•]. This is reminiscent to the regulation of *scavenger receptor B1* (*Scarb1*) by LRH-1 in mouse liver [45••,46]. These studies suggest that the role of SUMOylated LRH-1 in cholesterol and lipid homeostasis might be evolutionary conserved.

SUMOylation of LRH-1 also plays an important role in the generation of induced pluripotent stem cells (iPS) [25••]. The four common factors that are used to induce iPS are OCT4, SOX2, KLF4, and c-MYC [47]. Interestingly, LRH-1 can be used to replace OCT4, and SUMOylation mutants of LRH-1 further enhance the reprogramming efficiency [25••], highlighting that this posttranslational modification affects diverse molecular functions of LRH-1.

Binding of co-regulators

NRs are not only modulated by ligand binding and PTMs, but also by coregulator recruitment. Several tissue-specific coactivators and corepressor can fine-tune the transcriptional activity of LRH-1 in a context specific manner. In the ovary, for example, LRH-1 function is regulated by the coactivator peroxisome proliferator-activated receptor gamma coactivator 1-alpha (PGC-1α) and the corepressor DAX-1 (NR0B1) [48]. In the liver, other

Figure 2

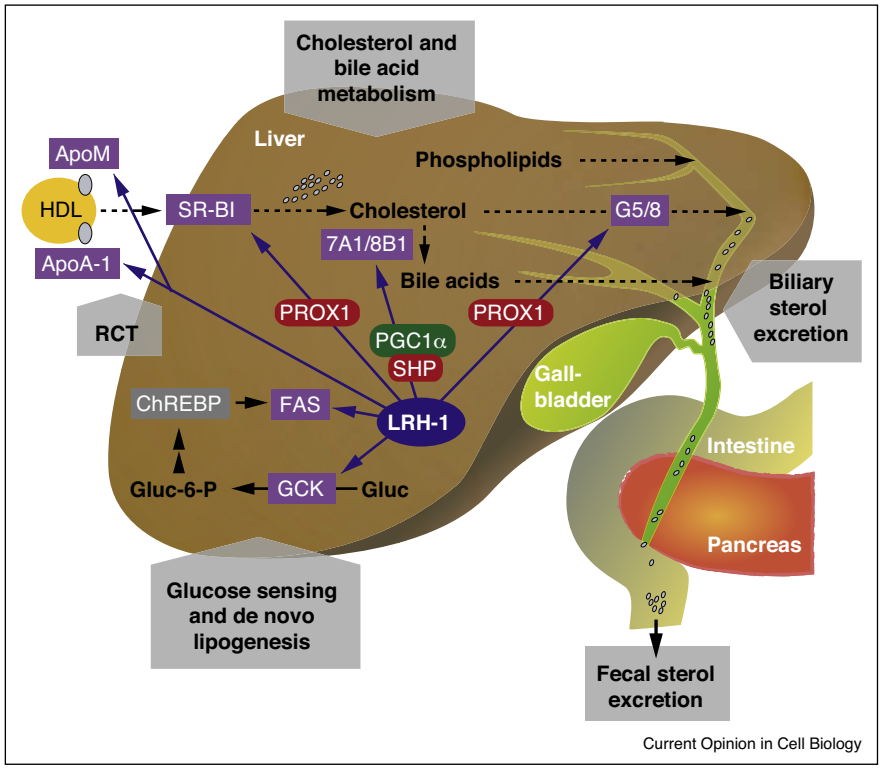

Scheme demonstrating the main hepatic functions of LRH-1 and the role of coregulators in target gene regulation. RCT, reverse cholesterol transport; HDL, high density lipoprotein; SR-BI, Scavenger receptor class B1; G5/G8, ABCG5/ABCG8; 7A1/8B1, CYP7A1/CYP8B1. Corepressors are illustrated in red, coactivators in green.

corepressors such as small heterodimer partner (SHP or NR0B2) and PROX1 as well as the NCOR1/HDAC3 corepressor complex can repress LRH-1 activity [34,35,41•,45••,49,50] (Figure 2). Importantly, as described in the previous section, several coregulators bind to domains whose structure has been changed by binding of ligands and/or PTMs. Whether the PTMs are crucial to initiate or maintain or simply facilitate the interaction has to be studied in more detail for each of the PTM and the affected coregulators.

SHP & DAX1

SHP (NR0B2) and DAX-1 (NR0B1) are closely related and atypical NRs that lack a typical DNA binding domain (DBD) and act as repressors of LRH-1 and SF-1. SHP binds to the C-terminal activation function (AF-2) domain of LRH-1 [31,50], reviewed in detail in [2,3]. Importantly, LRH-1 induces the expression of *Shp*, which in turn will reduce the transcriptional activity of LRH-1, thereby inhibiting its own expression in a negative feedback loop [34,35]. DAX-1 also represses the activity of LRH-1 by binding to its LBD [48,51,52]. Importantly, while *Shp* is primarily expressed in the liver, pancreas, stomach and heart, *Dax1* expression is mainly limited to embryonic stem cells, testis and ovary (see bioGPS.org). Therefore these proteins likely have the same repressive functions in different tissues.

NCOR1 & NCOR2

As described in detail above, SUMOylation of LRH-1 drives its interaction with a transcriptional corepressor complex consisting of NCOR1/HDAC3 via association with GPS2 [41•]. One of the consequences of this association is the transrepression of acute phase response proteins [53]. Another study showed that the close homologue of NCOR1, the silencing mediator for retinoic acid receptor and thyroid hormone receptor (SMRT, or NCOR2) also represses the transcriptional activity of LRH-1 in different cell lines [54]. However, the authors were not able to detect a direct interaction between LRH-1 and SMRT. Possibly, as for NCOR1, an associating protein such as GPS2 is necessary to bring these proteins into close proximity.

PROX1

The corepressor PROX1 binds to different LRH-1 domains in *Drosophila* and human cell lines [49,55], and similar to DAX1 and SHP, its expression is limited to few organs, such as the liver, heart and hippocampus (see bioGPS.org). Moreover, PROX1 is essential for lymphatic vessel development and maintenance [56,57]. Interaction studies demonstrated that PROX1 interacts with both the DNA binding domain (DBD) and the LBD of LRH-1 in different cell lines [49], or requires the entire LBD in *Drosophila* [55]. Although PROX1 seems to bind to different domains, its transrepressive potential affects similar metabolic pathways in the two organisms. The LRH-1/PROX1 interaction leads to the transrepression of different LRH-1 target genes, including *Cyp7a1* and *Shp*, which play a crucial role in the liver [49,55]. This is consistent with our own findings, showing that LRH-1/PROX1 interaction transrepresses the expression of genes regulating hepatic reverse cholesterol transport in mice [45••]. Importantly, since PROX1 is highly expressed in the liver, but not in intestinal fractions, only hepatic RCT regulators are affected by PROX1 transrepression [45••].

SRCs

The three homologous members of the steroid receptor co-activator (SRC) p160 family, SRC-1, SRC-2 and SRC-3, also act as strong LRH-1 regulators by binding to its LBD and potentiating its transcriptional activity [50,58]. For example, stimulation of rat primary granulosa cells with pregnant mare serum gonadotropin (PMSG) leads to the SRC-1/LRH-1 transactivation of the inhibin alpha-subunit gene, a gene that inhibits the release of follicle-stimulating hormone (FSH) [10]. In the transcriptional regulation of the *Cyp11a1* gene, SRC-1 and protein inhibitor of activated STAT (signal transducer and activator of transcription) y (PIASy) compete to bind LRH-1 [59]. While SRC-1 stimulates, PIASy transrepresses LRH-1-dependent Cyp11a1 promoter activation. Although PIASy is an E3 SUMO-ligase, its transrepressive function does not seem to result from changes in the LRH-1 SUMOylation status [59]. In another study that investigated the transcriptional regulation of the *Lrh-1* gene upon sphingosine-1-phosphate and prostaglandin E2 stimulation, it was shown that CCAAT/enhancer binding proteins δ (C/EBPδ) and the coactivators CREB-binding protein (CBP) and SRC-3 potentiate the interaction of cAMP response element binding protein (CREB) and LRH-1 [60].

PGC-1α

Peroxisome proliferator-activated receptor gamma (PPARγ) coactivator 1α (PGC-1α) has been described as an LRH-1 co-activator [48,61,62]. Binding of PGC-1α to the AF2 domain of LRH-1 stimulates *Cyp7a1* expression in the liver [61], *aromatase* (*Cyp19a1*) expression in the breast [62], and the expression of steroidogenesis genes in granulosa cells [48]. The PGC-1α-mediated transactivation of LRH-1 is blocked by binding of SHP in the liver or of DAX1 in granulosa cells [48,61].

Beta-catenin

In intestinal crypt cells β-catenin (CTNNB1) works synergistically with LRH-1 to activate the expression of cell cycle genes and promote proliferation [18]. LRH-1 drives the expression of *cyclin E1* (*Ccne1*), and this transcriptional effect is further augmented by β-catenin. Conversely, LRH-1 acts as a coactivator of β-catenin in the transcriptional regulation of *cyclin D1* (*Ccnd1*) [18], by direct binding of the β-catenin armadillo repeat to the LBD of LRH-1 [63].

MBF-1

Multiprotein bridging factor (MBF-1) is a transcriptional regulator that interacts with the *Drosophila* LRH-1 homologue Ftz-F1 as well as with human LRH-1 in mammalian cells [64,65]. Rather than acting as a direct co-activator, MBF-1 links LRH-1 to the transcriptional machinery through its interaction with the transcription factor IID (TFIID) complex [64].

Combinatorial regulation of NR target genes

Expression of the gene *Cyp7a1* encoding the rate-limiting enzyme of the bile acid biosynthesis pathway, is regulated by a regulatory cascade of NRs including the farnesoid X receptor (FXR or NR1H4), LRH-1, hepatic nuclear factor 4α (HNF4α or NR2A1) and SHP [34,35,66]. LRH-1 potentiates the expression of liver X receptors (LXRs) target genes, including *cholesteryl ester transfer protein* (*Cetp*) [67], *fatty acid synthase* (*Fas*) [68], and *ATP-binding cassette sub-family G member 5* and *8* (*Abcg5* and *Abcg8*) [69], suggesting that LRH-1 acts as a competence factor for LXR. Whether LRH-1 and FXR act in a similar fashion is an intriguing question. While one study reported that the combined activity of FXR and LRH-1 augments the expression of the FXR target genes *Shp*, *retinol dehydrogenase 9* (*Rdh9*), *pyruvate carboxylase* (*Pcx*), and *phosphatidylethanolamine N-methyltransferase* (*Pemt*) [70], another study showed that FXR mediates *Shp* expression by docking to an LRH-1 binding site independent of LRH-1 [71].

Hepatic functions of LRH-1

The liver plays a crucial role in different metabolic processes, ranging from glucose processing and production to cholesterol and bile acid homeostasis. Hepatocytes also exhibit immunoregulatory responses after various stress stimuli and its high capacity to synthesize and secrete proteins makes them also susceptible to ER stress. To illustrate the complexity of the regulatory circuits controlled by LRH-1, we will here describe how the above described mechanisms of LRH-1 regulation, including ligand activation, cofactor recruitment or SUMOylation, can impact on liver homeostasis. For coverage of its role in other tissues, we refer the interested reader to a series of other recent reviews [3,72].

Bile acid metabolism

The two key genes involved in bile acid synthesis, *Cyp7a1* and *Cyp8b1*, have been amongst the first LRH-1 target genes identified [73,74]. SHP and PGC-1α compete to bind to the AF2 domain of LRH-1 in the liver, and thus modulate the expression of both genes (Figure 2) [34,35,61]. Interestingly, liver-specific *Lrh-1* knockout mice have an altered composition of bile with basically no cholic acid and an increased amount of less amphipathic bile acids, such as muricholic acid and ursodeoxycholic acid, which is attributed to the dramatically reduced expression of *Cyp8b1*, but not *Cyp7a1* [75–77]. Importantly, this altered bile acid composition leads to a compromised intestinal lipid absorption and enhances the fecal excretion of lipids [75,77]. Besides regulating several enzymes involved in bile acid synthesis, LRH-1 also activates the transcription of the *bile salt export pump* (*Bsep*) in Huh7 cells, a transporter that drives the canalicular secretion of bile acids [78], highlighting its crucial role in bile acid homeostasis.

Reverse cholesterol transport

Reverse cholesterol transport is an anti-atherogenic process in which excessive cholesterol from peripheral tissues is transported to the liver and finally excreted via the bile. LRH-1 governs the expression of genes involved in this process [46,79–81]. Of interest, SUMOylation of LRH-1 promotes its interaction with PROX1 and leads to the transrepression of hepatic reverse cholesterol transport genes such as *Scarb1*, *Abcg5*, and *Abcg8* [45••] (Figure 2). The increased biliary sterol excretion and RCT observed in an atherosclerosis-prone non-SUMOylatable LRH-1 K289R mouse model, decreases the development of atherosclerosis [45••]. Moreover, LRH-1 regulates the expression of *Apoa1* and *Apom*, two proteins that associate with HDL and facilitate cholesterol clearance (Figure 2) [80,81]. These studies suggest that LRH-1 could be pharmacologically targeted to prevent atherosclerosis development, which is the primary cause of myocardial infarction and stroke in humans.

Glucose homeostasis

The function of LRH-1 in hepatic glucose sensing and intermediary metabolism has been studied in liver-specific *Lrh-1* knockout mice under postprandial conditions. These mice display reduced hepatic glucokinase and glycogen synthase fluxes as a consequence of reduced expression of glucokinase (GCK), a direct target gene of LRH-1 (Figure 2). This in turn leads to reduced availability of glucose-6-phosphate, an intermediate that acts as a substrate for the pathways that support glycogen synthesis, glycolysis, and *de novo* lipogenesis (DNL) and controls the nuclear translocation and activity of the glucose-responsive transcription factor ChREBP (Figure 2) [82•].

The role of LRH-1 in glucose management has also been studied in obese and diabetic mouse models. DLPC, a phospholipid that binds to and induces LRH-1 activity, improves glucose tolerance and insulin resistance without affecting the body weight in diet-induced or genetically obese and diabetic mice [32••]. Another study showed that the heterozygous *Lrh-1*+/− mice have a mild but significant increase in body weight when exposed to a high-fat diet, but conversely do not exhibit changes in glucose or insulin tolerance [83]. These studies suggest that receptor activation has more pronounced metabolic effects on glucose homeostasis than genetic haploinsufficiency of *Lrh-1*.

Table 1

List of some key studies that show endogenous and synthetic LRH-1 ligands, known posttranslational modifications (PTMs) and their effects, and binding of other transcription factors or coregulators.

Binding of	Specification	References
Ligands and drugs		
Endogenous ligands	Phospholipids and phosphatidyl inositols	[28,29]
	Dilauroyl phosphatidylcholine (DLPC)	[32••,33•]
Agonists	Small molecule agonists	[88,89]
Antagonists	Small molecule antagonists	[87•]
PTMs		
Phosphorylation	Phosphorylation of S238 and S243 of human LRH-1	[36]
Acetylation	Acetylation of LRH-1 at basal state	[37]
SUMOylation	SUMOylation of different lysines residues	[39,40,41•,42,43•]
	Regulation of SUMOylation of LRH-1 by adenylate cyclase activators	[44]
	Recruitment of NCOR1/HDAC3	[41•]
	Recruitment of PROX1	[45••]
	Drosophila lipid homeostasis and steroidogenesis	[43•]
	Induction of iPS cells	[25••]
Coregulators and other NRs		
Coactivators	PGC-1α	[48,61,62]
	SRCs	[10,50,58–60]
	Beta-catenin	[18,63]
Corepressors	DAX-1 (NR0B1)	[48,51,52]
	SHP (NR0B2)	[31,34,35,50]
	PROX1	[41•,45••,49,55]
	NCOR1 & NCOR2	[41•,54]
Bridging factor	MBF-1	[64,65]
Other NRs	FXRs	[34,35]
	LXRs	[67–69]

Hepatic acute phase response

Upon inflammatory stimuli due to injury, infection or chronic metabolic stress, immune cells secrete various cytokines into the bloodstream, which may activate the acute phase response in the liver. As described above, SUMOylation of hepatic LRH-1 leads to the recruitment of different co-repressors. Binding of SUMOylated LRH-1 to the NCOR1/HDAC3 complex via GPS2 mediates the transrepression of acute phase response genes [41•,84], and therefore modulates this hepatic response. Besides transrepressing APPs, LRH-1 induces the expression of interleukin-1 receptor antagonist (IL-1RA), an inhibitor of IL-1 signaling, thereby exerting additional anti-inflammatory roles in the liver [85].

ER stress

A recent study suggests that LRH-1 ameliorates hepatic ER stress resolution independent of the canonical unfolded protein response (UPR) pathways [86•]. The authors demonstrated that liver-specific *Lrh-1* knockout mice display a defective ER stress resolution due to reduced expression of *polo-like kinase 3* (*Plk3*), which phosphorylates activating transcription factor 2 (ATF2) and thus induces its stress response target genes. Importantly, ectopic restoration of Plk3 in liver-specific *Lrh-1* knockout mice restored phosphorylation of ATF2 and rescued ER stress resolution [86•].

Conclusion and perspective

The identification of small molecule agonists and antagonists as well as the discovery that specific phospholipid species act as endogenous agonists of LRH-1 [32••,87•,88,89], suggest that the receptor could be a *bona fide* druggable target (Table 1). Given the multiple functions of LRH-1 in different tissues it is not easy to speculate whether activation or inhibition of this transcription factor could provide therapeutic advantages. Although increased activation of LRH-1 could be beneficial to promote RCT and biliary cholesterol excretion to prevent atherosclerosis development [45••,80,81] or to treat diabetes [32••,33•], its activation on the other side could induce the expression of cell-cycle regulators that could facilitate cell proliferation and possibly promote cancer development [87•,90]. In this regard, the selective induction of transcriptional programs by SUMO modification of LRH-1 may offer interesting therapeutic perspectives that could dissociate these effects. Further studies however will be required to fully understand the exact function of LRH-1 and its post-translational modifications in the different organs to develop a targeted and safe approach that could be useful to treat metabolic disorders or cancer.

Acknowledgements

This study was supported by EPFL funding and grants from the Swiss Heart Foundation (SHF) and the Swiss Cancer League (KLS-2809-08-2011). S. Stein is supported by a postdoctoral fellowship from the German Academy of Sciences Leopoldina (LPDS 2011-6).

References and recommended reading

Papers of particular interest, published within the period of review, have been highlighted as:

- • of special interest
- •• of outstanding interest

1. Ikeda Y, Lala DS, Luo X, Kim E, Moisan MP, Parker KL: **Characterization of the mouse FTZ-F1 gene, which encodes a key regulator of steroid hydroxylase gene expression**. *Mol Endocrinol* 1993, **7**:852-860.

2. Fayard E, Auwerx J, Schoonjans K: **LRH-1: an orphan nuclear receptor involved in development, metabolism and steroidogenesis**. *Trends Cell Biol* 2004, **14**:250-260.

3. Lazarus KA, Wijayakumara D, Chand AL, Simpson ER, Clyne CD: **Therapeutic potential of Liver Receptor Homolog-1 modulators**. *J Steroid Biochem Mol Biol* 2012, **130**:138-146.

4. Lee YK, Moore DD: **Liver receptor homolog-1, an emerging metabolic modulator**. *Front Biosci* 2008, **13**:5950-5958.

5. Duggavathi R, Volle DH, Mataki C, Antal MC, Messaddeq N, Auwerx J, Murphy BD, Schoonjans K: **Liver receptor homolog 1 is essential for ovulation**. *Genes Dev* 2008, **22**:1871-1876.

6. Falender AE, Lanz R, Malenfant D, Belanger L, Richards JS: **Differential expression of steroidogenic factor-1 and FTF/LRH-1 in the rodent ovary**. *Endocrinology* 2003, **144**:3598-3610.

7. Kim JW, Havelock JC, Carr BR, Attia GR: **The orphan nuclear receptor, liver receptor homolog-1, regulates cholesterol side-chain cleavage cytochrome p450 enzyme in human granulosa cells**. *J Clin Endocrinol Metab* 2005, **90**:1678-1685.

8. Saxena D, Escamilla-Hernandez R, Little-Ihrig L, Zeleznik AJ: **Liver receptor homolog-1 and steroidogenic factor-1 have similar actions on rat granulosa cell steroidogenesis**. *Endocrinology* 2007, **148**:726-734.

9. Saxena D, Safi R, Little-Ihrig L, Zeleznik AJ: **Liver receptor homolog-1 stimulates the progesterone biosynthetic pathway during follicle-stimulating hormone-induced granulosa cell differentiation**. *Endocrinology* 2004, **145**:3821-3829.

10. Weck J, Mayo KE: **Switching of NR5A proteins associated with the inhibin alpha-subunit gene promoter after activation of the gene in granulosa cells**. *Mol Endocrinol* 2006, **20**:1090-1103.

11. Peng N, Kim JW, Rainey WE, Carr BR, Attia GR: **The role of the orphan nuclear receptor, liver receptor homologue-1, in the regulation of human corpus luteum 3beta-hydroxysteroid dehydrogenase type II**. *J Clin Endocrinol Metab* 2003, **88**:6020-6028.

12. Liu DL, Liu WZ, Li QL, Wang HM, Qian D, Treuter E, Zhu C: **Expression and functional analysis of liver receptor homologue 1 as a potential steroidogenic factor in rat ovary**. *Biol Reprod* 2003, **69**:508-517.

13. • Zhang C, Large MJ, Duggavathi R, DeMayo FJ, Lydon JP, Schoonjans K, Kovanci E, Murphy BD: **Liver receptor homolog-1 is essential for pregnancy**. *Nat Med* 2013, **19**:1061-1066.

This study demonstrates that LRH-1 plays an indispensible role during mouse gestation.

14. • Atkin SD, Owen BM, Bookout AL, Cravo RM, Lee C, Elias CF, Elmquist JK, Kliewer SA, Mangelsdorf DJ: **Nuclear receptor LRH-1 induces the reproductive neuropeptide kisspeptin in the hypothalamus**. *Mol Endocrinol* 2013, **27**:598-605.

This work shows that LRH-1 affects ovarian follicle maturation and fertility through its actions in the hypothalamus.

15. Fayard E, Schoonjans K, Annicotte JS, Auwerx J: **Liver receptor homolog 1 controls the expression of carboxyl ester lipase**. *J Biol Chem* 2003, **278**:35725-35731.

16. Holmstrom SR, Deering T, Swift GH, Poelwijk FJ, Mangelsdorf DJ, Kliewer SA, MacDonald RJ: **LRH-1 and PTF1-L coregulate an exocrine pancreas-specific transcriptional network for digestive function**. *Genes Dev* 2011, **25**:1674-1679.

17. Benod C, Vinogradova MV, Jouravel N, Kim GE, Fletterick RJ, Sablin EP: **Nuclear receptor liver receptor homologue 1 (LRH-1) regulates pancreatic cancer cell growth and proliferation**. *Proc Natl Acad Sci U S A* 2011, **108**:16927-16931.

18. Botrugno OA, Fayard E, Annicotte JS, Haby C, Brennan T, Wendling O, Tanaka T, Kodama T, Thomas W, Auwerx J *et al.*: **Synergy between LRH-1 and beta-catenin induces G1 cyclin-mediated cell proliferation**. *Mol Cell* 2004, **15**:499-509.

19. Chand AL, Wijayakumara DD, Knower KC, Herridge KA, Howard TL, Lazarus KA, Clyne CD: **The orphan nuclear receptor LRH-1 and ERalpha activate GREB1 expression to induce breast cancer cell proliferation**. *PLoS One* 2012, **7**:e31593.

20. Mueller M, Cima I, Noti M, Fuhrer A, Jakob S, Dubuquoy L, Schoonjans K, Brunner T: **The nuclear receptor LRH-1 critically regulates extra-adrenal glucocorticoid synthesis in the intestine**. *J Exp Med* 2006, **203**:2057-2062.

21. Coste A, Dubuquoy L, Barnouin R, Annicotte JS, Magnier B, Notti M, Corazza N, Antal MC, Metzger D, Desreumaux P *et al.*: **LRH-1-mediated glucocorticoid synthesis in enterocytes protects against inflammatory bowel disease**. *Proc Natl Acad Sci U S A* 2007, **104**:13098-13103.

22. Chand AL, Herridge KA, Thompson EW, Clyne CD: **The orphan nuclear receptor LRH-1 promotes breast cancer motility and invasion**. *Endocr Relat Cancer* 2010, **17**:965-975.

23. Schoonjans K, Dubuquoy L, Mebis J, Fayard E, Wendling O, Haby C, Geboes K, Auwerx J: **Liver receptor homolog 1 contributes to intestinal tumor formation through effects on cell cycle and inflammation**. *Proc Natl Acad Sci U S A* 2005, **102**:2058-2062.

24. Gu P, Goodwin B, Chung AC, Xu X, Wheeler DA, Price RR, Galardi C, Peng L, Latour AM, Koller BH *et al.*: **Orphan nuclear receptor LRH-1 is required to maintain Oct4 expression at the epiblast stage of embryonic development**. *Mol Cell Biol* 2005, **25**:3492-3505.

25. •• Heng JC, Feng B, Han J, Jiang J, Kraus P, Ng JH, Orlov YL, Huss M, Yang L, Lufkin T *et al.*: **The nuclear receptor Nr5a2 can replace Oct4 in the reprogramming of murine somatic cells to pluripotent cells**. *Cell Stem Cell* 2010, **6**:167-174.

This study shows that LRH-1 can replace OCT4 during iPS generation and that LRH-1 SUMOylation mutants further enhance the reprogramming efficiency.

26. Wang W, Yang J, Liu H, Lu D, Chen X, Zenonos Z, Campos LS, Rad R, Guo G, Zhang S *et al.*: **Rapid and efficient reprogramming of somatic cells to induced pluripotent stem cells by retinoic acid receptor gamma and liver receptor homolog 1**. *Proc Natl Acad Sci U S A* 2011, **108**:18283-18288.

27. Wagner RT, Xu X, Yi F, Merrill BJ, Cooney AJ: **Canonical Wnt/beta-catenin regulation of liver receptor homolog-1 mediates pluripotency gene expression**. *Stem Cells* 2010, **28**:1794-1804.

28. Krylova IN, Sablin EP, Moore J, Xu RX, Waitt GM, MacKay JA, Juzumiene D, Bynum JM, Madauss K, Montana V *et al.*: **Structural analyses reveal phosphatidyl inositols as ligands for the NR5 orphan receptors SF-1 and LRH-1**. *Cell* 2005, **120**:343-355.

29. Wang W, Zhang C, Marimuthu A, Krupka HI, Tabrizizad M, Shelloe R, Mehra U, Eng K, Nguyen H, Settachatgul C *et al.*: **The crystal structures of human steroidogenic factor-1 and liver receptor homologue-1**. *Proc Natl Acad Sci U S A* 2005, **102**:7505-7510.

30. Sablin EP, Krylova IN, Fletterick RJ, Ingraham HA: **Structural basis for ligand-independent activation of the orphan nuclear receptor LRH-1**. *Mol Cell* 2003, **11**:1575-1585.

31. Ortlund EA, Lee Y, Solomon IH, Hager JM, Safi R, Choi Y, Guan Z, Tripathy A, Raetz CR, McDonnell DP *et al.*: **Modulation of human nuclear receptor LRH-1 activity by phospholipids and SHP**. *Nat Struct Mol Biol* 2005, **12**:357-363.

32. •• Lee JM, Lee YK, Mamrosh JL, Busby SA, Griffin PR, Pathak MC, Ortlund EA, Moore DD: **A nuclear-receptor-dependent phosphatidylcholine pathway with antidiabetic effects**. *Nature* 2011, **474**:506-510.

This is the first study that provides *in vitro* and *in vivo* evidence that unusual phospholipid species, such as dilauroylphosphatidylcholine, act as ligands for LRH-1 and exert anti-diabetic effects.

33. • Musille PM, Pathak MC, Lauer JL, Hudson WH, Griffin PR, Ortlund EA: **Antidiabetic phospholipid-nuclear receptor complex reveals the mechanism for phospholipid-driven gene regulation**. *Nat Struct Mol Biol* 2012, **19**:532-537 S1–2.
The authors describe the structure of the DLPC-LRH-1 complex and demonstrate that ligand binding is a dynamic process that alters coregulator selectivity.

34. Goodwin B, Jones SA, Price RR, Watson MA, McKee DD, Moore LB, Galardi C, Wilson JG, Lewis MC, Roth ME *et al.*: **A regulatory cascade of the nuclear receptors FXR, SHP-1, and LRH-1 represses bile acid biosynthesis**. *Mol Cell* 2000, **6**:517-526.

35. Lu TT, Makishima M, Repa JJ, Schoonjans K, Kerr TA, Auwerx J, Mangelsdorf DJ: **Molecular basis for feedback regulation of bile acid synthesis by nuclear receptors**. *Mol Cell* 2000, **6**:507-515.

36. Lee YK, Choi YH, Chua S, Park YJ, Moore DD: **Phosphorylation of the hinge domain of the nuclear hormone receptor LRH-1 stimulates transactivation**. *J Biol Chem* 2006, **281**:7850-7855.

37. Chanda D, Xie YB, Choi HS: **Transcriptional corepressor SHP recruits SIRT1 histone deacetylase to inhibit LRH-1 transactivation**. *Nucleic Acids Res* 2010, **38**:4607-4619.

38. Treuter E, Venteclef N: **Transcriptional control of metabolic and inflammatory pathways by nuclear receptor SUMOylation**. *Biochim Biophys Acta* 2011, **1812**:909-918.

39. Lee MB, Lebedeva LA, Suzawa M, Wadekar SA, Desclozeaux M, Ingraham HA: **The DEAD-box protein DP103 (Ddx20 or Gemin-3) represses orphan nuclear receptor activity via SUMO modification**. *Mol Cell Biol* 2005, **25**:1879-1890.

40. Chalkiadaki A, Talianidis I: **SUMO-dependent compartmentalization in promyelocytic leukemia protein nuclear bodies prevents the access of LRH-1 to chromatin**. *Mol Cell Biol* 2005, **25**:5095-5105.

41. • Venteclef N, Jakobsson T, Ehrlund A, Damdimopoulos A, Mikkonen L, Ellis E, Nilsson LM, Parini P, Janne OA, Gustafsson JA *et al.*: **GPS2-dependent corepressor/SUMO pathways govern anti-inflammatory actions of LRH-1 and LXRbeta in the hepatic acute phase response**. *Genes Dev* 2010, **24**:381-395.
This study describes the role of SUMOylated LRH-1 in the recruitment of co-repressor complexes to induce transrepression of acute phase response proteins.

42. Ward JD, Bojanala N, Bernal T, Ashrafi K, Asahina M, Yamamoto KR: **Sumoylated NHR-25/NR5A regulates cell fate during *C. elegans* vulval development**. *PLoS Genet* 2013, **9**:e1003992.

43. • Talamillo A, Herboso L, Pirone L, Perez C, Gonzalez M, Sanchez J, Mayor U, Lopitz-Otsoa F, Rodriguez MS, Sutherland JD *et al.*: **Scavenger receptors mediate the role of SUMO and Ftz-f1 in Drosophila steroidogenesis**. *PLoS Genet* 2013, **9**:e1003473.
The authors show that the Drosophila homolog of LRH-1 and SUMO regulate lipid homeostasis and steroidogenesis.

44. Yang FM, Pan CT, Tsai HM, Chiu TW, Wu ML, Hu MC: **Liver receptor homolog-1 localization in the nuclear body is regulated by sumoylation and cAMP signaling in rat granulosa cells**. *FEBS J* 2009, **276**:425-436.

45. •• Stein S, Oosterveer MH, Mataki C, Xu P, Lemos V, Havinga R, Dittner C, Ryu D, Menzies KJ, Wang X *et al.*: **SUMOylation-dependent LRH-1/PROX1 interaction promotes atherosclerosis by decreasing hepatic reverse cholesterol transport**. *Cell Metab* 2014, **20**:603-613.
This is the first study showing that a single mutation of a SUMOylatable site introduced by homologous recombination can dampen the progression of a chronic metabolic disease, like atherosclerosis, via loss of PROX1 corepressor recruitment.

46. Schoonjans K, Annicotte JS, Huby T, Botrugno OA, Fayard E, Ueda Y, Chapman J, Auwerx J: **Liver receptor homolog 1 controls the expression of the scavenger receptor class B type I**. *EMBO Rep* 2002, **3**:1181-1187.

47. Takahashi K, Yamanaka S: **Induction of pluripotent stem cells from mouse embryonic and adult fibroblast cultures by defined factors**. *Cell* 2006, **126**:663-676.

48. Yazawa T, Inaoka Y, Okada R, Mizutani T, Yamazaki Y, Usami Y, Kuribayashi M, Orisaka M, Umezawa A, Miyamoto K: **PPAR-gamma coactivator-1alpha regulates progesterone production in ovarian granulosa cells with SF-1 and LRH-1**. *Mol Endocrinol* 2010, **24**:485-496.

49. Qin J, Gao DM, Jiang QF, Zhou Q, Kong YY, Wang Y, Xie YH: **Prospero-related homeobox (Prox1) is a corepressor of human liver receptor homolog-1 and suppresses the transcription of the cholesterol 7-alpha-hydroxylase gene**. *Mol Endocrinol* 2004, **18**:2424-2439.

50. Lee YK, Moore DD: **Dual mechanisms for repression of the monomeric orphan receptor liver receptor homologous protein-1 by the orphan small heterodimer partner**. *J Biol Chem* 2002, **277**:2463-2467.

51. Suzuki T, Kasahara M, Yoshioka H, Morohashi K, Umesono K: **LXXLL-related motifs in Dax-1 have target specificity for the orphan nuclear receptors Ad4BP/SF-1 and LRH-1**. *Mol Cell Biol* 2003, **23**:238-249.

52. Suzuki T, Kasahara M, Yoshioka H, Umesono K, Morohashi K: **LXXLL motifs in Dax-1 have target specificity for the orphan nuclear receptors Ad4BP/SF-1 and LRH-1**. *Endocr Res* 2002, **28**:537.

53. Venteclef N, Jakobsson T, Steffensen KR, Treuter E: **Metabolic nuclear receptor signaling and the inflammatory acute phase response**. *Trends Endocrinol Metab* 2011, **22**:333-343.

54. Xu PL, Kong YY, Xie YH, Wang Y: **Corepressor SMRT specifically represses the transcriptional activity of orphan nuclear receptor hB1F/hLRH-1**. *Acta Biochim Biophys Sin (Shanghai)* 2003, **35**:897-903.

55. Steffensen KR, Holter E, Bavner A, Nilsson M, Pelto-Huikko M, Tomarev S, Treuter E: **Functional conservation of interactions between a homeodomain cofactor and a mammalian FTZ-F1 homologue**. *EMBO Rep* 2004, **5**:613-619.

56. Harvey NL, Srinivasan RS, Dillard ME, Johnson NC, Witte MH, Boyd K, Sleeman MW, Oliver G: **Lymphatic vascular defects promoted by Prox1 haploinsufficiency cause adult-onset obesity**. *Nat Genet* 2005, **37**:1072-1081.

57. Hong YK, Harvey N, Noh YH, Schacht V, Hirakawa S, Detmar M, Oliver G: **Prox1 is a master control gene in the program specifying lymphatic endothelial cell fate**. *Dev Dyn* 2002, **225**:351-357.

58. Xu PL, Liu YQ, Shan SF, Kong YY, Zhou Q, Li M, Ding JP, Xie YH, Wang Y: **Molecular mechanism for the potentiation of the transcriptional activity of human liver receptor homolog 1 by steroid receptor coactivator-1**. *Mol Endocrinol* 2004, **18**:1887-1905.

59. Hsieh HT, Wang CH, Wu ML, Yang FM, Tai YC, Hu MC: **PIASy inhibits LRH-1-dependent CYP11A1 expression by competing for SRC-1 binding**. *Biochem J* 2009, **419**:201-209.

60. Hadizadeh S, King DN, Shah S, Sewer MB: **Sphingosine-1-phosphate regulates the expression of the liver receptor homologue-1**. *Mol Cell Endocrinol* 2008, **283**:104-113.

61. Shin DJ, Osborne TF: **Peroxisome proliferator-activated receptor-gamma coactivator-1alpha activation of CYP7A1 during food restriction and diabetes is still inhibited by small heterodimer partner**. *J Biol Chem* 2008, **283**:15089-15096.

62. Safi R, Kovacic A, Gaillard S, Murata Y, Simpson ER, McDonnell DP, Clyne CD: **Coactivation of liver receptor homologue-1 by peroxisome proliferator-activated receptor gamma coactivator-1alpha on aromatase promoter II and its inhibition by activated retinoid X receptor suggest a novel target for breast-specific antiestrogen therapy**. *Cancer Res* 2005, **65**:11762-11770.

63. Yumoto F, Nguyen P, Sablin EP, Baxter JD, Webb P, Fletterick RJ: **Structural basis of coactivation of liver receptor homolog-1 by beta-catenin**. *Proc Natl Acad Sci U S A* 2012, **109**:143-148.

64. Brendel C, Gelman L, Auwerx J: **Multiprotein bridging factor-1 (MBF-1) is a cofactor for nuclear receptors that regulate lipid metabolism**. *Mol Endocrinol* 2002, **16**:1367-1377.

65. Li FQ, Ueda H, Hirose S: **Mediators of activation of fushi tarazu gene transcription by BmFTZ-F1**. *Mol Cell Biol* 1994, **14**:3013-3021.

66. Kir S, Zhang Y, Gerard RD, Kliewer SA, Mangelsdorf DJ: **Nuclear receptors HNF4alpha and LRH-1 cooperate in regulating Cyp7a1 in vivo**. *J Biol Chem* 2012, **287**:41334-41341.

67. Luo Y, Liang CP, Tall AR: **The orphan nuclear receptor LRH-1 potentiates the sterol-mediated induction of the human CETP gene by liver X receptor**. *J Biol Chem* 2001, **276**:24767-24773.

68. Matsukuma KE, Wang L, Bennett MK, Osborne TF: **A key role for orphan nuclear receptor liver receptor homologue-1 in activation of fatty acid synthase promoter by liver X receptor**. *J Biol Chem* 2007, **282**:20164-20171.

69. Back SS, Kim J, Choi D, Lee ES, Choi SY, Han K: **Cooperative transcriptional activation of ATP-binding cassette sterol transporters ABCG5 and ABCG8 genes by nuclear receptors including Liver-X-Receptor**. *BMB Rep* 2013, **46**:322-327.

70. Chong HK, Infante AM, Seo YK, Jeon TI, Zhang Y, Edwards PA, Xie X, Osborne TF: **Genome-wide interrogation of hepatic FXR reveals an asymmetric IR-1 motif and synergy with LRH-1**. *Nucleic Acids Res* 2010, **38**:6007-6017.

71. Hoeke MO, Heegsma J, Hoekstra M, Moshage H, Faber KN: **Human FXR regulates SHP expression through direct binding to an LRH-1 binding site, independent of an IR-1 and LRH-1**. *PLoS One* 2014, **9**:e88011.

72. Fernandez-Marcos PJ, Auwerx J, Schoonjans K: **Emerging actions of the nuclear receptor LRH-1 in the gut**. *Biochim Biophys Acta* 2011, **1812**:947-955.

73. del Castillo-Olivares A, Gil G: **Alpha 1-fetoprotein transcription factor is required for the expression of sterol 12alpha-hydroxylase, the specific enzyme for cholic acid synthesis. Potential role in the bile acid-mediated regulation of gene transcription**. *J Biol Chem* 2000, **275**:17793-17799.

74. Nitta M, Ku S, Brown C, Okamoto AY, Shan B: **CPF: an orphan nuclear receptor that regulates liver-specific expression of the human cholesterol 7alpha-hydroxylase gene**. *Proc Natl Acad Sci U S A* 1999, **96**:6660-6665.

75. Mataki C, Magnier BC, Houten SM, Annicotte JS, Argmann C, Thomas C, Overmars H, Kulik W, Metzger D, Auwerx J *et al.*: **Compromised intestinal lipid absorption in mice with a liver-specific deficiency of liver receptor homolog 1**. *Mol Cell Biol* 2007, **27**:8330-8339.

76. Lee YK, Schmidt DR, Cummins CL, Choi M, Peng L, Zhang Y, Goodwin B, Hammer RE, Mangelsdorf DJ, Kliewer SA: **Liver receptor homolog-1 regulates bile acid homeostasis but is not essential for feedback regulation of bile acid synthesis**. *Mol Endocrinol* 2008, **22**:1345-1356.

77. Out C, Hageman J, Bloks VW, Gerrits H, Sollewijn Gelpke MD, Bos T, Havinga R, Smit MJ, Kuipers F, Groen AK: **Liver receptor homolog-1 is critical for adequate up-regulation of Cyp7a1 gene transcription and bile salt synthesis during bile salt sequestration**. *Hepatology* 2011, **53**:2075-2085.

78. Song X, Kaimal R, Yan B, Deng R: **Liver receptor homolog 1 transcriptionally regulates human bile salt export pump expression**. *J Lipid Res* 2008, **49**:973-984.

79. Freeman LA, Kennedy A, Wu J, Bark S, Remaley AT, Santamarina-Fojo S, Brewer HB Jr: **The orphan nuclear receptor LRH-1 activates the ABCG5/ABCG8 intergenic promoter**. *J Lipid Res* 2004, **45**:1197-1206.

80. Delerive P, Galardi CM, Bisi JE, Nicodeme E, Goodwin B: **Identification of liver receptor homolog-1 as a novel regulator of apolipoprotein AI gene transcription**. *Mol Endocrinol* 2004, **18**:2378-2387.

81. Venteclef N, Haroniti A, Tousaint JJ, Talianidis I, Delerive P: **Regulation of anti-atherogenic apolipoprotein M gene expression by the orphan nuclear receptor LRH-1**. *J Biol Chem* 2008, **283**:3694-3701.

82. • Oosterveer MH, Mataki C, Yamamoto H, Harach T, Moullan N, van Dijk TH, Ayuso E, Bosch F, Postic C, Groen AK *et al.*: **LRH-1-dependent glucose sensing determines intermediary metabolism in liver**. *J Clin Invest* 2012, **122**:2817-2826.
This study identifies hepatic LRH-1 as a regulator of glucose-6-phosphate availability that controls ChREBP nuclear translocation and activity.

83. Hattori T, Iizuka K, Horikawa Y, Takeda J: **LRH-1 heterozygous knockout mice are prone to mild obesity**. *Endocr J* 2014, **61**:471-480.

84. Venteclef N, Smith JC, Goodwin B, Delerive P: **Liver receptor homolog 1 is a negative regulator of the hepatic acute-phase response**. *Mol Cell Biol* 2006, **26**:6799-6807.

85. Venteclef N, Delerive P: **Interleukin-1 receptor antagonist induction as an additional mechanism for liver receptor homolog-1 to negatively regulate the hepatic acute phase response**. *J Biol Chem* 2007, **282**:4393-4399.

86. • Mamrosh JL, Lee JM, Wagner M, Stambrook PJ, Whitby RJ, Sifers RN, Wu SP, Tsai MJ, Demayo FJ, Moore DD: **Nuclear receptor LRH-1/NR5A2 is required and targetable for liver endoplasmic reticulum stress resolution**. *Elife (Cambridge)* 2014, **3**:e01694.
This work shows that LRH-1 ameliorates hepatic ER stress resolution independent of the canonical unfolded protein response pathways.

87. • Benod C, Carlsson J, Uthayaruban R, Hwang P, Irwin JJ, Doak AK, Shoichet BK, Sablin EP, Fletterick RJ: **Structure-based discovery of antagonists of nuclear receptor LRH-1**. *J Biol Chem* 2013, **288**:19830-19844.
This study shows that treatment of different cancer cell lines with specific LRH-1 antagonists inhibits cancer cell proliferation.

88. Whitby RJ, Dixon S, Maloney PR, Delerive P, Goodwin BJ, Parks DJ, Willson TM: **Identification of small molecule agonists of the orphan nuclear receptors liver receptor homolog-1 and steroidogenic factor-1**. *J Med Chem* 2006, **49**:6652-6655.

89. Whitby RJ, Stec J, Blind RD, Dixon S, Leesnitzer LM, Orband-Miller LA, Williams SP, Willson TM, Xu R, Zuercher WJ *et al.*: **Small molecule agonists of the orphan nuclear receptors steroidogenic factor-1 (SF-1, NR5A1) and liver receptor homologue-1 (LRH-1, NR5A2)**. *J Med Chem* 2011, **54**:2266-2281.

90. Rey J, Hu H, Kyle F, Lai CF, Buluwela L, Coombes RC, Ortlund EA, Ali S, Snyder JP, Barrett AG: **Discovery of a new class of liver receptor homolog-1 (LRH-1) antagonists: virtual screening, synthesis and biological evaluation**. *ChemMedChem* 2012, **7**:1909-1914.

nature COMMUNICATIONS

ARTICLE

Received 30 Jan 2015 | Accepted 27 Feb 2015 | Published 15 Apr 2015

DOI: 10.1038/ncomms7801 OPEN

LRH-1 mediates anti-inflammatory and antifungal phenotype of IL-13-activated macrophages through the PPARγ ligand synthesis

Lise Lefèvre[1,2], Hélène Authier[1,2], Sokrates Stein[3], Clarisse Majorel[2], Bettina Couderc[4], Christophe Dardenne[1,2], Mohamad Ala Eddine[2], Etienne Meunier[1,2], José Bernad[1,2], Alexis Valentin[2], Bernard Pipy[1,2,*], Kristina Schoonjans[3,*] & Agnès Coste[1,2,*]

Liver receptor homologue-1 (LRH-1) is a nuclear receptor involved in the repression of inflammatory processes in the hepatointestinal tract. Here we report that LRH-1 is expressed in macrophages and induced by the Th2 cytokine IL-13 via a mechanism involving STAT6. We show that loss-of-function of LRH-1 in macrophages impedes IL-13-induced macrophage polarization due to impaired generation of 15-HETE PPARγ ligands. The incapacity to generate 15-HETE metabolites is at least partially caused by the compromised regulation of CYP1A1 and CYP1B1. Mice with LRH-1-deficient macrophages are, furthermore, highly susceptible to gastrointestinal and systemic *Candida albicans* infection. Altogether, these results identify LRH-1 as a critical component of the anti-inflammatory and fungicidal response of alternatively activated macrophages that acts upstream from the IL-13-induced 15-HETE/PPARγ axis.

[1] UMR MD3, EA2405 Polarisation des Macrophages et Récepteurs Nucléaires dans les Pathologies Inflammatoires et Infectieuses, UPS, Toulouse 31400, France. [2] Université de Toulouse, UMR 152, UPS, Toulouse 31400, France. [3] Metabolic Signaling, Institute of Bioengineering, Ecole Polytechnique Fédérale de Lausanne, Lausanne 1015, Switzerland. [4] EA4553 Individualisation des traitements des cancers ovariens et ORL, UPS, Toulouse 31400, France. * These authors contributed equally to this work. Correspondence and requests for materials should be addressed to A.C. (email: agnes.coste@univ-tlse3.fr).

Macrophages orchestrate innate immune responses by initiating and resolving inflammatory signalling programmes. Emerging evidence indicates that the state of macrophage polarization plays a critical role in the regulation of these inflammatory processes. Two different programmes of macrophage activation, the classical (M1) and the alternative differentiation, classify polarized macrophages with either persistence or resolution of inflammation[1–3]. M1 macrophages express high levels of opsonic receptors, involved in the production of pro-inflammatory effector molecules such as reactive oxygen and nitrogen intermediates and pro-inflammatory cytokines (interleukin (IL)-1β, tumour-necrosis factor alpha (TNFα), IL-6 and IL-12). These macrophages contribute to inflammation, microbial killing, regulation of cell proliferation and apoptosis. Alternatively activated macrophages are characterized by abundant levels of the anti-inflammatory cytokine IL-10 and non-opsonic receptors, such as C-type lectin receptors and scavenger receptors (CD36), and resolve inflammation by increasing CD36-mediated efferocytosis and secretion of tissue remodelling/repair mediators[3,4].

The balance of macrophage differentiation in favour of alternatively activated macrophages can be shifted by the activation of the nuclear receptor peroxisome proliferator-activated receptor gamma (PPARγ) (refs 5,6). PPARγ expression and activity in macrophages is negatively regulated during inflammatory processes[7,8]. In addition, activated PPARγ transrepresses many inflammation-activated transcription factors, including nuclear factor-kappaB (NF-κB), signal transducers and activators of transcription (STATs), activator protein 1 (AP1) and nuclear factor of activated T-cells NFAT), resulting in pro-inflammatory mediator inhibition[9]. PPARγ is activated by endogenous ligands derived from the metabolism of arachidonic acid (AA)[9]. Among these ligands, 15-deoxy-$\Delta^{12,14}PGJ_2$ (15d-PGJ2), metabolized through the COX1/COX2 cyclooxygenases, and the 12- and 15-hydroxyeicosatrienoic acids (HETEs), metabolized through 5 and 12/15 lipoxygenases, are essential for PPARγ endogenous activation[5,10,11]. In addition to cyclooxygenases and lipoxygenases, cytochrome P450 (CYP) enzymes are also considered to be critical for the metabolism of AA in epoxy (EETs) and in hydroxy (HETEs) derivatives[10,11]. Within the CYP family, the CYP1 family is mainly involved in the generation of 12- and 15-HETEs through CYP1A1 and CYP1B1 (refs 12,13).

Liver receptor homologue-1 (LRH-1, NR5A2) is a nuclear receptor highly expressed in the intestine, liver, pancreas and ovary[14,15]. Although LRH-1 has been recognized as an orphan receptor, phospholipids, including the phosphatidyl inositol second messengers, and more recently the 12C-fatty acyl-containing phospholipid, dilauroyl phosphatidylcholine (DLPC), have been described to bind the ligand-binding pocket and to act as LRH-1 agonists[16–18]. LRH-1 plays important roles in embryonic development, cholesterol and bile acid homeostasis[14,15] and promotes hepatic glucose sensing through the regulation of the glucokinase enzyme[19]. Several lines of evidence also support a role for LRH-1 in the control of the inflammatory response. While pro-inflammatory factors such as TNFα and lipopolysaccharide (LPS) decrease LRH-1 expression in murine models of human colon tumorigenesis, deficiency of LRH-1 in the intestinal epithelium predisposes mice to intestinal inflammation as a result of a defect in local glucocorticoid production. In the colon from patients with inflammatory bowel disease, inflammation is inversely correlated with the expression of LRH-1 (refs 20,21). In line with these reports, Venteclef *et al.*[22,23] identified a role for LRH-1 in the negative modulation of the hepatic acute-phase response by inhibiting IL-6- and IL-1β-stimulated haptoglobin, serum amyloid A gene expression in hepatocytes and inducing anti-inflammatory IL-1ra expression. Despite the numerous studies documenting the anti-inflammatory properties of LRH-1 in the liver and gut, no studies so far have focused on the role of LRH-1 in macrophages.

In the present study, we identify LRH-1 as an important regulator of the inflammatory response in macrophages. We demonstrate that LRH-1 is induced by IL-13 via a STAT6-dependent mechanism, which in turn induces the transcriptional activation of CYP1A1 and CYP1B1, two enzymes involved in the generation of 15-HETE PPARγ ligand. Finally, we also demonstrate the importance of intact LRH-1 signalling in the anti-inflammatory and antifungal functions of alternatively activated macrophages, indicating that modulators of LRH-1 activity may have therapeutic potential to restrain infectious and inflammatory diseases.

Results

IL-13-mediated LRH-1 gene expression is dependent on STAT6. The anti-inflammatory properties of LRH-1 are well established in the liver and gut[24]. To elucidate whether LRH-1 also participates in regulating the inflammatory response in macrophages, gene expression profiling was performed. *In situ* hybridization and reverse transcriptase–quantitative PCR (RT–qPCR) revealed that LRH-1 (encoded by the *Nr5a2* gene), known to be expressed in the colon and liver, is also expressed in macrophages but not in B and T immune cells (Fig. 1a). Consistent with the gene expression data, LRH-1 protein was also detected in macrophages (Supplementary Fig. 1b). We next analysed the impact of pro- and anti-inflammatory factors on *Nr5a2* gene expression in primary macrophages. As depicted in Fig. 1b, pro-inflammatory challenges, such LPS and IFNγ exposure, but not IL-6, significantly reduced or abolished *Nr5a2* mRNA expression. Conversely, IL-13, IL-4 and IL-10 cytokines significantly enhanced *Nr5a2* mRNA level in macrophages. Similar to findings in the murine model, *NR5A2* mRNA levels were significantly increased by IL-13 treatment in human monocytes (Fig. 1c). These results suggest that LRH-1 could be part of the transcriptional network mediating alternative activation of macrophages. To test this hypothesis, we analysed the downstream signalling components of IL-13 in more detail (Fig. 1d–i). STAT6, a transcription factor known to be activated by IL-13 is part of the signalling pathway that governs alternative activation[25]. Interestingly, exposure of macrophages with AG490, a Jak-2/STAT6 inhibitor, prevented the IL-13-mediated induction of LRH-1 (Fig. 1d). Consistent with these observations, IL-13 failed to increase *Nr5a2* mRNA and protein levels in macrophages deficient for STAT6 (Fig. 1e,f), suggesting that STAT6 mediates the transcriptional regulation of LRH-1. We then performed transient transfection assays in primary macrophages to assess the effect of IL-13 and STAT6 on *Nr5a2* promoter activity. While 4 h of IL-13 exposure was already sufficient to induce *Nr5a2* promoter activity in wild-type macrophages (Fig. 1g,h), chemical inhibition of STAT6 by AG490 (Fig. 1g) or genetic deletion of STAT6 (Fig. 1h) attenuated or even abolished this response.

To evaluate whether LRH-1 is subject to direct transcriptional control by STAT6, we performed an *in silico* analysis of the *Nr5a2* promoter region. Scanning of the *Nr5a2* promoter sequence for the STAT6 response element (STAT6-RE) canonical motif revealed four putative STAT6-RE (Fig. 1i). Chromatin immunoprecipitation (ChIP) analysis of macrophage DNA from C57BL/6 mice revealed specific recruitment of STAT6 to site 1 at −541, which is most proximal to the transcription initiation site of the gene (Fig. 1i).

To explore the functionality of this site, we next modified by *in vitro* mutagenesis its sequence and we evaluated the mutated *Nr5a2* reporter construct activity on IL-13 exposure (Fig. 1j).

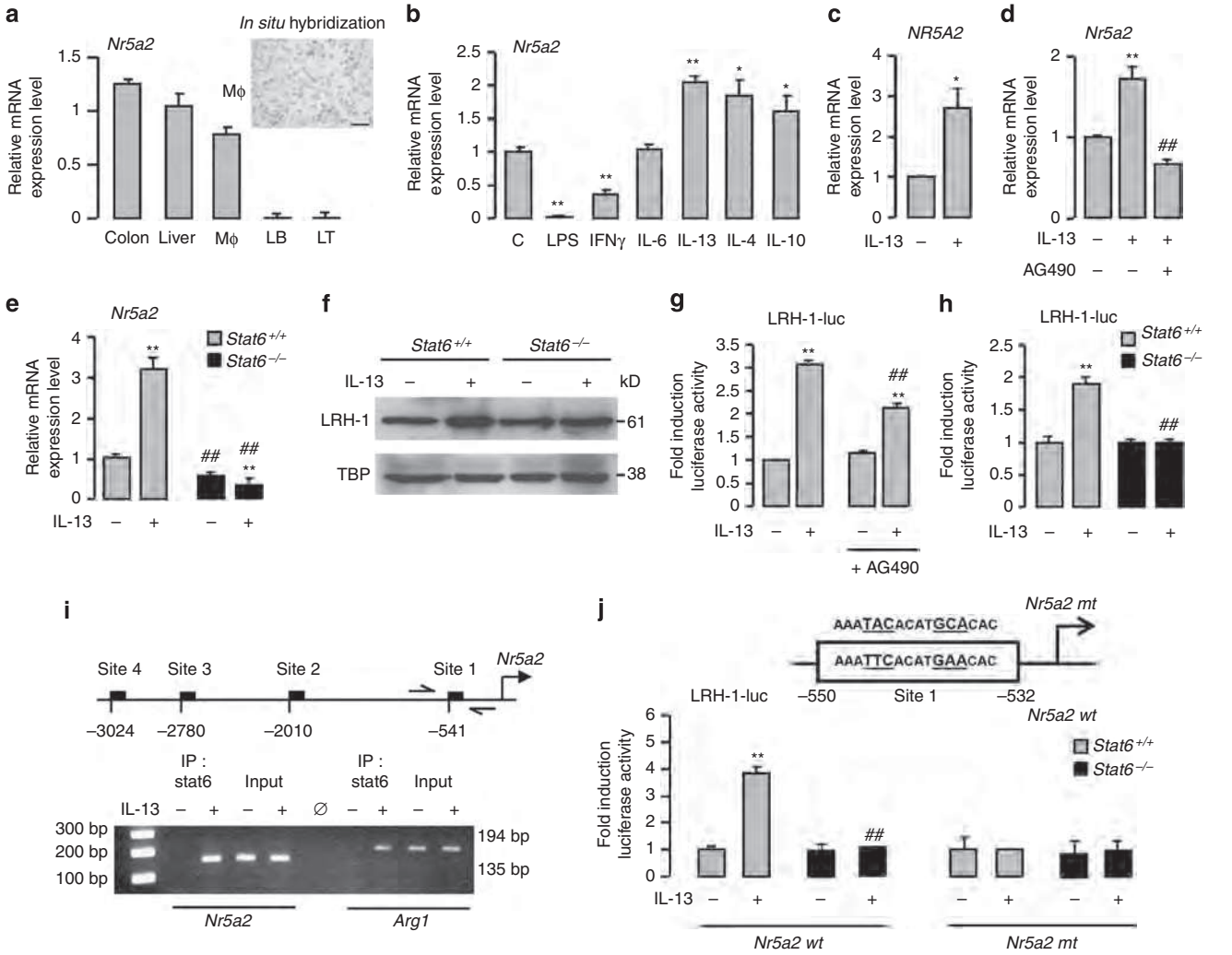

Figure 1 | IL-13-mediated LRH-1 gene expression is dependent on STAT6. (**a**) *Nr5a2* mRNA expression in the colon, liver, peritoneal macrophages (MΦ), B (LB) and T (LT) lymphocytes from C57BL/6 mice determined using RT-PCR. Inset shows *in situ* hybridization of *Nr5a2* mRNA in peritoneal macrophages from C57BL/6 mice (scale bar, 25 μm). (**b**,**c**) *Nr5a2* mRNA expression in macrophages from C57BL/6 mice (**b**) and in human macrophages (**c**) treated with the indicated cytokines for 4 h, determined using RT-PCR. The results were represented in fold induction relative to the untreated control or wild-type littermate. (**d**,**e**) *Nr5a2* mRNA expression in macrophages from C57BL/6 mice pretreated with AG490 and stimulated with IL-13 (**d**) and in macrophages from *Stat6*$^{+/+}$ and *Stat6*$^{-/-}$ mice stimulated with IL-13 for 4 h (**e**), determined using RT-PCR. The results were represented in fold induction relative to the untreated control or wild-type littermate. (**f**) Immunoblot analysis of the nuclear expression of LRH-1 and TBP (Tata-binding protein) in macrophages from *Stat6*$^{+/+}$ and *Stat6*$^{-/-}$ mice stimulated with IL-13 for 24 h. (**g**,**h**) Luciferase activity in macrophages from C57BL/6 mice transfected with LRH-1 (LRH-1-luc) promoter construct pretreated with AG490 (**g**) or from *Stat6*$^{+/+}$ and *Stat6*$^{-/-}$ mice (**h**), and treated with IL-13 for 24 h. The results were represented in fold induction relative to the untreated control or wild-type littermate. (**i**) Schematic presentation of the four putative STAT6 response elements in the mouse *Nr5a2* promoter identified by Genomatix algorithm and assessment of STAT6 recruitment to site 1 and to the *Arg1* promoter determined with the ChIP analysis using genomic DNA from C57BL/6 macrophages treated with IL-13 for 4 h. (**j**) Luciferase activity in macrophages from *Stat6*$^{+/+}$ and *Stat6*$^{-/-}$ mice transfected with LRH-1 promoter constructs and treated with IL-13 for 18 h. The results were represented in fold induction relative to the untreated control. Results correspond to mean ± s.e.m. of triplicates. Data are representative of three independent experiments. $^{*}P<0.05$ $^{**}P<0.01$ compared with the respective untreated control and $^{\#}P<0.05$, $^{\#\#}P<0.01$ compared with IL-13-treated wild-type littermate. *P* values were determined using Bonferroni–Dunnett method.

Mutation of the STAT6-RE abolished the activity of the Nr5a2 reporter construct in response to IL-13 in *Stat6*$^{+/+}$ and *Stat6*$^{M-/-}$ macrophages (Fig. 1j). These results demonstrate that STAT6 directly controls the transcription of LRH-1 in response to IL-13.

LRH-1 is involved in IL-13-induced macrophage activation. In order to assess the role of LRH-1 in IL-13-induced alternative macrophage differentiation, we generated mice in which the *Nr5a2* gene was selectively disrupted in myeloid-derived cells. To generate these animals, mice carrying floxed *Lrh-1* alleles were crossed with transgenic mice that express the Cre recombinase under the control of the mouse phagocyte-selective lysozyme promoter[21,26]. Compared with control (*Lrh-1*$^{M+/+}$) macrophages, LRH-1 mRNA and protein levels were almost undetectable in macrophages derived from the myeloid cell-specific LRH-1-deficient (*Lrh-1*$^{M-/-}$) mice (Supplementary Fig. 1a–c). Furthermore, the disruption of LRH-1 could not be detected in other LRH-1-expressing tissues, such as the liver and the colon (Supplementary Fig. 1d,e).

We then evaluated the expression of specific markers of classical and alternative activation in untreated or IL-13-treated

Lrh-1$^{M+/+}$ and *Lrh-1*$^{M-/-}$ macrophages during 4 h. Overall, *Lrh-1*$^{M-/-}$ macrophages displayed an upregulation of M1 markers such as *Nos2* (encoding the inducible nitric oxide synthase) and the Fcγ-receptors *Fcgr3* and *Fcgr*1 (encoding CD16 and CD64 proteins, respectively), which was mirrored by a downregulation of *Chi3l3* (YM1), *Mrc1* (MR), *Clec7a* (Dectin-1), *Il1rn* (IL-1ra) and *Tgfb1* (transforming growth factor (TGF)-β1) alternative activation markers (Fig. 2a,b). This was accompanied by an increase in the mRNA and protein levels of the inflammatory cytokines TNFα, IL-1β and IL-6 (encoded by *Tnfa, Il1b* and *Il-6* genes, respectively; Fig. 2a,c). *Il12* pro-inflammatory and *Il10* anti-inflammatory cytokine mRNA levels remained unchanged in *Lrh-1*$^{M+/+}$ and *Lrh-1*$^{M-/-}$ macrophages (Fig. 2a). Furthermore, the induction of MR, Dectin-1, CD36, *Arg1* (encoding the arginase 1), *Chi3l3* and *Il1rn* expression by IL-13 was strongly diminished in *Lrh-1*$^{M-/-}$ macrophages (Fig. 2a,b). Consistent with reduced alternative activation markers in *Lrh-1*$^{M-/-}$ macrophages, the M1 markers such as *Nos2, Itgam* (CD11b), *Fcgr3*, *Fcgr1*, *Il1b* and *Il-6* still remained highly expressed (Fig. 2a–c). Consistent with these findings, the induction of alternative activation gene markers observed after 4 h of IL-13 treatment was amplified after 24 h of IL-13 treatment in *Lrh-1*$^{M+/+}$ macrophages (Supplementary Fig. 2a). Moreover, the decrease in alternative activation markers in *Lrh-1*$^{M-/-}$ macrophages after 4 h of IL-13 treatment was sustained after 24 h of stimulation (Supplementary Fig. 2a). Altogether, these data indicate that LRH-1 is required for repression of pro-inflammatory state and for optimal induction of alternative macrophage activation by IL-13. These findings are consistent with the robust induction of *Il10*, *Tgfb1*, *Il1rn*, *Mrc1*, *Clec7a* and *Cd36* gene expression in *Lrh-1*$^{M+/+}$ macrophages treated with the LRH-1 agonist DLPC (Supplementary Fig. 2b).

LRH-1 activates 15-HETE secretion *via* the control of CYP1s. The nuclear receptor PPARγ is a key component of the signalling

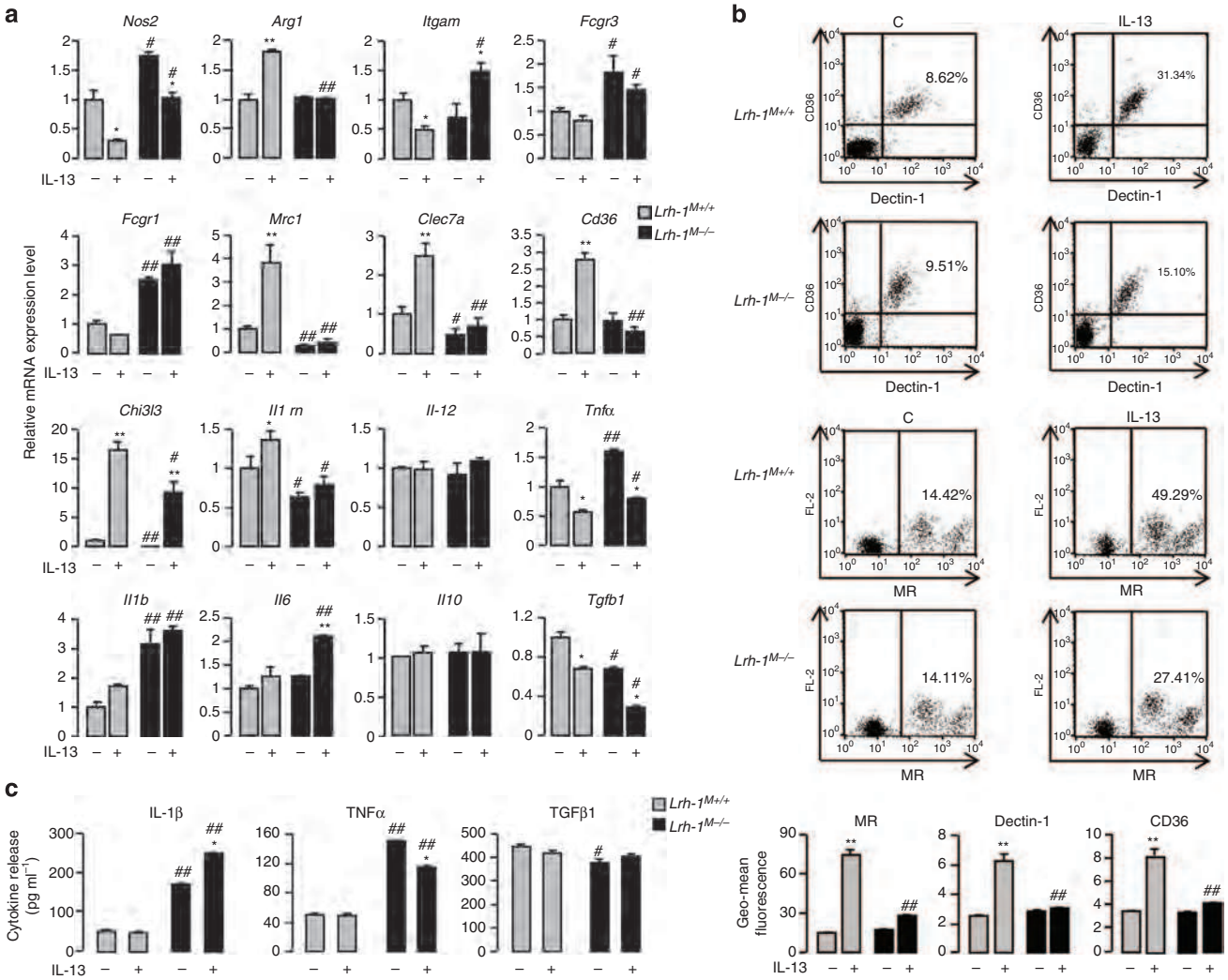

Figure 2 | LRH-1 is involved in IL-13-induced alternative activation of macrophages. (**a**) Gene expression analysis of markers of M1 and M2 polarization in peritoneal macrophages from *Lrh-1*$^{M+/+}$ and *Lrh-1*$^{M-/-}$ mice treated with IL-13 for 4 h, determined using RT-PCR. The results were represented in fold induction relative to the untreated *Lrh-1*$^{M+/+}$ littermate. (**b**) Dot-plot representing Dectin-1, CD36 and MR protein expression in macrophages from *Lrh-1*$^{M+/+}$ and *Lrh-1*$^{M-/-}$ mice treated with IL-13 for 24 h. Numbers indicate the % of positive cells. Graphs represent geomean fluorescence quantification for the indicated proteins. (**c**) Cytokine production of peritoneal macrophages from *Lrh-1*$^{M+/+}$ and *Lrh-1*$^{M-/-}$ mice after IL-13 treatment and *C. albicans* challenge for 8 h (ratio: 1 macrophage:3 yeasts), quantified by enzyme-linked immunosorbent assay. Results correspond to mean ± s.e.m. of triplicates. Data are representative of three independent experiments. $^{*}P<0.05$, $^{**}P<0.01$ compared to the respective untreated control and $^{\sharp}P<0.05$, $^{\sharp\sharp}P<0.01$ compared with *Lrh-1*$^{M+/+}$ + IL-13. *P* values were determined using the Bonferroni–Dunnett method.

pathway triggered by IL-13 and directly controls the expression of markers of alternative activation. To establish whether the increase in alternative activation markers by IL-13 results from direct regulation of PPARγ transcription by LRH-1, we first evaluated *Pparg* mRNA levels in *Lrh-1*$^{M+/+}$ and *Lrh-1*$^{M-/-}$ macrophages under basal conditions and after IL-13 exposure. The increased *Pparg* mRNA level by IL-13 in *Lrh-1*$^{M+/+}$ macrophages was not affected in *Lrh-1*$^{M-/-}$ macrophages (Fig. 3a). Moreover, in transient transfection studies, absence of LRH-1 in *Lrh-1*$^{M-/-}$ macrophages (Fig. 3b) or conversely ectopic expression of LRH-1 in wild-type macrophages (Fig. 3c) did not significantly affect IL-13-mediated PPARγ promoter induction, further indicating that LRH-1 does not regulate the transcription rate of PPARγ. Next, we examined whether LRH-1 was required for PPARγ activation by assessing the impact of IL-13 on a heterologous PPARγ reporter transfected in *Lrh-1*$^{M+/+}$ and *Lrh-1*$^{M-/-}$ macrophages. Remarkably, while in *Lrh-1*$^{M+/+}$ macrophages IL-13 significantly induced the PPRE luciferase reporter, no such response could be observed in *Lrh-1*$^{M-/-}$ macrophages (Fig. 3d). Conversely, co-transfection of the PPRE luciferase reporter with an expression vector for LRH-1 robustly increased PPARγ activation (Fig. 3e), suggesting that LRH-1 induces the activity of PPARγ.

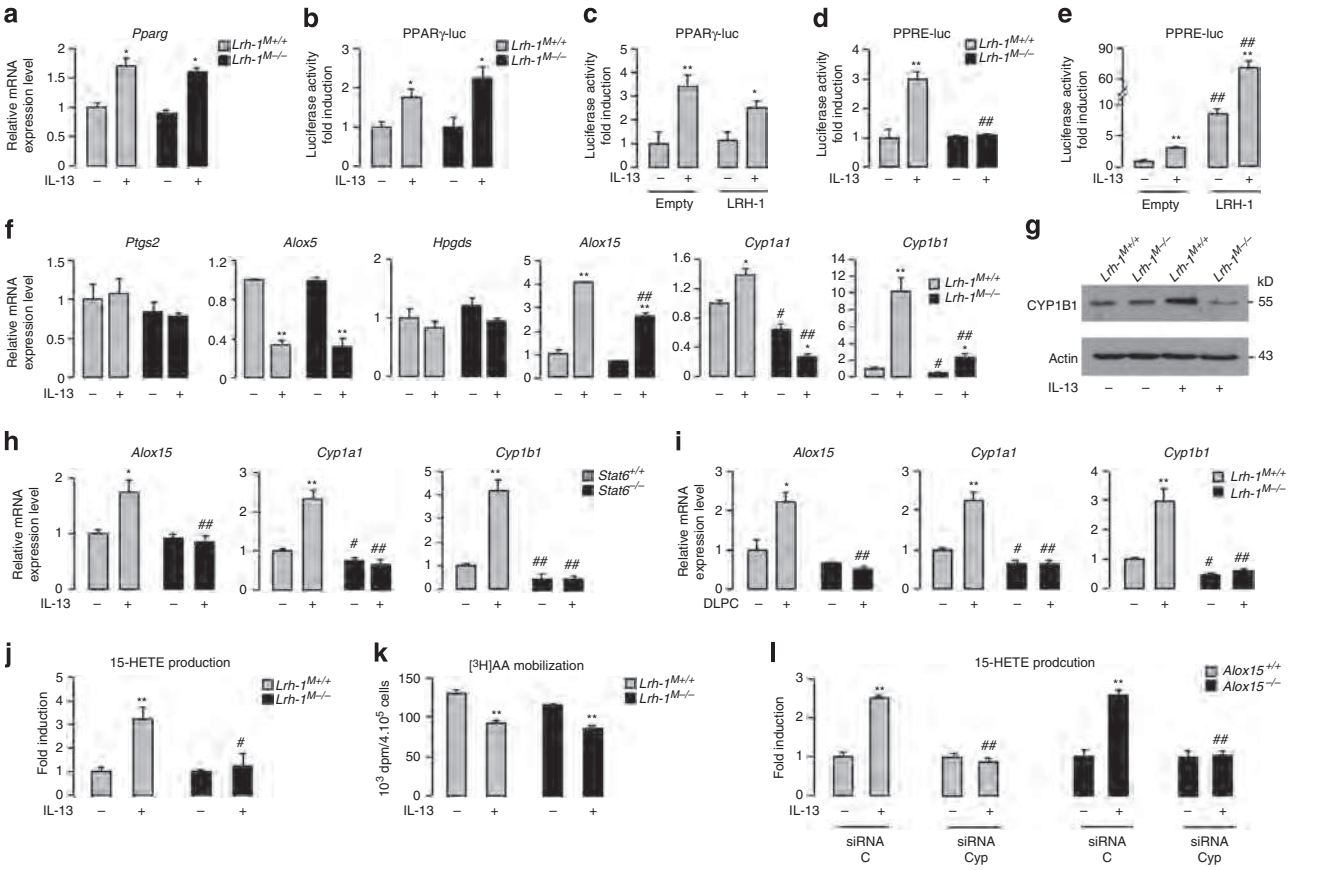

Figure 3 | LRH-1 activates CYP1A1- and CYP1B1-dependent 15-HETE production. (**a**) *Pparg* mRNA expression in macrophages from *Lrh-1*$^{M+/+}$ and *Lrh-1*$^{M-/-}$ mice treated with IL-13 for 4 h, determined using RT–PCR. The results were represented in fold induction relative to the untreated wild-type littermate. (**b**) Luciferase activity in macrophages from *Lrh-1*$^{M+/+}$ and *Lrh-1*$^{M-/-}$ mice transfected with PPARγ (PPARγ-luc) promoter construct and treated with IL-13 for 4 h. The results were represented in fold induction relative to the respective control. (**c**) Luciferase activity in macrophages from C57BL/6 mice co-transfected with PPARγ (PPARγ-luc) promoter construct in presence (LRH-1) or absence (empty) of LRH-1 (pCMX-LRH-1) and treated with IL-13 for 4 h. The results were represented in fold induction relative to the untreated control (empty). (**d**) Luciferase activity in macrophages from *Lrh-1*$^{M+/+}$ and *Lrh-1*$^{M-/-}$ mice transfected with a PPRE (PPRE-luc) construct treated with IL-13 for 24 h. The results were represented in fold induction relative to the respective untreated control. (**e**) Luciferase activity of macrophages from C57BL/6 macrophages co-transfected with PPRE (PPRE-luc) construct in presence (LRH-1) or absence (empty) of LRH-1 (pCMX-LRH-1), treated with IL-13 for 24 h. The results were represented in fold induction relative to the respective control. (**f**) Gene expression analysis of arachidonic acid metabolic enzymes in macrophages from *Lrh-1*$^{M+/+}$ and *Lrh-1*$^{M-/-}$ mice treated with IL-13 for 4 h, determined using RT–PCR. The results were represented in fold induction relative to untreated *Lrh-1*$^{M+/+}$. (**g**) Immunoblot analysis of Cyp1b1 and Actin in macrophages from *Lrh-1*$^{M+/+}$ and *Lrh-1*$^{M-/-}$ mice stimulated with IL-13 for 24 h. (**h**,**i**) Gene expression analysis of *Alox15*, *Cyp1a1* and *Cyp1b1* in macrophages from *Stat6*$^{+/+}$ and *Stat6*$^{-/-}$ mice treated with IL-13 (**h**) and in macrophages from *Lrh-1*$^{M-/-}$ and *Lrh-1*$^{M+/+}$ mice stimulated with DLPC for 4 h (**i**), determined using RT–PCR. The results were represented in fold induction relative to untreated wild-type littermate. (**j**) 15-HETE production by macrophages from *Lrh-1*$^{M-/-}$ and *Lrh-1*$^{M+/+}$ mice stimulated with or without IL-13 quantified by enzyme immunoassay (EIA). The results were represented in fold induction relative to untreated *Lrh-1*$^{M+/+}$. (**k**) $^{[3H]}$AA mobilization in membrane phospholipids of macrophages from *Lrh-1*$^{M-/-}$ and *Lrh-1*$^{M+/+}$ mice stimulated with IL-13 for 2 h. (**l**) 15-HETE production by macrophages from *Alox15*$^{-/-}$ and *Alox15*$^{+/+}$ mice stimulated with IL-13 for 24 h and silenced or not for Cyp1a1 and Cyp1b1 (siRNA Cyp) measured by EIA. The results were represented in fold induction relative to respective untreated control (siRNA C). Results correspond to the mean ± s.e.m. of triplicates. Data are representative of three independent experiments. $^{*}P<0.05$, $^{**}P<0.01$ compared with the respective untreated control and $^{\#}P<0.05$, $^{\#\#}P<0.01$ compared with the corresponding treated or untreated wild-type littermate. *P* values were determined using Bonferroni–Dunnett method.

PPARγ is activated by endogenous ligands derived from the metabolism of AA. The COX1/COX2 cyclooxygenases, 5 and 12/15 lipoxygenases and CYP enzymes are considered to be critical for the conversion of AA into endogenous PPARγ ligands. To identify how LRH-1 may have an impact on PPARγ activation, we next explored whether LRH-1 can coordinate PPARγ ligand availability through the control of the expression of these enzymes. The mRNA levels of *Ptgs2* (cyclooxygenase 2), *Alox5* (5 lipoxygenase) and *Hpgds* (prostaglandin-D synthase) after IL-13 stimulation were not differentially expressed in *Lrh-1*$^{M+/+}$ and *Lrh-1*$^{M-/-}$ macrophages (Fig. 3f). However, IL-13 robustly induced *Alox15* (12/15 lipoxygenase), *Cyp1a1* and *Cyp1b1* gene expression in *Lrh-1*$^{M+/+}$ macrophages, while this induction was blunted in *Lrh-1*$^{M-/-}$ macrophages. Moreover, Cyp1b1 protein levels were only induced in *Lrh-1*$^{M+/+}$ macrophages on IL-13 exposure, but not in *Lrh-1*$^{M-/-}$ macrophages (Fig. 3g). Unlike *Cyp1a1* and *Cyp1b1* mRNA levels, which were unresponsive to the IL-13 treatment in *Lrh-1*$^{M-/-}$ macrophages, *Alox15* expression was still moderately induced (Fig. 3f), indicating that *Alox15* is only partially controlled by LRH-1.

Consistent with these findings, a strong decrease in *Alox15*, *Cyp1a1* and *Cyp1b1* expression could be observed in both untreated and IL-13-treated *Stat6*$^{-/-}$ macrophages (Fig. 3h), further supporting the importance of STAT6 in the regulation of these genes.

To further explore whether STAT6 controls the expression of *Alox15*, *Cyp1a1* and *Cyp1b1* directly or indirectly through the induction of LRH-1, we performed an *in silico* analysis of *Alox15*, *Cyp1a1* and *Cyp1b1* promoters (Supplementary Fig. 3a). This analysis revealed one putative LRH-1 and two putative STAT6-RE in the *Alox15* promoter, with more than 95% of similarity to the consensus REs. Scanning of the *Cyp1a1* and *Cyp1b1* promoter sequences indicated the presence of conserved LRH-1 REs in both promoters, while no conserved STAT6 REs (matrix similarity <0.8) could be identified in these regulatory regions (Supplementary Fig. 3a). Consistent with these findings, DLPC treatment increased *Alox15, Cyp1a1* and *Cyp1b1* gene expression in *Lrh-1*$^{M+/+}$ macrophages, but not in *Lrh-1*$^{M-/-}$ macrophages (Fig. 3i). These data confirm the importance of LRH-1 in the regulation of *Alox15, Cyp1a1* and *Cyp1b1*.

Finally, to assess whether these effects on gene expression also translate into changes in endogenous ligand availability, 15-HETE production was assessed. Interestingly, while IL-13 exposure robustly enhanced 15-HETE levels in *Lrh-1*$^{M+/+}$ macrophages, this effect was completely lost in *Lrh-1*$^{M-/-}$ macrophages (Fig. 3j). These findings indicate that LRH-1 is critically required for IL-13-induced 15-HETE production in macrophages. Importantly, IL-13-induced mobilization of AA was similar in *Lrh-1*$^{M+/+}$ and *Lrh-1*$^{M-/-}$ macrophages (Fig. 3k), indicating that the generation of 15-HETE metabolites through LRH-1 is dependent on AA metabolism.

To further dissect how LRH-1 promotes the production of 15-HETEs in response to IL-13, we assessed 15-HETE production in *Alox15-deficient* macrophages on *Cyp1a1* and *Cyp1b1* short interfering RNA (siRNA)-mediated silencing (Fig. 3l and Supplementary Fig. 3b). Interestingly, the increased 15-HETE production by IL-13 was still conserved in *Alox15*$^{-/-}$ macrophages. Furthermore, the simultaneous gene silencing for *Cyp1a1* and *Cyp1b1* in both *Alox15* $^{+/+}$ *and Alox15*$^{-/-}$ macrophages abolished this induction (Fig. 3l). Altogether, these data indicate that LRH-1 drives the generation of 15-HETE metabolites through its impact on CYP1 gene expression.

To define whether *Cyp1a1* and *Cyp1b1* are direct transcriptional targets of LRH-1, transfection assays in *Lrh-1*$^{M+/+}$ and *Lrh-1*$^{M-/-}$ macrophages were performed using a luciferase reporter containing ± 1.2 kb of the promoter of the *Cyp1a1* and *Cyp1b1* genes. IL-13 exposure of *Lrh-1*$^{M+/+}$ macrophages

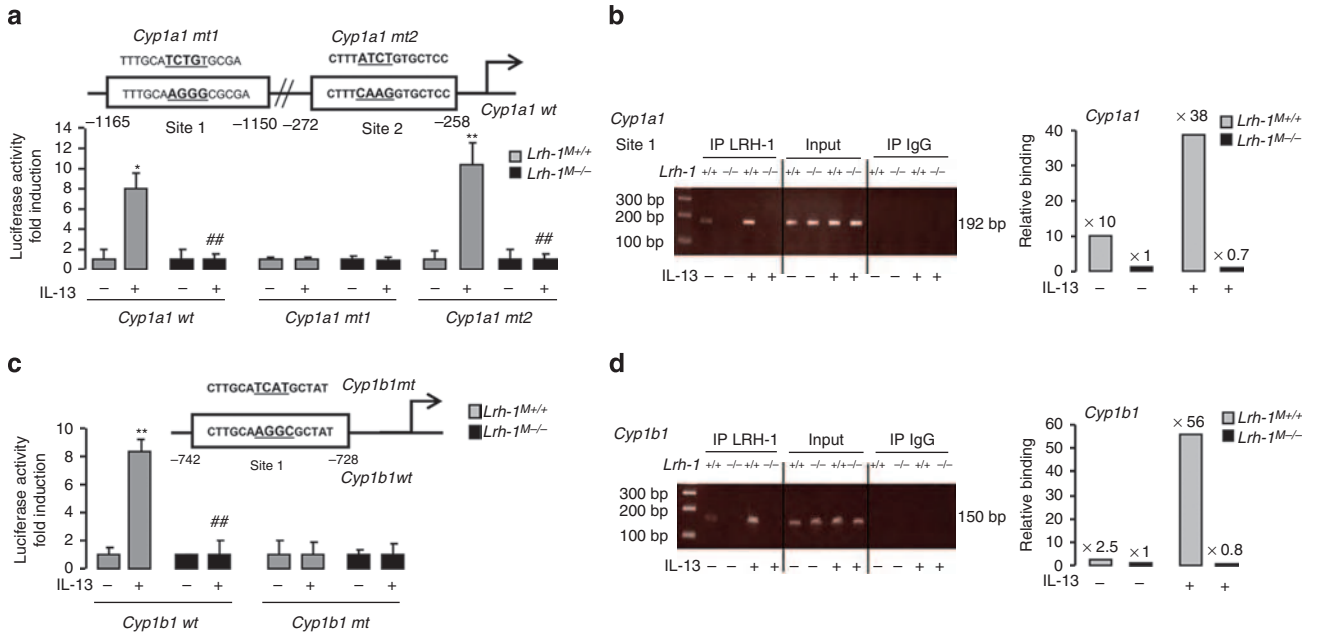

Figure 4 | LRH-1 controls the transcription of *Cyp1a1* and *Cyp1b1* genes in response to IL-13. (**a**–**c**) Luciferase activity in macrophages from *Lrh-1*$^{M+/+}$ and *Lrh-1*$^{M-/-}$ mice transfected with Cyp1a1 promoter constructs (**a**) or Cyp1b1 promoter constructs (**c**) and treated with IL-13 for 18 h. The results were represented in fold induction relative to the untreated control. (**b**,**d**) Assessment of LRH-1 recruitment to site 1 to the *Cyp1a1* promoter (**b**) or *Cyp1b1* promoter (**d**) determined with the ChIP analysis using genomic DNA from *Lrh-1*$^{M+/+}$ and *Lrh-1*$^{M-/-}$ macrophages treated with IL-13 for 18 h. Results correspond to mean ± s.e.m. of triplicates. Data are representative of three independent experiments. $^{*}P<0.05$, $^{**}P<0.01$ compared with the respective untreated control and $^{\#}P<0.05$, $^{\#\#}P<0.01$ compared with the corresponding treated wild-type littermate. *P* values were determined using the Bonferroni–Dunnett method.

resulted in an eightfold increase in reporter activity of both *Cyp1a1* and *Cyp1b* promoters (Fig. 4a,c). Interestingly, genetic deletion of LRH-1 abolished this response, demonstrating that *Cyp1a1* and *Cyp1b1* promoters are directly activated by LRH-1.

To identify the critical LRH-1 REs in the *Cyp1a1* and *Cyp1b1* promoters, we mutagenized the putative RE that were found by in *silico* analysis (Supplementary Fig. 3a), and their response to LRH-1 on IL-13 exposure was compared (Fig. 4a–c). For the *Cyp1a1* promoter, mutation of the first LRH-1 RE (site 1) abolished the activity of the reporter construct in response to IL-13, whereas mutation of site 2 was still responsive in *Lrh-1*$^{M+/+}$ macrophages (Fig. 4a). Furthermore, whole inhibition of mutated reporter construct activities in *Lrh-1*$^{M-/-}$ macrophages established that site 1 is the principal site transmitting the effect of LRH-1 on the *Cyp1a1* promoter. Thus, this result identified specific recruitment of LRH-1 to site 1, which is most distal to the transcription initiation site in the *Cyp1a1* promoter.

For the *Cyp1b1* promoter, IL-13 treatment failed to increase the activity of the mutated *Cyp1b1* reporter in both *Lrh-1*$^{M+/+}$ or *Lrh-1*$^{M-/-}$ macrophages (Fig. 4c), indicating that LRH-1 binds and activates the *Cyp1b1* promoter through a unique sequence between −742 and −728 bp upstream of the transcription initiation site of the gene. Finally, ChIP assays were performed. IL-13 enhanced the recruitment of LRH-1 on both *Cyp1a1* and *Cyp1b1* sites in *Lrh-1*$^{M+/+}$ macrophages, but not in *Lrh-1*$^{M-/-}$ macrophages (Fig. 4b–d). Altogether, these results demonstrate that LRH-1 directly binds *Cyp1a1* and *Cyp1b1* promoters and hence controls the transcription of *Cyp1a1* and *Cyp1b1* genes in response to IL-13.

LRH-1/CYP1-dependent 15-HETE release induces PPARγ activation. To further determine whether the generation of 15-HETE metabolites through LRH-1 are involved in PPARγ activation, we assessed whether supplementation of 15-HETE can rescue the loss of PPARγ activation in *Lrh-1*$^{M-/-}$ macrophages. In contrast to IL-13, which could not induce PPARγ activation in *Lrh-1*$^{M-/-}$ macrophages, addition of exogenous 15-HETE efficiently restored the induction of both a PPRE luciferase reporter (Fig. 5a) and of PPARγ target genes such as *Mrc1, Clec7a* and *Cd36* (Fig. 5b) in *Lrh-1*$^{M-/-}$ macrophages, indicating that the PPARγ activation through LRH-1 is critically dependent on 15-HETE production.

To confirm that 15-HETE production through the LRH-1/CYP1 axis induces PPARγ activation, we evaluated PPARγ activation in macrophages silenced for *Cyp1a1* and *Cyp1b1*. Interestingly, PPARγ activity as determined by the induction of a PPRE luciferase reporter (Fig. 5c) and the induction of PPARγ target genes (Fig. 5d) by IL-13 were totally inhibited in macrophages deficient for *Cyp1a1* and *Cyp1b1*. Moreover, the induction of a PPRE luciferase reporter (Fig. 5c) and of PPARγ target genes (Fig. 5d) was still significantly enhanced by IL-13 in *Alox15*$^{-/-}$ macrophages, showing that the 12/15 lipoxygenase is not required for PPARγ activation mediated by LRH-1. These data are in support of a critical role of CYP1A1 and CYP1B1 in LRH-1-mediated PPARγ activation through 15-HETE synthesis.

IL-13 activation of macrophages requires STAT6/LRH-1/PPARγ. To determine whether STAT6 controls both directly the transcription of markers of IL-13-mediated alternative activation and indirectly through the activation of the LRH-1/PPARγ axis, we studied the mRNA level of alternative activation markers in STAT6-deficient macrophages. IL-13-augmented induction of *Arg1*, *Chi3l3* (*YM1*), *Retnla (Fizz1), MR, Clec7a* and *CD36* was detected in *Stat6*$^{+/+}$ macrophages but not in *Stat6*$^{-/-}$ macrophages (Fig. 5e). The lack of IL-13-augmented induction of alternative markers was associated with a failure of *Stat6*$^{-/-}$ macrophages to produce 15-HETE in response to IL-13 (Fig. 5f). Interestingly, the addition of exogenous 15-HETE restored the induction of alternative polarization markers in *Stat6*$^{-/-}$ macrophages and not in *Pparγ*$^{M-/-}$ macrophages (Fig. 5e and Supplementary Fig. 3c). These data suggest that STAT6 is required for induction of macrophage-alternative activation markers and further support the existence of a PPARγ-dependent mechanism in the regulation of these genes.

Moreover, induction of *Arg1*, *Retnla (Fizz1)* and *Chi3l3* (*YM1*) in response to IL-13 was slightly decreased in *Pparγ*$^{M-/-}$ macrophages, whereas the induction of *Mrc1 (MR), Clec7a* and CD36 was completely abrogated in *Pparγ*$^{M-/-}$ macrophages (Fig. 5g). These results indicate the existence of distinct regulatory mechanisms involving either STAT6 with a modest contribution of PPARγ or predominantly controlled by the LRH-1/PPARγ axis. In line, the overexpression of *Mrc1*, *Clec7a* and *Cd36* after treatment with DLPC in *Pparγ*$^{M+/+}$ macrophages was not detected in *Pparγ*$^{M-/-}$ macrophages (Fig. 5h), clearly establishing that LRH-1 acts upstream from PPARγ in the signalling cascade leading to the PPARγ-dependent gene expression.

IL-13-induced fungicidal properties of macrophages via LRH-1. Previous work from our laboratory established the importance of PPARγ in the fungicidal functions of alternatively activated macrophages[27]. On the basis of the current findings suggesting a role for LRH-1 in PPARγ-mediated alternative polarization following IL-13 stimulation, we next investigated whether deletion of LRH-1 in macrophages could have an impact on the outcome of *Candida albicans* infection. The severe systemic infection of mice with *C. albicans* resulted in a significantly lower survival rate of *Lrh-1*$^{M-/-}$ mice compared with *Lrh-1*$^{M+/+}$ mice ($P<0.001$; Fig. 6a), supporting a role for LRH-1 in antifungal defence. To further explore the exact function of LRH-1 in the pathophysiology of fungal infection, we evaluated the fungal burden in the intestinal tract and the macrophage microbicidal functions in a murine experimental model of gastrointestinal candidiasis. *Lrh-1*$^{M-/-}$ mice infected with *C. albicans* had more severe gastrointestinal infection than their wild-type littermates and showed worsened fungal burden in the caecum (Fig. 6b). Remarkably, IL-13, 15-HETE, as well as DLPC, diminished *C. albicans* gastrointestinal colonization in *Lrh-1*$^{M+/+}$ mice. However, these effects were lost in *Lrh-1*$^{M-/-}$ mice treated with IL-13 or DLPC, but not when the PPARγ ligand, 15-HETE, was administered to the animals (Fig. 6b).

To investigate whether LRH-1 in macrophages has any relevant microbicidal phenotype, we evaluated the capacity of *Lrh-1*$^{M+/+}$ and *Lrh-1*$^{M-/-}$ macrophages to kill yeasts *in vitro*. Compared with *Lrh-1*$^{M+/+}$ macrophages, *Lrh-1*$^{M-/-}$ macrophages showed a defect in their ability to kill *C. albicans,* demonstrating the contribution of LRH-1 in macrophage-intrinsic antifungal activity (Fig. 6c). Consistent with our observation, *Lrh-1*$^{M-/-}$ macrophages were less efficient in engulfing *C. albicans* and producing reactive oxygen species (ROS) after fungal challenge (Fig. 6d,e). Moreover, the defect of *Lrh-1*$^{M-/-}$ macrophages to exert their antifungal activity was correlated with lower MR and Dectin-1 protein levels after *C. albicans* challenge (Supplementary Fig. 3d). As expected, treatment with IL-13 of *Lrh-1*$^{M+/+}$ macrophages increased the killing and the phagocytosis of *C. albicans* and also ROS production in response to *C. albicans*. These inductions were abrogated in *Lrh-1*$^{M-/-}$ macrophages, underscoring the importance of LRH-1 in these fungicidal functions (Fig. 6c–e). Similar effects were obtained when macrophages were stimulated with DLPC (Fig. 6c–e).

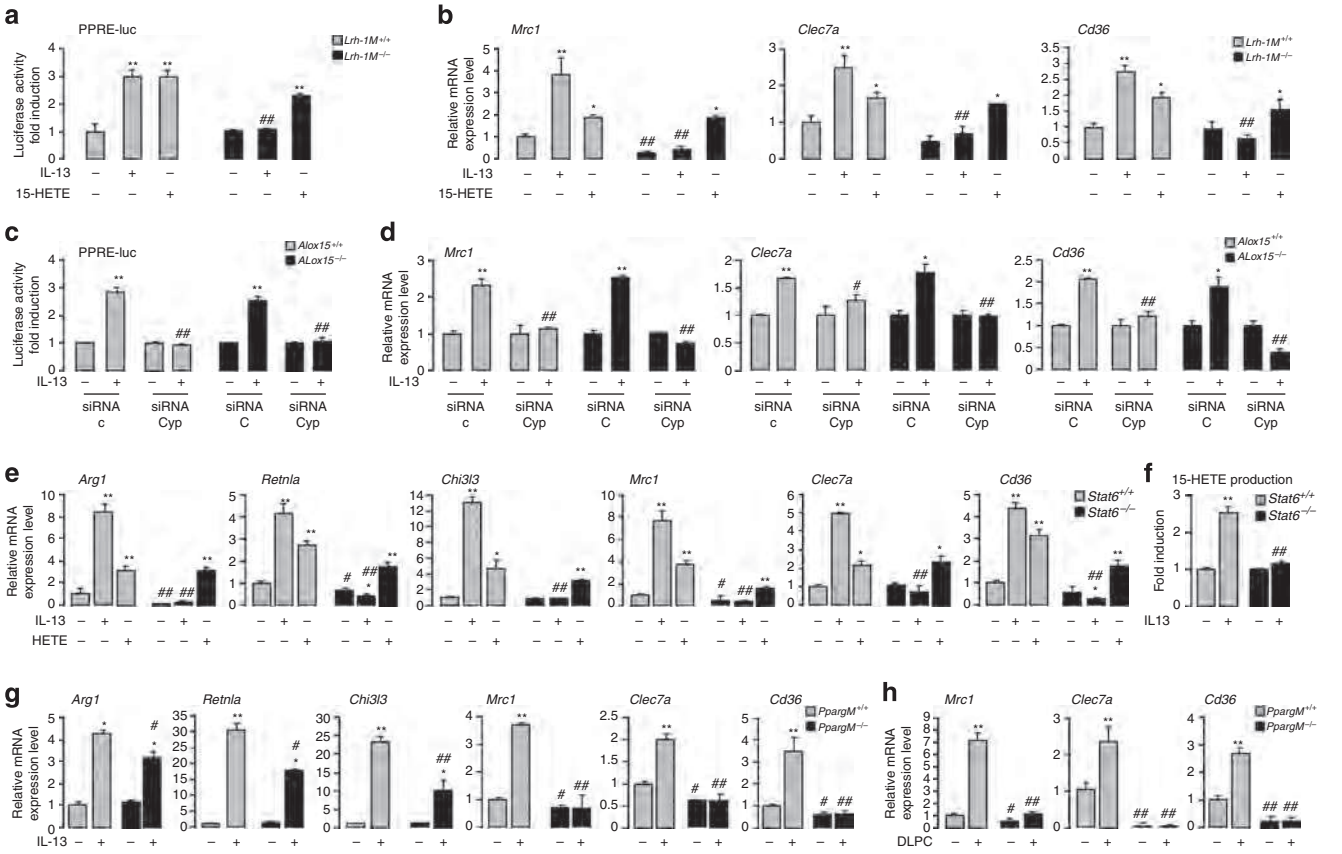

Figure 5 | STAT6/LRH-1/PPARγ signaling is required for IL-13-mediated alternative activation of macrophages. (**a**) Luciferase activity in peritoneal macrophages from *Lrh-1*$^{M+/+}$ and *Lrh-1*$^{M-/-}$ mice transfected with a PPRE (PPRE-luc) construct and treated with IL-13 or 15-HETE for 24 h. (**b**) Gene expression analysis of *Mrc1, Clec7a* and *Cd36* in macrophages from *Lrh-1*$^{M+/+}$ and *Lrh-1*$^{M-/-}$ mice treated with IL-13 or 15-HETE for 4 h, determined by RT-PCR. (**c**) Luciferase activity of macrophages from *ALox15*$^{+/+}$ and *ALox15*$^{-/-}$ mice transfected with a PPRE (PPRE-luc) construct and siRNA targeting Cyp1a1 and Cyp1b1 (siRNA Cyp) and treated with IL-13 for 24 h. (**d**) Gene expression analysis of *Mrc1, Clec7a* and *Cd36* in macrophages from *ALox15*$^{+/+}$ and *ALox15*$^{-/-}$ mice transfected with siRNA targeting Cyp1a1 and Cyp1b1 (siRNA Cyp) treated with IL-13 for 4 h and determined by RT-PCR. (**e**,**g**) Gene expression analysis of *Arg1* (arginase 1), *Retnla* (Fizz1), *Chi3l3* (YM1), *Mrc1, Clec7a* and *Cd36* in macrophages from *Stat6*$^{+/+}$ and *Stat6*$^{-/-}$ mice (**e**) or from *Pparg*$^{M+/+}$ and *Pparg*$^{M-/-}$ mice (**g**) treated with IL-13 or 15-HETE (**e**) for 24 h, determined by RT-PCR. (**f**) 15-HETE production by macrophages from *Stat6*$^{-/-}$ and *Stat6*$^{+/+}$ mice stimulated with IL-13 for 24 h measured by EIA. (**h**) Gene expression analysis of *Mrc1, Clec7a* and *Cd36* in macrophages from *Pparg*$^{M+/+}$ and *Pparg*$^{M-/-}$ treated with DLPC for 4 h, determined by RT-PCR. Results were represented in fold induction compared to the respective untreated control or wild-type littermate and correspond to mean ± s.e.m. of triplicates. Data are representative of three independent experiments. $^{*}P<0.05$, $^{**}P<0.01$ compared to the respective floxed or not untreated control and $^{\#}P<0.05$, $^{\#\#}P<0.01$ compared to the corresponding untreated or treated wild-type littermate or siRNA control. *P* values were determined using Bonferroni–Dunnett method.

Interestingly, treatment with 15-HETE increased the fungicidal functions in both *Lrh-1*$^{M+/+}$ and *Lrh-1*$^{M-/-}$ macrophages (Fig. 6c–e). Moreover, treatment with IL-13, DLPC and 15-HETE of *Pparg*$^{M-/-}$ macrophages did not increase the killing of *C. albicans* (Fig. 6f), corroborating our findings that PPARγ is downstream from LRH-1 in the signalling pathway triggered by IL-13, leading to macrophage fungicidal activities.

To unequivocally establish that the LRH-1/CYP1/HETE axis is involved in macrophage-intrinsic antifungal activity of IL-13, we evaluated the ability of macrophages silenced for Cyp1a1 and Cyp1b1 (Cyp1) to kill *C. albicans*. Interestingly, the increase in *C. albicans* killing by IL-13 and DLPC was inhibited by the simultaneous gene silencing for Cyp1a1 and Cyp1b1 (Cyp1), but not after 15-HETE stimulation (Fig. 6g). Taken together, these data provide *in vivo* evidence that LRH-1 is involved in the PPARγ-dependent antifungal functions elicited by IL-13 through CYP1-induced 15-HETE production.

Discussion

The nuclear receptor PPARγ is essential for IL-13-induced alternative differentiation of macrophages[6,28,29]. We have previously demonstrated that IL-13, via the cPLA$_2$ signalling pathway, induced AA mobilization associated with the nuclear localization of 15d-PGJ2, an endogenous PPARγ ligand[5]. Once activated, PPARγ induces the transcription of *Dectin-1*, *MR* and *CD36*, three genes characteristic of the alternative activation[5,30,31]. Therefore, the processes leading to PPARγ activation, such as AA release and its subsequent metabolic conversion, could be important aspects of alternative polarization because they are limiting factors for PPARγ ligand synthesis.

AA can be metabolized by the COX1/COX2 cyclooxygenases to PGH2, which in turn is transformed by the PGD synthase into 15d-PGJ2 (refs 32,33). AA can also be directly metabolized to 12- and HETEs, other endogenous PPARγ ligands, through 12/15 lipoxygenases[34]. A third pathway of AA metabolism leading to endogenous PPARγ ligand production is associated with its conversion by the enzymes of the CYP family[35–37]. The CYP enzymes generate two biological and active classes of eicosanoids, the epoxy (EETs) and hydroxy (HETEs) derivatives[10,11]. The CYP1 family is mainly involved in the formation of mid-chain HETEs, such as 12- and 15-HETEs, through CYP1A1 and CYP1B1 (refs 12,13).

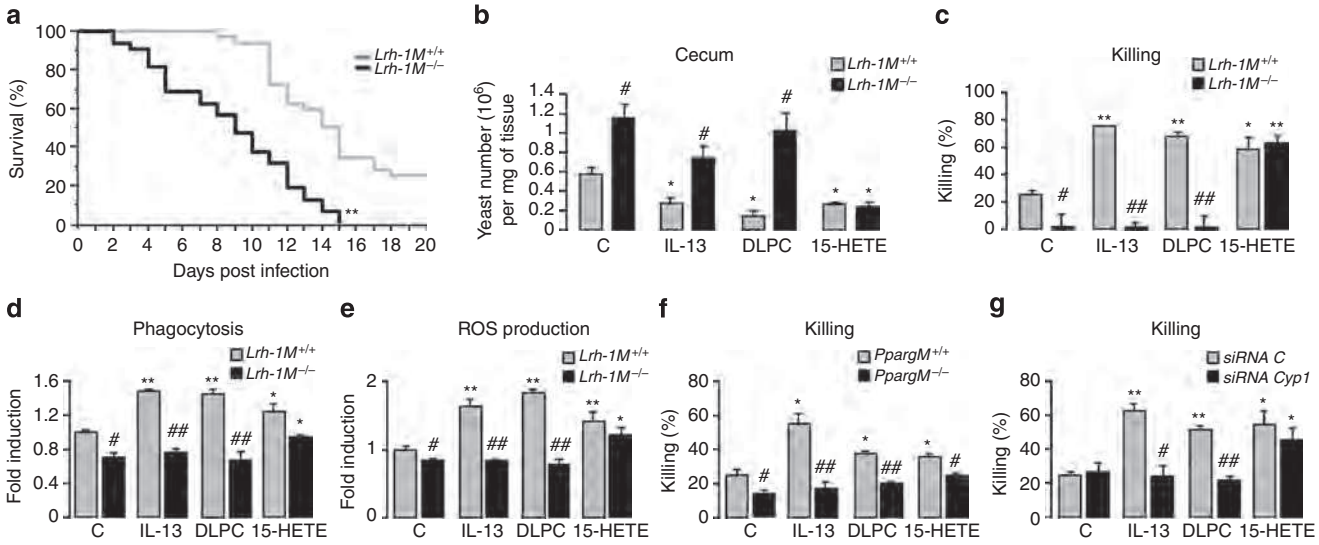

Figure 6 | IL-13-induced antifungal properties of macrophages require LRH-1. (**a**) Survival of *Lrh-1*$^{M-/-}$ and *Lrh-1*$^{M+/+}$ mice to an intraperitoneal injection of *C. albicans* (1.10^8 yeasts per mouse, $n=32$ per group). Survival (%) was assessed twice daily. $^*P<0.001$ compared with *Lrh-1*$^{M+/+}$ mice using log-rank test. (**b**) *Lrh-1*$^{M+/+}$ and *Lrh-1*$^{M-/-}$ mice were infected with *C. albicans*, and treated i.p. without (C) or with IL-13, DLPC or 15-HETE. *C. albicans* gastrointestinal colonization in the caecum was determined on day 7 using RT–PCR. Data are represented as mean ± s.e.m. $^*P<0.05$ compared with the respective untreated control and $^{\#}P<0.05$ compared with the corresponding untreated or treated *Lrh-1*$^{M+/+}$. The data are representative of at least two independent experiments ($n=10$ per group). (**c**) Killing assay of *Lrh-1*$^{M+/+}$ and *Lrh-1*$^{M-/-}$ macrophages incubated with *C. albicans*. (**d**,**e**) Phagocytosis (**d**) and ROS induction (**e**) of *C. albicans* were measured in macrophages from *Lrh-1*$^{M-/-}$ and *Lrh-1*$^{M+/+}$ mice. Data are expressed as fold induction relative to the fluorescence (**c**) or chemiluminescence (**d**) observed for untreated *Lrh-1*$^{M+/+}$. (**f**) Killing assay of *Pparg*$^{M+/+}$ and *Pparg*$^{M-/-}$ macrophages incubated with *C. albicans*. (**g**) Killing assay of macrophages silenced for Cyp1a1 and Cyp1b1 incubated with *C. albicans*. $^*P<0.05$, $^{**}P<0.01$ compared with the respective untreated control and $^{\#}P<0.05$ $^{\#\#}P<0.01$ compared with the corresponding treated wild-type littermate or siRNA control. *P* values were determined using Bonferroni–Dunnett method. Results correspond to mean ± s.e.m. of triplicates and are representative of at least three independent experiments. For indicated measurements, treatments with IL-13, 15-HETE and DLPC were performed 24 h before the challenge with *C. albicans*.

Here we report that the nuclear receptor LRH-1 is expressed in macrophages and in response to IL-13 directly binds CYP1A1 and CYP1B1 promoters to positively regulate their transcription. Moreover, 15-HETE production following IL-13 stimulation is impaired in macrophages deficient for LRH-1 and not in macrophages lacking 12/15 lipoxygenase, indicating that LRH-1 drives the generation of 15-HETE metabolites through its impact on CYP1 gene expression. Consistently, our findings showing that the concurrent gene silencing of *Cyp1a1* and *Cyp1b1* in macrophages abolishes the generation of 15-HETE, provide evidence that its production through the LRH-1/CYP1s axis is crucial in PPARγ activation. This is corroborated by the findings that PPARγ activation on IL-13 stimulation is lost in macrophages silenced simultaneously for CYP1A1/CYP1B1 and restored by the addition of exogenous 15-HETE in macrophages lacking LRH-1. Consistent with these observations, treatment of macrophages with the LRH-1 agonist, DLPC, increased the expression of CD36, MR and Dectin-1 PPARγ target genes in wild-type macrophages but not in macrophages lacking PPARγ. Altogether, these results establish that PPARγ activation by IL-13 is dependent on the LRH-1/CYP1/15-HETE pathway. Another endogenous activator to consider in PPARγ activation is 15d-PGJ2. Although we have previously shown that IL-13 generates 15d-PGJ2 production and its nuclear localization in macrophages[5], the results in this study suggest that it is not sufficient to activate PPARγ. This is supported by previous reports showing that 15d-PGJ2 concentration required to stimulate PPARγ is in the μM range, in contrast to other prostaglandins that are normally active at low nM concentrations[38,39]. Thus, the levels generated *in vivo* are not sufficient to be compatible with a role for this metabolite as an endogenous PPARγ ligand[38,40].

Despite the growing knowledge with regard to the biological function of LRH-1, little is known about how LRH-1 is controlled at the transcriptional level. We identified STAT6 as a transcriptional regulator of LRH-1. This was evidenced by the induction of LRH-1 promoter activity by binding of STAT6 to its RE in the LRH-1 promoter and by the decrease in LRH-1 mRNA and protein levels in macrophages lacking STAT6. On the basis of the established role of STAT6 in PPARγ activation and macrophage polarization[41], these findings identify LRH-1 as a critical component in the signalling cascades that drive PPARγ-mediated alternative macrophage activation. This was further highlighted by the fact that macrophages lacking LRH-1 present an increase in pro-inflammatory cytokines and the simultaneous expression of other M1 markers. The involvement of LRH-1 in anti-inflammatory responses was supported by the robust reduction of LRH-1 gene expression in response to Th1 cytokines and conversely by the upregulation by Th2 cytokines. Interestingly, LRH-1 was also induced in human macrophages in response to the Th2 cytokine IL-13 via a mechanism that is most likely also STAT6-dependent, given the presence of several conserved STAT6 REs in the human *LRH-1* promoter (Supplementary Fig. 3a). Our findings may further explain why during Crohn's disease, characterized by a Th1 cytokine profile, mRNA expression levels of LRH-1 are lower than in ulcerative colitis, characterized by a Th2 immune response[21]. Consistent with the anti-inflammatory role of LRH-1, IL-13-induced alternative activation was impaired in macrophages lacking LRH-1. Indeed, on IL-13 treatment, the induction of several signature genes of alternative activation, including *Arginase 1, YM1, IL-1 receptor antagonist (IL-1ra), MR, Dectin-1* and *CD36*, was significantly impaired in macrophages lacking LRH-1. This is

in agreement with reports showing that LRH-1 controls the expression of anti-inflammatory IL-1ra and the scavenger receptor class B type I, two markers specific of alternatively activated macrophages[22,23,42].

In addition to the key role of LRH-1 in the acquisition of alternative activation of macrophages, this study also provides mechanistic insight into the hierarchy between STAT6, LRH-1 and PPARγ to achieve this phenotype. Our findings showing that loss of induction of alternative activation markers in $Stat6^{-/-}$ macrophages can be restored by exogenous 15-HETE support the notion that STAT6 is required for macrophage-alternative activation through PPARγ-dependent mechanism. Moreover, the use of $Pparγ^{M-/-}$ macrophages provides evidence for the existence of distinct mechanisms in the transcriptional regulation of genes characteristics of alternative activation. Our results demonstrate that the transcriptional regulation of Arginase 1, Fizz 1 and YM1 involves directly STAT6 with a modest contribution of PPARγ and that Dectin-1, MR and CD36 are regulated indirectly by STAT6 through the LRH-1/PPARγ axis. These observations are not only consistent with the requirement of STAT6 to induce the majority of PPARγ target genes[41] but also with the identification of PPARγ as a positive regulator of alternative activation[6].

Consistent with the involvement of the LRH-1/PPARγ pathway in inducing MR and Dectin-1 expression during IL-13-mediated alternative activation, loss of LRH-1 and PPARγ in macrophages also severely compromised their capacity to kill, to engulf *C. albicans* and to produce ROS. This is in line with the fact that LRH-1 is upstream from PPARγ in the signalling pathway leading to the induction of MR and Dectin-1, two C-type lectin receptors strongly involved in the antifungal functions of macrophages against *C. albicans*[5,27,31]. LRH-1 deficiency in myeloid cells also rendered the mice highly susceptible to gastrointestinal and systemic *C. albicans* infection, highlighting LRH-1 of myeloid lineage as a key effector of host fungicidal functions. Although we have not characterized the role of neutrophils in this infectious context, our *in vitro* and *in vivo* results identify LRH-1 as a nuclear receptor indispensable for alternative activation of macrophages and for its associated antifungal functions.

In conclusion, we have shown that loss of LRH-1 in macrophages prevents IL-13-induced alternative activation of macrophages, demonstrating the pivotal role of LRH-1 in the differentiation of macrophages towards an anti-inflammatory and antifungal phenotype. In response to IL-13, LRH-1 expression is increased in macrophages through STAT6 and controls the expression of CYP1A1 and CYP1B1 enzymes, which catalyses the generation of 15-HETE PPARγ ligand. Altogether, these results establish that the alternative polarization of macrophages by IL-13 is dependent on the STAT6/LRH-1/CYPs/15-HETE/PPARγ axis (Fig. 7). Finally, deletion of LRH-1 in myeloid cells renders mice susceptible to gastrointestinal and systemic *C. albicans* infection, highlighting LRH-1 as a critical factor for antifungal functions. Synthetic agonists of LRH-1 activity may, hence, constitute promising compounds for the treatment of anti-infectious and anti-inflammatory diseases.

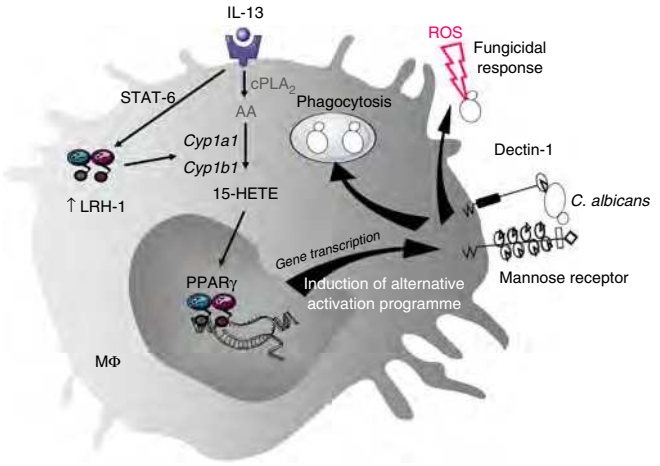

Figure 7 | Schematic illustration of the role of LRH-1 in IL-13-alternative activation program of macrophages and in associated fungicidal activities. The alternative polarization of macrophages by IL-13 is dependent on the increase of LRH-1 expression through STAT-6 which controls the expression of Cyp1a1 and Cyp1b1 enzymes leading to the generation of 15-HETE PPARγ ligand.

Methods

Mice. Male mice aged 10–12 weeks on C57BL/6 background were used for *in vitro* and *in vivo* experiments. Mice were bred and handled by following protocols approved by the Conseil Scientifique du Centre de Formation et de Recherche Experimental Médico Chirurgical and the ethics board of the Midi-Pyrénées ethic committee for animal experimentation (Experimentation permit number 31–067, approval no. B3155503). All cages were changed twice weekly, and all manipulations of the animals were carried out in a laminal blow hood under aseptic conditions. The photoperiod was adjusted to 12-h light and 12-h dark. C57BL/6 mice were purchased from Janvier (France) and $Stat6^{-/-}$ mice and $ALox15^{-/-}$ mice were purchased from Jackson Laboratories. $Pparg^{M-/-}$ mice deleted for *Pparg* specifically in macrophages have been described earlier[30,43]. *Nr5a2* (encoding LRH-1) macrophage specific knockout mice (referred as $Lrh\text{-}1^{M-/-}$ mice) were obtained by crossing mice carrying floxed *Lrh-1* alleles with transgenic mice expressing the Cre recombinase under the control of the mouse phagocyte-selective lysozyme promoter[21,26]. For $Lrh\text{-}1^{M-/-}$ and $Pparg^{M-/-}$ mice, the corresponding floxed littermates were used as controls throughout all the experiments. Corresponding littermates were used as controls for $Stat6^{-/-}$ and $ALox15^{-/-}$ mice.

For the *in vivo* experiments, a gastrointestinal infection with the *C. albicans* strain was established by gavage with 50×10^6 *C. albicans* per mouse ($n = 10$ per group). Mice were treated or not intraperitoneally (i.p.) with IL-13 (Clinisciences), DLPC (Sigma) or 15-HETE (Cayman). For IL-13 treatment, injections of 4 µg per mouse were performed 1 day before and 3 days after the infection with *C. albicans* (two injections). For DLPC (300 µg per 10 g of mouse) and 15-HETE (28 µg per 10 g of mouse), i.p. injections were realized 1 day before the day of the infection with *C. albicans* and then every 2 days (five injections). Control groups received saline solution only with DMSO. After 6 days of infection, the ceca were removed aseptically for the experiments.

For *C. albicans* systemic infection, yeasts were administered i.p. (100×10^6yeasts per mouse). Survival studies were conducted using 32 mice per group and were repeated twice.

Human macrophages. Monocytes were obtained from healthy blood donors (Etablissement Français du Sang, EFS Toulouse). Written informed consents were obtained from the donors under EFS contract no. 21/PVNT/TOU/UPS04/2010–0025. Following articles L1243-4 and R1243-61 of the French Public Health Code, the contract was approved by the French Ministry of Science and Technology (agreement no. AC 2009-921). Human peripheral blood mononuclear cells were isolated from the blood of healthy volunteers by a density gradient centrifugation method on Lymphoprep (Abcys). Monocytes were isolated by adherence to plastic for 2 h in SFM (Gibco) at 37 °C, 5% CO_2. The macrophages were obtained after 3 days of culture only in SFM medium.

Preparation of mouse resident peritoneal macrophages. After being killed, resident peritoneal cells were harvested by washing the peritoneal cavity with 5 ml of sterile NaCl 0.9%. Collected cells were centrifuged at 1,500 r.p.m. for 10 min and the cell pellet was suspended in Dulbecco's modified Eagle's medium (Invitrogen) supplemented with glutamine (Invitrogen), penicillin, streptomycin (Invitrogen) and 5% heat-inactivated fetal calf serum. Cells were allowed to adhere for 2 h at 37 °C and 5% CO_2. Nonadherent cells were then removed by washing with PBS.

Reverse transcription and real-time PCR. After washing, adherent macrophages were immediately stimulated with IFNγ (40 UI ml^{-1}, Clinisciences), IL-6 (50 ng ml^{-1}, Clinisciences), LPS (1 ng ml^{-1}, Sigma), IL-4 (50 ng ml^{-1}, Miltenyi Biotech), IL-13 (50 ng ml^{-1}, Clinisciences), IL-10 (50 ng ml^{-1}, Clinisciences), 15-HETE (1 µM, Cayman) or DLPC (50 µM, Sigma) for 4 or 24 h. In indicated experiments, adherent macrophages were pre-incubated or not with a Jak-2/STAT6 inhibitor, AG490 (1 nM, Tebu-Bio).

The mRNA preparation was made using the EZ-10 Spin Column Total RNA Minipreps Super Kit (Bio Basic) using the manufacturer's protocol. Synthesis of cDNA was performed according to the manufacturer's recommendations (Thermo electron). RT–qPCR was performed on a LightCycler 480 system using LightCycler SYBR Green I Master (Roche Diagnostics). The primers (Eurogentec) were designed with the software Primer 3. *Actb* (Actin) mRNA was used as the invariant control. Serially diluted samples of pooled cDNA were used as external standards in each run for the quantification. Primer sequences are listed in Supplementary Table 1.

***In situ* hybridization.** *In situ* hybridization was performed with digoxigenin-labelled RNA probe (Plasmid pBSSK Lrh-1) as previously described[44]. Briefly, this manual nonradioactive method allows to detect specific complementary mRNA sequences at the cellular level using digoxigenin-labelled probes in a five-step procedure: hybridization of the probe to pretreated tissue at 65 °C; post-hybridization stringent washes; blocking steps to prepare for the immunodetection; primary antibody anti-DIG-AP incubation; and colorimetric enzymatic detection. The detection step lasts for 2–3 days.

Western blot analysis. Nuclear protein extracts were prepared, and lysates were subjected to western blotting as described previously[45]. Briefly, nuclear protein lysates were extracted following standard procedures. Protein extracts were separated using SDS–PAGE. After protein transfer, membranes were incubated overnight at 4 °C with either a rabbit anti-Lrh-1 (ref. 21; 1/1,000), a rabbit polyclonal anti-Tbp (Abcam, ab63766, ½,000), a rabbit anti-Cyp1b1 (Santa Cruz, sc-133490, 1/200) or a Actin (Santa Cruz, sc-1615, 1/1,000) and then for 1 h at room temperature with a peroxidase conjugated secondary antibody. Membranes were washed, and proteins were visualized with the SuperSignal West Pico Chemiluminescent Substrate (ThermoScientific). Images have been cropped for presentation. Full-size images are presented in Supplementary Fig. 4.

Transfection experiments. Macrophages were pre-incubated or not with AG490 (1 nM) and then incubated with 1 µg of DNA per well of the indicated plasmids (pGL3 promoter LRH-1-luciferase, pCMX-LRH-1, PPRE luciferase, pGL3 promoter PPARγ-luciferase, pGL4.12 promoter Cyp1a1-luciferase or pGL4.12 promoter Cyp1b1-luciferase) with JetPei (Polyplus transfection) for 8 h according to the manufacturer's instructions. Then, the cells were stimulated or not with IL-13 (50 ng ml^{-1}) for 18 h. Supernatant was removed, luciferase substrate was added and luminescence was measured with the Envision luminometer (Perkin Elmer).

For siRNA experiments, mouse Cyp1a1 and Cyp1b1 and control siRNA were purchased from Origene. Macrophages were incubated with 20 nM of control siRNA or Cyp1a1 and Cyp1b1 siRNA and with Lipofectamine 2000 (Invitrogen) for 18 h according to the manufacturer's instructions. Cells were then stimulated with IL-13, DLPC or 15-HETE for 18 h.

ChIP. ChIP analysis was performed as described previously with minor adaptations[46]. Briefly, the liver and colon from Lrh-1 +/+ and Lrh-1 −/− mice were lysed (5 mM PIPES pH 8.0, 85 mM KCl, 0.5% NP40 with protease inhibitors). The pellets or adherent macrophages from indicated mice were cross-linked with 1% formaldehyde for 15 min at room temperature. The cells were then lysed in nuclear lysis buffer (50 mM Tris-HCl pH 8.1, 10 mM EDTA, 1% SDS with protease inhibitors) and sonicated at 30% maximum power eight times. The supernatant was diluted in immunoprecipitation-dilution buffer (0.01% SDS, 1.1% Trition X-100, 1.2 mM EDTA, 16.7 mM Tris-Cl pH 8.1 and 167 mM NaCl with protease inhibitor) and precleared with Protein A agarose/salmon sperm DNA beads (Invitrogen 101141). The samples were immunoprecipitated overnight at 4 °C with a rabbit Lrh-1 antibody[21], normal rabbit IgG (Santa Cruz, sc-2027, 7 µl/ml) or with a rabbit STAT6 antibody (Santa Cruz, sc-981, 7 µl ml^{-1}). The beads were then washed in low-salt buffer (0.1% SDS, 1% Triton X-100, 2 mM EDTA, 20 mM Tris-HCl pH 8 and 150 mM NaCl), high-salt buffer (0.1% SDS, 1% Triton X-100, 2 mM EDTA, 20 mM Tris-HCl pH 8 and 500 mM NaCl) and LiCl buffer (1% NP40, 1% deoxycholate, 1 mM EDTA, 10 mM Tris-HCl pH 8 and 250 mM LiCl). The samples were then boiled in chelex followed by incubation with proteinase K solution (10 µg ml^{-1} proteinase K; 10 mM EDTA; and 37 mM Tris-HCl, pH 6.5) at 55 °C for 30 min. DNA was purified using the EZ-10 Spin Column Total RNA Minipreps Super Kit (Bio Basic), after which qPCR was performed. Data were normalized for GAPDH promoter binding and expressed relative to IgG. ChIP primer sequences are listed in Supplementary Table 2.

Reporter assays and site-directed mutagenesis. Genomic DNA was extracted from mouse kidneys and the corresponding Cyp1a1 and Cyp1b1 promoter fragments were amplified by PCR with primers containing KpnI and XhoI restriction sites. The PCR products were then cloned into pENTR-D/TOPO (Invitrogen/Lifetechnologies) plasmids, which were digested with KpnI and XhoI and then ligated into pGL4.12 (Promega) reporter plasmids.

Mutagenesis was carried out with the GeneArt mutagenesis kit (Invitrogen/Lifetechnologies) according to the manufacturer's instructions. The sequences of reporter constructs were analysed and confirmed.

Flow cytometry. The analysis was performed on nonadherent macrophages[47] harvested by washing the peritoneal cavity with 5 ml of sterile NaCl 0.9%. Collected cells were centrifuged at 1,500 r.p.m. for 10 min and the cell pellet was suspended in PBS medium supplemented with 1% fetal calf serum (FCS). Surface expressed Dectin-1 or CD36 was detected, respectively, using fluoroscein isothiocyanate (FITC)-Dectin-1 monoclonal antibody (mAb; Serotec MCA2289F, 1/100) or PE-CD36 mAb (Santa Cruz, sc-13572, 1/100) and was compared with an irrelevant appropriate isotype control. To evaluate the mannose receptor (MR) surface expression, we have used MR-specific ligand conjugated with FITC (Sigma A7790, 1 mg ml^{-1}). All stainings were performed on PBS—1% FCS medium. A population of 10,000 cells was analysed for each data point. All analyses were carried out in a Becton Dickinson FACScalibur using the CellQuestPro software.

B and T lymphocytes were isolated from the mouse spleen with a PE-B220 mAb (RD System FAB1217P, 1/10) and a PE-CD3 mAb (eBiosciences MCA500, 1/10) using a Becton Dickinson Influx cell sorter.

ELISA Cytokine titration and EIA quantification of 15-HETE. Peritoneal macrophages were stimulated with IL-13 for 18 h and challenged with non-opsonized *C. albicans* at a yeast-to-macrophage ratio of 3:1 for 8 h. The production of TNF-α, IL-1β and TGF-β in the cell supernatants was determined with a commercially available OptiEIA kit (BD Biosciences) according to the manufacturer's instructions.

For 15-HETE quantification, the macrophages were stimulated with IL-13 for 18 h and 15-HETE were measured using EIA as recommended by the manufacturer's protocol (15(S)-HETE EIA kit, Cayman).

AA mobilization. Peritoneal macrophages were prelabelled with [^{3}H]AA (1 µCi per well, Perkin Elmer) for 18 h. The prelabelled macrophages were then treated with IL-13 (50 ng ml^{-1}) for 1 h. The cellular lipids were extracted twice with hexane/isopropanol (3:2, v/v) and the [^{3}H]AA content in membrane phospholipids was quantified by measurement of the radioactivity by beta liquid scintillation counting, as described with minor adaptations[48].

***C. albicans* strain.** The strain of *C. albicans* used throughout these experiments was isolated from a blood culture of a Toulouse-Rangueil Hospital patient[5]. Fluorescent *C. albicans* was prepared by adding *C. albicans* to FITC (Sigma) dissolved in sodium carbonate buffer (pH 9.5) at room temperature for 3 h and washed by centrifugation three times in sodium carbonate buffer before storage in aliquots of water at 4 °C.

Phagocytosis assay and ROS quantification. For analysis of phagocytosis of *C. albicans*, cultured macrophages were pretreated or not with IL-13, 15-HETE or DLPC for 18 h and then challenged with six FITC-labelled yeasts per macrophage. Phagocytosis was initiated at 37 °C with 5% CO_2 and stopped after 1 h by washing the macrophages with ice-cold PBS. The number of *C. albicans* engulfed by macrophages was determined with fluorescence quantification using the Envision (Perkin Elmer) fluorimetry-based approach.

The oxygen-dependent respiratory burst of macrophages (ROS production) was measured by chemiluminescence in the presence of 5-amino-2,3-dihydro-1,4-phthalazinedione (luminol) using a thermostatically (37 °C) controlled luminometer (Wallac 1420 Victor2). The generation of chemoluminescence was monitored continuously for 1 h after incubation of the cells with luminol (66 µM) and pretreatment with IL-13, 15-HETE or DLPC for 18 h and challenge with *C. albicans* (yeast-to-macrophage ratio: 3:1). Statistical analysis was performed using the area under the curve expressed in counts × seconds.

Killing assay. The killing assay was performed as previously described[49]. Cells were allowed to interact for 30 min at 37 °C with *C. albicans* (at a ratio of 0.3 yeast per macrophage) and unbound yeasts were removed by four washes with medium. Macrophages were then incubated at 37 °C for 4 h. Control plates were kept at 4 °C to provide a measure of live *C. albicans* in the wells. After incubation, the medium was removed and cells were lysed by incubation for 5 min at 25 °C with water at a pH of 11. An excess of PBS was used to neutralize the lysis buffer, and CFU *C. albicans* was determined by plating on Sabouraud plates and incubation overnight at 37 °C.

Quantification of *C. albicans* in the caecum. *Cell lysis and DNA extraction*. After mouse infection, ceca were aseptically removed and then crushed using lysing matrix tubes (MP Biomedicals). Tissue sample homogenate (250 µl) was resuspended in 200 µl of lysis buffer for 2 h at 65 °C and DNA was then extracted with isopropanol and eluted with an elution buffer (High Pure PCR Template preparation kit, Roche Diagnostics).

Light cycler-based PCR assay. The Light Cycler PCR and detection system (Roche Diagnostics) was used for amplification and online quantification. PCR analysis was performed as described previously[27]. Serially diluted samples of genomic fungal DNA obtained from *C. albicans* cultures (40×10^6 cells) were used as external standards in each run. Cycle numbers of the logarithmic linear phase were plotted against the logarithm of the concentration of template DNA to evaluate the number of yeast cells present in each tissue sample homogenate.

Statistical analysis. For each experiment, the data were subjected to one-way analysis of variance followed by the means multiple comparison method of Bonferroni–Dunnett. For survival study, statistical significance was determined by a log-rank test. $P<0.05$ was considered as the level of statistical significance.

References

1. Gilroy, D. W., Lawrence, T., Perretti, M. & Rossi, A. G. Inflammatory resolution: new opportunities for drug discovery. *Nat. Rev. Drug Discov.* **3,** 401–416 (2004).
2. Gordon, S. & Martinez, F. O. Alternative activation of macrophages: mechanism and functions. *Immunity* **32,** 593–604 (2010).
3. Mantovani, A. *et al.* The chemokine system in diverse forms of macrophage activation and polarization. *Trends Immunol.* **25,** 677–686 (2004).
4. Greenberg, M. E. *et al.* Oxidized phosphatidylserine-CD36 interactions play an essential role in macrophage-dependent phagocytosis of apoptotic cells. *J. Exp. Med.* **203,** 2613–2625 (2006).
5. Coste, A. *et al.* PPARgamma promotes mannose receptor gene expression in murine macrophages and contributes to the induction of this receptor by IL-13. *Immunity* **19,** 329–339 (2003).
6. Odegaard, J. I. *et al.* Macrophage-specific PPARgamma controls alternative activation and improves insulin resistance. *Nature* **447,** 1116–1120 (2007).
7. Boyer, J. F. *et al.* Tumor necrosis factor alpha and adalimumab differentially regulate CD36 expression in human monocytes. *Arthritis Res. Ther.* **9,** R22 (2007).
8. Mrácek, T., Cannon, B. & Houstek, J. IL-1 and LPS but not IL-6 inhibit differentiation and downregulate PPAR gamma in brown adipocytes. *Cytokine* **26,** 9–15 (2004).
9. Daynes, R. A. & Jones, D. C. Emerging roles of PPARs in inflammation and immunity. *Nat. Rev. Immunol.* **2,** 748–759 (2002).
10. Liu, Y. *et al.* The antiinflammatory effect of laminar flow: the role of PPARgamma, epoxyeicosatrienoic acids, and soluble epoxide hydrolase. *Proc. Natl Acad. Sci. USA* **102,** 16747–16752 (2005).
11. Zhao, G. *et al.* Epoxyeicosatrienoic acids protect rat hearts against tumor necrosis factor-α-induced injury. *J. Lipid Res.* **53,** 456–466 (2012).
12. Choudhary, D., Jansson, I., Stoilov, I., Sarfarazi, M. & Schenkman, J. B. Metabolism of retinoids and arachidonic acid by human and mouse cytochrome P450 1b1. *Drug Metab. Dispos.* **32,** 840–847 (2004).
13. Elbekai, R. H. & El-Kadi, A. O. S. Cytochrome P450 enzymes: central players in cardiovascular health and disease. *Pharmacol. Ther.* **112,** 564–587 (2006).
14. Fayard, E., Auwerx, J. & Schoonjans, K. LRH-1: an orphan nuclear receptor involved in development, metabolism and steroidogenesis. *Trends Cell Biol.* **14,** 250–260 (2004).
15. Lee, Y.-K. & Moore, D. D. Liver receptor homolog-1, an emerging metabolic modulator. *Front. Biosci.* **13,** 5950–5958 (2008).
16. Krylova, I. N. *et al.* Structural analyses reveal phosphatidyl inositols as ligands for the NR5 orphan receptors SF-1 and LRH-1. *Cell* **120,** 343–355 (2005).
17. Lee, J. M. *et al.* A nuclear-receptor-dependent phosphatidylcholine pathway with antidiabetic effects. *Nature* **474,** 506–510 (2011).
18. Musille, P. M. *et al.* Antidiabetic phospholipid-nuclear receptor complex reveals the mechanism for phospholipid-driven gene regulation. *Nat. Struct. Mol. Biol.* **19,** 532–537 (2012).
19. Oosterveer, M. H. *et al.* LRH-1-dependent glucose sensing determines intermediary metabolism in liver. *J. Clin. Invest.* **122,** 2817–2826 (2012).
20. Schoonjans, K. *et al.* Liver receptor homolog 1 contributes to intestinal tumor formation through effects on cell cycle and inflammation. *Proc. Natl Acad. Sci. USA* **102,** 2058–2062 (2005).
21. Coste, A. *et al.* LRH-1-mediated glucocorticoid synthesis in enterocytes protects against inflammatory bowel disease. *Proc. Natl Acad. Sci. USA* **104,** 13098–13103 (2007).
22. Venteclef, N. & Delerive, P. Interleukin-1 receptor antagonist induction as an additional mechanism for liver receptor homolog-1 to negatively regulate the hepatic acute phase response. *J. Biol. Chem.* **282,** 4393–4399 (2007).
23. Venteclef, N., Smith, J. C., Goodwin, B. & Delerive, P. Liver receptor homolog 1 is a negative regulator of the hepatic acute-phase response. *Mol. Cell Biol.* **26,** 6799–6807 (2006).
24. Fernandez-Marcos, P. J., Auwerx, J. & Schoonjans, K. Emerging actions of the nuclear receptor LRH-1 in the gut. *Biochim. Biophys. Acta* **1812,** 947–955 (2011).
25. Goenka, S. & Kaplan, M. H. Transcriptional regulation by STAT6. *Immunol. Res.* **50,** 87–96 (2011).
26. Clausen, B. E., Burkhardt, C., Reith, W., Renkawitz, R. & Förster, I. Conditional gene targeting in macrophages and granulocytes using LysMcre mice. *Transgenic Res.* **8,** 265–277 (1999).
27. Coste, A. *et al.* IL-13 attenuates gastrointestinal candidiasis in normal and immunodeficient RAG-2(− / −) mice via peroxisome proliferator-activated receptor-gamma activation. *J. Immunol.* **180,** 4939–4947 (2008).
28. Lawrence, T. & Natoli, G. Transcriptional regulation of macrophage polarization: enabling diversity with identity. *Nat. Rev. Immunol.* **11,** 750–761 (2011).
29. Olefsky, J. M. & Glass, C. K. Macrophages, inflammation, and insulin resistance. *Annu. Rev. Physiol.* **72,** 219–246 (2010).
30. Berry, A. *et al.* IL-13 induces expression of CD36 in human monocytes through PPARgamma activation. *Eur. J. Immunol.* **37,** 1642–1652 (2007).
31. Galès, A. *et al.* PPARgamma controls dectin-1 expression required for host antifungal defense against *Candida albicans*. *PLoS Pathog.* **6,** e1000714 (2010).
32. Kliewer, S. A. *et al.* A prostaglandin J2 metabolite binds peroxisome proliferator-activated receptor gamma and promotes adipocyte differentiation. *Cell* **83,** 813–819 (1995).
33. Smith, W. L., Garavito, R. M. & DeWitt, D. L. Prostaglandin endoperoxide H synthases (Cyclooxygenases)-1 and -2. *J. Biol. Chem.* **271,** 33157–33160 (1996).
34. Huang, J. T. *et al.* Interleukin-4-dependent production of PPAR-γ ligands in macrophages by 12/15-lipoxygenase. *Nature* **400,** 378–382 (1999).
35. Bellien, J., Joannides, R., Richard, V. & Thuillez, C. Modulation of cytochrome-derived epoxyeicosatrienoic acids pathway: a promising pharmacological approach to prevent endothelial dysfunction in cardiovascular diseases? *Pharmacol. Ther.* **131,** 1–17 (2011).
36. Capdevila, J. H., Falck, J. R. & Harris, R. C. Cytochrome P450 and arachidonic acid bioactivation: molecular and functional properties of the arachidonate monooxygenase. *J. Lipid Res.* **41,** 163–181 (2000).
37. Zordoky, B. N. M. & El-Kadi, A. O. S. Effect of cytochrome P450 polymorphism on arachidonic acid metabolism and their impact on cardiovascular diseases. *Pharmacol. Ther.* **125,** 446–463 (2010).
38. Abdelrahman, M., Sivarajah, A. & Thiemermann, C. Beneficial effects of PPAR-gamma ligands in ischemia-reperfusion injury, inflammation and shock. *Cardiovasc. Res.* **65,** 772–781 (2005).
39. Powell, W. S. 15-Deoxy-delta12,14-PGJ2: endogenous PPARgamma ligand or minor eicosanoid degradation product? *J. Clin. Invest.* **112,** 828–830 (2003).
40. Bell-Parikh, L. C. *et al.* Biosynthesis of 15-deoxy-delta12,14-PGJ2 and the ligation of PPARgamma. *J. Clin. Invest.* **112,** 945–955 (2003).
41. Szanto, A. *et al.* STAT6 transcription factor is a facilitator of the nuclear receptor PPARγ-regulated gene expression in macrophages and dendritic cells. *Immunity* **33,** 699–712 (2010).
42. Schoonjans, K. *et al.* Liver receptor homolog 1 controls the expression of the scavenger receptor class B type I. *EMBO Rep.* **3,** 1181–1187 (2002).
43. Olagnier, D. *et al.* Nrf2, a PPARγ alternative pathway to promote CD36 expression on inflammatory macrophages: implication for malaria. *PLoS Pathog.* **7,** e1002254 (2011).
44. Modica, S. *et al.* The intestinal nuclear receptor signature with epithelial localization patterns and expression modulation in tumors. *Gastroenterology* **138,** 636–648 (2010).
45. Mataki, C. *et al.* Compromised intestinal lipid absorption in mice with a liver-specific deficiency of liver receptor homolog 1. *Mol. Cell Biol.* **27,** 8330–8339 (2007).
46. Stein, S. *et al.* SUMOylation-dependent LRH-1/PROX1 interaction promotes atherosclerosis by decreasing hepatic reverse cholesterol transport. *Cell Metab.* **20,** 603–613 (2014).
47. Lefèvre, L. *et al.* PPARγ ligands switched high fat diet-induced macrophage M2b polarization toward M2a thereby improving intestinal *Candida* elimination. *PLoS ONE* **5,** e12828 (2010).
48. Del Bufalo, A. *et al.* Contact sensitizers modulate the arachidonic acid metabolism of PMA-differentiated U-937 monocytic cells activated by LPS. *Toxicol. Appl. Pharmacol.* **256,** 35–43 (2011).
49. Taylor, P. R. *et al.* Dectin-1 is required for beta-glucan recognition and control of fungal infection. *Nat. Immunol.* **8,** 31–38 (2007).

Acknowledgements

We thank Philippe Batigne and Bénédicte Bertrand from the Université Paul Sabatier for excellent technical support, and Alexia Zakaroff-Girard and Christiane Pécher (TRI imaging platform, IFR150/I2MC) for flow cytometry technical assistance. This research project has received, through BIOASTER investment, funding from the French Government through the Investissement d'Avenir programme (grant n°ANR-10-AIRT-03). This research was also supported by a grant from l'Association de la Recherche contre le Cancer (ARC) awarded to L.L. (DOC20120605122) and Swiss Cancer Ligue (to K.S.).

Author contributions

A.C., K.S., B.P. and L.L. designed the study, analysed the data and wrote the manuscript. L.L. and A.H. performed and analysed the experiments. S.S., C.M., B.C., C.D., M.A.E., E.M., J.B. and A.V. generated tools and/or helped with specific experiments.

Additional information

Supplementary Information accompanies this paper at http://www.nature.com/naturecommunications

Competing financial interests: The authors declare no competing financial interests.

How to cite this article: Lefèvre, L. *et al.* LRH-1 mediates anti-inflammatory and antifungal phenotype of IL-13-activated macrophages through the PPARγ ligand synthesis. *Nat. Commun.* 6:6801 doi: 10.1038/ncomms7801 (2015).

Impaired SUMOylation of nuclear receptor LRH-1 promotes nonalcoholic fatty liver disease

Sokrates Stein,[1,2] Vera Lemos,[1,3] Pan Xu,[1] Hadrien Demagny,[1] Xu Wang,[4] Dongryeol Ryu,[4] Veronica Jimenez,[5] Fatima Bosch,[5] Thomas F. Lüscher,[2] Maaike H. Oosterveer,[6] and Kristina Schoonjans[1]

[1]Laboratory of Metabolic Signaling, Institute of Bioengineering, School of Life Sciences, École Polytechnique Fédérale de Lausanne, Lausanne, Switzerland. [2]Center for Molecular Cardiology, University of Zurich, Zurich, Switzerland. [3]Abel Salazar Biomedical Sciences Institute, University of Porto, Porto, Portugal. [4]Laboratory of Integrative and Systems Physiology, Institute of Bioengineering, School of Life Sciences, École Polytechnique Fédérale de Lausanne, Lausanne, Switzerland. [5]Center of Animal Biotechnology and Gene Therapy and Department of Biochemistry and Molecular Biology, School of Veterinary Medicine, Universitat Autònoma de Barcelona, Bellaterra, and Centro de Investigación Biomédica en Red de Diabetes y Enfermedades Metabólicas Asociadas (CIBERDEM), Barcelona, Spain. [6]Department of Pediatrics, Center for Liver Digestive and Metabolic Diseases, University of Groningen, University Medical Center Groningen, Groningen, The Netherlands.

Hepatic steatosis is caused by metabolic imbalances that could be explained in part by an increase in de novo lipogenesis that results from increased sterol element binding protein 1 (SREBP-1) activity. The nuclear receptor liver receptor homolog 1 (LRH-1) is an important regulator of intermediary metabolism in the liver, but its role in regulating lipogenesis is not well understood. Here, we have assessed the contribution of LRH-1 SUMOylation to the development of nonalcoholic fatty liver disease (NAFLD). Mice expressing a SUMOylation-defective mutant of LRH-1 (LRH-1 K289R mice) developed NAFLD and early signs of nonalcoholic steatohepatitis (NASH) when challenged with a lipogenic, high-fat, high-sucrose diet. Moreover, we observed that the LRH-1 K289R mutation induced the expression of oxysterol binding protein-like 3 (OSBPL3), enhanced SREBP-1 processing, and promoted de novo lipogenesis. Mechanistically, we demonstrated that ectopic expression of OSBPL3 facilitates SREBP-1 processing in WT mice, while silencing hepatic *Osbpl3* reverses the lipogenic phenotype of LRH-1 K289R mice. These findings suggest that compromised SUMOylation of LRH-1 promotes the development of NAFLD under lipogenic conditions through regulation of OSBPL3.

Introduction

Hepatic steatosis is characterized by the excessive accumulation of triglycerides as a consequence of an imbalance between the acquisition and disposal of fatty acids. Increased hepatic uptake of adipose tissue–derived fatty acids, defective breakdown via β-oxidation, reduced VLDL-triglyceride secretion, and induced activity of master regulators of de novo lipogenesis, such as sterol element binding protein 1 (SREBP-1, encoded by *Srebf1*), are factors that contribute to the development of steatosis (1). Nonalcoholic fatty liver disease (NAFLD) comprises a spectrum of disorders, of which the earliest stage is characterized by the deposition of lipid droplets within the cytoplasm of the hepatocytes. NAFLD increases the susceptibility to hepatocyte damage and inflammation, a condition termed nonalcoholic steatohepatitis (NASH), and can ultimately progress to cirrhosis and hepatocellular carcinoma (HCC) (1–4).

Liver receptor homolog 1 (LRH-1) is a nuclear receptor with diverse biological functions ranging from cell cycle regulation to the control of steroid homeostasis. In the liver, LRH-1 is an important regulator of glucose, cholesterol, and bile acid metabolism (5). Liver-specific *Lrh-1* knockout mice display reduced glycolytic flux and de novo lipogenesis secondary to impaired glucokinase activity (6). On the other hand, treatment of mice with the LRH-1 agonist 1,2-dilauroyl-*sn*-glycero-3-phosphocholine (DLPC) protects animals from developing NAFLD and insulin resistance in genetic and dietary models of diabesity (7, 8). To address this apparent contradictory role of LRH-1 in hepatic triglyceride metabolism, we chose to study lipogenesis in our recently described *Lrh-1* K289R knockin mouse model (LRH-1 K289R mice), which displays selective gain of function of LRH-1 as a result of impaired SUMOylation at K289 (9).

In this study, we demonstrate that LRH-1 K289R induces the expression of oxysterol binding protein-like 3 (OSBPL3, encoded by *Osbpl3*, also known as *Orp3*), which in turn promotes the posttranslational activation of SREBP-1. As a consequence, LRH-1 K289R mice display increased de novo lipogenesis upon refeeding in comparison with WT mice. In fact, compared with what is seen in LRH-1 WT mice, this chronic lipogenic stress promotes NAFLD in LRH-1 K289R mice accompanied by early signs of NASH when mice are exposed to a lipogenic, high-fat, high-sucrose (HFHS) diet.

Results

Increased hepatic SREBP-1 processing in LRH-1 K289R mice. In order to evaluate the role of an LRH-1 SUMO–defective pathway on intermediary liver metabolism, we subjected LRH-1 K289R mice, which exhibit partial gain of function of LRH-1, and control LRH-1 WT mice (9) to fasting-refeeding challenges in which mice were fasted and then refed for a period of 6 hours. We then evaluated the expression of metabolic genes in refed livers of both genotypes using microarray analysis. Interestingly, the expression of

Authorship note: S. Stein and V. Lemos contributed equally to this work.
Conflict of interest: The authors have declared that no conflict of interest exists.
Submitted: November 11, 2015; **Accepted:** November 22, 2016.
Reference information: *J Clin Invest*. 2017;127(2):583–592.
https://doi.org/10.1172/JCI85499.

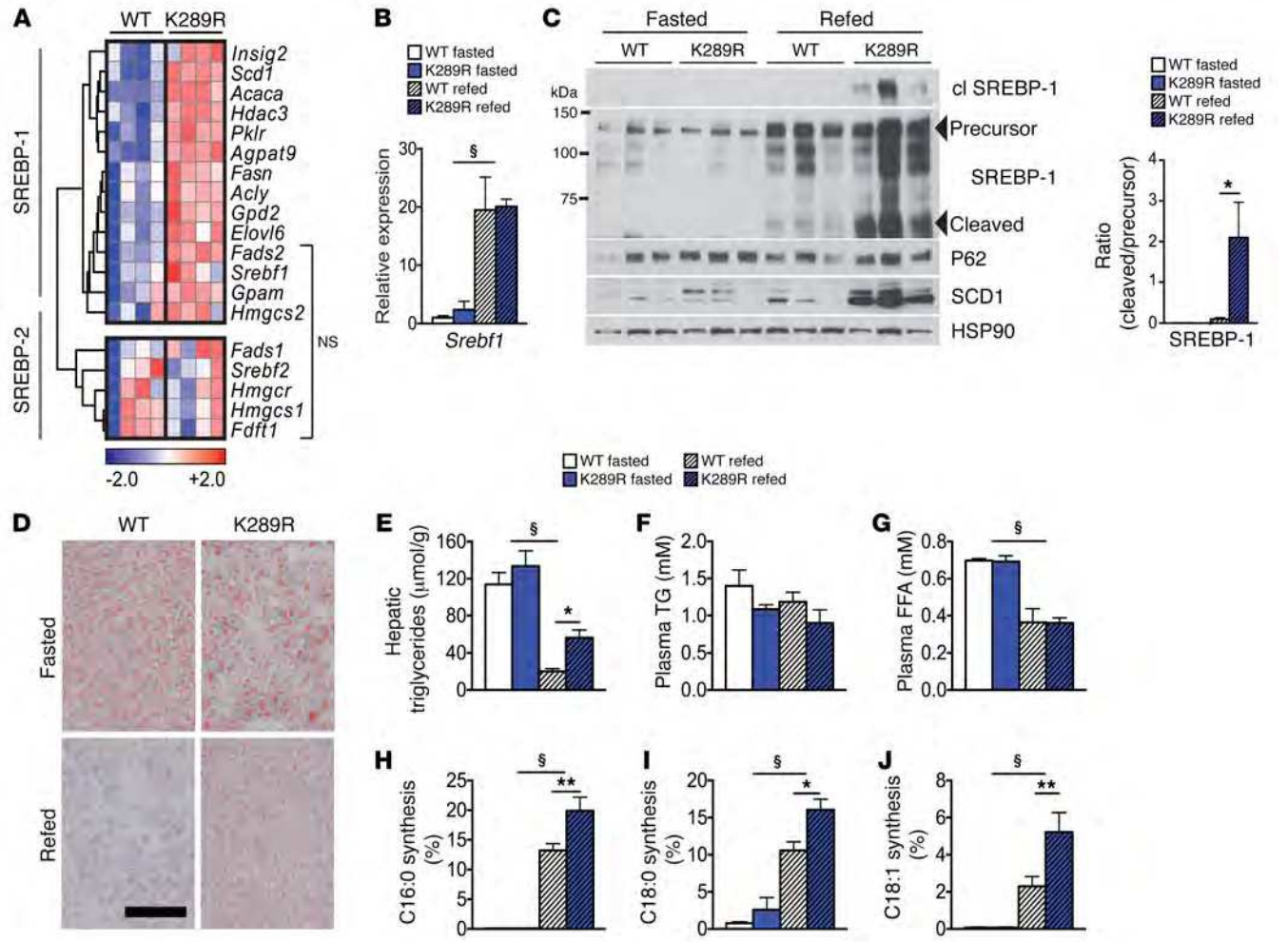

Figure 1. LRH-1 K289R mice display increased de novo lipogenesis. (**A**) Heat map showing the expression of genes involved in de novo fatty acid and cholesterol synthesis in refed WT and K289R mice. Normalized expression values are in $\log_2$ scale. SREBP-1, depicting mainly SREBP-1 target genes; SREBP-2, mostly SREBP-2 target genes; NS, transcripts that are not significantly changed between the indicated genotypes. For all other transcripts $P < 0.05$. (**B**) Hepatic mRNA expression of *Srebf1* in K289R and WT mice. $n = 10$ per genotype. (**C**) Left, immunoblots of precursor and cleaved (cl) SREBP-1, SCD1, HSP90, and P62 in hepatic lysates of WT or K289R livers. Right, graph displaying the ratio of cleaved to precursor SREBP-1. (**D**) Representative images of liver sections of K289R or WT mice stained with oil red O to visualize neutral lipids. Scale bar: 200 μm. (**E**) Quantification of hepatic triglyceride content in WT and K289R mice. $n = 10$ per group. (**F** and **G**) Plasma triglyceride (TG) and free fatty acid (FFA) contents in WT and K289R mice. $n = 10$ per group. (**H**–**J**) Fractional de novo synthesis rates of palmitate (**H**), stearate (**I**), and oleate (**J**) in WT and K289R mice. $n = 6$ per group. Error bars represent mean ± SEM. $^*P < 0.05$, $^{**}P < 0.01$ relative to WT within each nutritional state; $^{§}P < 0.001$ refed relative to fasted mice, as determined by unpaired Student's *t* test (**A**) or 2-way ANOVA with Bonferroni's post-hoc test (**B**, **C**, **E**–**J**). WT, LRH-1 WT; K289R, LRH-1 K289R mice.

many SREBP-1 target genes was increased in 6-hour–refed LRH-1 K289R compared with LRH-1 WT livers, whereas SREBP-2 targets were not altered (Figure 1A). Although no changes in *Srebf1* mRNA (Figure 1B) or uncleaved precursor SREBP-1 (Figure 1C) could be observed between both genotypes, refed LRH-1 K289R livers displayed significantly more of the cleaved and transcriptionally active SREBP-1 protein in comparison with the LRH-1 WT livers (Figure 1C), indicating that the posttranslational processing and maturation of SREBP-1 is increased in LRH-1 K289R mice. We then performed acute insulin challenges as well as shorter 2-hour refeeding experiments to analyze whether early signaling events could explain the increased SREBP-1 activity. Insulin did not induce an additional increase in AKT phosphorylation or a consistent induction of early response genes, such as activating transcription factor 3 (*Atf3*) or early growth response 1 (*Egr1*) (Supplemental Figure 1, A and B; supplemental material available online with this article; https://doi.org/10.1172/JCI85499DS1) (10, 11), in LRH-1 K289R versus LRH-1 WT livers. Similarly, we did not observe differences in *Srebf1a* and *Srebf1c* expression in 2-, 6-, or 12-hour–refed LRH-1 K289R and LRH-1 WT mice (Supplemental Figure 1C). Taken together, these data suggest that LRH-1 K289R induces SREBP-1 signaling primarily at the posttranscriptional level independently of early insulin-AKT signaling.

Enhanced de novo lipogenesis in LRH-1 K289R mice. To verify whether the increased expression of lipogenic genes is accompanied by hepatic fat accumulation, we next quantified hepatic triglyceride content in LRH-1 K289R and LRH-1 WT mice. The content of neutral lipids and triglycerides was significantly increased in LRH-1 K289R compared with LRH-1 WT livers upon refeeding (Figure 1, D and E). Of note, plasma triglycerides and free fatty

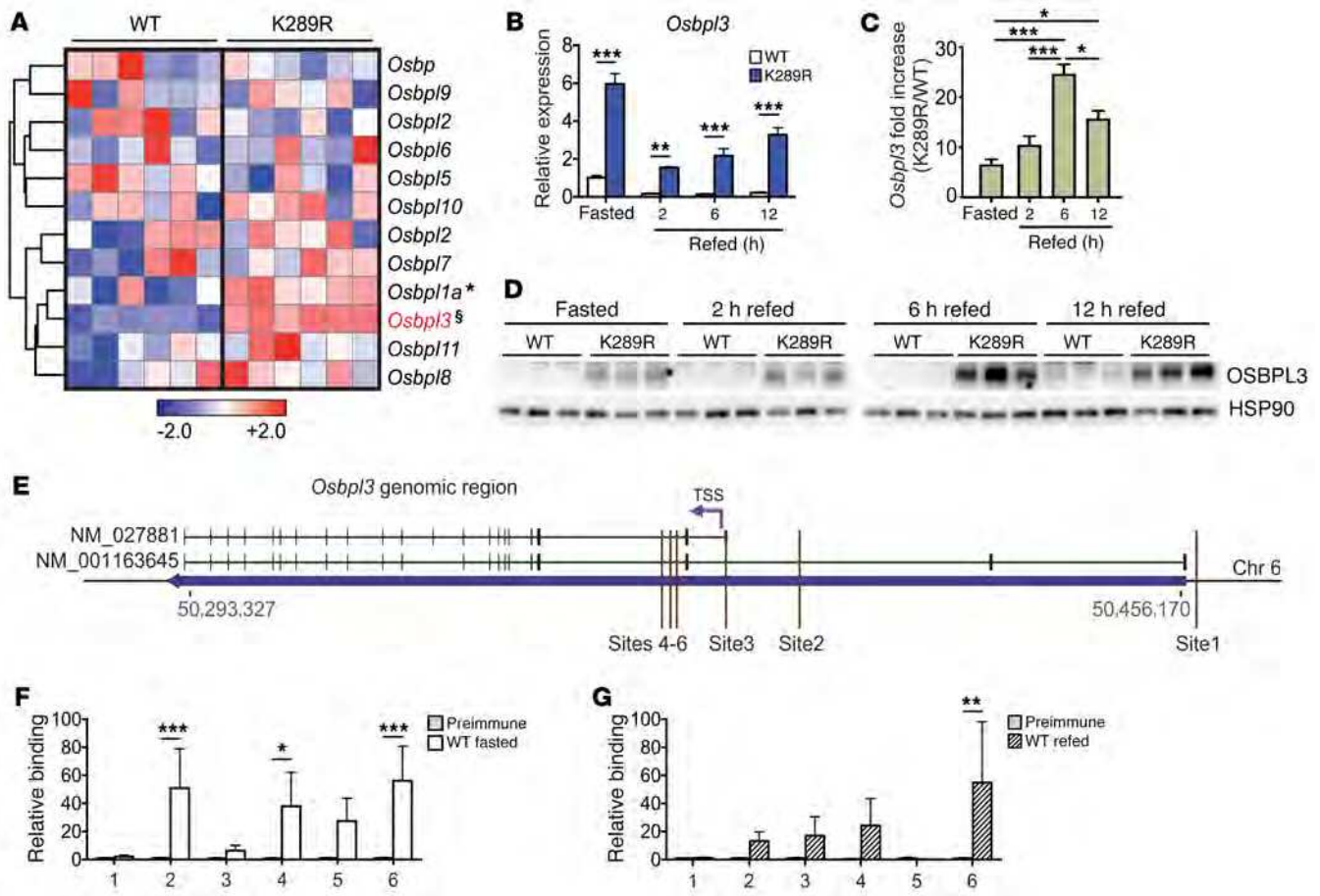

Figure 2. *Osbpl3* is a direct LRH-1 target gene and overexpressed in LRH-1 K289R mice. (**A**) Heat map showing the hepatic expression of oxysterol-binding protein family members in WT and K289R mice. Normalized expression values are in $\log_2$ scale. (**B** and **C**) Expression of *Osbpl3* mRNA in hepatic lysates of fasted and refed WT and K289R mice (**B**) and the fold change between the genotypes (**C**). $n = 4$ per fasted, 2-hour–, or 12-hour–refed groups, and $n = 5$ per 6-hour–refed groups. (**D**) Expression levels of OSBPL3 protein in hepatic lysates of fasted and refed WT and K289R mice. (**E**) Schematic showing the genomic area containing the *Osbpl3* gene and the sites used for ChIP-qPCR experiments (mouse genome assembly mm10). (**F** and **G**) Binding of LRH-1 to the different *Osbpl3* promoter sites assessed by ChIP analysis using genomic DNA from fasted WT (**F**) and refed WT livers (**G**). $n = 5$ WT fasted, $n = 5$ WT refed. Error bars represent mean ± SEM. $^*P < 0.05$, $^{**}P < 0.01$, $^{***}P < 0.001$, $^{§}P = 2 \times 10^{-7}$ relative to WT, as determined by unpaired Student's *t* test (**A**), or 1-way (**C**) or 2-way (**B**, **F**, **G**) ANOVA with Bonferroni post-hoc test. TSS, transcription start site.

acids did not show significant alterations between LRH-1 K289R and LRH-1 WT mice (Figure 1, F and G). To verify whether the enhanced expression of lipogenic genes translates into increased de novo lipogenesis, animals received ^{13}C-acetate prior to sacrifice to quantify de novo lipogenesis (6). In line with the increased lipogenic gene expression, de novo synthesis of palmitate (C16:0), stearate (C18:0), and oleate (C18:1) was significantly higher in LRH-1 K289R compared with LRH-1 WT livers (Figure 1, H–J). Of note, chain elongation of preexisting fatty acids was not altered between the 2 genotypes (Supplemental Figure 1, D and E). Collectively, these data show that LRH-1 K289R mice display increased de novo lipogenesis and that enhanced activation of SREBP-1 likely contributes to this process.

SUMOylation-defective LRH-1 drives the expression of Osbpl3. We next analyzed the transcriptome of livers from refed LRH-1 K289R and LRH-1 WT mice and searched for transcripts that are linked to SREBP-1 processing. One of the top hits on the list of genes that was increased in LRH-1 K289R compared with LRH-1 WT livers corresponded to *Osbpl3*, a member of a class of lipid transfer proteins recently implicated in the shuttling of lipids between the plasma and endoplasmic reticulum membrane (12–14). The expression of *Osbpl3*, and to a lesser extent *Osbpl1a*, was robustly induced in LRH-1 K289R livers, while that of most other OSBP family members did not differ between the 2 genotypes (Figure 2A). Of interest, overexpression of certain oxysterol-binding proteins has been suggested as increasing SREBP-1 processing and hepatic lipogenesis (15). Analysis of livers of LRH-1 K289R versus LRH-1 WT mice confirmed the enhanced expression of *Osbpl3* mRNA during fasting and refeeding (Figure 2B), while the expression of other OSBP family members did not differ between the 2 genotypes (Supplemental Figure 2A). Notably, the expression of *Osbpl3* was high during fasting and then reduced upon refeeding (Figure 2B). This postprandial suppression of *Osbpl3* mRNA expression was also observed upon overexpression of *Osbpl3* in mice using an adenovirus (Supplemental Figure 2B), suggesting that during the refed state, *Osbpl3* is regulated by posttranscriptional mechanisms occurring independently of LRH-1. Despite this feeding-dependent regulation of the mRNA, hepatic *Osbpl3* mRNA levels were consistently higher in the LRH-1 K289R

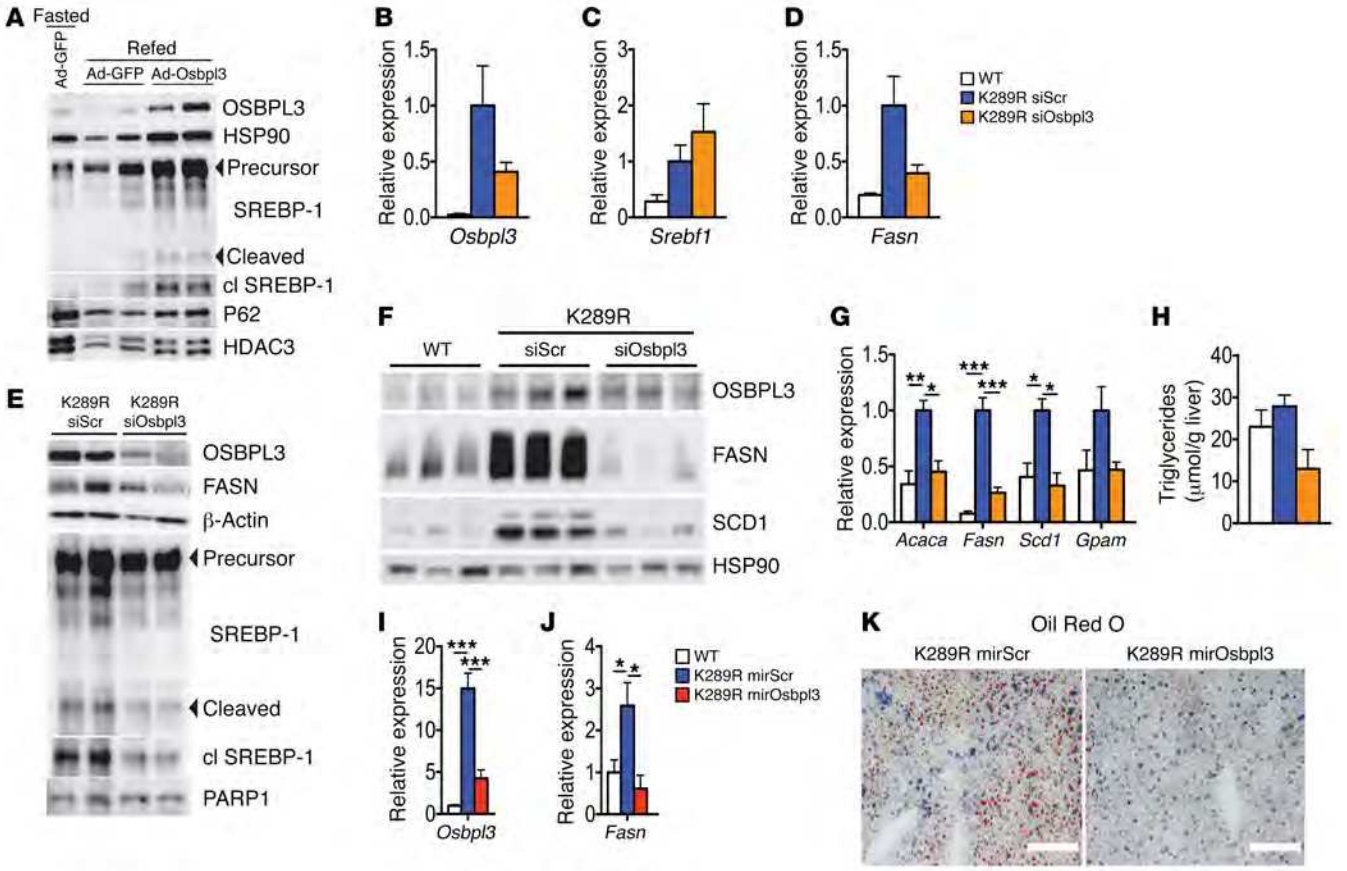

Figure 3. *Osbpl3* silencing rescues the lipogenic phenotype of LRH-1 K289R mice. (**A**) Immunoblots of OSBPL3, HSP90, precursor and cleaved SREBP-1, P62, and HDAC3 in hepatic lysates of fasted or refed WT plus Ad-GFP or refed WT plus Ad-OSBPL3 livers. (**B**–**D**) Hepatic mRNA expression of *Osbpl3* (**B**), *Srebf1* (**C**), and *Fasn* (**D**) in refed K289R and WT mice. WT, $n = 3$; K289R siScr or K289R siOsbpl3, $n = 9$ per genotype. (**E**) Immunoblots of OSBPL3, FASN, β-actin, precursor and cleaved SREBP-1, and PARP1 in hepatic lysates of refed K289R siScr or K289R siOsbpl3 livers. (**F**) Hepatic expression of OSBPL3, FASN, SCD1, and HSP90 in livers of ad libitum–fed WT, K289R siScr, and K289R siOsbpl3 mice. (**G**) Hepatic mRNA expression of genes involved in de novo lipogenesis in ad libitum–fed WT, K289R siScr, and K289R siOsbpl3 mice. $n = 3$ per genotype. (**H**) Quantification of hepatic triglycerides in hepatic lipid extracts from ad libitum–fed WT, K289R siScr, and K289R siOsbpl3 mice. $n = 3$ per genotype. (**I** and **J**) Hepatic mRNA expression of *Osbpl3* (**I**) and *Fasn* (**J**) in 6-hour–refed WT, K289R, or K289R mirOsbpl3 mice. $n = 3$ per genotype. (**K**) Representative oil red O staining in liver cryosections from refed K289R mirScrambled or K289R mirOsbpl3 mice. Scale bars: 100 μm. Error bars represent mean ± SEM. $^*P < 0.05$, $^{**}P < 0.01$, $^{***}P < 0.001$ relative to K289R siScr, as determined by 1-way ANOVA with Bonferroni's post-hoc test (**B**–**D**, **G**–**J**). WT, LRH-1 WT; K289R siOsbpl3, LRH-1 K289R mice injected with Osbpl3-siRNA complexes; K289R siScr, LRH-1 K289R mice injected with scrambled-siRNA complexes; K289R mirOsbpl3, LRH-1 K289R mice injected with AAV8 viral vectors containing an miRNA targeting *Osbpl3*.

mice in all nutritional states, but were particularly high under 6-hour–refeeding conditions (Figure 2C), and these differences were translated into similar changes at the protein level (Figure 2D).

To investigate whether *Osbpl3* is directly controlled by LRH-1, we first analyzed the *Osbpl3* genomic region in available ChIP-Seq data for potential LRH-1–binding sites (16, 17). We identified 3 main sites from the ChIP-Seq data from Holmstrom et al. (sites 1–3; ref. 16), and 3 additional sites with an LRH-1 consensus sequence close to one of the transcription start sites of the *Osbpl3* gene (sites 4–6) were identified by computational analysis (Figure 2E). We then performed site-specific ChIP analysis to evaluate whether these sites are bound by LRH-1 in fasted and refed mice. LRH-1 was recruited at different sites under both nutritional conditions (Figure 2, F and G), suggesting that *Osbpl3* is a direct LRH-1 target gene.

Based on the fact that LRH-1 and the nuclear receptor liver X receptor (LXR) have been shown to crosstalk in the regulation of hepatic acute-phase response proteins (18, 19) and that various LRH-1 target genes, including lipogenic genes, are coregulated by members of the LXR subfamily (20–22), we assessed the possibility that the LRH-1 mutant may modulate the recruitment of LXRα to its target genes, *Abca1*, *Chrebp*, and *Srebf1*. Although recruitment of LXRα was detected on these promoters in the genomic lysates of LRH-1 K289R and LRH-1 WT livers, no differences were observed between both genotypes, suggesting that LXRα binding is not altered due to the LRH-1 K289R mutation (Supplemental Figure 3A). Furthermore, Hepa 1.6 and AML-12 cells treated with the LXR agonist GW3965 did not alter *Osbpl3* expression (Supplemental Figure 3, B and C), indicating that *Osbpl3* expression is not regulated by LXR.

Osbpl3 silencing rescues the steatotic phenotype of LRH-1 K289R mice. To establish whether the increased expression of OSBPL3 in LRH-1 K289R livers is causatively linked to exacerbated de novo lipogenesis, we performed in vivo overexpression and silencing experiments. Adenoviral overexpression of OSBPL3 increased

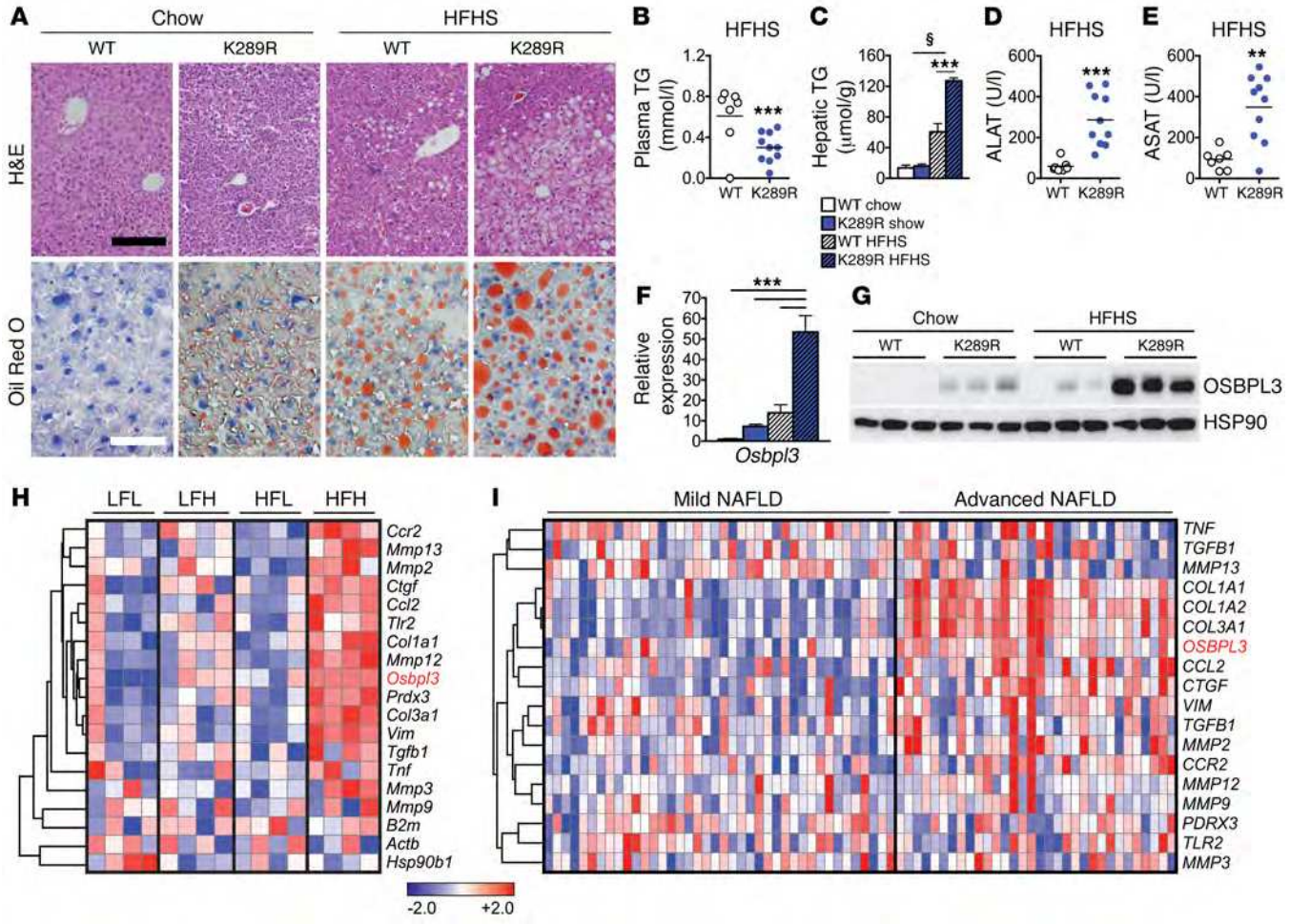

Figure 4. LRH-1 K289R mice develop NAFLD upon HFHS diet feeding. (**A**) Representative images of liver sections of K289R or WT mice stained with H&E or oil red O to visualize the tissue structure and neutral lipids, respectively. Black scale bar: 200 μm; white scale bar: 50 μm. (**B** and **C**) Quantification of triglyceride content in plasma (**B**) and in hepatic lipid extracts (**C**) in WT and K289R mice. WT, $n = 7$; K289R, $n = 10$. (**D** and **E**) Plasma levels of ALAT (**D**) and ASAT (**E**) in mice fed a HFHS diet. WT, $n = 7$; K289R, $n = 10$. (**F** and **G**) Expression of *Osbpl3* mRNA (**F**) and protein (**G**) levels in livers of WT and K289R mice fed chow and HFHS diets. $n = 9$ per genotype. (**H**) Heat map displaying the expression of *Osbpl3* as well as markers of matrix degradation, fibrosis, and inflammation in mice that were classified as LFL responders, LFH responders, HFL responders, and HFH responders according to the development of NAFLD/NASH upon chow or high-fat diet feeding (24). (**I**) Expression of *OSBPL3* and markers of matrix degradation, fibrosis, and inflammation in transcriptomic data from human patients that were categorized for mild or advanced NAFLD (25). Normalized expression values are in $\log_2$ scale. Error bars represent mean ± SEM. $^{**}P < 0.01$, $^{***}P < 0.001$ relative to WT; $^{§}P < 0.001$ refed relative to fasted mice, as determined by unpaired Student's *t* test (**B**, **D**, **E**) or 2-way ANOVA with Bonferroni's post-hoc test (**C**, **F**).

SREBP-1 cleavage in refed LRH-1 WT mice (Figure 3A), suggesting that elevated OSBPL3 levels promote SREBP-1 activation. We next silenced *Osbpl3* in LRH-1 K289R mice using siRNAs in LRH-1 K289R mice under fast-refeeding conditions. The hepatic mRNA expression of *Osbpl3* showed a clear trend of effective silencing (Figure 3B), while *Srebf1* expression was not altered (Figure 3C). Importantly, we observed a robust decrease in OSBPL3 protein along with a reduction in the maturation of SREBP-1 and a blunted expression of the fatty acid synthase (FASN) transcript and protein in the livers of refed LRH-1 K289R mice treated with siOsbpl3 (Figure 3, D and E). We next assessed the effect of *Osbpl3* silencing under normal-fed conditions. Western blot analysis revealed reduced OSBPL3 expression (Figure 3F) and a robust decrease in the lipogenic proteins FASN and stearoyl–coenzyme A desaturase 1 (SCD-1) in ad libitum–fed LRH-1 K289R mice treated with siOsbpl3 compared with control mice (Figure 3F). Of interest, mRNA expression levels of the lipogenic enzymes acetyl–coenzyme A carboxylase alpha (*Acaca*), *Fasn*, *Scd1*, and glycerol-3-phosphate acyltransferase (*Gpam)* were often normalized to values observed in LRH-1 WT mice (Figure 3G), suggesting that *Osbpl3* silencing rescues the lipogenic phenotype of LRH-1 K289R mice. In line with the reduced expression of lipogenic genes, *Osbpl3* silencing also decreased hepatic triglyceride and neutral lipid content (Figure 3H). As an additional approach to silence *Osbpl3*, we injected mice with an AAV8 viral vector containing an miRNA targeting *Osbpl3* in the liver. Here again, we observed a robust silencing of *Osbpl3,* which was accompanied by the suppression of *Fasn* and a striking reduction of hepatic lipid droplets (Figure 3, I–K).

Finally, we also examined whether other mechanisms, directly or indirectly regulated by LRH-1, may contribute to the lipogenic phenotype. Of interest, both hepatic glucose-6-phosphate content (6) and VLDL secretion (23) were unchanged between

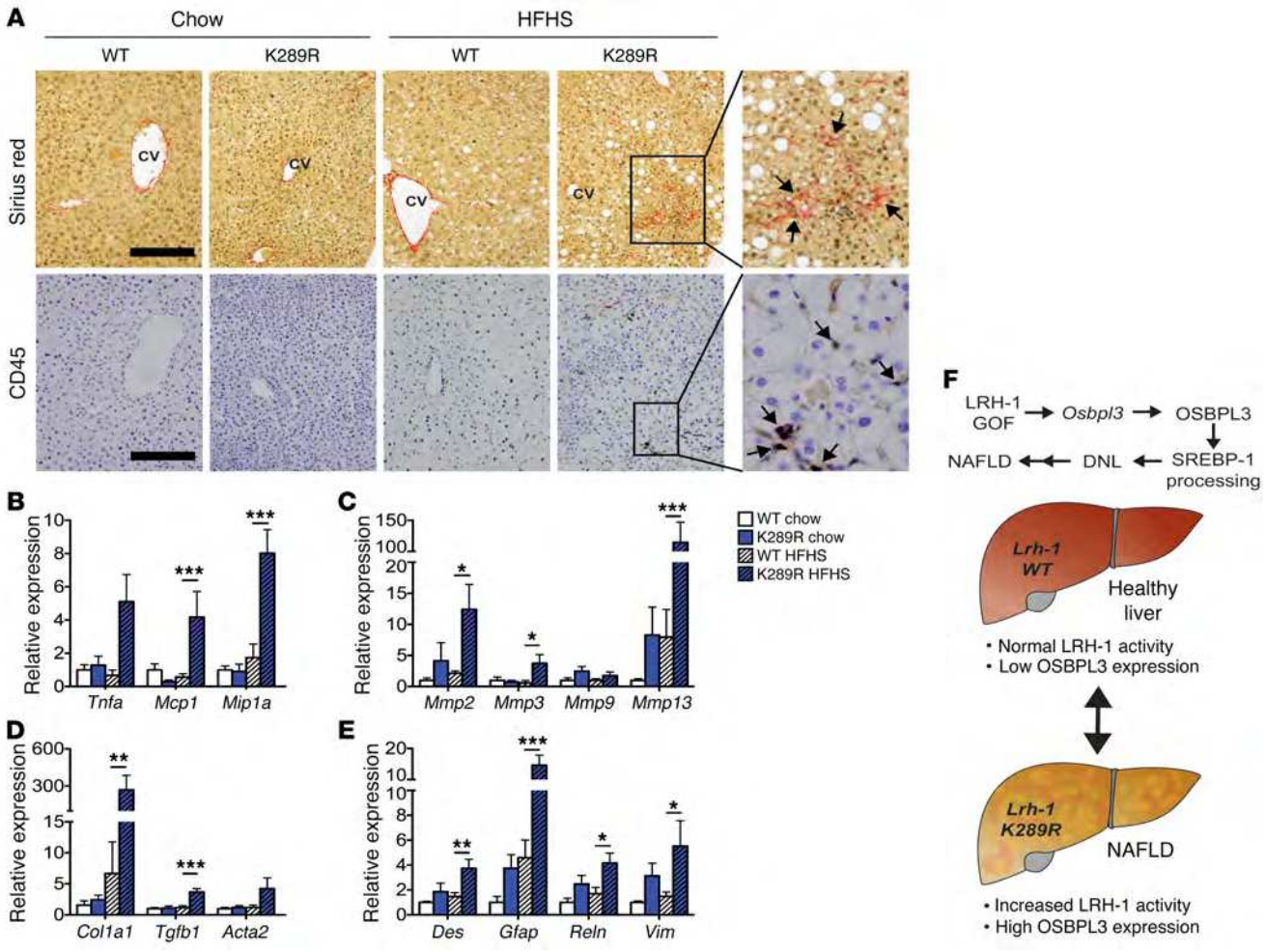

Figure 5. LRH-1 K289R mice display increased inflammation and early signs of fibrosis upon HFHS diet feeding. (**A**) Representative images of liver sections of K289R or WT mice stained with sirius red or CD45 to visualize collagen depositions and CD45-positive cells, respectively. Scale bars: 200 μm. CV, central vein. (**B**–**E**) Hepatic mRNA expression of genes involved in inflammation (**B**), matrix degradation (**C**), fibrosis (**D**), and stellate cells (**E**) in K289R and WT mice. n = 9 per genotype. (**F**) Graphical presentation showing how the LRH-1/OSBPL3 axis drives the accumulation of hepatic lipids. Error bars represent mean ± SEM. $^*P < 0.05$, $^{**}P < 0.01$, $^{***}P < 0.001$ relative to WT within each diet, as determined by 2-way ANOVA with Bonferroni's post-hoc test (**B**–**E**).

LRH-1 K289R and LRH-1 WT mice (Supplemental Figure 4, A–C), making it unlikely that these processes account for the exacerbated lipid accumulation in liver.

Together, these data suggest that the LRH-1-OSBPL3 signaling axis contributes to the increased maturation of SREBP-1, the induction of lipogenic enzymes, and the hepatic accumulation of triglycerides observed in LRH-1 K289R mice.

LRH-1 K289R mice are prone to developing NAFLD upon lipogenic diet feeding. Excessive de novo lipogenesis contributes to the development of NAFLD, a condition that can eventually progress to NASH (1, 3). In order to investigate whether LRH-1 affects the development of NAFLD, LRH-1 K289R and LRH-1 WT mice were fed a highly lipogenic HFHS diet or a chow diet for 17 weeks, and then sacrificed under normal-fed conditions. Stainings of hepatic sections with H&E and oil red O revealed that LRH-1 K289R mice developed a stronger steatotic phenotype compared with LRH-1 WT mice fed a HFHS diet (Figure 4A). While plasma cholesterol levels were unchanged (Supplemental Figure 5A), triglyceride content in plasma (Figure 4B) or in VLDL fractions (Supplemental Figure 5B) was reduced in HFHS-fed LRH-1 K289R mice. This reduction was accompanied with a robust accumulation of hepatic triglycerides (Figure 4C) as well as an induction of plasma levels of the enzymes alanine transaminase (ALAT) and aspartate aminotransferase (ASAT) in the HFHS-challenged LRH-1 K289R mice (Figure 4, D and E). Similar to our earlier observations in normal chow diet conditions (Figure 2, A–D), *Osbpl3* mRNA and OSBPL3 protein were significantly induced in LRH-1 K289R compared with LRH-1 WT mice fed a HFHS diet (Figure 4, F and G), while the expression of other *Osbp* genes did not differ between the genotypes (Supplemental Figure 5C).

The development of hepatic steatosis in mice is known to be highly heterogeneous (24). Therefore, we analyzed the data from a study in which mice were fed a chow or high-fat diet and then classified according to the development of NAFLD/NASH into low-fat low (LFL) responders, low-fat high (LFH) responders, high-fat low (HFL) responders, and high-fat high (HFH) responders (24). Interestingly, the expression of *Osbpl3* was significantly induced in the HFH responders along with markers of inflammation and

necrosis (Figure 4H) and was by far the most strikingly increased *Osbp* among all family members (Supplemental Figure 5D). We also analyzed *OSBPL3* expression in 2 cohorts of NAFLD/NASH patients. In the first cohort, livers were categorized as showing mild or advanced NAFLD (25). In the second study, subjects had livers ranging from healthy controls to showing steatosis and further to NASH (26). *OSBPL3* expression was low in healthy livers, but increased in advanced stages of NAFLD/NASH and clustered with markers of fibrosis (Figure 4I and Supplemental Figure 6), suggesting that OSBPL3 could be a novel biomarker for advanced liver diseases, such as NASH. Taken together, these data show that *Osbpl3* is markedly increased in LRH-1 K289R mice as well as in mice and humans with NAFLD/NASH.

LRH-1 K289R mice display increased inflammation and early signs of fibrosis in response to lipogenic diet feeding. Given the strong steatotic phenotype and the high levels of ALAT and ASAT markers in LRH-1 K289R mice fed a HFHS diet as well as the clustering of *Osbpl3* with genes involved in inflammation and fibrosis in mice and humans with NAFLD, we next analyzed inflammatory and fibrotic markers in LRH-1 K289R and LRH-1 WT mice. Stainings of hepatic sections with sirius red and CD45 revealed that, in contrast with LRH-1 WT mice, LRH-1 K289R mice developed small fibrotic lesions and accumulated CD45-positive immune cells upon HFHS feeding (Figure 5A). Moreover, LRH-1 K289R livers displayed higher levels of the inflammatory genes *Tnfα*, monocyte chemoattractant protein-1 (*Mcp1* or *Ccl2*), and macrophage inflammatory protein-1 α (Mip1α or *Ccl3*) (Figure 5B), indicating increased inflammation in livers of HFHS-fed LRH-1 K289R mice. The expression of MMPs, such as *Mmp2* and *Mmp13*, as well as early markers of fibrosis, such as α-1 type I collagen (*Col1a1*) and *Tgfb1*, was also elevated in LRH-1 K289R in comparison with LRH-1 WT mice fed a HFHS diet (Figure 5, C and D). Hepatic stellate cells are the primary hepatic cell type promoting fibrogenesis (27). The expression of different hepatic stellate cell markers, such as desmin (*Des*), glial fibrillary acidic protein (*Gfap*), and reelin (*Reln*), was also increased in HFHS-fed LRH-1 K289R compared with LRH-1 WT mice (Figure 5E), suggesting that HFHS-treated LRH-1 K289R mice exhibit early signs of NASH.

Previous studies showed that LRH-1 and the SUMOylation machinery might affect the hepatic acute phase response (APR) (18, 19, 28). While induction of the APR by short exposure of LPS led to reduced hepatic expression of *Crp* and *Tnf* in LRH-1 K289R compared with LRH-1 WT mice, it did not alter the hepatic expression of other APR and inflammatory genes (Supplemental Figure 7A). Moreover, no difference in plasma IL-6, MCP-1 (also known as CCL-2), or TNF-α could be observed in LPS-challenged LRH-1 K289R and LRH-1 WT mice (Supplemental Figure 7B), suggesting that the APR is likely not driving the observed inflammatory phenotype in our NAFLD-model.

Taken together, these data show that SUMOylation-defective LRH-1 promotes the development of NAFLD and displays early signs of NASH in mice fed a HFHS diet. This process is at least partially driven by the LRH-1-OSBPL3 signaling axis, which contributes to increased maturation of SREBP-1, the induction of lipogenic enzyme expression, and hepatic triglyceride accumulation in LRH-1 K289R mice (Figure 5F).

Discussion

In this study, we analyzed the contribution of a selective LRH-1 gain of function on hepatic de novo lipogenesis and fatty liver development and identified *Osbpl3* as a critical component in the regulation of this process. While the hepatic expression of *Osbpl3* is normally low in mice under basal conditions, LRH-1 K289R mice express high levels of this specific OSBP family member. Consistent with our observations, the analyses of independent mouse and human transcriptomic data sets revealed that *Osbpl3* expression is often induced in NAFLD/NASH. Our work furthermore strengthens the putative role of OSBPL3 in SREBP-1 maturation. As a consequence, LRH-1 K289R mice display increased de novo lipogenesis and accumulation of triglycerides upon refeeding in a manner that is independent of enhanced LXRα recruitment or activity. Importantly, silencing of OSBPL3 in vivo reverts the increased lipogenesis observed in these animals. Moreover, when exposed to a lipogenic HFHS diet, LRH-1 K289R mice develop NAFLD accompanied by early signs of NASH, most likely as a consequence of chronic fat accumulation (1, 3).

The excessive accumulation of hepatic lipids and increased de novo lipogenesis could also have other causes. A previous study using liver-specific *Lrh-1* knockout mice showed that LRH-1 promotes glucokinase expression, hence regulating glycolysis and de novo lipogenesis (6). However, we did not observe a difference in hepatic glucose-6-phosphate content between LRH-1 WT and LRH-1 K289R mice, suggesting that the selective gain of function of LRH-1 driven by the K289R mutation does not increase substrate availability for the glycolytic pathway. Based on the finding that the primary corepressor of LRH-1 affects microsomal triglyceride transfer protein levels and consequently hepatic VLDL-triglyceride secretion (23), we also performed in vivo VLDL-secretion assays, but could not detect any difference between refed LRH-1 K289R and LRH-1 WT mice. Finally, LRH-1 SUMOylation has been linked to the induction of the hepatic APR (18, 19, 28), which could explain the excessive inflammation observed in the livers of mice receiving a chronic HFHS diet. To study the APR in vivo, we challenged LRH-1 WT and LRH-1 K289R mice with lipopolysaccharide for 2.5 hours. Besides the reduction in *Crp* and *Tnf*, the inflammatory signature was comparable between the genotypes, suggesting that the exacerbated inflammatory phenotype of the LRH-1 K289R mice is most likely not driven by changes in the APR.

While the induction of SREBP-2 processing has been well described, the mechanisms that trigger SREBP-1 processing are less well understood (29). Insulin receptor/AKT/mTOR signaling is considered one of the main pathways triggering SREBP-1 signaling (30). A recent study showed that insulin promotes SREBP-1 activation and de novo lipogenesis via mTORC1-dependent and -independent mechanisms (31). Others proposed that while insulin signaling is required for SREBP-1 activation in insulin-resistant conditions, it is not critical for inducing the feeding-dependent induction of SREBP-1 under physiological conditions (32, 33). In breast epithelial cells, the expression of oncogenic forms of the PI3K or K-Ras are sufficient to induce SREBP-1 maturation and de novo lipogenesis through induction of mTOR signaling (34). Whereas these and many other studies demonstrate that the expression of *Srebf1* and the posttranslational maturation of SREBP-1 can be triggered by insulin signaling, other downstream

or parallel pathways exist. One recent example is the induction of SREBP-1 processing upon depletion of phosphatidylcholine, whose synthesis is dependent on S-adenosylmethionine, a methionine derivative that is generated in the one-carbon cycle (35). We did not observe a difference in AKT phosphorylation between LRH-1 WT and LRH-1 K289R mice, suggesting other signaling pathways to induce the processing of SREBP-1. Indeed, our current study highlights the existence of an alternative mechanism of SREBP-1 activation involving a SUMO-dependent LRH-1/OSBPL3 pathway.

The first oxysterol-binding proteins were identified, purified, and cloned in the 1980s (36–38). Recent studies suggest that OSBPs act as sterol transfer and/or sensor proteins that may also play important roles in cell signaling (39, 40). OSBPL3, a member of subfamily III, contains a conserved sterol-binding OSBP homology domain (OHD) as well as a phosphatidylinositol lipid species–binding pleckstrin homology (PH) domain and two 2-phenylalanines in an acidic tract (FFAT) domains that bind to the vesicle-associated membrane protein–associated (VAMP-associated) protein (VAP) (39, 41, 42). Recently, it has been shown that this last interaction can activate R-RAS, thus reorganizing the actin cytoskeleton and affecting cell polarity and cell-cell adhesion (43). Future studies will be necessary to dissect the exact mechanisms by which OSBPL3 modulates SREBP-1 processing, but its association with the ER could indicate a possible site of regulation.

In addition to the identification of OSBPL3 as a target of LRH-1, our study also highlights the existence of complex regulatory mechanisms to which OSBPL3 is subjected. We observed a discrepancy between mRNA and protein levels of OSBPL3 between fasting and refed conditions despite its persistent increase in LRH-1 K289R mice. The marked reduction in mRNA levels upon refeeding was also noticed when OSBPL3 was overexpressed using an adenovirus, indicating that additional posttranscriptional mechanisms independent of LRH-1 regulate the expression of OSBPL3. Moreover, while the expression of OSBPL3 is low in healthy livers, it is increased in NAFLD, suggesting that this protein could be a novel biomarker for NAFLD.

In this study, we described a function of LRH-1 in the development of fatty liver disease. It is noteworthy that other nuclear receptors also contribute to the development of NAFLD by affecting steatosis, glucose homeostasis, inflammation, and/or fibrosis in the liver. For instance, while activation of LXRs or pregnane x receptor (PXR) promotes lipogenesis and the development of NAFLD, activation of other nuclear receptors such as PPARs or farnesoid X-activated receptor (FXR) has opposite effects (reviewed in ref. 44). Clinical trials performed in NASH patients using PPARγ or FXR agonists showed that the beneficial effects observed on hepatic steatosis and inflammation were accompanied by adverse effects on obesity and hypercholesterolemia, respectively (45, 46), highlighting the functional complexity of nuclear receptors (44). Therefore, the development of drugs targeting specific nuclear receptor targets, such as OSBPL3, might provide alternative therapeutic options for treating NAFLD.

Methods

Animal studies. Congenic C57BL/6J LRH-1 WT or LRH-1 K289R (9) as well as C57BL/6J *Lrh-1*$^{hep-/-}$ and *Lrh-1*$^{hep+/+}$ mice (6) were kept under normal housing conditions. For fast-refeeding protocols, 12- to 16-week-old male mice were initially fasted for 24 hours, followed by refeeding for 12 hours (8 pm to 8 am), 6 hours (2 am to 8 am), or 2 hours (6 am to 8 am), and finally sacrificed together at 8 am to avoid confounding effects of the circadian rhythm. To induce a chronic hepatic steatosis, male mice were fed ad libitum with a HFHS diet (TD.08811, Harlan Laboratories) for 17 weeks and sacrificed at 9 am. To study the APR, male mice fed a chow diet received an intraperitoneal injection of either 500 μl PBS or 40 μg LPS dissolved in 500 μl PBS. Mice were sacrificed 2.5 hours after injection and tissues collected.

Subcellular fractionation of liver tissues and Western blotting. From 50 to 100 mg of liver pieces were incubated in 400 μl of hypotonic buffer (10 mM HEPES-KOH, pH 7.4, 10 mM KCl, 1.5 mM $MgCl_2$, 0.5 mM DTT, protease and phosphatase inhibitor cocktails; Roche) and lysed with 10 strokes in a Dounce homogenizer. The supernatant fraction containing mainly cytoplasmic proteins was collected after centrifugation (14,000 *g* for 5 minutes, 4°C), and the pellets were washed twice with hypotonic buffer. The pellets were resuspended in 100 to 200 μl of hypertonic buffer (50 mM Tris-HCl pH 7.4, 150 mM NaCl, 0.1 % NP-40, protease and phosphatase inhibitor cocktails) for 30 minutes on ice. The supernatant containing mainly nucleoplasm and membrane fractions was collected by centrifugation (2,000 *g* for 5 minutes, 4°C), and the remaining insoluble pellet containing mainly chromatin was resuspended in 100 μl of hypertonic buffer and sonicated. Before running SDS-PAGE, protein lysates were boiled for 5 minutes at 95°C. The following proteins were used for Western blotting: anti-Hsp90, anti–SREBP-1, and anti-P62 (BD Biosciences catalog 610418, 557036, and 610497); anti-OSBPL3 (Novus Biologicals, catalog NBP-155151), anti-FASN (Abcam, catalog ab22759), anti-SCD1 (Thermo Fisher, catalog A13996), anti–α-tubulin, anti-PARP1, and anti–β-actin (Santa Cruz Biotechnology Inc., catalog sc-5286, sc-7150, and sc-47778). Anti–SREBP-1, anti-P62, and anti-PARP1 were blotted on nuclear/membrane fractions and all other antibodies on cytoplasmic fractions.

Gene expression and analysis. RNA was extracted from the livers of mice that were fasted for 24 hours followed by 6 hours of refeeding, LRH-1 WT ($n = 6$) and LRH-1 K289R ($n = 6$). Extraction was performed using TRIZOL (Invitrogen) and purified with the RNeasy Cleanup Kit for Microarray Analysis (QIAGEN). For quantitative reverse-transcription PCR (RT-qPCR), cDNA was generated using the QuantiTect Reverse Transcription Kit (QIAGEN) and analyzed by qPCR using a LightCycler 480 Real-Time PCR System (Roche) and the primers listed in Supplemental Table 1. Expression data were normalized to *36b4* or *B2m* mRNA levels. Microarray analysis was performed using the Affymetrix MouseGene 1.0 ST array and normalized using the robust multi-array average (RMA) method. All original microarray data were deposited in the NCBI's Gene Expression Omnibus (GEO GSE89877). Heat maps were generated using GENE-E (http://www.broadinstitute.org/cancer/software/GENE-E/index.html), and rows were clustered using the one minus Pearson correlation metric.

ChIP-PCR. ChIP analysis was performed as described previously, with minor modifications (9). ChIPed DNA was purified using the PCR Clean-up Extraction Kit (Macherey-Nagel), after which qPCR was performed as described previously (47). Data were normalized to the input (fold differences = $2^{-(\text{Ct-sample} - \text{Ct-input})}$). ChIP primer sequences are listed in Supplemental Table 2. For LXR ChIP assays, an anti-LXRα antibody (Abcam, catalog ab41902) was used. For LRH-1 ChIP experiments, a custom LRH-1 antibody was generated. A synthetic peptide ([H]-QEQSNRNRQEKLSAFG-[NH2]) was used to immunize 2 rab-

bits (AbFRONTIER). The antiserum with the highest ELISA titer was selected and used in ChIP experiments. The preimmunization serum from the same rabbit was used as a negative control.

LXR agonist treatment. Hepa 1.6 (ATCC, catalog CRL1830) or AML-12 (ATCC, catalog CRL2254) cells were treated with 1 μM of GW3965 (Selleckchem), a dual LXRα and LXRβ agonist, for 6 hours in full medium.

In vivo siRNA transfection. siRNA sequences are listed in Supplemental Table 4. HPLC-purified siRNAs (3 nmol, Microsynth) were tail-vein injected into each recipient mouse using in vivo-JetPEI (Polyplus) according to the manufacturer's instructions. Mice were fast-refed as described above and sacrificed 2 days after injection.

Adenoviral infection. *Osbpl3* cDNA was cloned into a pENTR/D-TOPO plasmid (Invitrogen; the Topo primer is listed in Supplemental Table 3) and then subcloned in the pAd/CMV-DEST plasmid (Invitrogen). After linearization with *PacI*, the construct was transfected into HEK 293A cells to produce the adenoviruses. Mice were tail-vein injected with Ad-*gfp* or Ad-*Osbpl3*, 2.5×10^9 PFU, fast-refed as described above, and sacrificed 3 days after injection.

AAV8 miRNA injection. The *Osbpl3*-siRNA sequence (Supplemental Table 4) was engineered to create a pre-miRNA sequence targeting *Osbpl3*, which was cloned into an AAV vector construct driven by the liver-specific *hAAT* promoter. AAV8 mirOsbpl3 viral vectors were generated and titrated as described previously (48, 49) and injected into jugular vein under isoflurane anesthesia (5×10^{11} vg). Two weeks after the injection, mice were fasted for 24 hours followed by 6 hours refeeding, then sacrificed, and tissues were snap-frozen.

Lipid analyses and plasma parameters. Hepatic lipids were extracted according to the Bligh and Dyer protocol (50). Triglycerides, free fatty acids, and cholesterol contents in plasma and/or hepatic lipid fractions were quantified using enzymatic assays (Roche). To asses fatty acid synthesis rates in vivo, mice received sodium [1-^{13}C] acetate via their drinking water (2%) 24 hours prior to sacrifice. Fatty acids derived from hepatic lipid extracts were liberated, derivatized, and subjected to gas chromatography–mass spectrometry (GC-MS) analysis in order to calculate the fractional synthesis rates from the incorporation of ^{13}C-acetate as described previously (51). ASAT and ALAT concentrations in blood were determined using standard clinical chemistry methods.

VLDL secretion assay and glucose-6-phosphate quantification. The VLDL secretion assay was performed as described previously (51). Thirteen-week-old male LRH-1 K289R or LRH-1 WT mice were subjected to the fasting-refeeding protocol and treated with 50 mg/ml poloxamer 407 (Sigma-Aldrich, catalog 16758) 8 hours after refeeding was initiated. Blood samples were collected once before and every hour after poloxamer treatment to determine the triglyceride content. Glucose-6-phosphate content was determined using enzymatic assays as described previously (6).

Immunohistochemistry. Liver sections were cut into 5-μm–thick serial cryosections for oil red O staining to visualize neutral lipids or paraffin cryosections to stain collagen with sirius red, CD45-positive cells using rat anti-CD45 antibody (eBioscience, catalog 30-F11), or H&E.

Statistics. Data are expressed as mean ± SEM. Comparison of differences between 2 groups was assessed using unpaired 2-tailed Student's *t* tests. Multiple group comparisons were assessed by ANOVA and Bonferroni's post-hoc *t* tests. $P < 0.05$ was considered statistically significant.

Study approval. All animal procedures were approved by the Swiss authorities (Canton of Vaud, animal protocols ID 2380, 2561, and 2768) and performed in accordance with École Polytechnique Fédérale de Lausanne institutional guidelines.

Author contributions

SS and VL designed and carried out most of the experiments, analyzed data, prepared the figures, and wrote the manuscript. PX and DR helped with Western blotting, histology, adenovirus production, and/or in vivo experiments. HD carried out the ChIP-qPCR experiments. XW helped with bioinformatic analyses. VJ and FB designed and generated the AAV8 constructs. MHO performed GC-MS analysis and quantification of fatty acids. TFL and MHO provided useful advice on the experimental procedures. KS supervised all aspects of the work.

Acknowledgments

We thank Vasco de Campos and Norman Moullan for help with tail-vein and jugular-vein injections and Theo van Dijk, Theo Boer, Sara Oppi, Thibaud Clerc, Sabrina Bichet, and Soline Odouard for technical help. This study was funded by École Polytechnique Fédérale de Lausanne and the Swiss National Science Foundation (31003A_1666695 and CRSII3_160798/1). SS was supported by postdoctoral fellowships from the German Academy of Sciences Leopoldina (LPDS 2011-6) and the Novartis Consumer Health Foundation and an Ambizione grant from the Swiss National Science Foundation (PZOOP3_161521). VL was supported by a PhD grant from the Portuguese Foundation for Science and Technology (SFRH/BD/52046/2012) through the Graduate Program in Basic and Applied Biology (GABBA) PhD program. MHO holds a Rosalind Franklin Fellowship from the University of Groningen. FB is an ICREA Academia recipient, Generalitat de Catalunya, Spain. AAV vector generation and production were funded by the Ministerio de Economía y Competitividad, Plan Nacional I+D+I (SAF2014-54886-R), Spain.

Address correspondence to: Kristina Schoonjans, Institute of Bioengineering, School of Life Sciences, École Polytechnique Fédérale de Lausanne, EPFL SV SSV-GE, AI 1149 (Bâtiment AI), Station 19, CH-1015 Lausanne, Switzerland. Phone: 41.21.693.18.91; E-mail: kristina.schoonjans@epfl.ch.

1. Cohen JC, Horton JD, Hobbs HH. Human fatty liver disease: old questions and new insights. *Science*. 2011;332(6037):1519–1523.
2. Villanueva A, Llovet JM. Liver cancer in 2013: Mutational landscape of HCC--the end of the beginning. *Nat Rev Clin Oncol*. 2014;11(2):73–74.
3. Angulo P. Nonalcoholic fatty liver disease. *N Engl J Med*. 2002;346(16):1221–1231.
4. Perry RJ, Samuel VT, Petersen KF, Shulman GI. The role of hepatic lipids in hepatic insulin resistance and type 2 diabetes. *Nature*. 2014;510(7503):84–91.
5. Stein S, Schoonjans K. Molecular basis for the regulation of the nuclear receptor LRH-1. *Curr Opin Cell Biol*. 2015;33:26–34.
6. Oosterveer MH, et al. LRH-1-dependent glucose sensing determines intermediary metabolism in liver. *J Clin Invest*. 2012;122(8):2817–2826.
7. Lee JM, et al. A nuclear-receptor-dependent phosphatidylcholine pathway with antidiabetic effects. *Nature*. 2011;474(7352):506–510.
8. Musille PM, Pathak MC, Lauer JL, Hudson WH, Griffin PR, Ortlund EA. Antidiabetic phospholipid-nuclear receptor complex reveals the mech-

anism for phospholipid-driven gene regulation. *Nat Struct Mol Biol*. 2012;19(5):532–537.
9. Stein S, et al. SUMOylation-dependent LRH-1/PROX1 interaction promotes atherosclerosis by decreasing hepatic reverse cholesterol transport. *Cell Metab*. 2014;20(4):603–613.
10. Keeton AB, Bortoff KD, Bennett WL, Franklin JL, Venable DY, Messina JL. Insulin-regulated expression of Egr-1 and Krox20: dependence on ERK1/2 and interaction with p38 and PI3-kinase pathways. *Endocrinology*. 2003;144(12):5402–5410.
11. Keeton AB, Bortoff KD, Franklin JL, Messina JL. Blockade of rapid versus prolonged extracellularly regulated kinase 1/2 activation has differential effects on insulin-induced gene expression. *Endocrinology*. 2005;146(6):2716–2725.
12. Chung J, et al. Intracellular transport. PI4P/phosphatidylserine countertransport at ORP5- and ORP8-mediated ER-plasma membrane contacts. *Science*. 2015;349(6246):428–432.
13. Moser von Filseck J, et al. Intracellular transport. Phosphatidylserine transport by ORP/Osh proteins is driven by phosphatidylinositol 4-phosphate. *Science*. 2015;349(6246):432–436.
14. Maeda K, et al. Interactome map uncovers phosphatidylserine transport by oxysterol-binding proteins. *Nature*. 2013;501(7466):257–261.
15. Yan D, et al. Oxysterol binding protein induces upregulation of SREBP-1c and enhances hepatic lipogenesis. *Arterioscler Thromb Vasc Biol*. 2007;27(5):1108–1114.
16. Holmstrom SR, et al. LRH-1 and PTF1-L coregulate an exocrine pancreas-specific transcriptional network for digestive function. *Genes Dev*. 2011;25(16):1674–1679.
17. Chong HK, Biesinger J, Seo YK, Xie X, Osborne TF. Genome-wide analysis of hepatic LRH-1 reveals a promoter binding preference and suggests a role in regulating genes of lipid metabolism in concert with FXR. *BMC Genomics*. 2012;13:51.
18. Venteclef N, Smith JC, Goodwin B, Delerive P. Liver receptor homolog 1 is a negative regulator of the hepatic acute-phase response. *Mol Cell Biol*. 2006;26(18):6799–6807.
19. Venteclef N, et al. GPS2-dependent corepressor/SUMO pathways govern anti-inflammatory actions of LRH-1 and LXRbeta in the hepatic acute phase response. *Genes Dev*. 2010;24(4):381–395.
20. Cha JY, Repa JJ. The liver X receptor (LXR) and hepatic lipogenesis. The carbohydrate-response element-binding protein is a target gene of LXR. *J Biol Chem*. 2007;282(1):743–751.
21. Joseph SB, et al. Direct and indirect mechanisms for regulation of fatty acid synthase gene expression by liver X receptors. *J Biol Chem*. 2002;277(13):11019–11025.
22. Matsukuma KE, Wang L, Bennett MK, Osborne TF. A key role for orphan nuclear receptor liver receptor homologue-1 in activation of fatty acid synthase promoter by liver X receptor. *J Biol Chem*. 2007;282(28):20164–20171.
23. Huang J, et al. Molecular characterization of the role of orphan receptor small heterodimer partner in development of fatty liver. *Hepatology*. 2007;46(1):147–157.
24. Duval C, et al. Adipose tissue dysfunction signals progression of hepatic steatosis towards nonalcoholic steatohepatitis in C57BL/6 mice. *Diabetes*. 2010;59(12):3181–3191.
25. Moylan CA, et al. Hepatic gene expression profiles differentiate presymptomatic patients with mild versus severe nonalcoholic fatty liver disease. *Hepatology*. 2014;59(2):471–482.
26. Ahrens M, et al. DNA methylation analysis in nonalcoholic fatty liver disease suggests distinct disease-specific and remodeling signatures after bariatric surgery. *Cell Metab*. 2013;18(2):296–302.
27. Yin C, Evason KJ, Asahina K, Stainier DY. Hepatic stellate cells in liver development, regeneration, and cancer. *J Clin Invest*. 2013;123(5):1902–1910.
28. Venteclef N, Delerive P. Interleukin-1 receptor antagonist induction as an additional mechanism for liver receptor homolog-1 to negatively regulate the hepatic acute phase response. *J Biol Chem*. 2007;282(7):4393–4399.
29. Horton JD, Goldstein JL, Brown MS. SREBPs: activators of the complete program of cholesterol and fatty acid synthesis in the liver. *J Clin Invest*. 2002;109(9):1125–1131.
30. Krycer JR, Sharpe LJ, Luu W, Brown AJ. The Akt-SREBP nexus: cell signaling meets lipid metabolism. *Trends Endocrinol Metab*. 2010;21(5):268–276.
31. Yecies JL, et al. Akt stimulates hepatic SREBP1c and lipogenesis through parallel mTORC1-dependent and independent pathways. *Cell Metab*. 2011;14(1):21–32.
32. Haas JT, et al. Hepatic insulin signaling is required for obesity-dependent expression of SREBP-1c mRNA but not for feeding-dependent expression. *Cell Metab*. 2012;15(6):873–884.
33. Leavens KF, Easton RM, Shulman GI, Previs SF, Birnbaum MJ. Akt2 is required for hepatic lipid accumulation in models of insulin resistance. *Cell Metab*. 2009;10(5):405–418.
34. Ricoult SJ, Yecies JL, Ben-Sahra I, Manning BD. Oncogenic PI3K and K-Ras stimulate de novo lipid synthesis through mTORC1 and SREBP. *Oncogene*. 2016;35(10):1250–1260.
35. Walker AK, et al. A conserved SREBP-1/phosphatidylcholine feedback circuit regulates lipogenesis in metazoans. *Cell*. 2011;147(4):840–852.
36. Kandutsch AA, Shown EP. Assay of oxysterol-binding protein in a mouse fibroblast, cell-free system. Dissociation constant and other properties of the system. *J Biol Chem*. 1981;256(24):13068–13073.
37. Dawson PA, Ridgway ND, Slaughter CA, Brown MS, Goldstein JL. cDNA cloning and expression of oxysterol-binding protein, an oligomer with a potential leucine zipper. *J Biol Chem*. 1989;264(28):16798–16803.
38. Dawson PA, Van der Westhuyzen DR, Goldstein JL, Brown MS. Purification of oxysterol binding protein from hamster liver cytosol. *J Biol Chem*. 1989;264(15):9046–9052.
39. Ridgway ND. Oxysterol-binding proteins. *Subcell Biochem*. 2010;51:159–182.
40. Olkkonen VM, Li S. Oxysterol-binding proteins: sterol and phosphoinositide sensors coordinating transport, signaling and metabolism. *Prog Lipid Res*. 2013;52(4):529–538.
41. Weber-Boyvat M, et al. OSBP-related protein 3 (ORP3) coupling with VAMP-associated protein A regulates R-Ras activity. *Exp Cell Res*. 2015;331(2):278–291.
42. Lehto M, Hynynen R, Karjalainen K, Kuismanen E, Hyvärinen K, Olkkonen VM. Targeting of OSBP-related protein 3 (ORP3) to endoplasmic reticulum and plasma membrane is controlled by multiple determinants. *Exp Cell Res*. 2005;310(2):445–462.
43. Lehto M, et al. The R-Ras interaction partner ORP3 regulates cell adhesion. *J Cell Sci*. 2008;121(Pt 5):695–705.
44. Cave MC, et al. Nuclear receptors and nonalcoholic fatty liver disease. *Biochim Biophys Acta*. 2016;1859(9):1083–1099.
45. Neuschwander-Tetri BA, et al. Farnesoid X nuclear receptor ligand obeticholic acid for non-cirrhotic, non-alcoholic steatohepatitis (FLINT): a multicentre, randomised, placebo-controlled trial. *Lancet*. 2015;385(9972):956–965.
46. Sanyal AJ, et al. Pioglitazone, vitamin E, or placebo for nonalcoholic steatohepatitis. *N Engl J Med*. 2010;362(18):1675–1685.
47. Mataki C, et al. Compromised intestinal lipid absorption in mice with a liver-specific deficiency of liver receptor homolog 1. *Mol Cell Biol*. 2007;27(23):8330–8339.
48. Ayuso E, et al. High AAV vector purity results in serotype- and tissue-independent enhancement of transduction efficiency. *Gene Ther*. 2010;17(4):503–510.
49. Lock M, et al. Characterization of a recombinant adeno-associated virus type 2 Reference Standard Material. *Hum Gene Ther*. 2010;21(10):1273–1285.
50. Bligh EG, Dyer WJ. A rapid method of total lipid extraction and purification. *Can J Biochem Physiol*. 1959;37(8):911–917.
51. Oosterveer MH, et al. High fat feeding induces hepatic fatty acid elongation in mice. *PLoS One*. 2009;4(6):e6066.

RESEARCH COMMUNICATION

LRH-1-dependent programming of mitochondrial glutamine processing drives liver cancer

Pan Xu,[1] Maaike H. Oosterveer,[2,6] Sokrates Stein,[1,6] Hadrien Demagny,[1] Dongryeol Ryu,[3] Norman Moullan,[1,3] Xu Wang,[3] Emine Can,[4] Nicola Zamboni,[5] Arnaud Comment,[4] Johan Auwerx,[3] and Kristina Schoonjans[1]

[1]Metabolic Signaling, Institute of Bioengineering, Ecole Polytechnique Fédérale de Lausanne, CH-1015 Lausanne, Switzerland; [2]Department of Pediatrics, Center for Liver Digestive and Metabolic Diseases, University of Groningen, NL-9700 RB Groningen, The Netherlands; [3]Laboratory of Integrative and Systems Physiology, Institute of Bioengineering, Ecole Polytechnique Fédérale de Lausanne, CH-1015 Lausanne, Switzerland; [4]Institute of the Physics of Biological Systems, School of Basic Sciences, Ecole Polytechnique Fédérale de Lausanne, CH-1015 Lausanne, Switzerland; [5]Department of Biology, Institute for Molecular Systems Biology, Eidgenössische Technische Hochschule Zürich, CH-8093 Zurich, Switzerland

Various tumors develop addiction to glutamine to support uncontrolled cell proliferation. Here we identify the nuclear receptor liver receptor homolog 1 (LRH-1) as a key regulator in the process of hepatic tumorigenesis through the coordination of a noncanonical glutamine pathway that is reliant on the mitochondrial and cytosolic transaminases glutamate pyruvate transaminase 2 (GPT2) and glutamate oxaloacetate transaminase 1 (GOT1), which fuel anabolic metabolism. In particular, we show that gain and loss of function of hepatic LRH-1 modulate the expression and activity of mitochondrial glutaminase 2 (GLS2), the first and rate-limiting step of this pathway. Acute and chronic deletion of hepatic LRH-1 blunts the deamination of glutamine and reduces glutamine-dependent anaplerosis. The robust reduction in glutaminolysis and the limiting availability of α-ketoglutarate in turn inhibit mTORC1 signaling to eventually block cell growth and proliferation. Collectively, these studies highlight the importance of LRH-1 in coordinating glutamine-induced metabolism and signaling to promote hepatocellular carcinogenesis.

Supplemental material is available for this article.

Received January 7, 2016; revised version accepted May 12, 2016.

During tumorigenesis, cancer cells usually switch from oxidative metabolism to a highly glycolytic metabolic status (Vander Heiden et al. 2009). While glucose is predominantly metabolized into lactate rather than entering the tricarboxylic acid (TCA) cycle, cancer cells particularly rely on glutamine to replenish TCA cycle intermediates. This process, termed anaplerosis, is accomplished through the conversion of glutamine to α-ketoglutarate (α-KG) via a two-step deamination reaction catalyzed by glutaminases and then by glutamate dehydrogenase 1 (GLUD1) or transaminases (DeBerardinis et al. 2008; Wise et al. 2008; Csibi et al. 2013; Son et al. 2013). Cancer cells therefore critically depend on glutamine as a fuel for proliferation, and abrogation of glutamine metabolism blocks tumorigenesis, indicating an accessible therapeutic window for cancer treatment (Hensley et al. 2013).

Liver receptor homolog 1 (LRH-1; also called NR5A2) is a nuclear receptor that is enriched in enterohepatic tissues, where it has diverse molecular and physiological functions (Stein and Schoonjans 2015). LRH-1 has been linked to cell proliferation and cancer development in the intestine (Botrugno et al. 2004; Schoonjans et al. 2005) and pancreas (Petersen et al. 2010; Benod et al. 2011). In the liver, LRH-1 regulates various metabolic processes, including bile acid synthesis (Mataki et al. 2007; Lee et al. 2008; Out et al. 2011), glucose sensing and processing (Oosterveer et al. 2012), and reverse cholesterol transport (Stein et al. 2014). Although the function of LRH-1 in the liver has been extensively studied, its commanding role in intermediary metabolism has never been connected to tumorigenesis.

In this study, we report that LRH-1 promotes diethylnitrosamine (DEN)-induced hepatocellular carcinoma (HCC) by coordinating glutamine-induced anabolic metabolism. We demonstrate that LRH-1 facilitates the production of NADPH from glutamine by favoring a noncanonical glutamine pathway that optimizes reductive biosynthesis. Importantly, chronic and acute disruption of LRH-1 also impairs glutamine-induced anaplerosis and α-KG availability, ultimately leading to reduced mTORC1 signaling. These results unveil an unexpected role of LRH-1 in cancer intermediary metabolism with broad-ranging implications on mTORC1 signaling.

Results and Discussion

Hepatic loss of LRH-1 prevents DEN-induced liver carcinogenesis

To investigate the specific contribution of hepatic LRH-1 on HCC formation, we used the well-established DEN method to induce liver cancer (Bakiri and Wagner 2013). Liver-specific *Lrh-1*-deficient ($Lrh\text{-}1^{hep-/-}$) and wild-type control ($Lrh\text{-}1^{hep+/+}$) mice were injected with DEN on postnatal day 14. Tumor burden was assessed 6 mo (mid-term) or 10 mo (long-term) after injection (Fig. 1A). While long-term DEN-challenged $Lrh\text{-}1^{hep+/+}$ littermates developed multiple hepatic tumors, $Lrh\text{-}1^{hep-/-}$ mice were strikingly protected (Fig. 1B,C). The robust reduction of total tumor number and size was not caused by differences in DEN carcinogenicity as evidenced by the equal accumulation of DNA adducts induced by DEN

[*Keywords*: Hepatocellular carcinoma; cancer metabolism; nuclear receptor NR5A2; mitochondria; anaplerosis; mTOR; NADPH]
[6]**These authors contributed equally to this work.**
Corresponding author: kristina.schoonjans@epfl.ch
Article is online at http://www.genesdev.org/cgi/doi/10.1101/gad.277483.116. Freely available online through the *Genes & Development* Open Access option.

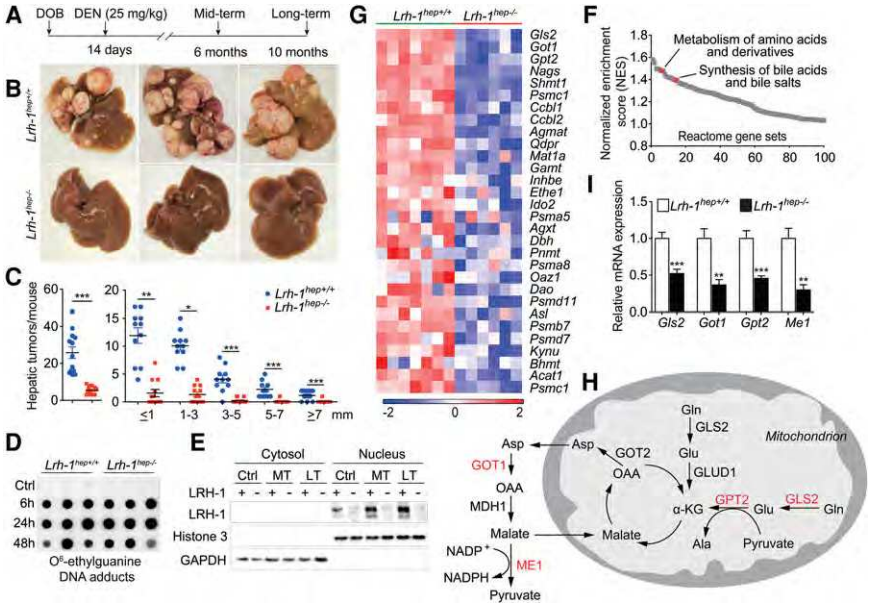

Figure 1. Hepatic *Lrh-1*-deficient mice are protected against DEN-induced HCC formation and display reduced glutamine-dependent anaplerosis. (*A*) Experimental strategies of DEN administration. (DOB) Date of birth. (*B*) Representative livers of 10-mo DEN-treated *Lrh-1*$^{hep+/+}$ and *Lrh-1*$^{hep-/-}$ mice. (*C*) Hepatic tumor number (*left*) and tumor size (*right*) in the corresponding genotypes. (*D*) Hepatic O^6-ethylguanine DNA adducts 6, 24, and 48 h after DEN injection to 14-d-old *Lrh-1*$^{hep+/+}$ and *Lrh-1*$^{hep-/-}$ mice. $n = 5$–6 per genotype and time point. (*E*) LRH-1 protein levels in cytosol and nucleus fractions of livers from untreated control (Ctrl), 6-mo DEN-treated (MT), and 10-mo DEN-treated (LT) *Lrh-1*$^{hep+/+}$ and *Lrh-1*$^{hep-/-}$ mice. (*F*) Gene set enrichment analysis (GSEA) demonstrates down-regulated pathways that were ranked by normalized enrichment scores (NES) in livers of 6-mo DEN-treated *Lrh-1*$^{hep-/-}$ ($n = 6$) mice compared with *Lrh-1*$^{hep+/+}$ ($n = 7$) mice. Specific pathways are indicated. (*G*) Heat map displaying the core-enriched gene set "metabolism of amino acids and derivatives," expressed in the livers of the mice described in *F*. (*H*) Graphical representation of enzymes involved in glutamine breakdown and metabolism. Enzymes highlighted in red are reduced in *Lrh-1*$^{hep-/-}$ livers, as shown in *I*. (*I*) Hepatic mRNA levels of *glutaminase 2* (*Gls2*), *glutamate oxaloacetate transaminase 1* (*Got1*), *glutamate pyruvate transaminase 2* (*Gpt2*), and *malic enzyme 1* (*Me1*) in livers of mice described in *F*. Data represent mean ± SEM. (*) $P < 0.05$; (**) $P < 0.01$; (***) $P < 0.001$ by two-tailed Student's *t*-test.

exposure in 14-d-old *Lrh-1*$^{hep+/+}$ and *Lrh-1*$^{hep-/-}$ livers (Fig. 1D; see the Supplemental Material for more details). Furthermore, DEN moderately increased LRH-1 protein abundance but did not affect its nuclear compartmentalization (Fig. 1E). We then performed histological and immunohistochemical analysis on the long-term DEN-treated liver sections. H&E staining of *Lrh-1*$^{hep-/-}$ liver sections demonstrated fewer microscopic tumor foci, while BrdU and Ki67 staining confirmed reduced cell proliferation in *Lrh-1*-deficient livers (Supplemental Fig. S1A). Moreover, long-term DEN-treated *Lrh-1*$^{hep-/-}$ livers were significantly lighter compared with *Lrh-1*$^{hep+/+}$ livers, while the body weight did not differ between the two genotypes (Supplemental Fig. S1B–D). Together, these results indicate that LRH-1 is required for efficient HCC induction and progression in response to DEN treatment.

Hepatic loss of LRH-1 inhibits noncanonical glutamine processing

LRH-1 coordinates intestinal cell renewal and tumor formation through cross-talk with the β-catenin pathway (Botrugno et al. 2004; Schoonjans et al. 2005). It is also required for hepatic endoplasmic reticulum (ER) stress resolution through transcriptional control of *polo-like kinase 3* (*Plk3*) and subsequent phosphorylation of activating transcription factor 2 (ATF2) (Mamrosh et al. 2014). To understand the robust tumor-suppressive phenotype, we first assessed the β-catenin pathway in mid-term DEN-treated livers in which tumors were not yet developed (Supplemental Fig. S1E). In contrast to the findings in intestinal crypts of germline *Lrh-1*$^{+/-}$ mice (Botrugno et al. 2004), β-catenin targets *c-Myc*, *Ccnd1*, and *Ccne1* were not reduced in the unchallenged (Supplemental Fig. S1F) or DEN-challenged (Supplemental Fig. S1G) *Lrh-1*$^{hep-/-}$ livers. We also evaluated the Plk3–ATF2 cascade in response to acute DEN exposure. *Plk3* mRNA levels and ATF2 phosphorylation were not induced by DEN (Supplemental Fig. S1H; data not shown), indicating that, in our model, LRH-1 impacts hepatocarcinogenesis via other mechanisms. We then performed microarray analysis to compare the transcriptomes of mid-term DEN-exposed *Lrh-1*$^{hep+/+}$ and *Lrh-1*$^{hep-/-}$ livers. As expected, gene set enrichment analysis (GSEA) confirmed previously established functions and target pathways of LRH-1, such as synthesis of bile acids (Fig. 1F; Supplemental Fig. S1I,J). Of interest, metabolism of amino acid and derivatives scored among the most significantly enriched pathways (Fig. 1F; Supplemental Fig. S1K). We next analyzed this gene set in more detail. While transcripts of several proteasomal subunits were down-regulated in *Lrh-1*$^{hep-/-}$ livers, a more striking reduction of several enzymes involved in glutamine catabolism was observed (Fig. 1G). Glutamine plays an essential role in tumor growth to support anaplerosis and reductive biosynthesis (DeBerardinis et al. 2008). Several genes involved in the processing of glutamine were reduced in mid-term DEN-exposed *Lrh-1*$^{hep-/-}$ livers, including mitochondrial *glutaminase 2* (*Gls2*), cytosolic *glutamate oxaloacetate transaminase 1* (*Got1*), and mitochondrial *glutamate pyruvate transaminase 2* (*Gpt2*) (Fig. 1G,H). This pathway is reminiscent of a noncanonical pathway of glutamine breakdown that was earlier reported in human glioma (Wise et al. 2008) and pancreatic ductal adenocarcinoma (PDAC) cells as an alternative mechanism to support NADPH production via malic enzyme (Son et al. 2013). Not only these genes but also *malic enzyme 1* (*Me1*) were significantly blunted, as confirmed by quantitative RT–PCR (qRT–PCR) (Fig. 1I). Many cancer cells typically rely on GLUD1 to fuel the TCA cycle through repleting α-KG (DeBerardinis et al. 2008). Transcript levels of *Glud1*, however, remained unchanged upon hepatic loss of function (LOF) of LRH-1 (Supplemental Fig. S1L). Moreover, mRNA expression of *Gls1*, *Got2*, and TCA cycle-related genes was not altered between the two

genotypes (Supplemental Fig. S1L,M). Collectively, these data indicate that an alternative pathway involved in hepatic glutamine processing is most likely compromised in *Lrh-1*$^{hep-/-}$ mice.

LRH-1 regulates reductive biosynthesis fueled by glutamine processing

We previously showed that LRH-1 coordinates glucose intermediary metabolism via glucokinase (GCK) activation and subsequent carbohydrate response element-binding protein (ChREBP) nuclear translocation (Oosterveer et al. 2012). Consistent with this study, the ChREBP pathway was significantly enriched between both genotypes (Supplemental Fig. S2A,B). Because *Me1* is a known ChREBP target gene (Iizuka et al. 2004; Chambers et al. 2013), we first analyzed whether the reduction of our candidate genes (Fig. 1I) results from impaired GCK–ChREBP signaling. GCK reconstitution in *Lrh-1*$^{hep-/-}$ livers restored *Chrebp*β and *Me1* (Fig. 2A), but not *Gls2*, *Got1*, or *Gpt2* expression (Supplemental Fig. S2C), indicating that LRH-1 regulates only *Me1* via the GCK–ChREBP axis. In parallel to the reduced *Me1* expression, NADPH/NADP$^+$ levels were significantly reduced in unchallenged (Fig. 2B) or DEN-challenged (Fig. 2C) *Lrh-1*$^{hep-/-}$ livers and was accompanied by a corresponding reduction of the GSH/GSSG ratio in DEN-treated livers (Fig. 2D). Although *Me1* was readily rescued upon GCK reconstitution (Fig. 2A), normalization of NADPH/NADP$^+$ levels was still incomplete (Fig. 2B), supporting the notion that the generation of NADPH from glutamine is also attenuated in *Lrh-1*$^{hep-/-}$ livers.

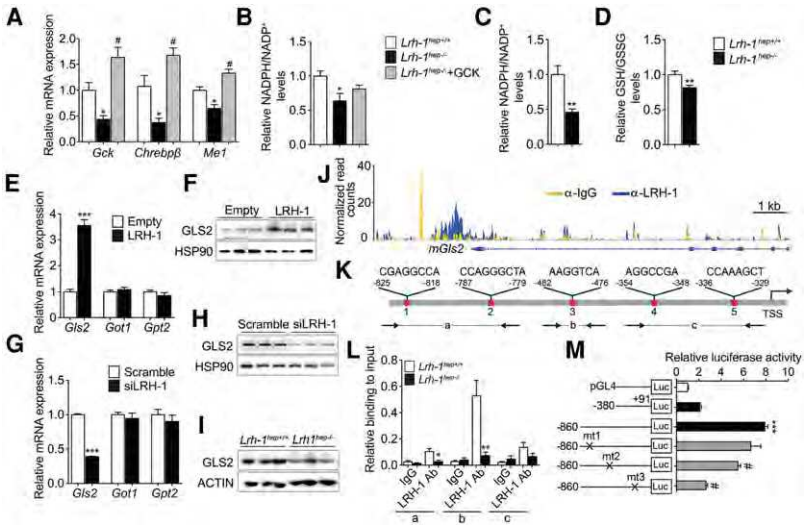

Figure 2. *Gls2* is a direct transcriptional target of LRH-1. (*A*,*B*) Hepatic mRNA levels of *Gck*, *Chrebp*β, and *Me1* (*A*) and NADPH/NADP$^+$ levels (*B*) in control virus-infected *Lrh-1*$^{hep+/+}$ and *Lrh-1*$^{hep-/-}$ mice and AAV8-GCK virus-infected *Lrh-1*$^{hep-/-}$ mice. $n = 4$–5 per group. Data represent mean ± SEM. (*) $P < 0.05$ versus *Lrh-1*$^{hep+/+}$; (#) $P < 0.05$ versus *Lrh-1*$^{hep-/-}$ by one-way ANOVA and Tukey's post-hoc test. (*C*,*D*) Relative NADPH/NADP$^+$ (*C*) and GSH/GSSG (*D*) levels in livers of 6-mo DEN-treated *Lrh-1*$^{hep+/+}$ ($n = 7$) and *Lrh-1*$^{hep-/-}$ ($n = 6$) mice. (*E*,*F*) mRNA levels of *Gls2*, *Got1*, and *Gpt2* (*E*) and protein levels of GLS2 (*F*) in Hepa 1.6 cells transfected with control or *Lrh-1* expression plasmids. $n = 3$ per group. (*G*,*H*) mRNA levels of *Gls2*, *Got1*, and *Gpt2* (*G*) and protein levels of GLS2 (*H*) in Hepa 1.6 cells transfected with scrambled or *Lrh-1* targeted siRNAs. $n = 3$ per group. Data represent mean ± SEM. (**) $P < 0.01$; (***) $P < 0.001$ by two-tailed Student's *t*-test. (*I*) Hepatic protein levels of GLS2 in mice described in *C*. (*J*) University of California at Santa Cruz (UCSC) genome browser (mm9) view displaying the occupancy of mouse *Gls2* by IgG and LRH-1 (Chong et al. 2012). (*K*) Schematic representation of the five putative LRH-1 response elements in the proximal mouse *Gls2* promoter. (*L*) ChIP-qPCR (chromatin immunoprecipitation [ChIP] combined with qPCR) assay to evaluate the relative LRH-1 binding to the mouse *Gls2* promoter. Amplified regions (a, b and c) are depicted in Figure 1K. (*M*) Luciferase activities in HEK293A cells after cotransfection of a *Lrh-1* expression vector and with empty luciferase reporter (pGL4) and long or short *Gls2* promoter constructs with or without the indicated mutations. Data represent mean ± SEM. (***) $P < 0.001$ versus empty reporter (pGL4); (#) $P < 0.05$ versus long *Gls2* promoter construct by one-way ANOVA and Tukey's post-hoc test.

We next investigated the molecular mechanism through which LRH-1 regulates glutamine metabolism. Overexpression of LRH-1 in mouse hepatoma Hepa 1.6 cells resulted in an increase of GLS2 transcripts and protein, while *Got1* and *Gpt2* transcripts were unchanged (Fig. 2E,F). Conversely, siRNA-mediated silencing of LRH-1 exclusively reduced the expression of GLS2 mRNA and protein (Fig. 2G,H). In *Lrh-1*$^{hep-/-}$ mice, reduced hepatic *Gls2* mRNA expression (Fig. 1H) translated into lower GLS2 protein levels (Fig. 2I). Of interest, *Gls2* is highly expressed in the liver compared with *Gls1* (Supplemental Fig. S2D). GLS2 deaminates mitochondrial glutamine, thus controlling a major anaplerotic step for hepatic glutamine utilization (Hensley et al. 2013). We then asked whether *Gls2* is subjected to direct transcriptional regulation by LRH-1. Analysis of a genome-wide hepatic LRH-1 ChIP-seq (chromatin immunoprecipitation [ChIP] combined with high-throughput sequencing) data set (Chong et al. 2012) revealed LRH-1 recruitment at the *Gls2* promoter (Fig. 2J), and computational analysis identified five putative LRH-1 response elements within the *Gls2* promoter under the LRH-1 ChIP-seq peak (Fig. 2K). Site-specific ChIP assays using DNA from mid-term DEN-treated *Lrh-1*$^{hep+/+}$ and *Lrh-1*$^{hep-/-}$ livers revealed LRH-1 recruitment to putative binding sites 1, 2, and 3 (Fig. 2L). Mutation of these binding sites in mouse *Gls2*-luciferase reporter constructs further mapped site 3, which is conserved in the human *Gls2* promoter (Supplemental Fig. S2E), as the major site that confers LRH-1 responsiveness (Fig. 2M). Accordingly, silencing of LRH-1 in human hepatoma HepG2 cells also led to a significant reduction of *Gls2* transcripts (Supplemental Fig. S2F).

LRH-1 regulates GLS2 to promote glutamine-induced anaplerosis

Given the marked reduction of GLS2 in *Lrh-1*$^{hep-/-}$ mice, we hypothesized that hepatic loss of LRH-1 blunts the conversion of glutamine to glutamate. To test the flux through GLS2 in vivo, we performed ^{13}C nuclear magnetic resonance (^{13}C MR) spectroscopy measurements following hyperpolarized [5-^{13}C]glutamine injection (Cabella et al. 2013; Cheng et al. 2013). [5-^{13}C]glutamine was hyperpolarized using dissolution dynamic nuclear polarization (DNP) and rapidly injected into DEN-treated *Lrh-1*$^{hep-/-}$ and *Lrh-1*$^{hep+/+}$ mice followed by real-time recording of its conversion to [5-^{13}C]glutamate (Fig. 3A,B). As expected, *Lrh-1*$^{hep-/-}$ showed a strong decrease in hepatic

[5-^{13}C]glutamate content compared with *Lrh-1*$^{hep+/+}$ mice (Fig. 3C). Unlike the expression levels of glutamine transporters *Slc1a5* and *Slc7a5*, which were unchanged (Supplemental Fig. S3A), hepatic α-KG levels were diminished in *Lrh-1*$^{hep-/-}$ mice (Fig. 3D), indicating that LRH-1 LOF may attenuate glutamine-fueled anaplerosis. To further explore the direct roles of LRH-1 and GLS2 in maintaining glutaminolysis and intracellular α-KG pools, we examined the effect of glutamine metabolism on α-KG levels. Hepa 1.6 cells were starved of glutamine for 6 h, and removal of glutamine significantly reduced the intracellular levels of α-KG (Supplemental Fig. S3B), demonstrating that glutamine sustains glutaminolysis. We then acutely modulated LRH-1 or GLS2 expression in Hepa 1.6 cells. In line with the reduced α-KG abundance in *Lrh-1*$^{hep-/-}$ livers, overexpression of LRH-1 or GLS2 increased, while siRNA-mediated silencing of LRH-1 or GLS2 decreased, α-KG levels in Hepa 1.6 cells (Fig. 3E–H). Together, these results demonstrate that LRH-1 promotes glutamine-induced anaplerosis via the induction of GLS2.

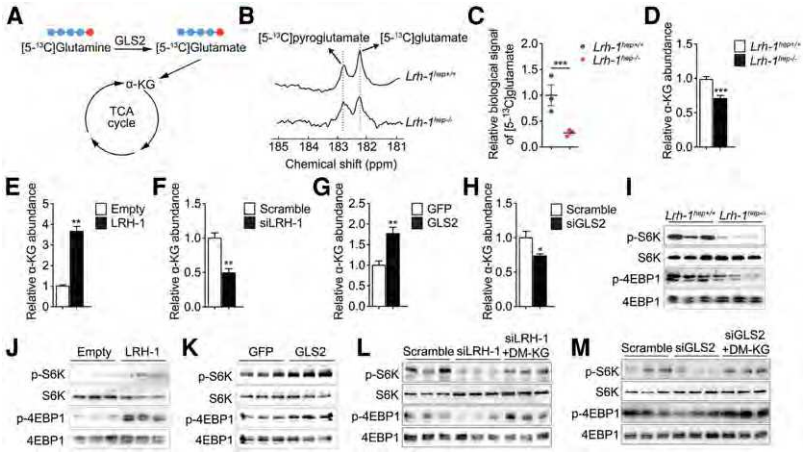

Figure 3. LRH-1 controls glutamine-induced anaplerosis and regulates mTORC1 activity. (*A*) GLS2-mediated biochemical reaction with hyperpolarized [5-^{13}C]glutamine. Red dots indicate the labelling of C5. (*B–D*) Representative in vivo ^{13}C MR spectra showing hyperpolarized [5-^{13}C]glutamate production with the by-product signal of hyperpolarized [5-^{13}C]pyroglutamate (*B*), the mean signal intensity of the hyperpolarized [5-^{13}C]glutamate formed via glutaminase (*C*), and intracellular α-KG levels (*D*) in the livers of DEN-treated *Lrh-1*$^{hep+/+}$ and *Lrh-1*$^{hep-/-}$ mice. (*E–H*) Intracellular α-KG levels in Hepa 1.6 cells transfected with either control or *Lrh-1* expression plasmids ($n = 3$ per group) (*E*) or scrambled or *Lrh-1* targeted siRNAs ($n = 3$ per group) (*F*), transduced with either AdGFP or AdGLS2 viruses ($n = 3$ per group) (*G*), or transfected with scrambled or *Gls2* targeted siRNAs ($n = 3$ per group) (*H*). (*I*) Phosphorylation states of S6K and 4EBP1 in the livers of mice described in *B*. (*J–M*) Phosphorylation states of S6K and 4EBP1 in Hepa 1.6 cells transfected as in *E* (*J*), transduced as in *G* (*K*), transfected as in *F* (*L*), or transfected as in *H* (*M*) with or without dimethyl-KG (DM-KG) supplementation (*L*,*M*). Data represent mean ± SEM. (*) $P < 0.05$; (**) $P < 0.01$; (***) $P < 0.001$ by two-tailed Student's *t*-test.

LRH-1 modulates the mTORC1 pathway in an α-KG-dependent manner

Glutamine is metabolized through glutaminolysis to produce α-KG. Previous studies showed that increased glutamine (Duran et al. 2012; Bar-Peled and Sabatini 2014) or α-KG (Duran et al. 2012) availability stimulates the mTORC1 signaling pathway. Of note, a robust reduction of mTORC1 activation was observed in *Lrh-1*$^{hep-/-}$ livers, as evidenced by the decreased phosphorylation of 4EBP1 and S6K (Fig. 3I). We then investigated the importance of glutamine in the activation of mTORC1 in Hepa 1.6 cells. Depletion of glutamine for 6 h reduced α-KG levels (Supplemental Fig. S3B) and inhibited mTORC1 activity (Supplemental Fig. S3C). Moreover, supplementation of a cell-permeable α-KG analog, dimethyl-KG (DM-KG), restored the activation of mTORC1 signaling upon glutamine deprivation (Supplemental Fig. S3D), indicating that intracellular glutamine and its derived α-KG are essential to stimulate mTORC1. Based on these results, we overexpressed LRH-1 or GLS2 in Hepa 1.6 cells. In both settings, mTORC1 activity was induced in the presence of glutamine (Fig. 3J,K). These effects were reversed upon glutamine starvation (Supplemental Fig. S3E,F). Furthermore, RNAi-mediated suppression of LRH-1 or GLS2 interfered with phosphorylation of 4EBP1 and S6K in the presence of glutamine, while addition of DM-KG or overexpression of GLS2 or LRH-1, respectively, rescued mTORC1 activities (Fig. 3L,M; Supplemental Fig. S3G, H). These data hence suggest that the LRH-1–GLS2 axis increases α-KG levels and consequently activates mTORC1.

The LRH-1–GLS2 axis promotes cell proliferation

Activation of mTORC1 inhibits autophagy (Kim et al. 2011), activates protein translation (Ma and Blenis 2009), and promotes cell growth (Schmelzle and Hall 2000). To investigate the importance of the LRH-1–GLS2–mTORC1 pathway, we first assessed autophagy in mid-term DEN-treated livers. As expected, disruption of LRH-1 induced autophagy, as evidenced by reduced phosphorylation of ULK-1 at Ser757, blunted P62, and increased LC3-II levels (Supplemental Fig. S4A). Silencing of LRH-1 or GLS2 decreased global protein translation as measured by incorporation of ^{35}S-labelled methionine in Hepa 1.6 cells (Fig. 4A, B), while their overexpression enhanced translation (Supplemental Fig. S4B,C). We then evaluated the link between LRH-1, α-KG, and cell proliferation. As expected, LRH-1 or GLS2 overexpression promoted cell proliferation, while additional glutamine deprivation prevented the increase in cell proliferation (Fig. 4C,D). Conversely, inhibition of glutaminolysis by LRH-1 or GLS2 silencing inhibited cell proliferation, while overexpression of LRH-1 or GLS2 rescued this effect (Supplemental Fig. S4D,E). Moreover, diminished cell proliferation upon LRH-1 or GLS2 suppression could also be rescued by addition of DM-KG (Fig. 4E,F), indicating that the LRH-1–GLS2 axis activates cell proliferation in an α-KG-dependent manner. It has been shown that GLS2-catalyzed deamination of glutamine is also essential for the control of intracellular reactive oxygen species (ROS) levels (Hu et al. 2010). Supplementation with the antioxidant N-acetyl-cysteine (NAC), however, could not rescue the inhibited cell proliferation upon LRH-1 or GLS2 silencing in Hepa 1.6 cells (Supplemental Fig. S4F,G), suggesting that reduced mTORC1 signaling rather than induced oxidative stress accounts for the reduction in cell proliferation. Furthermore, Hepa 1.6 cells silenced for LRH-1 or GLS2 induced significantly less tumor growth after propagation in athymic nude mice (Fig. 4G). Taken together, these findings

highlight that LRH-1 promotes cell proliferation through glutaminolysis and mTORC1 signaling.

In conclusion, our study assigns a critical role to LRH-1 in hepatic fuel metabolism with a striking impact on hepatic tumorigenesis. Unlike the role of LRH-1 in the intestine and pancreas, the oncogenic potential of hepatic LRH-1 is independent from the β-catenin/Wnt signaling pathway and is instead driven by the regulation of specific gene programs involved in mitochondrial glutamine catabolism (Fig. 4H). The enhanced mTORC1 signaling upon LRH-1-induced glutaminolysis indicates that the effect of LRH-1 on glutamine processing also impinges on established kinases in cell growth and cancer, thereby further amplifying the overall growth-stimulating effect. These observations, together with our previous findings linking LRH-1 to glucose-dependent fatty acid biosynthesis via ChREBP activation (Oosterveer et al. 2012), support the notion that LRH-1 confers a protumorigenic status to hepatocytes by promoting the metabolism of the principal fuel substrates of cancer cells. Further studies are warranted to fully understand its role in human HCC and explore its potential as a drug target.

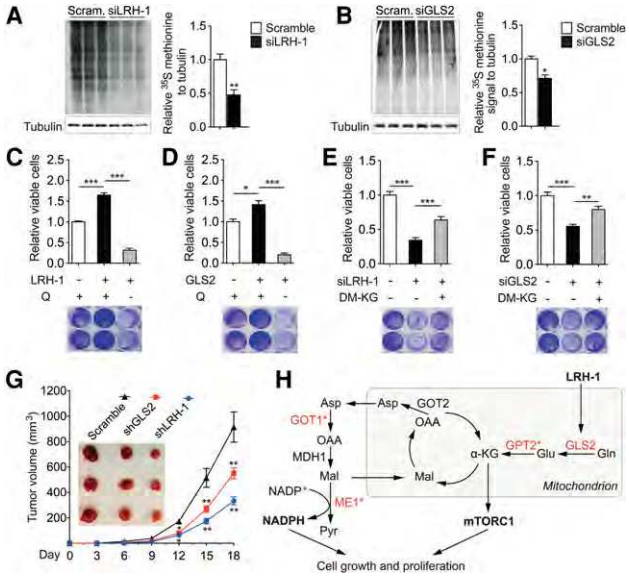

Figure 4. The LRH-1–GLS2 axis promotes protein translation and cell proliferation. (*A*,*B*) Global protein synthesis measured by ^{35}S-labelled methionine incorporation in Hepa 1.6 cells transfected with either scrambled or *Lrh-1* targeted siRNAs ($n = 3$ per group) (*A*) or scrambled or *Gls2* targeted siRNAs ($n = 3$ per group) (*B*). Relative ^{35}S methionine signals were normalized to Tubulin. Data represent mean ± SEM. (*) $P < 0.05$; (**) $P < 0.01$ by two-tailed Student's *t*-test. (*C–F*) Relative viable cells and representative Crystal Violet staining images of Hepa 1.6 cells transfected with either control or *Lrh-1* expression plasmids ($n = 3$ per group) (*C*) or transduced with either AdGFP or AdGLS2 viruses ($n = 3$ per group) (*D*) with or without glutamine deprivation or scrambled or *Lrh-1* targeted siRNAs ($n = 3$ per group) (*E*) or scrambled or *Gls2* targeted siRNAs ($n = 3$ per group) (*F*) with or without DM-KG supplementation. Data represent mean ± SEM. (*) $P < 0.05$; (***) $P < 0.001$ by one-way ANOVA and Tukey's post-hoc test. (*G*) Comparison of tumor growth and volume of mice subcutaneously injected with Hepa 1.6 cells that were transduced with scrambled, LRH-1 targeted, or GLS2 targeted shRNA. $n = 6$ per group. (*H*) Graphical summary illustrating how LRH-1 promotes glutamine-induced anaplerosis and reductive biosynthesis in hepatic cancer cells. Enzymes highlighted in red are reduced in *Lrh-1*$^{hep-/-}$ livers, and an asterisk indicates indirect regulation by LRH-1.

Materials and methods

Animal studies

Hepatocyte-specific LRH-1 knockout (*Lrh-1*$^{hep-/-}$) and wild-type (*Lrh-1*$^{hep+/+}$) mice were previously reported (Oosterveer et al. 2012). Congenic neonatal mice at 14 d old were intraperitoneally injected with DEN at a dose of 25 mg per kilogram of body weight to initiate tumor formation. Six months (mid-term DEN) or 10 mo (long-term DEN) after injection, mice were sacrificed, and liver tissue was collected. The experiments with the AAV8 viruses have been described previously (Oosterveer et al. 2012). Five-week-old male BALB/c nu/nu mice were purchased from Charles River and maintained in the animal facilities. All animal procedures were approved by the Swiss authorities (Canton of Vaud, animal protocol IDs 2375 and 2768) and performed in accordance with our institutional guidelines.

ChIP

ChIP analysis was performed as described previously with minor modifications (Stein et al. 2014). DNA was purified using the PCR clean-up extraction kit (Macherey-Nagel), after which qRT-PCR was performed as described previously (Mataki et al. 2007). Data were normalized to the input [fold differences = $2^{-(\text{Ct sample} - \text{Ct input})}$]. ChIP primer sequences are listed in Supplemental Table 1.

Measurements of metabolites

For NADPH/NADP$^+$ and GSH/GSSG ratios, liver biopsies were extracted with 70% ethanol, and biomass was separated by centrifugation at 4000 rpm for 10 min. Liquid extracts were then dried by vacuum centrifugation, resuspended in 10 µL of water per milligram of wet weight, and analyzed by targeted liquid chromatography-tandem mass spectrometry on a Thermo Quantum Ultra instrument equipped with a Waters Acquity ultra high performance liquid chromatographer (UPLC). Intracellular α-KG levels were determined using commercial kits (Abcam, ab83431) according to the manufacturer's instructions.

In vivo hyperpolarized ^{13}C MR measurements

DEN-treated *Lrh-1*$^{hep+/+}$ and *Lrh-1*$^{hep-/-}$ mice were anesthetized with ~1.8% isoflurane, 0.5% O_2, and 0.5% air. A 750-µL bolus containing a dose of 0.57 mmol/kg ± 0.02 mmol/kg hyperpolarized [5-^{13}C]glutamine was administered in 9 sec. A series of 30°C BIR4 adiabatic RF excitation pulses were applied using a custom-built dual ^{1}H/^{13}C probe (two ^{1}H surface coils placed in quadrature on top of a ^{13}C single-loop surface coil) placed under the animal on the shaved skin located above the mouse's liver. In vivo ^{13}C MR measurements were respiratory-gated and triggered with simulated cardiac signal with a repetition time of 1 sec. Acquisitions were performed with an INOVA spectrometer (Varian/Magnex). The peak integrals were obtained from summed spectra analyzed using VNMRJ.

Allograft tumor study

Hepa 1.6 cells suspended in phosphate-buffered saline were injected subcutaneously into the left flanks of nude mice (4×10^6 cells per flank). The diameters of the tumors were measured every 3 d, and tumor volumes (V) were calculated using the formula $V = L \times W^2/2$, where L is length, and W is width.

Statistical analysis

Data represent mean ± SEM. Comparison of differences between two groups was assessed using two-tailed Student's *t*-tests. Multiple group comparisons were assessed by one-way ANOVA and Tukey's post-hoc test. Differences under $P < 0.05$ were considered statistically significant ($P < 0.05$ [*], $P < 0.01$ [**], and $P < 0.001$ [***]).

More experimental Materials and Methods are included in the Supplemental Material.

Acknowledgments

We thank V. Lemos for assistance with in vivo experiments, and H.A.I. Yoshihara for hyperpolarized ^{13}C data analysis. This study was supported by École Polytechnique Fédérale de Lausanne funding, the Swiss Cancer League (KFS-2809-08-2011, KFS-3082-02-2013, and KFS-3444-08-2014), and the Swiss National Science Foundation (CRSII3_160798/1). S.S. is supported by a post-doctoral fellowship from the Novartis Consumer Health Foundation, and J.A. is the Nestle Chair in Energy Metabolism.

References

Bakiri L, Wagner EF. 2013. Mouse models for liver cancer. *Mol Oncol* **7:** 206–223.

Bar-Peled L, Sabatini DM. 2014. Regulation of mTORC1 by amino acids. *Trends Cell Biol* **24:** 400–406.

Benod C, Vinogradova MV, Jouravel N, Kim GE, Fletterick RJ, Sablin EP. 2011. Nuclear receptor liver receptor homologue 1 (LRH-1) regulates pancreatic cancer cell growth and proliferation. *Proc Natl Acad Sci* **108:** 16927–16931.

Botrugno OA, Fayard E, Annicotte JS, Haby C, Brennan T, Wendling O, Tanaka T, Kodama T, Thomas W, Auwerx J, et al. 2004. Synergy between LRH-1 and β-catenin induces G1 cyclin-mediated cell proliferation. *Mol Cell* **15:** 499–509.

Cabella C, Karlsson M, Canape C, Catanzaro G, Colombo Serra S, Miragoli L, Poggi L, Uggeri F, Venturi L, Jensen PR, et al. 2013. In vivo and in vitro liver cancer metabolism observed with hyperpolarized [5-^{13}C]glutamine. *J Magn Reson* **232:** 45–52.

Chambers KT, Chen Z, Lai L, Leone TC, Towle HC, Kralli A, Crawford PA, Finck BN. 2013. PGC-1β and ChREBP partner to cooperatively regulate hepatic lipogenesis in a glucose concentration-dependent manner. *Mol Metab* **2:** 194–204.

Cheng T, Mishkovsky M, Bastiaansen JA, Ouari O, Hautle P, Tordo P, van den Brandt B, Comment A. 2013. Automated transfer and injection of hyperpolarized molecules with polarization measurement prior to in vivo NMR. *NMR Biomed* **26:** 1582–1588.

Chong HK, Biesinger J, Seo YK, Xie X, Osborne TF. 2012. Genome-wide analysis of hepatic LRH-1 reveals a promoter binding preference and suggests a role in regulating genes of lipid metabolism in concert with FXR. *BMC Genomics* **13:** 51.

Csibi A, Fendt SM, Li C, Poulogiannis G, Choo AY, Chapski DJ, Jeong SM, Dempsey JM, Parkhitko A, Morrison T, et al. 2013. The mTORC1 pathway stimulates glutamine metabolism and cell proliferation by repressing SIRT4. *Cell* **153:** 840–854.

DeBerardinis RJ, Lum JJ, Hatzivassiliou G, Thompson CB. 2008. The biology of cancer: metabolic reprogramming fuels cell growth and proliferation. *Cell Metab* **7:** 11–20.

Duran RV, Oppliger W, Robitaille AM, Heiserich L, Skendaj R, Gottlieb E, Hall MN. 2012. Glutaminolysis activates Rag-mTORC1 signaling. *Mol Cell* **47:** 349–358.

Hensley CT, Wasti AT, DeBerardinis RJ. 2013. Glutamine and cancer: cell biology, physiology, and clinical opportunities. *J Clin Invest* **123:** 3678–3684.

Hu W, Zhang C, Wu R, Sun Y, Levine A, Feng Z. 2010. Glutaminase 2, a novel p53 target gene regulating energy metabolism and antioxidant function. *Proc Natl Acad Sci* **107:** 7455–7460.

Iizuka K, Bruick RK, Liang G, Horton JD, Uyeda K. 2004. Deficiency of carbohydrate response element-binding protein (ChREBP) reduces lipogenesis as well as glycolysis. *Proc Natl Acad Sci* **101:** 7281–7286.

Kim J, Kundu M, Viollet B, Guan KL. 2011. AMPK and mTOR regulate autophagy through direct phosphorylation of Ulk1. *Nat Cell Biol* **13:** 132–141.

Lee YK, Schmidt DR, Cummins CL, Choi M, Peng L, Zhang Y, Goodwin B, Hammer RE, Mangelsdorf DJ, Kliewer SA. 2008. Liver receptor homolog-1 regulates bile acid homeostasis but is not essential for feedback regulation of bile acid synthesis. *Mol Endocrinol* **22:** 1345–1356.

Ma XM, Blenis J. 2009. Molecular mechanisms of mTOR-mediated translational control. *Nat Rev Mol Cell Biol* **10:** 307–318.

Mamrosh JL, Lee JM, Wagner M, Stambrook PJ, Whitby RJ, Sifers RN, Wu SPO, Tsai MJ, Demayo FJ, Moore DD. 2014. Nuclear receptor LRH-1/NR5A2 is required and targetable for liver endoplasmic reticulum stress resolution. *Elife* **3:** e01694.

Mataki C, Magnier BC, Houten SM, Annicotte JS, Argmann C, Thomas C, Overmars H, Kulik W, Metzger D, Auwerx J, et al. 2007. Compromised intestinal lipid absorption in mice with a liver-specific deficiency of liver receptor homolog 1. *Mol Cell Biol* **27:** 8330–8339.

Oosterveer MH, Mataki C, Yamamoto H, Harach T, Moullan N, van Dijk TH, Ayuso E, Bosch F, Postic C, Groen AK, et al. 2012. LRH-1-dependent glucose sensing determines intermediary metabolism in liver. *J Clin Invest* **122:** 2817–2826.

Out C, Hageman J, Bloks VW, Gerrits H, Sollewijn Gelpke MD, Bos T, Havinga R, Smit MJ, Kuipers F, Groen AK. 2011. Liver receptor homolog-1 is critical for adequate up-regulation of Cyp7a1 gene transcription and bile salt synthesis during bile salt sequestration. *Hepatology* **53:** 2075–2085.

Petersen GM, Amundadottir L, Fuchs CS, Kraft P, Stolzenberg-Solomon RZ, Jacobs KB, Arslan AA, Bueno-de-Mesquita HB, Gallinger S, Gross M, et al. 2010. A genome-wide association study identifies pancreatic cancer susceptibility loci on chromosomes 13q22.1, 1q32.1 and 5p15.33. *Nat Genet* **42:** 224–228.

Schmelzle T, Hall MN. 2000. TOR, a central controller of cell growth. *Cell* **103:** 253–262.

Schoonjans K, Dubuquoy L, Mebis J, Fayard E, Wendling O, Haby C, Geboes K, Auwerx J. 2005. Liver receptor homolog 1 contributes to intestinal tumor formation through effects on cell cycle and inflammation. *Proc Natl Acad Sci* **102:** 2058–2062.

Son J, Lyssiotis CA, Ying H, Wang X, Hua S, Ligorio M, Perera RM, Ferrone CR, Mullarky E, Shyh-Chang N, et al. 2013. Glutamine supports pancreatic cancer growth through a KRAS-regulated metabolic pathway. *Nature* **496:** 101–105.

Stein S, Schoonjans K. 2015. Molecular basis for the regulation of the nuclear receptor LRH-1. *Curr Opin Cell Biol* **33:** 26–34.

Stein S, Oosterveer MH, Mataki C, Xu P, Lemos V, Havinga R, Dittner C, Ryu D, Menzies KJ, Wang X, et al. 2014. SUMOylation-dependent LRH-1/PROX1 interaction promotes atherosclerosis by decreasing hepatic reverse cholesterol transport. *Cell Metab* **20:** 603–613.

Vander Heiden MG, Cantley LC, Thompson CB. 2009. Understanding the Warburg effect: the metabolic requirements of cell proliferation. *Science* **324:** 1029–1033.

Wise DR, DeBerardinis RJ, Mancuso A, Sayed N, Zhang XY, Pfeiffer HK, Nissim I, Daikhin E, Yudkoff M, McMahon SB, et al. 2008. Myc regulates a transcriptional program that stimulates mitochondrial glutaminolysis and leads to glutamine addiction. *Proc Natl Acad Sci* **105:** 18782–18787.

CellPress

Cell Metabolism
Article

A SIRT7-Dependent Acetylation Switch of GABPβ1 Controls Mitochondrial Function

Dongryeol Ryu,[1] Young Suk Jo,[1,2] Giuseppe Lo Sasso,[1] Sokrates Stein,[3] Hongbo Zhang,[1] Alessia Perino,[3] Jung Uee Lee,[4] Massimo Zeviani,[5,6] Raymond Romand,[7] Michael O. Hottiger,[8] Kristina Schoonjans,[3] and Johan Auwerx[1,*]

[1]Laboratory of Integrative and Systems Physiology, School of Life Sciences, École Polytechnique Fédérale de Lausanne, 1015 Lausanne, Switzerland
[2]Division of Endocrinology, Department of Internal Medicine, Yonsei University College of Medicine, Seoul 120-752, Republic of Korea
[3]Metabolic Signaling, Institute of Bioengineering, École Polytechnique Fédérale de Lausanne, 1015 Lausanne, Switzerland
[4]Department of Pathology, Daejeon St. Mary's Hospital, College of Medicine, the Catholic University of Korea, Seoul 137-701, Republic of Korea
[5]Unit of Molecular Neurogenetics, the Carlo Besta Institute of Neurology IRCCS, 20133 Milan, Italy
[6]MRC Mitochondrial Biology Unit, Cambridge CB2 0XY, UK
[7]Institut de Génétique et de Biologie Moléculaire et Cellulaire, BP 10142, 67404 Illkirch Cedex, France
[8]Institute of Veterinary Biochemistry and Molecular Biology, University of Zurich, 8057 Zurich, Switzerland
*Correspondence: admin.auwerx@epfl.ch
http://dx.doi.org/10.1016/j.cmet.2014.08.001

SUMMARY

Mitochondrial activity is controlled by proteins encoded by both nuclear and mitochondrial DNA. Here, we identify *Sirt7* as a crucial regulator of mitochondrial homeostasis. *Sirt7* deficiency in mice induces multisystemic mitochondrial dysfunction, which is reflected by increased blood lactate levels, reduced exercise performance, cardiac dysfunction, hepatic microvesicular steatosis, and age-related hearing loss. This link between SIRT7 and mitochondrial function is translatable in humans, where SIRT7 overexpression rescues the mitochondrial functional defect in fibroblasts with a mutation in *NDUFS1*. These wide-ranging effects of SIRT7 on mitochondrial homeostasis are the consequence of the deacetylation of distinct lysine residues located in the hetero- and homodimerization domains of GABPβ1, a master regulator of nuclear-encoded mitochondrial genes. SIRT7-mediated deacetylation of GABPβ1 facilitates complex formation with GABPα and the transcriptional activation of the GABPα/GABPβ heterotetramer. Altogether, these data suggest that SIRT7 is a dynamic nuclear regulator of mitochondrial function through its impact on GABPβ1 function.

INTRODUCTION

Mitochondria are unique cellular organelles derived from endosymbiotic α-proteobacteria that evolved within our cells (Gray et al., 1999). Mitochondria contain multiple copies of their own circular DNA (mtDNA), which encodes for only 13 proteins. Hence, the bulk of the mitochondrial proteins are encoded by nuclear DNA (nDNA) and subsequently imported, folded, and assembled within the mitochondria, exposing them to proteotoxic stress (Schmidt et al., 2010; Wallace, 1999). Mitochondria harvest energy from nutrients and convert it via oxidative phosphorylation (OXPHOS) into ATP, the cellular energy source, making them also vulnerable to metabolic stress. This exposure to distinct stressors explains the existence of multiple quality control mechanisms and adaptive pathways, including mitochondrial biogenesis, mitophagy, and the mitochondrial unfolded protein response, which all act to maintain proper mitochondrial function (Andreux et al., 2014; Poyton and McEwen, 1996). Chronic overload of these quality control pathways is a major cause for mitochondrial dysfunction and contributes to the pathogenesis of mitochondrial diseases, ranging from rare inherited mitochondrial diseases to a palette of common age-related disorders that include metabolic diseases, neurodegeneration, and cancer (Larsson, 2010; Nunnari and Suomalainen, 2012; Wallace, 1999). Many of the adaptive processes in the mitochondria are governed by a small set of nuclear transcription factors, including nuclear respiratory factor 1 (NRF1), GA binding protein (GABP, also known as nuclear respiratory factor or NRF2 [NCBI Gene Expression Omnibus (GEO) IDs 14390 for GABPα and 14391 for GABPβ1] but not to be confused with Nrf2/Nfe2l2 [NCBI GEO ID 18024]) and nuclear receptors, such as the peroxisome proliferator-activated receptors (PPARs) and estrogen-related receptors (ERRs) as well as transcriptional coregulators, such as PPARγ coactivator 1α, nuclear receptor corepressor 1, and the sirtuins (Andreux et al., 2013; Houtkooper et al., 2012; Scarpulla, 2008).

The sirtuins, an evolutionarily conserved protein family named after the prototypical yeast sirtuin enzyme Sir2p (Ivy et al., 1985; Shore et al., 1984), are central regulators of mitochondrial homeostasis (Guarente, 2008; Haigis and Sinclair, 2010; Houtkooper et al., 2012). Mammals have seven sirtuins (SIRT1–SIRT7) with distinct subcellular localization and biological actions (Houtkooper et al., 2012). The enzymatic activity of sirtuins is critically dependent on the obligatory cosubstrate NAD^+, making them intracellular sensors of the metabolic environment (Houtkooper et al., 2010; Imai and Guarente, 2010). The function of SIRT7, which, along with SIRT1 and SIRT6, is present in the nucleus, is only partially understood. SIRT7 is enriched in the nucleoli, where it facilitates the activation of

the DNA-dependent RNA polymerase I holoenzyme by interacting with one of its subunits (Ford et al., 2006) and the upstream binding transcription factor (UBTF) (Grob et al., 2009) and by the deacetylation of PAF53 (Chen et al., 2013). SIRT7 also deacetylates lysine 18 of histone H3, which is involved in the stabilization of transformed cancer cells (Barber et al., 2012), and *Sirt7*$^{-/-}$ mice display cardiac hypertrophy, which has been linked to p53 hyperacetylation (Vakhrusheva et al., 2008). Interestingly, two very recent studies linked SIRT7 to the control of liver function using independently generated mouse models, though diametrically opposed effects on liver lipid accumulation were observed (Shin et al., 2013; Yoshizawa et al., 2014).

By the combination of bioinformatic, molecular, and in vivo studies using independently generated germline- and liver-specific *Sirt7*$^{-/-}$ mouse models, we show that SIRT7 deacetylates GABPβ1, thereby enabling it to form the transcriptionally active GABPα/GABPβ heterotetramer. Through this effect on GABPβ1 acetylation, SIRT7 is crucial for promoting proper mitochondrial function and preventing mitochondrial-related diseases.

RESULTS

Sirt7 Expression Positively Correlates with nDNA-Encoded Mitochondrial Genes

As a first step for identifying functions of SIRT7, we applied a reverse genetic approach with the GeneNetwork database (www.genenetwork.org) (Andreux et al., 2012). The *Sirt7* expression pattern in livers or hematopoietic cells varied across the different BXD (Singer et al., 2004) or B6XBTBR-F2-ob/ob (F2) (Keller et al., 2008) mouse strains (Figures S1A–S1C available online). To identify putative targets of SIRT7, we selected those strains showing the highest or lowest *Sirt7* expression levels in each data set (indicated in red or blue, respectively; Figures S1A–S1C) and performed gene set enrichment analysis (GSEA; www.broadinstitute.org/gsea). Interestingly, GSEA showed a significant positive correlation between *Sirt7* and the gene set encompassing mitochondrial ribosomal proteins (MRPs; Figure 1A), whereas no correlation was observed with cytosolic ribosomal proteins (CRPs; Figures 1B–1C and Table S1). Next, to avoid possible inbreeding-related confounding factors potentially present in the recombinant inbred BXD strains, we analyzed the correlation of *Sirt7* to mitochondrial genes in lungs of outbred heterogeneous mice stocks (Valdar et al., 2006) and 457 human liver biopsies (Schadt et al., 2008). Again, a highly significant positive correlation between *Sirt7* and MRP genes was observed in both the lungs of heterogeneous outbred mice strains (Figures 1D–1E and S1D and Table S2) and human liver biopsies (Figures 1F and S1E and Table S3). In addition, the expression of several other nDNA-encoded mitochondrial genes such as *Clpp*, *Polrmt*, *Mfn1*, *Fars2*, *Elac2*, and *Nt5m* also correlated positively with *Sirt7* (Figures 1D–1F and Tables S2 and S3).

Multisystemic Mitochondrial Dysfunction in Sirt7$^{-/-}$ Mice

These results encouraged us to explore the role of SIRT7 in mitochondrial homeostasis with the use of a different *Sirt7*-deficient mouse line (*Sirt7*$^{-/-}$), which was generated by the targeted deletion of exons 6–9 of the *Sirt7* gene (see the Supplemental Information). Exons 6–9 encode the sirtuin deacetylase domain; in particular, exon 6 includes the putative proton acceptor histidine 188, the critical residue for the enzymatic activity of sirtuins (Figure S2A). The offspring of heterozygous *Sirt7* breeders (*Sirt7*$^{+/-}$) were born under normal Mendelian (+/+:+/−:−/− = 22.8%:52.4%:24.9%) and sex ratio (male:female = 48%:52%; Figure S2B).

A frequent feature of mitochondrial disease is the accumulation of lactate in the blood (Chi et al., 1992). Therefore, we monitored lactate and glucose levels in the basal state, during an oral glucose tolerance test (OGTT), and after exercise. Although basal lactate and glucose levels were not different between genotypes, lactate, but not glucose, was higher in *Sirt7*$^{-/-}$ mice after a glucose challenge (Figure 2A) and a 30 min treadmill run (Figure 2B). Consistent with increased lactate levels, endurance performance was reduced in *Sirt7*$^{-/-}$ mice (Figure 2C). Given that SIRT7 was undetectable in skeletal muscle (Figure S2C), this phenotype likely originates from cardiac dysfunction in our *Sirt7*$^{-/-}$ mice, which was ascertained by a comprehensive set of functional, molecular, and morphological analyses (Figures S2D–S2M) and was consistent with a previous report in an independently generated SIRT7 knockout mouse line (Vakhrusheva et al., 2008). The liver, the main tissue for metabolic transformation, is also sensitive to mitochondrial dysfunction. Although body weight and composition were indistinguishable between both genotypes (Figures S2N and S2O), livers of *Sirt7*$^{-/-}$ mice were heavier because of microvesicular hepatosteatosis, a hallmark of hepatic mitochondrial dysfunction (Figures 2D–2F) (Fromenty et al., 1997). In addition to the microvesicular hepatosteatosis, plasma triglycerides and free fatty acids were also elevated in *Sirt7*$^{-/-}$ mice (Figures 2G and 2H).

Inherited forms of deafness as well as age-related hearing loss are linked with mitochondrial dysfunction (Yamasoba et al., 2007). Among all nuclear sirtuins, *Sirt7* is highest expressed in the inner ear (Ct values: *Sirt1* = 29.18 ± 0.479, *Sirt6* = 38.29 ± 1.162, and *Sirt7* = 25.60 ± 0.343; Figure S2P). On the basis of this finding, we analyzed the auditory brainstem response (ABR), a standard electrophysiological test for auditory function. Hearing loss usually initiates from the high-frequency region and then extends to the low-frequency region (Hunter and Willott, 1987). ABR was not different in young *Sirt7*$^{+/+}$ and *Sirt7*$^{-/-}$ mice (Figure 2I, left and right). However, in older mice, *Sirt7*$^{-/-}$ deficiency increased the ABR threshold at all the frequencies (Figure 2I, right) although this was only evident for the highest frequency (30 kHz) in wild-type (WT) littermates (Figure 2I, left). Collectively, these phenotypic changes suggest that *Sirt7*$^{-/-}$ mice suffer from a multisystemic mitochondrial dysfunction.

Perturbed OXPHOS Function in Sirt7$^{-/-}$ Mice

As a next step, we analyzed gene and protein expression in different tissues. Although expression of several nDNA-encoded mitochondrial transcripts was reduced in the heart, liver, inner ear, bone-marrow-derived cells, and lung of *Sirt7*$^{-/-}$ mice, the expression of the CRP genes, such as *Rpl32*, *Rpl24*, and *Rps12*, was not altered (Figures 3A and S3A–S3C). Expression of the nDNA-encoded MRPL49, a component of the mitochondrial large ribosomal subunit, and ClpP, an ATP-dependent Clp

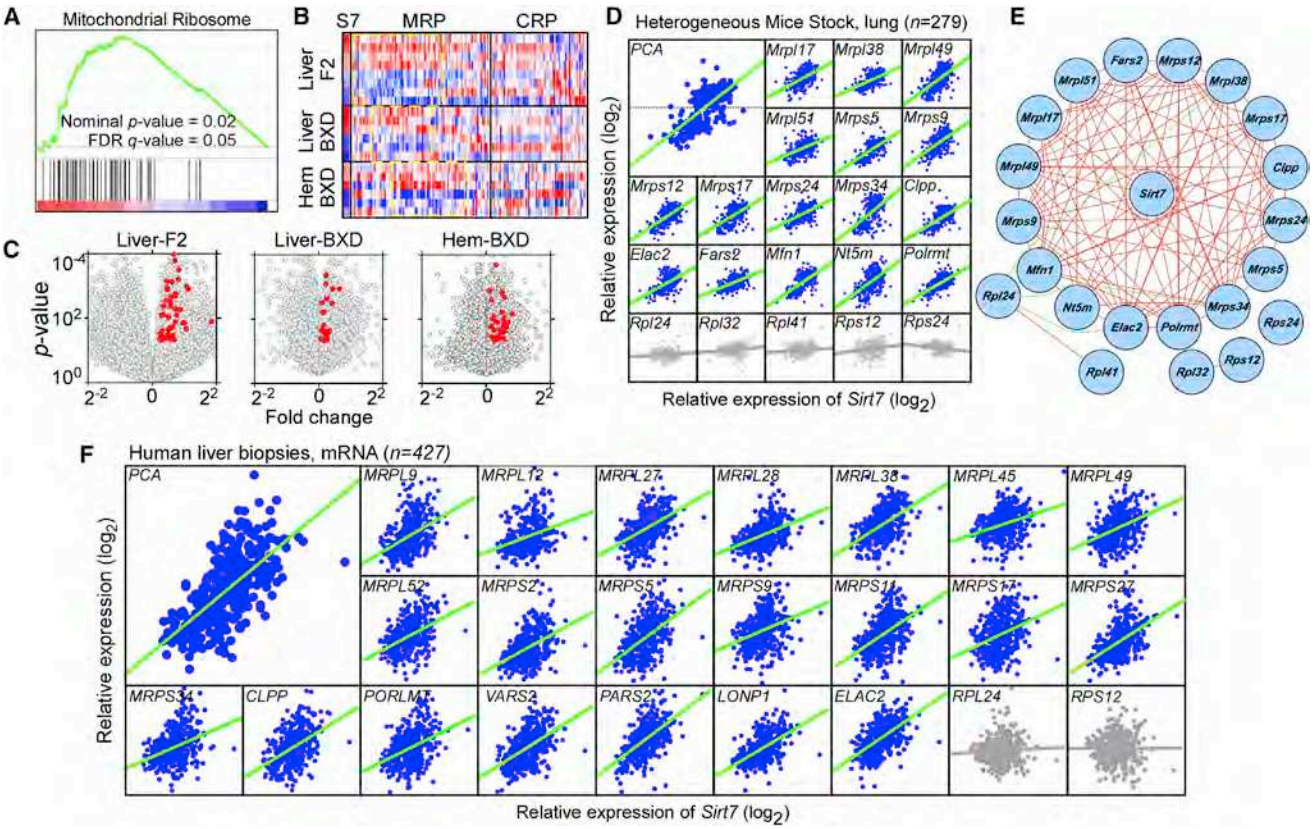

Figure 1. *Sirt7* Correlates with Nuclear-Encoded Mitochondrial Genes

(A) GSEA of the gene expression profiles in livers of B6xBTBR-F2-ob/ob (F2) mice. The gene set encompassing mitochondrial ribosomal proteins has an enrichment score = 0.55, nominal p = 0.02, false discovery rate (FDR) q = 0.05, and family-wise error rate p = 0.01.

(B) Corresponding heat maps displaying the expression values for *Sirt7* (S7) and the MRP and CRP genes in livers of BXD and F2 strains and in hematopoietic cells (Hem) of the BXD strains.

(C) Volcano plots of the p values (Student's t test) versus fold change in BXD and F2 livers and hematopoietic cells of the BXDs. MRP genes showing positive correlations with statistically significant p values are represented in red. See Table S1.

(D) Covariation between mRNA expression of *Sirt7* (x axis) and indicated mitochondrial genes (y axis) in lungs of heterogeneous mice stocks (n = 279). PCA combined all positively correlated mitochondrial genes. See Table S2.

(E) Interaction network between *Sirt7*, *MRPs*, *CRPs*, and genes involved in mitochondrial function from the lung mRNA data set in heterogeneous mice stocks. Positive ($r > 0.5$) and negative correlations ($r < -0.5$, Pearson's correlation coefficient) between the nodes are represented by red and green edges, respectively.

(F) Covariation between mRNA expression of *Sirt7* (x axis) and each indicated gene (y axis) in the human livers (n = 427). See also Table S3, including Pearson's r correlation coefficient with corresponding p values.

protease, as well as the mtDNA-encoded MT-CO1 protein was reduced in the heart and liver of *Sirt7*$^{-/-}$ mice (Figures 3B and 3C). Other OXPHOS subunits, such as ATP5A and UQCRC2, were only reduced in the heart and not in the liver (Figures 3B and 3C). To verify whether the changes in individual OXPHOS proteins impacted on the OXPHOS complexes, we performed blue native PAGE (BN-PAGE). SIRT7 deficiency differently affected OXPHOS composition in heart and liver. Complex IV was decreased in both tissues, whereas complex III was stable. Complexes I and II were slightly reduced in heart, whereas complexes II and V were slightly reduced in liver (Figures 3D and 3E). Moreover, complex I activity was clearly reduced during in-gel activity assays in both heart and liver (Figures 3D–3E, bottom). In line with the BN-PAGE results, respiration through complexes I, II, and IV was reduced in heart, liver, inner ear, and lung tissues, as determined by high-resolution respirometry (Figures 3F–3H and S3D).

Mitochondrial Dysfunction Is Induced in a Cell-Autonomous Fashion

Then, we tested whether the effect of SIRT7 on mitochondrial function was cell autonomous. After infection of *Sirt7*-floxed mouse embryonic fibroblasts (*Sirt7*$^{L2/L2}$ MEFs) with a Cre-recombinase (Ad-Cre), but not the control GFP-expressing (Ad-GFP) adenovirus, mRNA levels of various mitochondrial genes were reduced (Figure S4A). Moreover, nDNA-encoded MRPL49 as well as mtDNA-encoded MT-CO1 and MT-ND1 proteins were robustly reduced upon induction of *Sirt7* deficiency in primary mouse hepatocytes (Figure S4B). Although a recent report suggested that SIRT7 suppresses ER stress in the liver (Shin et al., 2013), the expression of the ER stress marker GRP78/BiP was not altered in *Sirt7*-deficient primary hepatocytes (Figure S4B), suggesting that a different mechanism underlies our phenotype. In addition, *Sirt7*-deficient hepatocytes also had a reduced oxygen consumption rate (OCR) in

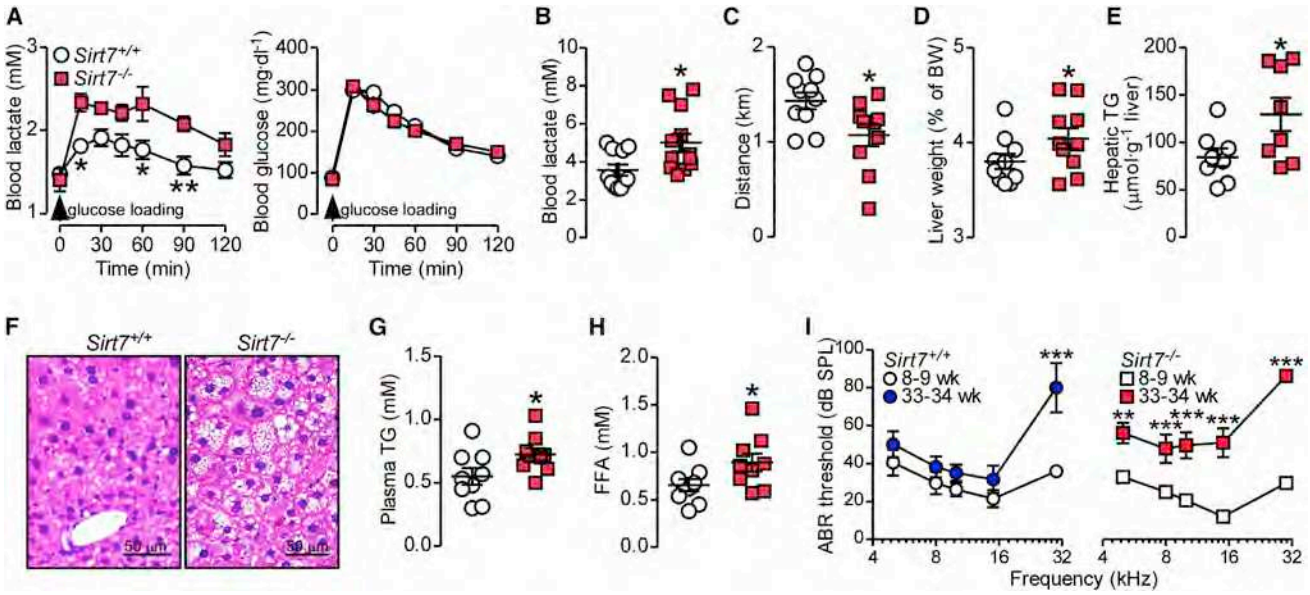

Figure 2. *Sirt7* KO Mice Show the Hallmarks of Mitochondrial Disease

(A) Blood lactate (left) and glucose (right) levels before and during OGTT in 30-week-old male $Sirt7^{+/+}$ (n = 11) and $Sirt7^{-/-}$ (n = 12) mice.

(B) Exercise-induced blood lactate levels after a 30 min treadmill run in 34-week-old male $Sirt7^{+/+}$ (n = 11) and $Sirt7^{-/-}$ (n = 12) mice.

(C) Maximum endurance was determined, and the running distance achieved by each mouse is represented ($Sirt7^{+/+}$, n = 10; $Sirt7^{-/-}$, n = 10, 34-week-old males).

(D) Liver weights of $Sirt7^{+/+}$ (n = 10) and $Sirt7^{-/-}$ (n = 10) mice of 42 weeks of age normalized to body weight.

(E) Triglyceride (TG) content in $Sirt7^{+/+}$ and $Sirt7^{-/-}$ livers (n = 8 per group, 42-week-old males).

(F) Hematoxylin and eosin staining of representative 42-week-old male livers of the indicated genotype.

(G and H) Plasma TG (G) and free fatty acid levels (H) in $Sirt7^{+/+}$ and $Sirt7^{-/-}$ mice (n = 8 per group, 42-week-old males).

(I) ABR auditory thresholds were monitored at 5, 8, 10, 15, and 30 kHz ($Sirt7^{+/+}$, n = 8; $Sirt7^{-/-}$, n = 10).

Graphs in (B–E) and (G and H) are mean ± SEM. *p < 0.05, **p < 0.01, ***p < 0.001.

low-glucose medium, whereas the glycolytic activity was unchanged as measured through the extracellular acidification rate (ECAR) (Figure S4C, left). In high glucose, ECAR was increased, whereas OCR was unaltered (Figure S4C, right). Cellular fatty acid uptake and ATP levels were reduced, whereas more superoxide was produced, in *Sirt7*-deficient primary hepatocytes (Figures S4D–S4F). Interestingly, no major alterations in the levels of key enzymes involved in lipogenesis and fatty acid oxidation (i.e., medium-chain acyl-CoA dehydrogenase and acetyl-CoA carboxylase; Figure S4G) and of transcripts of lipogenesis, fatty acid oxidation, lipid uptake, lipid storage, and triglyceride (TG) secretion genes were observed (Figure S4H).

In addition to primary hepatocytes, we also evaluated the cell-autonomous effect of SIRT7 on mitochondrial function in primary cardiomyocytes that were isolated from 1- to 2-day-old C57BL/6J WT pups and infected with either shCtrl- or shSirt7-RNA-expressing adenoviruses. As in *Sirt7*-deficient primary hepatocytes, the expression level of nDNA-encoded mitochondrial genes was clearly attenuated in *Sirt7*-deficient primary cardiomyocytes (Figure S4I). Furthermore, levels of both nDNA- (ClpP, UBQCR3, and SDHB) and mtDNA-encoded (MT-CO1) mitochondrial proteins were reduced (Figure S4J), which translated into reduced complexes II and IV activity upon respirometry performed with homogenized lysates of primary cardiomyocytes (Figure S4K).

A recent study used adeno-associated virus 8 (AAV8)-mediated silencing of SIRT7 to support the cell-autonomous nature of its effects in vivo (Shin et al., 2013). Given that tail vein-injection of AAV8 infects various tissues besides the liver, including heart, skeletal muscle, lung, and brain (Zincarelli et al., 2008), we have chosen to generate liver-specific *Sirt7* KO ($Sirt7^{hep-/-}$) mice in order to analyze its cell-autonomous effects. In full support of a cell-autonomous effect of SIRT7 on mitochondrial function, $Sirt7^{hep-/-}$ mice displayed similar clinical (e.g., normal body weight with microvesicular steatosis; Figures 4A–4E), molecular (e.g., reduction in *Mrpl49* mRNA and MRPL49 and MT-CO1 protein expression; Figures 4F and 4G), and mitochondrial (reduction in mitochondrial complexes on BN-PAGE and in OXPHOS complexes I, II, and IV activity; Figures 4H and 4I) phenotypic alterations. However, we did not detect alterations in the expression of a comprehensive gene set involved in hepatic lipid metabolism (Figure 4J).

SIRT7 Is a Dynamic Nuclear Protein

Although SIRT7 was initially identified as a nucleolar protein (Ford et al., 2006), recent data have also attributed a role for SIRT7 outside the nucleolus (Barber et al., 2012; Chen et al., 2013; Pfister et al., 2008). We detected SIRT7 in both nucleoli and extranucleoli fractions upon subnuclear fractionation (Figure 5A). Immunocytochemistry assays further supported the extranucleolar localization of SIRT7 (Figure 5B). To unequivocally establish whether SIRT7 is a dynamic factor, we performed fluorescence recovery after photobleaching (FRAP) assays. SIRT7 showed a very high "diffusional mobility," given that

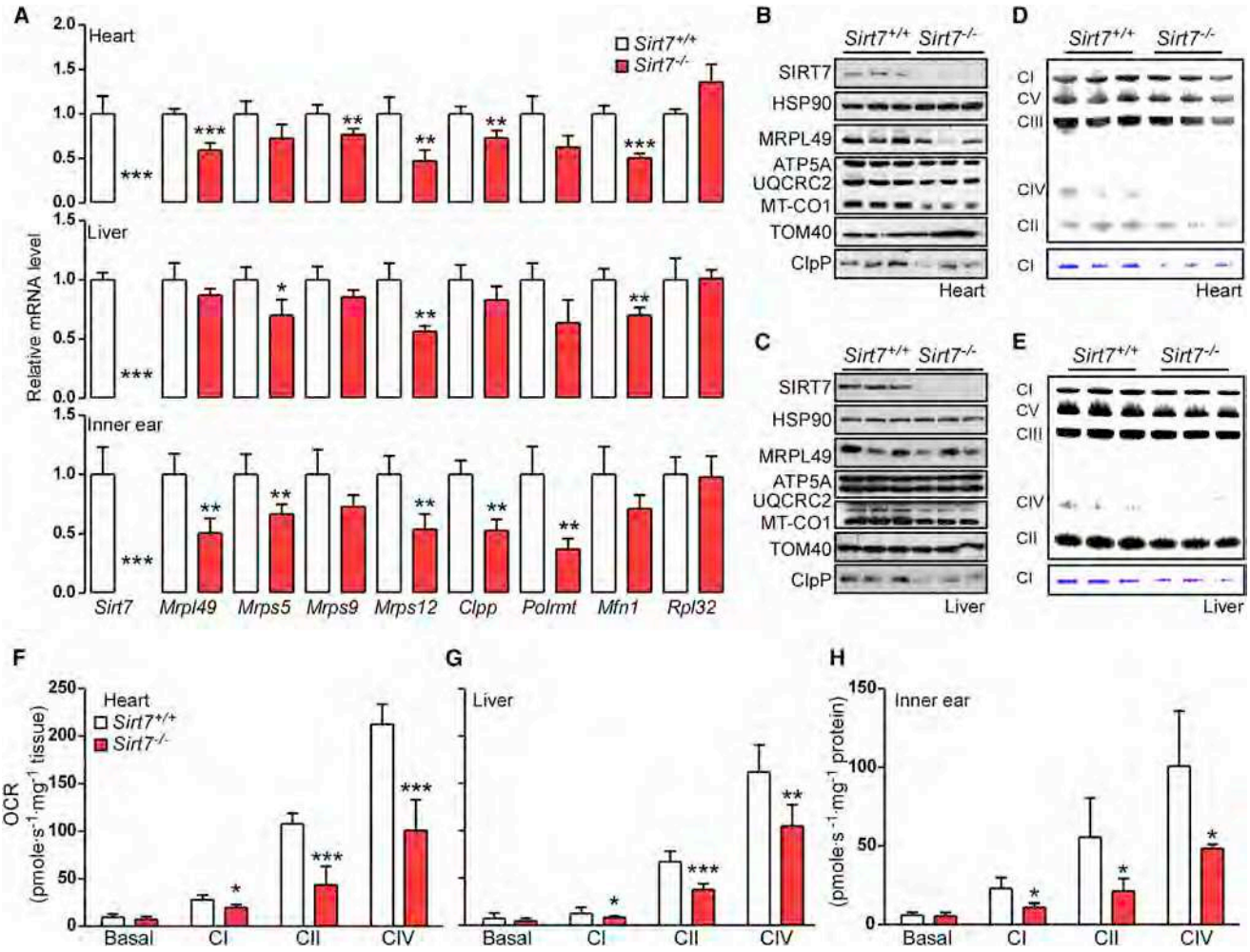

Figure 3. Lack of SIRT7 Triggers Mitochondrial Dysfunction

(A) mRNA levels of *Sirt7*, *Mrpl49*, *Mrps5*, *Mrps9*, *Mrps12*, *Clpp*, *Polrmt*, *Mfn1*, and *Rpl32* in heart, liver, and inner ear of 42-week-old $Sirt7^{+/+}$ (n = 4) and $Sirt7^{-/-}$ (n = 5) male mice.

(B and C) Western blot analysis showing SIRT7, MRPL49, ATP5A, UQCRC2, MT-CO1, TOM40, and ClpP levels in heart (B) and liver (C) of 42-week-old male $Sirt7^{+/+}$ and $Sirt7^{-/-}$ mice. HSP90 was used as a loading control.

(D and E) BN-PAGE of OXPHOS complexes (top) and complex I in-gel activity (bottom) in mitochondria isolated from heart (D) and liver (E) of 42-week-old male $Sirt7^{+/+}$ and $Sirt7^{-/-}$ mice.

(F–H) Oxygen consumption rates (OCR) of heart (F; n = 5), liver (G; n = 5), and inner ear (H; n = 4 per genotype) tissues of 42-week-old $Sirt7^{+/+}$ and $Sirt7^{-/-}$ male mice were monitored with specific substrates for each OXPHOS complex.

Data in (A) and (F–H) are mean ± SEM. *p < 0.05, **p < 0.01, ***p < 0.001.

approximately 50% of the initial fluorescence intensity was recovered in 2 s after photobleaching SIRT7-GFP in both nucleoplasm and nucleoli (Figures 5C and S5A). These cellular studies demonstrate that SIRT7 is a dynamic nuclear protein that is not restricted to nucleoli.

Bioinformatic Analysis Links SIRT7 Tightly to GABPβ1

On the basis of the striking correlations between the expression of *Sirt7* and mitochondrial genes, the mitochondrial dysfunction in $Sirt7^{-/-}$ mice, and the fact that SIRT7 is a dynamic nuclear factor, we hypothesized that SIRT7 might affect the expression of nDNA-encoded mitochondrial genes by impacting on transcription factors such as NRF1, GABPα, GABPβ1, GABPβ2, ERRα, and ERRγ (Scarpulla, 2008). Interestingly, the expression of *Sirt7* positively correlated with that of *Gabpa*, *Gabpb1*, *Gabpb2*, and *Esrrg*, but not *Nrf1* and *Esrra* (Figures 5D and S5B and Table S4). Pearson's and Spearman's correlation coefficients indicated that *Sirt7*, *Gabpa*, *Gabpb1*, *Gabpb2*, and *Esrrg* belong to the same gene cluster (Figure 5E and Table S4), and principal component analysis (PCA) confirmed the strong positive correlation between *Sirt7* and the components of the *GABP* complex (GABPα, GABPβ1, and GABPβ2; Figure 5F). Finally, in a factor-loading plot based on Pearson's correlation coefficients, *Gabpb1* was the strongest *Sirt7* correlate (Figure 5G). In addition to our bioinformatics analysis, we also reanalyzed data from three independent studies (Barber et al., 2012; Hollenhorst et al., 2009; Mercer et al., 2011). A recent genome-wide chromatin immunoprecipitation sequencing (ChIP-seq) study

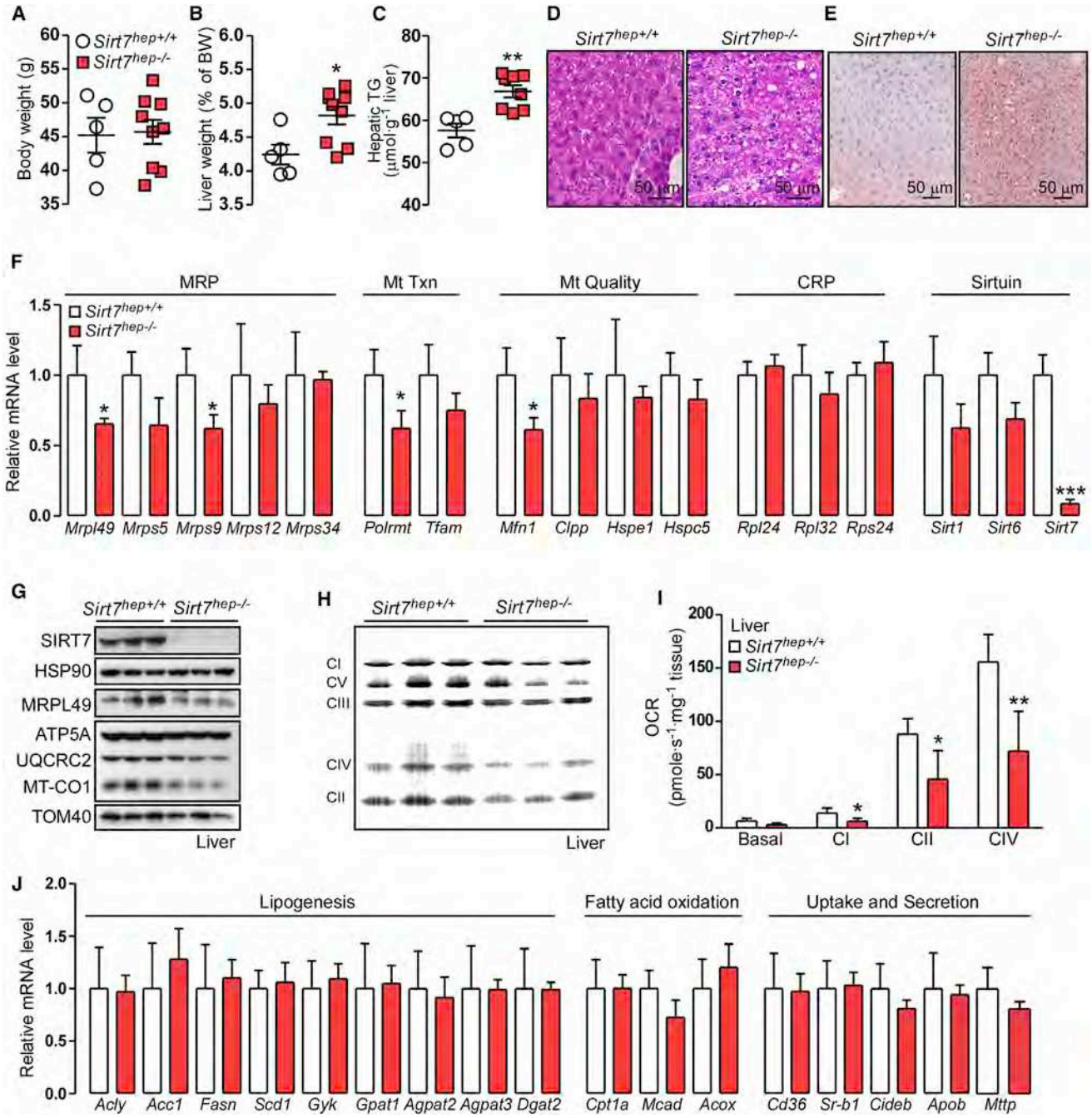

Figure 4. *Sirt7*$^{hep-/-}$ Mice Have Hepatic Mitochondrial Dysfunction

(A–C) Body weight (A), normalized liver weights (B), and hepatic TG content (C) of 55-week-old chow-fed male *Sirt7*$^{hep+/+}$ (n = 5) and *Sirt7*$^{hep-/-}$ (n = 7) mice.

(D and E) Hematoxylin and eosin (D) and Oil Red O staining (E) of representative 55-week-old male livers of the indicated genotype.

(F) Hepatic mRNA levels of *MRP*, *Polrmt*, *Tfam*, *Mfn1*, *Clpp*, *Hspe1*, *Hspc5*, *CRP*, and *Sirtuin* genes were evaluated by quantitative RT-PCR (qRT-PCR; *Sirt7*$^{hep+/+}$ n = 4 and *Sirt7*$^{hep-/-}$; n = 8, 55-week-old male mice; MRP, mitochondrial ribosomal proteins; Mt Txn, mitochondrial transcription related; Mt Quality, mitochondria quality control related; and CRP, cytosolic ribosomal proteins). Abbreviations are the same as in Figures 3A and S3A.

(G) Western blot analysis showing SIRT7, MRPL49, various OXPHOS subunits, and TOM40 in liver of *Sirt7*$^{hep+/+}$ and *Sirt7*$^{hep-/-}$. HSP90 was used as a loading control.

(H) BN-PAGE of hepatic OXPHOS complexes of the mice in (G).

(I) OCR of liver lysates from 42-week-old male *Sirt7*$^{hep+/+}$ and *Sirt7*$^{hep-/-}$ mice (n = 5 per group).

(J) Expression levels of hepatic genes involved in fatty acid and TG synthesis, fatty acid uptake, fatty acid oxidation, and TG secretion as evaluated by qRT-PCR (*Sirt7*$^{hep+/+}$ n = 4 and *Sirt7*$^{hep-/-}$ n = 8, 55-week-old male mice).

Graphs in (A–C), (F), and (I–J) are mean ± SEM. *p < 0.05, **p < 0.01, ***p < 0.001.

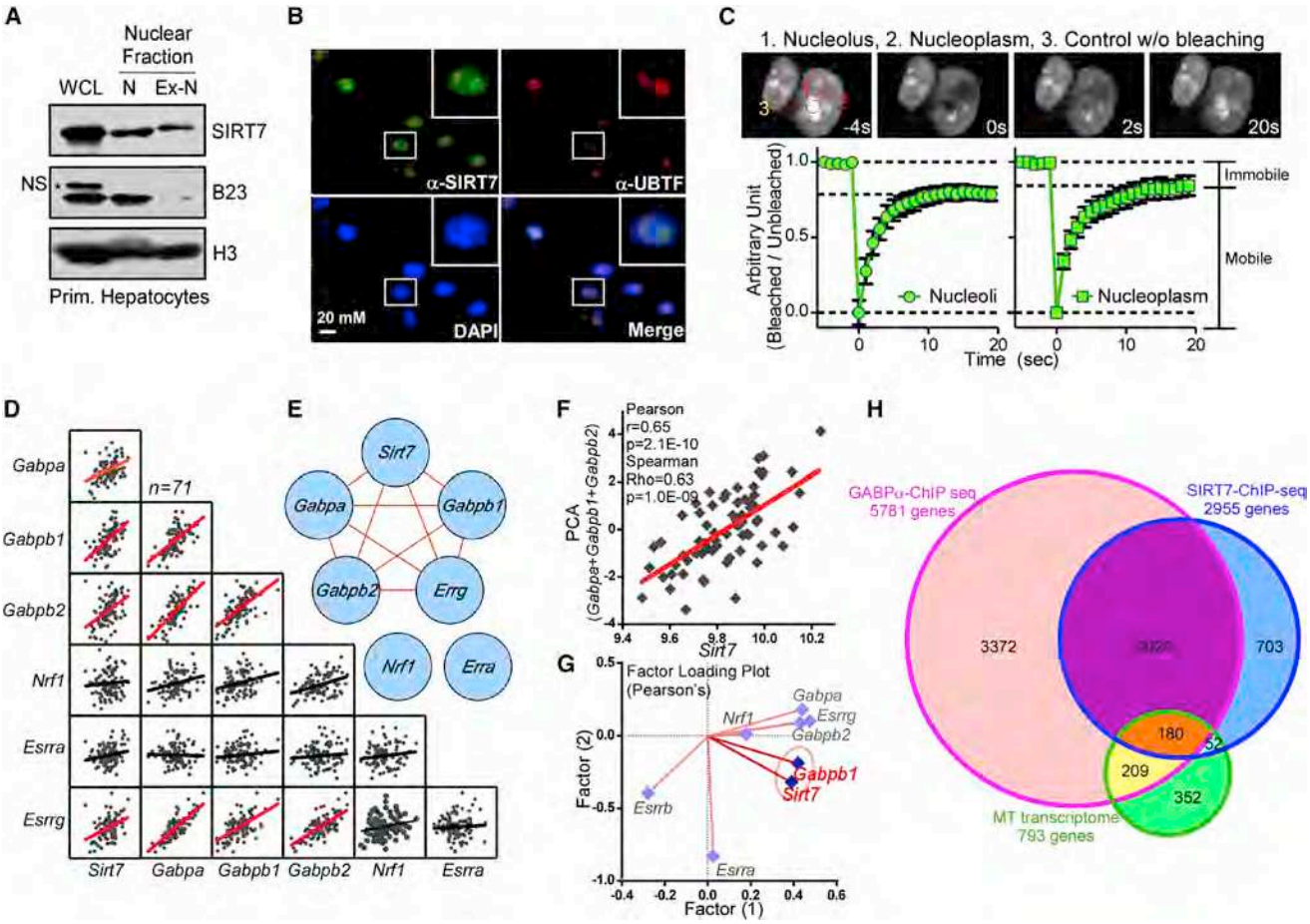

Figure 5. SIRT7 Is a Dynamic Nuclear Protein Regulating Mitochondrial Target Genes

(A) Western blot assays demonstrating the subnuclear localization of SIRT7. Whole-cell lysate (WCL), nucleoli (N), and extranucleoli (Ex-N) fractions were prepared from primary hepatocytes isolated from WT C57Bl/6J mice. B23 (also known as nucleophosmin) was used as a control for nucleoli, and histone H3 was used as a loading control (NS; a nonspecific band).

(B) Confocal microscopy of HeLa cells showing endogenous SIRT7 in the nucleus. UBTF was used as a positive control of nucleoli, and the nucleus was stained with DAPI.

(C) FRAP assay of SIRT7-GFP demonstrates the highly dynamic nature of SIRT7 in HEK293T cells. Time-series confocal images of SIRT7-GFP (left) and the fluorescence quantification of bleached areas (nucleolus, n = 9, and nucleoplasm, n = 6). Unbleached control areas were used for normalization of fluorescence intensity (right). Data shown as mean ± SEM.

(D and E) In order to evaluate a possible link between *Sirt7* expression and key transcription factors that control mitochondrial activity, a correlation analysis with gene expression data from the hippocampus, which contains all these nuclear factors (Figure S5B and Table S4) was performed. Correlation matrix (D) and interaction network (E) showing correlations between *Sirt7* and transcription factors involved in the expression of mitochondrial gene expression. Positive and statistically significant Pearson's correlation coefficients are represented by red edges (r = 0.5–1.0).

(F) PCA showing a significant positive correlation between the expression of *Sirt7* and all three genes in the GABP complex.

(G) Factor-loading plot based on Pearson's correlation coefficients highlighting that *Gabpb1* is most related to *Sirt7*.

(H) Area-proportional Venn diagram representing common genes between SIRT7-ChIP-seq (Barber et al., 2012), GABPα-ChIP-seq (Hollenhorst et al., 2009), and the human mitochondrial transcriptome data (Mercer et al., 2011).

See Table S5.

demonstrated that SIRT7 occupies the promoters of 232 mitochondrial genes (Figure 5H and Table S5), including the MRP promoters (Barber et al., 2012). Another study demonstrated that GABPα occupies the promoters of 389 mitochondrial genes (Hollenhorst et al., 2009). Interestingly, 75% of SIRT7-occupied genes were also identified in the GABPα-ChIP-seq. Moreover, 56% of the genes that are part of the human mitochondrial transcriptome (Mercer et al., 2011) are covered in these independent studies (Figure 5H and Table S5). In combination, these data suggest the existence of a link between SIRT7-GABP and the control of mitochondrial gene expression.

SIRT7 Impacts on Mitochondrial Function via the Deacetylation of GABPβ1

To analyze whether there is a functional link between SIRT7 and GABPβ1, we compared the acetylation of immunoprecipitated GABPβ1-Myc protein in human embryonic kidney 293T (HEK293T) cells overexpressing the nuclear sirtuins. Notably,

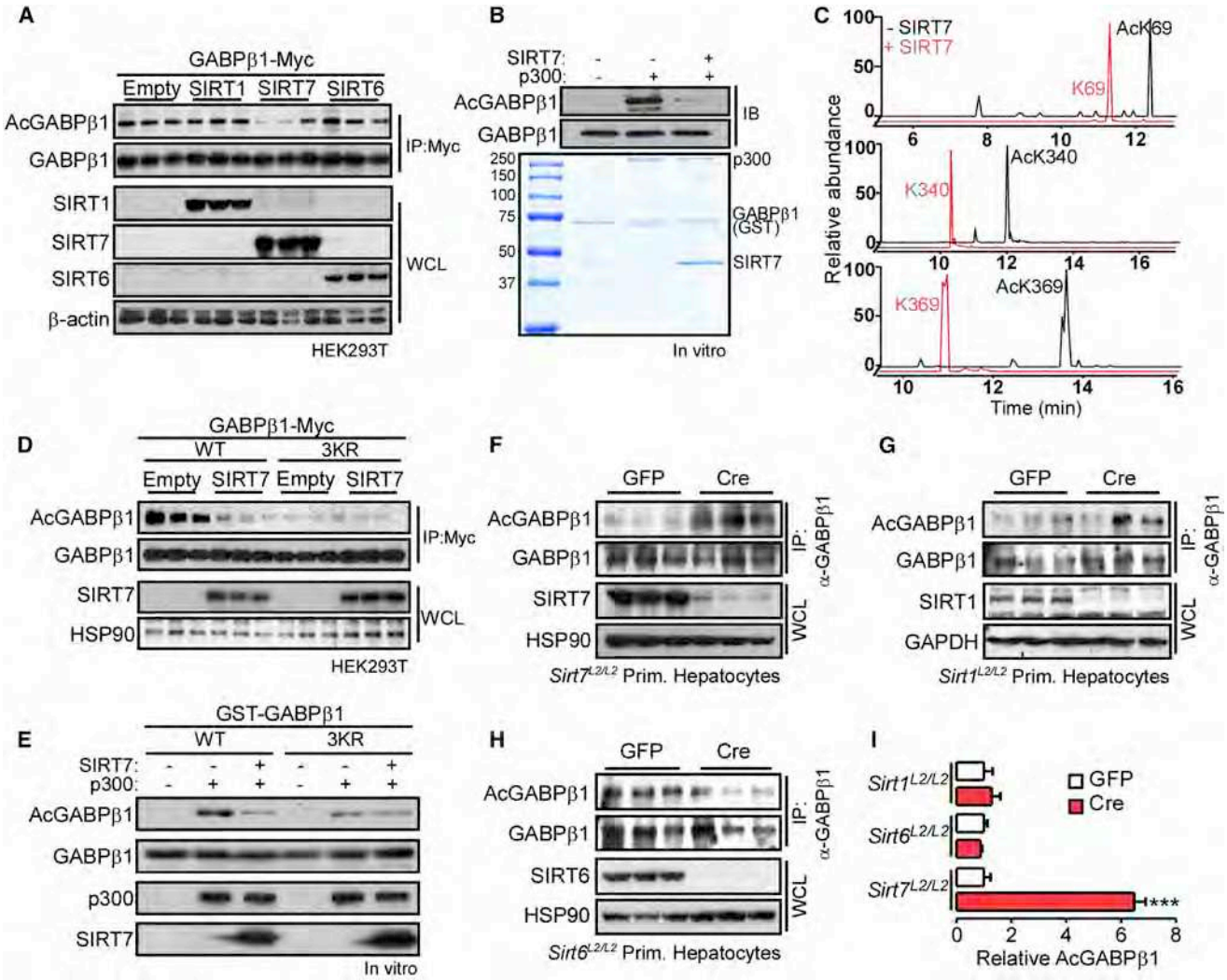

Figure 6. SIRT7 Is a Deacetylase of GABPβ1

(A) Western blot assay displaying reduced GABPβ1 acetylation in SIRT7-, but not SIRT1- or SIRT6-, overexpressing HEK293T cells.

(B) In vitro deacetylation assay demonstrating that p300 acetylates and SIRT7 deacetylates GABPβ1.

(C) Nano-LC-MS/MS analysis showing SIRT7-dependent in vitro deacetylation of AcK69, AcK340, and AcK396 of GABPβ1.

(D) Western blot assay demonstrating that, in contrast to the WT GABPβ1 protein, the GABPβ1-3KR mutant is not deacetylated in HEK293T cells overexpressing SIRT7.

(E) Reduced p300-mediated acetylation and abolished SIRT7-dependent deacetylation of the GABPβ1 3KR mutant relative to the WT GABPβ1 protein during in vitro acetylation/deacetylation studies.

(F–I) Western blot showing acetylated GABPβ1, total GABPβ1, SIRT7, and HSP90 (or GAPDH) expression in *Sirt7*$^{L2/L2}$ (F), *Sirt1*$^{L2/L2}$ (G), and *Sirt6*$^{L2/L2}$ (H) primary hepatocytes infected with either an Ad-GFP or Ad-Cre adenovirus. Bar graphs (I) show the quantification of the relative acetylation level of GABPβ1 in these *Sirt1*, *Sirt6*, and *Sirt7*$^{L2/L2}$ primary hepatocytes. Data are shown as mean ± SEM. *p < 0.05, **p < 0.01, ***p < 0.001.

the level of acetylated GABPβ1 was specifically reduced upon overexpression of SIRT7 but not SIRT1 or SIRT6 (Figure 6A). In addition, we observed a clear interaction between ectopically expressed SIRT7-GFP and GABPβ1-Myc in HEK293T cells, suggesting that SIRT7 could act as a GABPβ1 deacetylase (Figure S6A). To validate whether SIRT7 directly deacetylates GABPβ1, we performed an in vitro acetylation and deacetylation assay. Although p300 robustly acetylated GABPβ1, GCN5 and P/CAF displayed moderate or undetectable acetylation activity (data not shown). Notably, the strong p300-induced acetylation of GABPβ1 was reverted by SIRT7 (Figure 6B). Mass spectrometric analysis identified three acetylated lysines (K69, K340, and K369) in GABPβ1 displaying SIRT7-dependent deacetylation (Figures 6C and S6B–S6C). We generated a nonacetylatable GABPβ1 mutant in which these three lysine residues were replaced by arginines (GABPβ1-3KR). Upon transfection of HEK293T cells, the mutant GABPβ1-Myc-3KR displayed low acetylation levels in comparison to the GABPβ1-Myc-WT protein, and SIRT7 was unable to further reduce acetylation (Figure 6D). The same effect was observed in vitro, where GST-GABPβ1-3KR was poorly acetylated by p300, and SIRT7 had no deacetylase activity (Figure 6E). In addition, acetylated

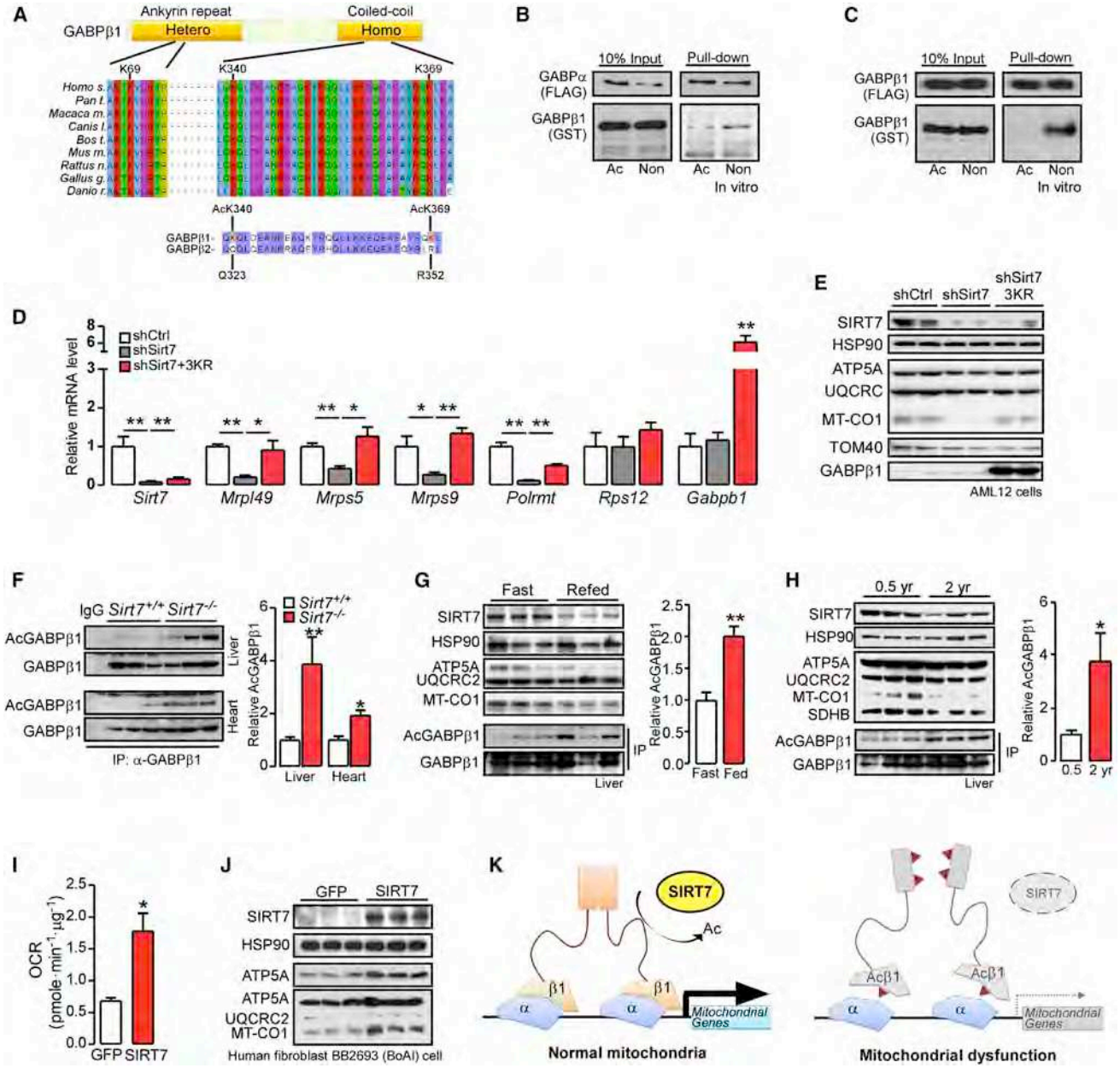

Figure 7. Deacetylation of GABPβ1 Promotes GABP Complex Formation and Governs Mitochondrial Activity In Vivo

(A) Sequence alignment showing three conserved lysine residues (K69, K340, and K369) in GABPβ1 of *Homo sapiens*, *Pan troglodytes*, *Macaca mulatta*, *Canis lupus*, *Bos taurus*, *Mus musculus*, *Rattus norvegicus*, *Gallus gallus*, and *Danio rerio* (top). Sequence alignment of the homodimerization domain of mouse GABPβ1 and GABPβ2. The residues K340 and K369 are unique to GABPβ1 (bottom).

(B and C) GST pulldown assays for comparing the heterodimerization between GABPα-FLAG with GST-GABPβ1 or acetylated GST-GABPβ1 (B) and the homodimerization between GABPβ1-FLAG with GST-GABPβ1 or acetylated GST-GABPβ1 (C). Acetylation of GABPβ1 reduces the hetero- as well as homodimerization in vitro. (Non; nonacetylated GABPβ1; Ac, acetylated GABPβ1).

(D) mRNA levels of *Sirt7*, *Mrpl49*, *Mrps5*, *Mrps9*, *Polrmt*, and *Rps12* in transiently transfected AML12 mouse hepatocytes expressing either a control shRNA (shCtrl), an shRNA targeting SIRT7 (shSirt7), or the shSirt7 in combination with a GABPβ1 3KR (3KR) expression vector.

(E) Western blot assay showing SIRT7, HSP90, ATP5A UQCRC2, MT-CO1, TOM40, and GABPβ1 proteins in AML12 cells in identical conditions as mentioned in (D).

(F) Western blot showing endogenous acetylated GABPβ1 levels in liver and heart of 42-week-old male $Sirt7^{+/+}$ and $Sirt7^{-/-}$ mice.

(G) Western blot assay showing reduced levels of SIRT7, ATP5A, and MT-CO1 proteins and increased acetylation levels of GABPβ1 in livers of 6 hr refed (Refed) versus 24 hr fasted (fast) 17-week-old male C57BL6/J mice.

(H) Western blot assay demonstrating reduced levels of SIRT7 and selected OXPHOS proteins and increased levels of GABPβ1 acetylation in livers of 2-year-old compared to 0.5-year-old male C57BL6/J mice.

(legend continued on next page)

GABPβ1 levels were specifically increased in *Sirt7*-, but not *Sirt1*- or *Sirt6*-, deficient primary hepatocytes (Figures 6F–6I). These studies indicate that SIRT7 deacetylates GABPβ1 on three specific lysine residues.

Deacetylation of GABPβ1 Promotes GABP Complex Formation and Activation

Previous reports showed that K69 of GABPβ1 is a critical residue facilitating the heterodimerization with GABPα and docking on DNA (Thompson et al., 1991), whereas the lysines K340 and K369 in the C-terminal domain (CTD) mediate GABPβ1 homodimerization (de la Brousse et al., 1994; Gugneja et al., 1995). These lysines are conserved in all vertebrate orthologs of GABPβ1 (Figure 7A, top), whereas the two lysines in the CTD are not conserved in GABPβ2, which also interacts with GABPα (Figure 7A, bottom). Notably, we found that heterodimerization between GABPα and β1 (Figure 7B) and homodimerization of GABPβ1 (Figure 7C) were reduced upon acetylation of these lysines. Then, we used a GABP-responsive luciferase reporter to test the effect of SIRT7-dependent deacetylation of GABPβ1 on its transcriptional activity. Therefore, murine AML12 hepatocyte cells were cotransfected with this GABP reporter and relevant combinations of SIRT7, WT GABPβ1, the nonacetylatable GABPβ1-3KR, or the acetylation-mimicking GABPβ1-3KQ. Notably, the nonacetylatable GABPβ1-3KR mutant induced GABP reporter activity to an equal extent as the coexpression of SIRT7 and GABPβ1, whereas the acetylation-mimicking GABPβ1-3KQ mutant failed to activate the reporter even in the presence of SIRT7 (Figure S7A). In addition, the effect of overexpressing the GABPβ1-3KR mutant was evaluated in AML12 cells in which SIRT7 was silenced (Figures 7D and 7E). Consistent with the results obtained in SIRT7-deficient tissues and cells, transcripts and protein levels of key mitochondrial genes, were reduced by the SIRT7 knockdown. The ectopic expression of GABPβ1-3KR in these SIRT7 silenced AML12 cells partially rescued the expression of several mitochondrial transcripts, including those encoding for MRP, Polrmt (Figure 7D), and the MT-CO1 protein (Figure 7E). These findings underscore the functional importance of the SIRT7-dependent GABPβ1 deacetylation.

Complementary to these in vitro interaction and cell-based studies, we next tested whether the acetylation levels of GABPβ1 also differ in vivo. As expected, endogenous acetylation levels of GABPβ1 (Ac-GABPβ1) were increased in hearts and livers of germline *Sirt7*$^{-/-}$ mice (Figure 7F) as well as those of *Sirt7*$^{hep-/-}$ mice in vivo (Figure S7B).

SIRT7/GABPβ1 Signaling and the Control of Mitochondrial Activity

Finally, we analyzed whether the SIRT7/GABPβ1 axis could control mitochondrial activity under physiological challenges. Food restriction is known to induce the expression of OXPHOS genes in the liver (Báez-Ruiz et al., 2005). Interestingly, SIRT7 expression was increased, whereas GABPβ1 acetylation was reduced in livers of fasted mice (Figure 7G). This was accompanied with induced MT-CO1 and ATPA5A levels. Reduced OXPHOS is associated with age-related decline in organ function (Yen et al., 1989). Previously, we also reported that OXPHOS is reduced in livers of old mice (Houtkooper et al., 2011). Expression of SIRT7 and some OXPHOS subunits, including MT-CO1, was robustly reduced, whereas Ac-GABPβ1 levels were induced in livers of 2-year- versus 6-month-old mice (Figure 7H). Moreover, adenoviral-mediated SIRT7 overexpression improved OCR and expression of mitochondrial proteins in human fibroblasts harboring a mutated NDUFSI (Figures 7I and 7J), testifying that SIRT7 can also improve human mitochondrial function. Altogether, our data suggest that the SIRT7/GABPβ1 signaling is linked to mitochondrial function in different genetic and physiological contexts.

DISCUSSION

Our work proposes that SIRT7 is a dynamic nuclear regulator of mitochondrial homeostasis acting on GABPβ1, a master regulator of mitochondrial biogenesis and function. A series of experimental observations led us to this conclusion. First, the expression of *Sirt7* is tightly correlated with the expression of many genes involved in the control of mitochondrial homeostasis. Second, from all the transcription factors known to regulate mitochondrial biogenesis and function, including PPARs, ERRs, NRF-1, and GABPs, SIRT7 expression tightly correlates only with that of GABPs. Third, two independent genome-wide ChIP-seq analyses suggest that SIRT7 and the GABP complex co-occupy multiple promoters of nDNA-encoded mitochondrial genes. Fourth, SIRT7 deacetylates GABPβ1 in critical residues including K69, which induces dimerization with GABPα (Batchelor et al., 1998), and K340 and K369, which stabilize GABPβ homodimerization (de la Brousse et al., 1994; Thompson et al., 1991). Fifth, deletion of Sirt7 in the mouse induces multiple defects in a wide range of tissues as a consequence of generalized mitochondrial dysfunction. Finally, SIRT7/GABPβ1 signaling is involved in mitochondrial adaptation to physiological challenges, such as fasting, feeding, and aging. In combination, these independent lines of evidence indicate a major role of SIRT7 in the nuclear control of mitochondrial homeostasis.

As stated above, the phenotype of *Sirt7*$^{-/-}$ mice, characterized by lactate accumulation, reduced exercise performance, cardiac dysfunction and hypertrophy, hepatic microvesicular steatosis, and hearing defects, resembles the clinical abnormalities observed in patients with mitochondrial disorders (Chinnery et al., 1999; Fosslien, 2003; Leone and Kelly, 2011; Nunnari and Suomalainen, 2012; Wallace, 1999; Yamasoba et al., 2007). The

(I) Oxygen consumption rates (OCR) were measured in human fibroblasts harboring a mutant NDUFS1 (BB2693: BoAI cells) infected with either a control Ad-GFP or Ad-SIRT7 adenovirus and grown in high glucose medium.
(J) Western blot assay showing increased OXPHOS in human fibroblasts harboring mutant NDUFS1, transduced with either Ad-SIRT7 adenovirus. Ad-GFP was used as a control.
(K) A schematic model summarizing how SIRT7 controls mitochondrial homeostasis via the deacetylation of GABPβ1 and the regulation of GABP complex formation (based on a model shown in Thompson et al., 1991).
Graphs in (D) and (F–I) show mean ± SEM. *$p < 0.05$, **$p < 0.01$, ***$p < 0.001$.

cardiac dysfunction phenotype was already reported in another study using an independently generated *Sirt7*$^{-/-}$ mouse line showing an increased rate of apoptosis in the myocardium (Vakhrusheva et al., 2008). However, our data indicate that, aside from regulating apoptosis, a pathway intimately linked to the mitochondria, SIRT7 has a broader role in mitochondrial homeostasis in the heart, through its impact on GABP activity. Hence, it is plausible that altered cardiac mitochondrial homeostasis contributes to the development of cardiac hypertrophy and dysfunction in the *Sirt7*$^{-/-}$ mice (Fosslien, 2003; Leone and Kelly, 2011; Wallace, 1999). The exercise intolerance in *Sirt7*$^{-/-}$ mice was most likely a consequence of cardiac problems, given that *Sirt7* is not or only marginally expressed in skeletal muscle.

Liver steatosis subsequent to reduced fatty acid oxidation and, in particular, microvesicular steatosis, as observed in our *Sirt7*$^{-/-}$ mice, is likewise a known feature of mitochondrial dysfunction (Fromenty et al., 1997). Two very recent studies (Shin et al., 2013; Yoshizawa et al., 2014) reported opposite hepatic phenotypes in *Sirt7*-deficient mice. Shin et al. (2013) observed a fatty liver, whereas Yoshizawa et al. (2014) report protection of their *Sirt7*-deficient mice against high-fat diet (HFD)-induced hepatic lipid accumulation. Although the *Sirt7*-deficient mouse lines and the proposed mechanisms in all three studies are different, our results showing that aged *Sirt7*-deficient mice fed a normal chow (NC) accumulate hepatic triglycerides (Figures 2E and 2F) are more consistent with the data of Shin et al. (2013). The fact that Yoshizawa et al. (2014) measured far fewer lipids in the livers of *Sirt7*-deficient mice under an HFD in comparison to WT or *Sirt7*-deficient mice under NC as well as the absence of acetylation changes in the proposed SIRT7 effector molecules makes their observations puzzling and devoid of conclusive mechanistic support. Altogether, all these phenotypic abnormalities in the *Sirt7*$^{-/-}$ mouse line reflect a severe multisystem mitochondrial dysfunction, supporting our hypothesis that SIRT7 is intimately linked to mitochondrial homeostasis.

From a more mechanistic point of view, the aforementioned correlation between SIRT7 and nDNA-encoded mitochondrial transcripts implies a more dynamic behavior of nuclear SIRT7, which seems not to be restricted to the nucleoli as previously reported (Ford et al., 2006; Grob et al., 2009). A purely nucleolar localization would dismiss a possible involvement of SIRT7 in the control of mRNA transcription and limit its function to the control of nucleoli-derived transcripts such as noncoding rRNAs and tRNAs. Using subnuclear fractionation, immunocytochemistry, and FRAP assays (Figures 5A–5C and S5), we confirmed that SIRT7 can shuttle between different nuclear compartments (Chen et al., 2013; Pfister et al., 2008). This dynamic nature of SIRT7 in the nucleus mechanistically underpins also how SIRT7 impacts on transcription factors involved in the control of nDNA-encoded mitochondrial genes. Nevertheless, future studies will be necessary to define whether the subnuclear localization of SIRT7 is a regulated process.

Although the transcription of nDNA-encoded mitochondrial genes involves several transcription factors, we established a specific link between SIRT7 and the activity of GABPα/GABPβ heterotetramer. GABPα continuously occupies its response elements on nuclear-encoded mitochondrial target genes but only induces their transcription when it forms the GABPα/GABPβ heterotetramer (de la Brousse et al., 1994; Scarpulla, 2008; Thompson et al., 1991; Virbasius et al., 1993). We demonstrated that SIRT7 deacetylates three critical residues of GABPβ1, K69, K340, and K369, which are involved in the stabilization of the GABPα/GABPβ complex (de la Brousse et al., 1994; Gugneja et al., 1995; Thompson et al., 1991). In particular, the hydrogen bond between Q321 of GABPα and K69 of GABPβ1 is vital for the stabilization of the GABPα-DNA complex (Batchelor et al., 1998), whereas K340 and K369, located in CTD of GABPβ1, stabilize GABPβ1 homodimerization (de la Brousse et al., 1994; Thompson et al., 1991). Interestingly, these two lysine residues (K340 and K369) are conserved in GABPβ1 but not GABPβ2 (Figure 7A). The acetylation of these two lysine residues could hence indicate a distinct role of GABPβ1 from GABPβ2. To our knowledge, this is the first study to unequivocally demonstrate the importance of acetylation on these lysine residues, which reduces GABPβ1 homodimerization. Furthermore, our work suggests a unique role of SIRT7 in the dynamic control of this acetylation switch, which stabilizes DNA binding and activation of the GABPα/GABPβ heterotetramer. This switch also allows the fine-tuning and synchronization of GABP activity with cellular energy levels, given that the activity of SIRT7, like that of all sirtuins, is strictly NAD^+-dependent (Haigis and Sinclair, 2010; Houtkooper et al., 2010; Imai et al., 2000). Through the control of the activity of the GABPα/GABPβ heterotetramer, which is vital for the expression of many mitochondrial gene sets, SIRT7 acquires a dominant position in the hierarchy of mitochondrial homeostasis.

This premise is not only corroborated by the phenotypic abnormalities seen in the *Sirt7*$^{-/-}$ mouse (see above) but also by a number of bioinformatic and physiological studies. The very tight correlation between the expression of *Sirt7* and that of many mitochondrial genes in several human and mouse tissues suggested a strong link between SIRT7 and mitochondrial activity (Figure 1). Many of the promoters of these mitochondrial proteins, including the MRP gene set, *Polrmt*, *Tfam*, and *Mfn1*, were further occupied by SIRT7 in an independent genome-wide ChIP-seq analysis in a human cell line (Barber et al., 2012). Notably, GABPα was shown to be permanently located on the promoter of many of the same genes that were occupied by SIRT7 (Hollenhorst et al., 2009). These two independent ChIP-seq analyses hence show that 75% of SIRT7-occupied genes are also bound by GABPα. In addition, more than half of the genes reported as being part of the mitochondrial transcriptome (Mercer et al., 2011) are covered in these two independent analyses (Figure 5H and Table S5), illustrating the wide ranging impact of the SIRT7/GABP tandem on the transcription of nDNA-encoded mitochondrial proteins. Finally, the reactivity of the SIRT7/GABP axis to physiological changes, such as fasting/feeding and aging, provides yet another compelling argument for their connectivity to mitochondrial function. It is also of note that the effect of the SIRT7/GABP signaling axis on mitochondrial function is amplified by their impact on the transcription of mitochondrial ribosomal proteins.

In summary, our work identifies a critical role for SIRT7/GABPβ1 signaling in the control of mitochondrial function. Mechanistically, SIRT7 controls mitochondrial homeostasis by the deacetylation of GABPβ1, which in turn triggers the formation of the active GABPα/GABPβ complex and enhance the expression of

mitochondrial genes (Figure 7K). Consequently, *Sirt7* deficiency in mice leads to multisystemic mitochondrial dysfunction. Furthermore, dynamic changes in SIRT7/GABPβ1 signaling might contribute to mitochondrial adaptation to physiological challenges, such as fasting recovery and aging. In combination, these genetic and physiological data underscore the importance of SIRT7/GABPβ1 signaling in mitochondrial homeostasis. A notable example was provided by the recovery of respiration rates and mitochondrial protein expression in fibroblasts of a patient with a mutation in NDUFSI. Activation of the SIRT7/GABPβ1 regulatory axis may offer an interesting approach for preventing and/or treating mitochondrial dysfunction in patients with inherited or acquired mitochondrial diseases.

EXPERIMENTAL PROCEDURES

All procedures are described in detail in the Supplemental Information.

Bioinformatic Analyses

Bioinformatic analyses with GSEA (http://www.broadinstitute.org/gsea) and GeneNetwork (http://www.genenetwork.org/) were performed as described in previous studies (Andreux et al., 2012; Lagouge et al., 2006). All transcriptome data sets were downloaded from GeneNetwork. Hepatic transcriptome data came from B6xBTBR-F2-ob/ob (B6XBTBR-F2 liver mRNA M430 RMA), BXD inbred mice (BXD GN373 GSE16780 UCLA Hybrid MDP-liver-Sep11 RMA), and a human population (the Human Liver Cohort). Hematopoietic cell transcriptome data came from BXD inbred mice (UMCG Stem Cells ILM6v1.1 original database). Lung transcriptome data came from heterogeneous stock mice (OX UK HS ILM6v1.1 lung RankInv). Hippocampus transcriptome data came from the BXD inbred mice (Hippocampus Consortium M430v2 PDNN).

In brief, GSEA was applied in these data sets as an unbiased bioinformatic analysis in order to define gene sets showing statistical correlation with *Sirt7* expression in both human and murine transcriptome data sets (Figures 1A–1C). Volcano plots were prepared on the basis of fold change and Student's t test. Correlation analyses were based on both Pearson product-moment correlation coefficient and Spearman's rank correlation coefficient with the GeneNetwork website (Figures 1D–1F and 5D–5H). The correlation analysis between Sirt7 and specific transcription factors (NRF1, GABP complex, ERRα, and ERRγ) was performed only in the hippocampus, given that all transcription factors are simultaneously expressed there, unlike in other tissues.

Animal Studies

Sirt7$^{-/-}$ mice were generated by a classical gene targeting strategy in 129Sv embryonic stem cells. Detailed information on gene targeting an be found in the Supplemental Experimental Procedures. The *Sirt7*$^{-/-}$ and *Sirt7*$^{L2/L2}$ mice were backcrossed for ten generations onto the C57BL/6J background. Phenotyping experiments were performed with validated Eumorphia /EMPReSS standard operating protocols (www.eumorphia.org). Animal experiments were approved by the ethics committee of the Canton of Vaud with permit ID #2444.

In Vitro Acetylation and Deacetylation Assays

In vitro acetylation and deacetylation assays were performed as originally described (Rothgiesser et al., 2010). In brief, 1 μg of recombinant GABPβ1 protein obtained from BL21 strain was incubated with 500 ng of recombinant p300 in acetylation buffer (50 mM Tris-HCl [pH 8], 100 mM NaCl, 10% glycerol, 1 mM phenylmethylsulfonyl fluoride [PMSF], 1 mM dithiothreitol [DTT], 1 μg/ml bepstatin, 1 μg/ml leupeptin, 1 μg/ml pepstatin, 1 mM sodium butyrate, and 150 μM acetyl-CoA) for 1 hr at 30°C. After incubation, samples were resolved on SDS-PAGE and analyzed by western blot or used for in vitro deacetylation assays. For deacetylation assays, 1 μg of acetylated GABPβ1 was incubated with 500 ng recombinant of SIRT7 protein in the deacetylation buffer (50 mM Tris-HCl [pH 9], 4 mM MgCl2, 0.2 mM DTT, 1 μg/ml bepstatin, 1 μg/ml leupeptin, 1 μg/ml pepstatin, and 1 mM NAD^+) for 30 min with constant agitation. The incubated samples were resolved on SDS-PAGE and analyzed by western blot or used to map an acetylated residue with nano liquid chromatography tandem mass spectrometry (LC-MS/MS). Recombinant proteins p300 and SIRT7 were kindly supplied by Michael O. Hottiger (University of Zurich).

Mass Spectrometry

Gel lanes were cut into pieces and subjected to in-gel digestion with endoproteinase Glu-C or trypsin. Peptide digests were resuspended and analyzed by nano LC-MS/MS with an Orbitrap Elite Mass Spectrometer (Thermo Fischer Scientific) coupled to an ultraperformance LC system (Thermo Fischer Scientific Ultimate 3000 RSLC). Data analysis was performed with Proteome Discoverer (v. 1.3), and searches were performed with Mascot and Sequest against a mouse database (UniProt release 2013_01). Data were further processed, inspected, and visualized with Scaffold 3.

Statistical Analyses

The comparison of different groups was carried out with Student's t test and two-way ANOVA, and differences under $p < 0.05$ were considered statistically significant (*$p < 0.05$, **$p < 0.01$, ***$p < 0.001$).

SUPPLEMENTAL INFORMATION

Supplemental Information contains Supplemental Experimental Procedures, seven figures, and six tables and can be found with this article online at http://dx.doi.org/10.1016/j.cmet.2014.08.001.

AUTHOR CONTRIBUTIONS

D.R. and J.A. conceived and designed the project. D.R. carried out bioinformatics analyses and performed all major experiments. Y.S.J., G.L.S., S.S., and A.P. helped with specific experiments. Y.S.J., G.L.S., and S.S. contributed equally. G.L.S., H.Z., and J.U.L. performed histological analyses. M.Z. provided human mutant fibroblasts. R.R. recorded and analyzed the ABR. M.O.H. advised and provided reagents for in vitro deacetylation assays. D.R., G.L.S., S.S., K.S., and J.A. wrote the manuscript.

ACKNOWLEDGMENTS

We thank V. Sirri (CNRS/Universités Paris 6 et 7) for providing SIRT7 rabbit polyclonal antibodies and the members of the different EPFL core facilities for help with various experiments. G.L.S. is supported by an Outgoing AIRC/Marie Curie Fellowship, S.S. by the German Academy of Sciences Leopoldina (LPDS 2011-6), and A.P. by a Long-Term EMBO Fellowship. Work in the laboratory of M.O.H. is supported by the SNSF (310030B-138667) and the Canton of Zurich. M.Z. is supported by the EU Ideas ERC program (AdG-322424). J.A. is the Nestlé Chair in Energy Metabolism. The research in his laboratory is supported by the EPFL, the EU Ideas program (AdG-231138), the NIH (R01AG043930), the Velux Stiftung, and the SNSF (31003A-140780 and CSRII3-136201 awarded to J.A. and 310030-143748 awarded to K.S.). We thank S.B. Lee, K. Kim, K.H. Kim (Sungkyunkwan University School of Medicine), and S.H. Koo (Korea University) and the members of the J.A. lab for discussion.

Received: April 14, 2014
Revised: June 30, 2014
Accepted: July 29, 2014
Published: September 4, 2014

REFERENCES

Andreux, P.A., Williams, E.G., Koutnikova, H., Houtkooper, R.H., Champy, M.F., Henry, H., Schoonjans, K., Williams, R.W., and Auwerx, J. (2012). Systems genetics of metabolism: the use of the BXD murine reference panel for multiscalar integration of traits. Cell *150*, 1287–1299.

Andreux, P.A., Houtkooper, R.H., and Auwerx, J. (2013). Pharmacological approaches to restore mitochondrial function. Nat. Rev. Drug Discov. *12*, 465–483.

Andreux, P.A., Mouchiroud, L., Wang, X., Jovaisaite, V., Mottis, A., Bichet, S., Moullan, N., Houtkooper, R.H., and Auwerx, J. (2014). A method to identify and validate mitochondrial modulators using mammalian cells and the worm C. elegans. Sci Rep *4*, 5285.

Báez-Ruiz, A., Escobar, C., Aguilar-Roblero, R., Vázquez-Martínez, O., and Díaz-Muñoz, M. (2005). Metabolic adaptations of liver mitochondria during restricted feeding schedules. Am. J. Physiol. Gastrointest. Liver Physiol. *289*, G1015–G1023.

Barber, M.F., Michishita-Kioi, E., Xi, Y., Tasselli, L., Kioi, M., Moqtaderi, Z., Tennen, R.I., Paredes, S., Young, N.L., Chen, K., et al. (2012). SIRT7 links H3K18 deacetylation to maintenance of oncogenic transformation. Nature *487*, 114–118.

Batchelor, A.H., Piper, D.E., de la Brousse, F.C., McKnight, S.L., and Wolberger, C. (1998). The structure of GABPalpha/beta: an ETS domain- ankyrin repeat heterodimer bound to DNA. Science *279*, 1037–1041.

Chen, S., Seiler, J., Santiago-Reichelt, M., Felbel, K., Grummt, I., and Voit, R. (2013). Repression of RNA polymerase I upon stress is caused by inhibition of RNA-dependent deacetylation of PAF53 by SIRT7. Mol. Cell *52*, 303–313.

Chi, C.S., Mak, S.C., Shian, W.J., and Chen, C.H. (1992). Oral glucose lactate stimulation test in mitochondrial disease. Pediatr. Neurol. *8*, 445–449.

Chinnery, P.F., Howell, N., Andrews, R.M., and Turnbull, D.M. (1999). Clinical mitochondrial genetics. J. Med. Genet. *36*, 425–436.

de la Brousse, F.C., Birkenmeier, E.H., King, D.S., Rowe, L.B., and McKnight, S.L. (1994). Molecular and genetic characterization of GABP beta. Genes Dev. *8*, 1853–1865.

Ford, E., Voit, R., Liszt, G., Magin, C., Grummt, I., and Guarente, L. (2006). Mammalian Sir2 homolog SIRT7 is an activator of RNA polymerase I transcription. Genes Dev. *20*, 1075–1080.

Fosslien, E. (2003). Review: Mitochondrial medicine—cardiomyopathy caused by defective oxidative phosphorylation. Ann. Clin. Lab. Sci. *33*, 371–395.

Fromenty, B., Berson, A., and Pessayre, D. (1997). Microvesicular steatosis and steatohepatitis: role of mitochondrial dysfunction and lipid peroxidation. J. Hepatol. *26* (*Suppl 1*), 13–22.

Gray, M.W., Burger, G., and Lang, B.F. (1999). Mitochondrial evolution. Science *283*, 1476–1481.

Grob, A., Roussel, P., Wright, J.E., McStay, B., Hernandez-Verdun, D., and Sirri, V. (2009). Involvement of SIRT7 in resumption of rDNA transcription at the exit from mitosis. J. Cell Sci. *122*, 489–498.

Guarente, L. (2008). Mitochondria—a nexus for aging, calorie restriction, and sirtuins? Cell *132*, 171–176.

Gugneja, S., Virbasius, J.V., and Scarpulla, R.C. (1995). Four structurally distinct, non-DNA-binding subunits of human nuclear respiratory factor 2 share a conserved transcriptional activation domain. Mol. Cell. Biol. *15*, 102–111.

Haigis, M.C., and Sinclair, D.A. (2010). Mammalian sirtuins: biological insights and disease relevance. Annu. Rev. Pathol. *5*, 253–295.

Hollenhorst, P.C., Chandler, K.J., Poulsen, R.L., Johnson, W.E., Speck, N.A., and Graves, B.J. (2009). DNA specificity determinants associate with distinct transcription factor functions. PLoS Genet. *5*, e1000778.

Houtkooper, R.H., Cantó, C., Wanders, R.J., and Auwerx, J. (2010). The secret life of NAD+: an old metabolite controlling new metabolic signaling pathways. Endocr. Rev. *31*, 194–223.

Houtkooper, R.H., Argmann, C., Houten, S.M., Cantó, C., Jeninga, E.H., Andreux, P.A., Thomas, C., Doenlen, R., Schoonjans, K., and Auwerx, J. (2011). The metabolic footprint of aging in mice. Sci Rep *1*, 134.

Houtkooper, R.H., Pirinen, E., and Auwerx, J. (2012). Sirtuins as regulators of metabolism and healthspan. Nat. Rev. Mol. Cell Biol. *13*, 225–238.

Hunter, K.P., and Willott, J.F. (1987). Aging and the auditory brainstem response in mice with severe or minimal presbycusis. Hear. Res. *30*, 207–218.

Imai, S., and Guarente, L. (2010). Ten years of NAD-dependent SIR2 family deacetylases: implications for metabolic diseases. Trends Pharmacol. Sci. *31*, 212–220.

Imai, S., Armstrong, C.M., Kaeberlein, M., and Guarente, L. (2000). Transcriptional silencing and longevity protein Sir2 is an NAD-dependent histone deacetylase. Nature *403*, 795–800.

Ivy, J.M., Hicks, J.B., and Klar, A.J. (1985). Map positions of yeast genes SIR1, SIR3 and SIR4. Genetics *111*, 735–744.

Keller, M.P., Choi, Y., Wang, P., Davis, D.B., Rabaglia, M.E., Oler, A.T., Stapleton, D.S., Argmann, C., Schueler, K.L., Edwards, S., et al. (2008). A gene expression network model of type 2 diabetes links cell cycle regulation in islets with diabetes susceptibility. Genome Res. *18*, 706–716.

Lagouge, M., Argmann, C., Gerhart-Hines, Z., Meziane, H., Lerin, C., Daussin, F., Messadeq, N., Milne, J., Lambert, P., Elliott, P., et al. (2006). Resveratrol improves mitochondrial function and protects against metabolic disease by activating SIRT1 and PGC-1alpha. Cell *127*, 1109–1122.

Larsson, N.G. (2010). Somatic mitochondrial DNA mutations in mammalian aging. Annu. Rev. Biochem. *79*, 683–706.

Leone, T.C., and Kelly, D.P. (2011). Transcriptional control of cardiac fuel metabolism and mitochondrial function. Cold Spring Harb. Symp. Quant. Biol. *76*, 175–182.

Mercer, T.R., Neph, S., Dinger, M.E., Crawford, J., Smith, M.A., Shearwood, A.M., Haugen, E., Bracken, C.P., Rackham, O., Stamatoyannopoulos, J.A., et al. (2011). The human mitochondrial transcriptome. Cell *146*, 645–658.

Nunnari, J., and Suomalainen, A. (2012). Mitochondria: in sickness and in health. Cell *148*, 1145–1159.

Pfister, J.A., Ma, C., Morrison, B.E., and D'Mello, S.R. (2008). Opposing effects of sirtuins on neuronal survival: SIRT1-mediated neuroprotection is independent of its deacetylase activity. PLoS ONE *3*, e4090.

Poyton, R.O., and McEwen, J.E. (1996). Crosstalk between nuclear and mitochondrial genomes. Annu. Rev. Biochem. *65*, 563–607.

Rothgiesser, K.M., Erener, S., Waibel, S., Lüscher, B., and Hottiger, M.O. (2010). SIRT2 regulates NF-κB dependent gene expression through deacetylation of p65 Lys310. J. Cell Sci. *123*, 4251–4258.

Scarpulla, R.C. (2008). Transcriptional paradigms in mammalian mitochondrial biogenesis and function. Physiol. Rev. *88*, 611–638.

Schadt, E.E., Molony, C., Chudin, E., Hao, K., Yang, X., Lum, P.Y., Kasarskis, A., Zhang, B., Wang, S., Suver, C., et al. (2008). Mapping the genetic architecture of gene expression in human liver. PLoS Biol. *6*, e107.

Schmidt, O., Pfanner, N., and Meisinger, C. (2010). Mitochondrial protein import: from proteomics to functional mechanisms. Nat. Rev. Mol. Cell Biol. *11*, 655–667.

Shin, J., He, M., Liu, Y., Paredes, S., Villanova, L., Brown, K., Qiu, X., Nabavi, N., Mohrin, M., Wojnoonski, K., et al. (2013). SIRT7 represses Myc activity to suppress ER stress and prevent fatty liver disease. Cell Rep *5*, 654–665.

Shore, D., Squire, M., and Nasmyth, K.A. (1984). Characterization of two genes required for the position-effect control of yeast mating-type genes. EMBO J. *3*, 2817–2823.

Singer, J.B., Hill, A.E., Burrage, L.C., Olszens, K.R., Song, J., Justice, M., O'Brien, W.E., Conti, D.V., Witte, J.S., Lander, E.S., and Nadeau, J.H. (2004). Genetic dissection of complex traits with chromosome substitution strains of mice. Science *304*, 445–448.

Thompson, C.C., Brown, T.A., and McKnight, S.L. (1991). Convergence of Ets- and notch-related structural motifs in a heteromeric DNA binding complex. Science *253*, 762–768.

Vakhrusheva, O., Smolka, C., Gajawada, P., Kostin, S., Boettger, T., Kubin, T., Braun, T., and Bober, E. (2008). Sirt7 increases stress resistance of cardiomyocytes and prevents apoptosis and inflammatory cardiomyopathy in mice. Circ. Res. *102*, 703–710.

Valdar, W., Solberg, L.C., Gauguier, D., Burnett, S., Klenerman, P., Cookson, W.O., Taylor, M.S., Rawlins, J.N., Mott, R., and Flint, J. (2006). Genome-wide genetic association of complex traits in heterogeneous stock mice. Nat. Genet. *38*, 879–887.

Virbasius, J.V., Virbasius, C.A., and Scarpulla, R.C. (1993). Identity of GABP with NRF-2, a multisubunit activator of cytochrome oxidase expression, reveals a cellular role for an ETS domain activator of viral promoters. Genes Dev. *7*, 380–392.

Wallace, D.C. (1999). Mitochondrial diseases in man and mouse. Science *283*, 1482–1488.

Yamasoba, T., Someya, S., Yamada, C., Weindruch, R., Prolla, T.A., and Tanokura, M. (2007). Role of mitochondrial dysfunction and mitochondrial DNA mutations in age-related hearing loss. Hear. Res. *226*, 185–193.

Yen, T.C., Chen, Y.S., King, K.L., Yeh, S.H., and Wei, Y.H. (1989). Liver mitochondrial respiratory functions decline with age. Biochem. Biophys. Res. Commun. *165*, 944–1003.

Yoshizawa, T., Karim, M.F., Sato, Y., Senokuchi, T., Miyata, K., Fukuda, T., Go, C., Tasaki, M., Uchimura, K., Kadomatsu, T., et al. (2014). SIRT7 controls hepatic lipid metabolism by regulating the ubiquitin-proteasome pathway. Cell Metab. *19*, 712–721.

Zincarelli, C., Soltys, S., Rengo, G., and Rabinowitz, J.E. (2008). Analysis of AAV serotypes 1-9 mediated gene expression and tropism in mice after systemic injection. Mol. Ther. *16*, 1073–1080.